



Swansea University Prifysgol Abertawe

Swansea University

Prifysgol Abertawe



Improving the Manufacture by Flexographic Printing of RFID Antennas for Intelligent Packaging

By

Caitlin Ann McCall

MEng (Hons), CEng.

Thesis submitted to Swansea University in fulfilment of the requirements for the Engineering
Doctorate (EngD)

September 2021



Abstract

Flexography is a well-established high-volume roll-to-roll industrial printing process that has shown promise for the manufacture of printed electronics for smart and intelligent packaging, particularly on to flexible substrates. Understanding is required of the relationship between print process parameters, including ink rheology, and performance of printed electronic circuits, sensors and in particular RFID antenna. The complexity of this printing process with its shear and extensional flows of complex inks and flexible substrates can lead to undesirable surface morphology to the detriment of electronic performance of the print. This thesis reports work that progresses the understanding of the complex relationships amongst relevant factors, particularly focusing on the printability of features that have an impact on printed RFID antenna where increases in resistance increase the antennas resonant frequency.

Flexography was successfully used to print RFID antenna. However, the large variation in print outcomes when using commercial inks and the limits on resistivity reduction even at the optimal print parameters necessitated the systematic development of an alternative silver flake ink. Increases in silver loading and TPU polymer viscosity grade (molecular weight) increased the viscosity. The ink maintained its geometry from the anilox cell between rollers, on to the substrate and print surface roughness increased. This, however, did not increase resistance of the track due to the high silver loading.

Better understanding of the relationship between print parameters, print outcomes, ink rheology and performance of an RFID antenna has been achieved. Increases in silver loading up to 60wt.% improved conductivity. However, further increasing the silver loading produced negligible additional benefit. An adaption of Krieger-Dougherty suspension model equation has been proposed for silver at concentrations over 60wt.% after assessing existing suspension models. Such a model has proven to better predict relative viscosities of inks than Einstein-Batchelor, Krieger-Dougherty and Maron-Pierce equations.

Increasing TPU viscosity grade was found to be a promising ink adjustment in the absence of changing print parameters, to produce a more consistent print. Better prediction of ink behaviour will allow for improved control of ink deposition, which for RFID applications can improve ink conductivity, essential for good response to signal. Further developments such as addition of non-flake particles and formulation refinement are required to enable the model ink to match the resistivity of the commercial ink.

Declaration and Statements

DECLARATION

This work has not previously been accepted in substance for any degree and is not being concurrently submitted in candidature for any degree.

Signed: C. A. McCall Date: 19/12/2021

Caitlin A. McCall

STATEMENT 1

This thesis is the result of my own investigations, except where otherwise stated. Other sources are acknowledged by footnotes giving explicit references and a bibliography is appended.

Signed: C. A. McCall Date: 19/12/2021

Caitlin A. McCall

STATEMENT 2

I hereby give consent for the thesis, if accepted, to be made available online in the University's Open Access Repository and for inter-library loan, and for the title and summary to be made available to outside organisations.

Signed: C. A. McCall Date: 19/12/2021

Caitlin A. McCall

STATEMENT 3

The University's ethical procedures have been followed and, where appropriate, ethical approval has been granted.

Signed: C. A. McCall Date: 19/12/2021

Caitlin A. McCall

Acknowledgements

I would like to express my gratitude to my supervisors Tim Claypole and Chris Phillips for the opportunity to embark as a researcher at icmPrint, and for their valuable assistance. I would like to thank icmPrint and WCPC for their guidance and support - in particular Alex Holder and Andrew Claypole for their expertise and enthusiasm for rheology which has motivated me throughout, and Ben Clifford for his guidance in the labs and on antennas.

Without my sponsors ESPRC, Swansea University, icmPrint and M2A this EngD would not have been possible, and I am very grateful to them all.

I am grateful to David Moody and his electronics team, and Alan McClelland and Eddie Iredia at CPI for access to their laboratories and the invaluable amount of feedback on my work.

My special thanks to my family and friends who have encouraged and supported me throughout this thesis. Thank you for the many great memories.

I would also like to thank Youmna Mouhamad, Sakulrat Foulston, Joy Ogeh-Hutfield, Jenny Baker, Andrew Rees, Catherine Critchley and Eleanor Norton with Discovery SVS in their support throughout my doctorate, helping me develop as a person and believing in me.

Caitlin McCall

Table of Contents

Abstract	ii
Declaration and Statements	iii
Acknowledgements	iv
Table of Contents	v
List of Tables.....	ix
List of Figures.....	xi
Nomenclature.....	xix
Chapter 1: Introduction	1
1.1 Operating Frequency	4
1.2 Chipless RFID	5
1.3 Printed RFID Antennas	6
1.3.1 Basic Principles of Flexographic Printing.....	10
1.4 Rheology of Printing Inks for RFID Manufacture.....	13
1.5 Closure.....	14
Chapter 2: Chapter 2 Literature Review	16
2.1 Introduction.....	16
2.2 Printed RFID Technology.....	16
2.2.1 Factors Affecting Antenna Performance	16
2.2.2 Process Parameters and Their Effects on Ink Transfer in Flexographic Printing.....	18
2.2.3 Process Settings and Their Effects on Ink Transfer in Flexographic Printing	22
2.2.4 Formulation of Conductive Flexographic Printing Inks.....	24
2.2.5 Drying, Curing and Sintering of Flexographic Inks	26
2.2.6 Design Feature Limits and Effect of Print Outcomes on Conductivity.....	28
2.2.7 Flexographic Printing Defects	28
2.3 Rheology	31
2.3.1 Shear Rheology	32
2.3.2 Silver Ink Rheology in Flexography	40
2.4 Chapter Closure.....	41
Chapter 3: Methodology	43
3.1 Introduction.....	43
3.2 Overview of the Antenna Design and Manufacture	43
3.3 RFID Antenna Measurement	43
3.3.1 RFID Antenna Measurement.....	43
3.3.2 Fundamentals of Complex Measurement of RFID Antenna	44
3.3.3 Antenna Reading Equipment.....	46
3.4 Antenna Design Software.....	49

3.4.1 CST Studio Suite 2019.....	50
3.5 Closure.....	52
3.6 Printing for RFID Manufacture.....	52
3.6.1 RK Control Coater (Bar Coater)	52
3.6.2 Flexographic Printing.....	53
3.6.3 Drying and Curing of Silver Ink.....	55
3.7 Surface Characterisation of Flexographic Printed Silver Ink.....	55
3.7.1 White light Interferometer: Veeco NT9300.....	56
3.7.2 Focus Variation Microscopy: Alicona Infinite Focus Microscope	57
3.8 Electrical Characterisation of Flexographic Printed Silver Lines.....	59
3.9 Manufacture of Inks for Flexographic Printing.....	60
3.9.1 Selection of Conductive Component.....	60
3.9.2 Resin Manufacture.....	60
3.10 Rheological Analysis.....	62
3.10.1 Rotational Rheometry	63
3.10.2 Bohlin Gemini	63
3.10.3 Kinexus Testing.....	63
3.10.4 Krieger-Dougherty, Maron-Pierce and Einstein-Batchelor Equations	64
3.11 Chapter Closure.....	65
Chapter 4: Preliminary Evaluation of Techniques for Measurement of Printed Antenna Electromagnetic Response	66
4.1 Introduction.....	66
4.2 Antenna Design	67
4.2.1 Monopole Antenna Design.....	68
4.2.2 Monopole Design Test Using a Spectrum Analyser and Arbitrary Generator	68
4.2.3 Testing Using a Vector Network Analyser.....	70
4.3 Simulation of Design	71
4.4 Chapter Closure.....	73
Chapter 5: Assessment of Flexographic Process Parameters	74
5.1 Introduction.....	74
5.2 Benchmarking of Antenna for Different Substrates.....	74
5.2.1 Benchmarking of Commercial Inks for Print Quality.....	74
5.2.2 Benchmarking of Resistance for Antenna Printed Tracks for Commercial Ink Selection	76
5.2.3 Substrate Selection.....	78
5.3 Revised Monopole Antenna Design for Testing Print Variation.....	79
5.3.1 Line Widths of Monopole Antenna Design.....	81
5.3.2 Film Thickness	82

5.3.3 Surface Roughness of Monopole Antenna Design.....	83
5.3.4 Resistances	85
5.4 Effect of Print Process Parameters on Print Quality.....	88
5.4.1 Effect of Anilox Roll Volume and Print Speed on Print Outcomes.....	88
5.4.2 Discussion.....	96
5.5 Substrate Optimisation	100
5.5.1 Effect of Substrate on Track Conductivity and Ageing.....	100
5.5.2 Discussion.....	101
5.6 Effect of Ink Drying Temperature and Duration on Printed Silver Tracks.....	101
5.7 Closure.....	105
Chapter 6: Effect of Printer Parameters: Anilox Volume and Print Speed on Frequency and Magnitude of Resonant Troughs	107
6.1 Introduction.....	107
6.2 Trough Magnitude and Corresponding Frequency for Print Parameters.....	107
6.3 Frequency at Highest Magnitude Resonant Trough Against Print Outcomes.....	110
6.4 Highest Magnitude Resonant Trough Against Print Outcomes.....	111
6.5 Effect of Line Width and Length on S22 at Resonant Frequency	113
6.6 Changes in Printed Line Performance on Biodegradable and PET Substrates Due to Environmental Exposure.....	114
6.6.1 Effect of Line Degradation on Resistance, Capacitance, and Inductance due to Environmental Exposure.....	115
6.6.2 Effect of Biodegradable Substrate on Printed Track Electrical Characteristics.....	117
6.7 Closure.....	118
Chapter 7: The Effect of Polymer Viscosity and Silver Loading on Ink Rheology and Printability	120
7.1 Introduction.....	120
7.2 Development of Optimised Carrier Ratio.....	120
7.3 Polymer Resin and Solvent.....	122
7.3.1 Effect of Silver Loading on Shear Viscosity	126
7.4 Effect of Polymer Molecular Structural Changes and Silver Loadings on Rheology	129
7.4.1 Effect of varying Polymer Viscosity Grade at Various Silver Loading.....	129
7.4.2 Varying Silver Loading.....	131
7.4.3 Equilibrium Shear Rate-Viscosity Curve	132
7.5 Modelling of Polymer Viscosity Grade and Silver Loading Suspension Behaviours for Viscosity and Phase Volume.....	133
7.6 Inclusion of Density in Viscosity Modelling.....	135
7.7 Chapter Conclusion.....	138
Chapter 8: Effect of Polymer Viscosity and Silver Loading on Printability	141
8.1 Introduction.....	141

8.2 Effect of Press Engagement.....	141
8.2.1 Effect of Engagement on Film Thickness	143
8.2.2 Effect of Engagement on Printed Line Width.....	147
8.2.3 Effect of Engagement on Resistance	148
8.3 Printing Trials Using Inks of Varying Viscosity Grade and Silver Content.....	150
8.3.1 Introduction	150
8.3.2 Effect of Polymer Viscosity Grade and Silver Loading on Line Widths	151
8.3.3 Effect of Polymer Viscosity Grade and Silver Loading on Film Thickness	156
8.3.4 Effect of Polymer Viscosity Grade and Silver Loading on Surface Roughness	157
8.3.5 Effect of Polymer Viscosity Grade and Silver Loading on Resistance	160
8.3.6 Effect of Polymer Viscosity Grade and Silver Loading on Resistivity.....	162
8.4 Antenna Performance Testing for Optimised Silver Ink.....	164
8.5 Discussion.....	168
8.6 Closure	173
Chapter 9: Discussion	175
Chapter 10: Conclusions and Future Work.....	183
10.1 Future Work Recommendations	184
10.1.1 Ink Formulation Method for Future Work	184
10.1.2 Future Work.....	184
References	186
Appendix	198
Appendix A: Discrete Component Model (Section 4.2.1.)	198
Appendix B: Simulation Array for Theoretical Impact of Surface Roughness on Frequency Response (Section 4.3)	200
Appendix C: Polymer Viscosity Grade at Various Silver Loadings (Section 7.4.1.)	204
Appendix D: Silver Loadings at Various Viscosity Grades (Section 7.4.2.)	207
Appendix E: Modelling of Polymer Viscosity Grade and Silver Loading Suspension Behaviours for Viscosity and Phase Volume (Section 7.5.)	210
Appendix F: Resin and Silver Ink Formulations (Section 7.3.1.).....	212

List of Tables

Table 1-1 – RFID Frequency Ranges and Typical Applications (1)	4
Table 1-2 – Comparison of Printing Techniques.....	8
Table 2-1 – List of typically used substrates in printing. Edited from presentation by department of Graphic Arts and Photophysics, Tampere University of Technology at the ActInPak Summer School (2017) (86).....	22
Table 3-1 – Modelled Silver ink properties	51
Table 3-2 – Modelled PET substrate properties.....	51
Table 3-3 – Anilox cell volume and screen line ruling.	55
Table 3-4 – Technic Inc. Engineered Powders Division particle size distributions as provided by manufacturer.....	60
Table 3-5 – Triple Roll Mill settings for two passes of silver ink.....	62
Table 3-6 – Densities used in calculations for volume.....	64
Table 4-1 – Printed tracks of various lengths and widths that are simulated on CST Studio Suite 2019	72
Table 5-1 – Commercial ink specifications	75
Table 5-2 – RK Flexiproof 100 print settings for print trials using Novacentrix PFI-722 and Inktec TEC-PR30.....	75
Table 5-3 – Design parameters of a plate with lines of various widths and lengths.....	80
Table 5-4 – Measured data for factors tested.....	90
Table 5-5 – Array of white light interferometry images of viscous finger effects from a print trial varying anilox volumes and print speeds.....	94
Table 5-6 – Print and oven settings used for the heat study.....	101
Table 6-1 – Design parameters of a plate with lines of various widths and lengths.....	113
Table 6-2 – Comparisons of resistance and Q Factors over a 12-week period for two substrate types.....	116
Table 7-1 – Commercial ink specifications.....	121
Table 7-2 – Polymer viscosity grades and silver loading (wt.%) contents for an ink array study with ink codes.....	129
Table 7-3 – Shear viscosity values at $0.01s^{-1}$ for polymer weights and silver loading contents for an ink array study.....	132
Table 7-4 – Shear viscosity values at $200s^{-1}$ for polymer weights and silver loading contents for an ink array study.....	132
Table 7-5 – Phase volumes at $1s^{-1}$ for each Ag wt.%.....	133

Table 7-6 – Error values between K-D model and measured results.....	136
Table 7-7 – Error values between newly proposed model and measured results.....	137
Table 7-8 – Highlights show improved alignment (green) or diverged alignment (red) compared to results in Table 7-9 for K-D Model. (Grey for anomaly result).....	137
Table 7-9 – Highlights show improved alignment (green) or diverged alignment (red) compared to results in Table 7-8 for New Model. (Grey for anomaly result).....	138
Table 8-1 – Design parameters of a plate with lines of various widths and lengths.....	142
Table 8-2 – Print settings for print engagement trial.....	143
Table 8-3 – Key to image array Figure 98.	144
Table 8-4 – Printed inks (red) from full factorial array.....	151
Table B-1 – Track length, widths and surface roughness for antenna design A	200
Table B-2 – Summary of resonant peaks from simulation tests of antenna from above table. ...	201
Table F-3 – Ag:DAA:TPU ratios for polymer Vgs 1.5 and 8.	212
Table F-4 – Ink formulations of 50:50 wt.% nano-Ag:(DAA-TPU formulation)	212

List of Figures

Figure 1-1 – Interaction between RFID, reader and computer (2).....	1
Figure 1-2 – Examples of RFID tags 1) (15), 2) (16).....	2
Figure 1-3 – Examples of monopole and dipole antennas.....	5
Figure 1-4 – Half-wave dipole antenna: two conductors connected to a central receiver ‘R’ (27).6	
Figure 1-6 – Key components of the flexographic printing process. Image from paper ‘Large-scale Roll-to-Roll Fabrication of Organic Solar Cells for Energy Production’ (60).....	11
Figure 1-7 – Flexographic Printing considerations for printed electronics (57)(62).....	12
Figure 1-8 – An extract from APEX International demonstrating the various cell structures available. The top row shows a cross section of three cell volumes of the same quantity, varying only in shape and the bottom row shows anilox cell geometries from surface (65).	13
Figure 2-1 – ‘Comparison of sintered microstructures of different types of silver pastes: (a) a conventional silver paste with microparticles, flakes and polymeric binder matrix left after sintering, and (b) the developed silver nano paste, ‘nano Coln E001’ (30).....	17
Figure 2-2 – Roller engagement schematic for printing nips.....	19
Figure 2-3 – Examples of flexographic print defects. halo effects (a) (117), viscous fingering (b) (118), dot gain (c) (119), print mottle (d) (120), pin holing (e) (121), filling in/bridging (f) (121), feathering (g) (121), dirty print (h) (121), and chatter (i) (gear marks) (121).....	29
Figure 2-4 – Alignment of particle orientation for a flowing suspension (142).	34
Figure 2-5 – The effect of concentration on shear rate and viscosity (143).....	34
Figure 2-6 – Nip junction schematic where tensile viscoelastic force is important.	39
Figure 2-7 – Shear (dotted lines) and extensional flow (solid lines) flow curves for aqueous solutions of polyacrylamide (tension thickening) and collagen (tension thinning) (124).....	40
Figure 3-1 – UHF RFID computer plugin reader.....	44
Figure 3-2 – An RLC circuit on a Tic-Tac ® Box.....	46
Figure 3-3 – Simple circuit diagram for chip-less antenna tests using a spectrum analyser and arbitrary generator.....	47
Figure 3-4 – Physical spectrum analyser, arbitrary generator and antenna set up.....	48
Figure 3-5 – Keysight Technologies N9923A FieldFox handheld RF Vector Network Analyser and printed sample.....	49
Figure 3-6 – Inductance, capacitance, resistance (LCR) bridge with wires for measuring antenna samples.....	49
Figure 3-7 – Typical Frequency – S22 graph from CST Studio Suite.....	50

Figure 3-8 – Frequency responses on: (a) spectrum analyser (b) vector network analyser and (c) CST Studio Suite 2019 simulations.	52
Figure 3-9 – RK Control Coater.....	53
Figure 3-10 - Flexiproof 100 and a schematic of the rollers.....	54
Figure 3-11 – Standard flexography plate design.....	55
Figure 3-12 - Analysis of average print thickness of printed track.....	56
Figure 3-13 – Surface roughness example from WYKO Vision 32 software for a printed track. .	57
Figure 3-14 – Alicona microscope in the Welsh Centre of Printing and Coatings laboratories. A flexographic printing plate is on the bed and shown on the screen.....	57
Figure 3-15 – Locations of the readings taken on the Alicona Infinite Focus Microscope.....	58
Figure 3-16 – Line width Measurements on Alicona MeasureSuite 5.3.5 software.....	58
Figure 3-17 – Line width Measurements on Alicona MeasureSuite 5.3.5 software.....	58
Figure 3-18 – Alicona microscope image of 24cm ³ /m ² anilox cell surface with blue measurement line.....	59
Figure 3-19 – Multimeter probe locations.....	59
Figure 3-20 – Overhead mixer used for ink formulations.....	61
Figure 3-21 – EXAKT Advanced Technologies GmbH three-roll mill (171).....	62
Figure 3-22 – Malvern Bohlin Gemini Rheometer at Swansea University with cone and plate set up.....	63
Figure 3-23 – Malvern Kinexus Pro Rheometer (174).....	64
Figure 4-1 – Layout of chip and antenna poles for a dipole antenna.....	67
Figure 4-2 – 1. Compact design dipole; 2. Straight-line dipole; 3. Meandering dipole. Insert: Contacts for chip placement.....	67
Figure 4-3 – Left: Design A - meandering monopole. Right: Design B - meandering monopole with four spiral resonators.....	68
Figure 4-4 – Solenoid and spectrum analyser.....	69
Figure 4-5 – Solenoid and printed antenna.....	69
Figure 4-6 – Frequency response shown on the spectrum analyser.....	70
Figure 4-7 – Screen grab of VNA screen when analysing a 0.5mm wide printed Novacentrix PFI 722 silver ink track.....	71
Figure 4-8 - CST Studio Suite 2019 simulations of printed tracks of increasing track lengths and widths.....	72
Figure 4-9 - CST Studio Suite 2019 simulations of printed tracks of increasing track lengths.....	72
Figure 5-1 – Design of the two sets of silver printed conductive lines labelled 1 and 2.....	76

Figure 5-2 – Comparison of the general trend of resistances between flexographic prints of the Novacentrix ink and the Inktec ink for antenna 3 design. 20 samples for each ink measured. Error bars show 1 standard deviations.....	76
Figure 5-3 – Average resistances for Novacentrix ink antenna #1 18mm in a straight line and 18mm with a corner. Error bars show 1 standard deviations.....	77
Figure 5-4 – Conductive silver track resistances for flexographic printed samples of the Novacentrix PFI-722 silver-based ink (a) antenna 1, (b) antenna 2.....	78
Figure 5-5 – Conductive silver track resistances for flexographic printed samples of the Inktec TEC-PR30 silver-based ink (a) antenna 1, (b) antenna 2.....	78
Figure 5-6 – Printed antenna designs A, B C D E and F.....	80
Figure 5-7 – Design for printed antennas with annotations outlined in Table 5-3.....	80
Figure 5-8 – Locations of the readings, 1, 2 and 3, taken on the Alicona Infinite Focus Microscope.	81
Figure 5-9 – (a) Line width % increase for designs A, C, D and E printed with a Novacentrix PFI-722 nano-silver ink. (b) Printed line widths at three points along the print direction for the design shown in Figure 5-8. Intended line width is shown via a red dashed line.....	82
Figure 5-10 – Film thickness for each print sample over the print sequence.....	83
Figure 5-11 – Surface roughness, Ra, of each print sample over the print sequence.	83
Figure 5-12 – View of a sample of the printed track on the Veeco White Light Interferometer software.....	84
Figure 5-13 – Film thickness against peak-to-peak distance for Novacentrix PFI-722 nano-silver ink.	85
Figure 5-14 – The average surface roughness across each printed antenna against the average film thickness for each antenna.....	85
Figure 5-15 – (a) : Resistances over print time for six designs of different line widths and line lengths. Error bars show 1 standard deviations. (b) : Resistance changes over print time for six designs of different line widths and line lengths.....	86
Figure 5-16 – Resistivities for four designs: A, C, D and E.....	87
Figure 5-17 – Log-log graph of viscosity against shear rate for a newly manufactured and a 1-year-old Novacentrix PFI 722 ink.....	88
Figure 5-18 – Print design with arrow labelling print direction. Arrow will enter printer last... 88	88
Figure 5-19 – Image of raise printing plate image overlaid on anilox surface.....	89
Figure 5-20 – Average print widths of Novacentrix PFI-722 ink for: (a) anilox volume 8cm ³ /m ² for print speeds 20m/min, 50m/min and 80m/min; (b) anilox volume 14cm ³ /m ² for print speeds 20m/min, 50m/min and 80m/min; (c) anilox volume 24cm ³ /m ² for print speeds 20m/min,	

50m/min and 80m/min. Error bars show 1 standard deviations. Intended line width is shown via a dashed line..... 91

Figure 5-21 – Locations on meandering line from which film thickness and surface roughness readings were measured..... 91

Figure 5-22 – Average film thickness of Novacentrix PFI-722 ink for: **(a)** anilox volume 8cm³/m² and print speeds; **(b)** anilox volume 14cm³/m² and print speeds; **(c)** anilox volume 24cm³/m² and print speeds. Error bars show 1 standard deviations..... 92

Figure 5-23 – Comparison of film thickness along print direction by taking measurements from the left (LHS) and the right (RHS) of the print. Error bars show 1 standard deviations..... 92

Figure 5-24 – Average surface roughness of Novacentrix PFI-722 ink for: **(a)** anilox volume 8cm³/m² for print speeds 20m/min, 50m/min and 80m/min; **(b)** anilox volume 14cm³/m² for print speeds 20m/min, 50m/min and 80m/min; **(c)** anilox volume 24cm³/m² for print speeds 20m/min, 50m/min and 80m/min. Error bars show 1 standard deviations. 93

Figure 5-25 – Average print resistance of Novacentrix PFI-722 ink for anilox volumes 8, 14 and 24cm³/m² at print speeds 20m/min, 50m/min and 80m/min. Error bars show standard deviations..... 95

Figure 5-26 – Average print resistivity of Novacentrix PFI-722 ink for: **(a)** anilox volume 8cm³/m² for print speeds 20m/min, 50m/min and 80m/min; **(b)** anilox volume 14cm³/m² for print speeds 20m/min, 50m/min and 80m/min; **(c)** anilox volume 24cm³/m² for print speeds 20m/min, 50m/min and 80m/min..... 96

Figure 5-27 – Resistance against film thickness for design C. 98

Figure 5-28 – Resistance changes over print time for Novacentrix PFI722 silver onto bio substrate and PET substrate. Error bars show 1 standard deviations..... 100

Figure 5-29 – **(a)** Track width measurements for four temperatures at four distinct heating intervals. **(b)** Film thickness measurements for four temperatures at four distinct heating intervals. **(c)** Surface roughness measurements for four temperatures at four distinct heating intervals. **(d)** Resistance measurements for four temperatures at four distinct heating intervals. **(e)** Resistivity measurements for four temperatures at four distinct heating intervals..... 103

Figure 5-30 – Drying pattern after one minute..... 103

Figure 6-1 – Frequencies at the point of largest trough magnitude for design A at anilox volumes 8cm²/m², 14cm²/m², 24cm²/m², and print speeds 20m/min, 50m/min and 80 m/min. Measured using a vector network analyser. Standard deviations are shown. **(a)**: Design A, **(b)**: Design B. 108

Figure 6-2 – Highest magnitude troughs recorded in the frequency sweep of 100 MHz to 1 GHz at anilox volumes 8cm²/m², 14cm²/m², 24cm²/m², and print speeds 20m/min, 50m/min and 80

m/min. Measured using a vector network analyser. Standard deviations are shown. (a) : Design A, (b) : Design B.....	109
Figure 6-3 – Effect of print speed on an amplitude – frequency graph for design A at anilox volumes 8cm ² /m ² , 14cm ² /m ² , 24cm ² /m ² , and print speeds 20m/min, 50m/min and 80 m/min with outliers removed. Measured using a vector network analyser. Error bars represent standard deviation.....	110
Figure 6-4 – For anilox volumes 8cm ² /m ² , 14cm ² /m ² , 24cm ² /m ² , and print speeds 20m/min, 50m/min and 80 m/min, and measured using a vector network analyser: (a) Frequency against surface roughness (b) Frequency against resistance. Error bars represent standard deviation.	111
Figure 6-5 – For antenna A, S22 against (a) Print thickness (b) Surface roughness (c) Surface roughness/ film thickness.	112
Figure 6-6 – Printed antenna designs A, C and E.....	113
Figure 6-7 – S22 for three track designs of varying length and width. One standard deviation is shown.	114
Figure 6-8 – Average resistances and Q-factors measured over 6-week intervals for printed Novacentrix PFI722 nano-silver ink onto PET substrate.	115
Figure 6-9 – Average capacitance and inductance measured over 6-week intervals for printed Novacentrix PFI722 nano-silver ink onto PET substrate.	116
Figure 6-10 – Average resistance, capacitance, inductance, and Q-factor measured on an LCR bridge for printed Novacentrix PFI722 nano-silver ink on HiFi Industrial Film 175µm thick PET substrate and on Eco Craft 30µm thick cellulose substrate.....	117
Figure 7-1 – Shear viscosity – shear rate graph for two commercial inks.....	121
Figure 7-2 – (a) Shear Viscosity against Shear Rate of the five resins composed of DAA and TPU with polymer Vgs (1.5, 8, 12, 19 and 25). Resins of DAA and TPU to ratios of 87.5:12.5 respectively. (b) Viscosity grades in resins at four shear rates.	123
Figure 7-3 – (a) Resins of DAA and TPU for 50wt.% Ag. (b) Viscosity grades in silver-resin formulations at four shear rates.....	124
Figure 7-4 – DAA-TPU resins of varying formulation ratios. (a) 1.5 Mw (b) 8 Mw.	125
Figure 7-5 – Resins of DAA and TPU. TPU wt.%s 1.5 and 8, in varying ratios of 12.5:87.5, 10:90 and 7.5:92.5 to DAA. All to 50:50 Resin: Ag.....	126
Figure 7-6 – (a) Shear viscosity against shear rate for five inks of 1.5 Vg and 92.5:7.5 DAA:TPU ratio with Ag wt.% of 40, 50, 60, 70 and 80. Commercial inks are also shown. (b) Shear viscosity for silver wt.%s at four shear rates for 1.5Vg resin-silver formulation.....	127

Figure 7-7 – (a) Shear viscosity against shear rate for five inks of 8 Vg and 92.5:7.5 DAA:TPU ratio with Ag wt.% of 40, 50, 60, 70 and 80. Commercial inks are also shown. (b) Shear viscosity for silver wt.%s at four shear rates for 8 Vg resin-silver formulation.	128
Figure 7-8 – Effect of polymer viscosity grades 1.5, 8, 12, 19 and 25 for: (a) 40 wt.%, (b) 50 wt.%, (c) 60 wt.%, (d) 70 wt.% and (e) 80 wt.% silver loading on shear viscosity. Shown on a shear viscosity against shear rate log-log graph.....	130
Figure 7-9 – Silver loadings: 40, 50, 60, 70 and 80 wt.% for 8 Vg polymer on a shear viscosity against shear rate.	131
Figure 7-10 – Relative viscosity against phase volume for an Ag-DAA-TPU (1.5 Vg.) flexographic printing ink for inks of 40wt.%, 50wt.%, 60wt.%, 70wt.% and 80wt.% Ag for 8 Vg polymer....	134
Figure 8-1 – Printed antenna designs A, C and E.....	142
Figure 8-2 – Engagement settings (Anilox Cylinder to Plate Cylinder Plate Cylinder to Impression Cylinder). Optimal profile for low resistance is highlighted in red.	145
Figure 8-3 – White light interferometry images of 1mm lines for engagements: (a) 200,280 μm (A-P,P-I), (b) 420,280 μm (A-P,P-I) and (c) 420,400 μm (A-P,P-I).....	146
Figure 8-4 – Effect of engagement on line width of a printed 1mm width track where (a) A-P engagement varies, and P-I engagement is set to 240 μm ; (b) Varying P-I engagement A-P engagement is set to 260 μm ; (c) A-P engagement and P-I engagement vary simultaneously. Error bars show one standard deviation.....	148
Figure 8-5 – Resistance measurements of a 1mm line width for: (a) increasing A-P engagement. P-I engagement is 280 μm ; (b) increasing P-I engagement. A-P engagement is 260 μm ; (c) increasing A-P and P-I engagement. Average resistance measurements are shown with one standard deviation.	150
Figure 8-6 – % increase in three line widths (design A:0.5mm, design C:1mm and design E:1.5mm) for changes in the silver ink of 60 wt.% loading with polymer (a) Vg1.5 (b) Vg8. Each point is an average increase for five measurements taken.	152
Figure 8-7 – Design A: Silver loading 60wt.%, polymer Vg 1.5, 8, 12, 19, 25.	153
Figure 8-8 – White light interferometry scans of 1.5 Vg (left) and 25 Vg (right) for a silver loading of 60wt.%.	153
Figure 8-9 – Design A: 8 Vg; Silver loading 40, 50, 60, 70 and 80wt.%.	154
Figure 8-10 – Overlays of anilox cells and printing plate track on (a) 12 Vg ink track (b) 80wt.% silver loading ink track. Anilox cell measurement outlined in Methodology.	154
Figure 8-11 – Cross-section of printed track on a flexographic printer. Demonstration of theorised movement of ink under the plate pressure.	155

Figure 8-12 – **(a)** Film thickness of three line widths (design A:0.5mm, design C:1mm and design E:1.5mm) for polymer Vg changes in the silver ink of 60 wt.% loading. **(b)** Film thickness of three line widths (design A:0.5mm, design C:1mm and design E:1.5mm) for silver loading changes in the silver ink of polymer 8 Vg. Error bars show standard deviation of 5 samples. 157

Figure 8-13 – **(a)** Surface roughness of three line widths (design A:0.5mm, design C:1mm and design E:1.5mm) for polymer Vg changes in the silver ink of 60 wt.% loading. **(b)** Surface roughness of three line widths (design A:0.5mm, design C:1mm and design E:1.5mm) for silver loading changes in the silver ink of 8 Vg polymer. Error bars show standard deviation of 5 samples. 158

Figure 8-14 – White Light Interferometry images of printed tracks for five silver loadings.1.5 Vg. 159

Figure 8-15 – White Light Interferometry images of printed tracks for five viscosity grades.... 160

Figure 8-16 – **(a)** Resistance of three line widths (design A:0.5mm, design C:1mm and design E:1.5mm) for polymer Vg changes in the silver ink of 60 wt.% loading. **(b)** Resistance of three line widths (design A:0.5mm, design C:1mm and design E:1.5mm) for silver loading changes in the silver ink of 8 Vg. Error bars show standard deviation of 5 samples. 162

Figure 8-17 – **(a)** Calculated resistivity of three line widths (design A:0.5mm, design C:1mm and design E:1.5mm) for polymer Vg changes in the silver ink of 60 wt.% loading. **(b)** Calculated resistivity of three line widths (design A:0.5mm, design C:1mm and design E:1.5mm) for silver loading changes in the silver ink of 8 Vg..... 163

Figure 8-18 – Designs A, C and E tested on a VNA machine at a frequency range of 1GHz to 5GHz. 165

Figure 8-19 – PCB designs A, C and E tested on a VNA machine at a frequency range of 1GHz to 5GHz..... 166

Figure 8-20 – PCB design A, and PET substrate design A tested on a VNA machine at a frequency range of 1GHz to 5GHz. 167

Figure A-1 – Rohde and Schwarz RTM 2024 Digital Oscilloscope output interface showing input and output voltages, input and output frequencies, and phase shifts of the signal. 198

Figure A-2 – Discrete component system showing measured output voltage for: **(a)** varying inductor values across a range of frequencies; **(b)** varying capacitor values across a range of frequencies; **(c)** varying resistor values across a range of frequencies..... 199

Figure C-3 – Polymer viscosity grades 1.5, 8, 12, 19 and 25 for: **(a)** 40 wt.%, **(b)** 50 wt.%, **(c)** 60 wt.%, **(d)** 70 wt.% and **(e)** 80 wt.% silver loading on a shear viscosity against shear rate log-log graph..... 206

Figure D-4 – 40 wt.%, 50 wt.%, 60 wt.%, 70 wt.% and 80 wt.% silver loadings for polymer: **(a)** 1.5 Vg, **(b)** 8 Vg, **(c)** 12 Vg, 19 **(d)** Vg **(e)** 25 Vg, on a shear viscosity against shear rate log-log graph.

.....209

Figure E-5 – Relative viscosity against phase volume for an Ag-DAA-TPU(1.5 Vg.) flexographic printing ink for inks of 40wt.%, 50wt.%, 60wt.%, 70wt.% and 80wt.% Ag. **(a)** TPU 1.5Vg; **(b)** 8 Vg; **(c)** 12 Vg, **(d)** 19 Vg, **(e)** 25 Vg.211

Nomenclature

A – cross-sectional area	λ – wavelength
Ag – silver	m – meter
A-P – anilox-plate cylinders	M-P – Maron-Pierce
BCM – billions of cubic microns	MEK – methyl-ethyl-ketone
C – capacitance	MHz – mega Hertz
c – speed of light	η – shear viscosity
cm – centimetre	$[\eta]$ – intrinsic viscosity
CP – cone and plate	η_0 – Newtonian continuous phase viscosity
cP – centipoise	nm – nanometre
DAA – diacetone alcohol	Ω – ohms
dB – decibels	Ω/\square – ohms per square
E – energy	Pa.s – Pascal seconds
E-B – Einstein-Batchelor	PE – printed electronics
EM – electromagnetic	PEDOT – polyethylenedioxythiophene
EN – European Standards	PET – polyethylene terephthalate
ERC – European Radiocommunications Committee	P-I – plate impression cylinders
ETSI – European Telecommunications Standards Institute	PLA – polylactic acid
f – frequency	PSI – phase shifting interferometry
g – gravitational acceleration	Q-factor – quality factor
GHz – giga Hertz	R – resistance
HF – high frequency	R_a – average roughness
I – current	R_q – root mean square roughness
ISO – International Standards Organisation	R_t – maximum peak-to-valley height
K – Kelvin	R_z – mean peak-to-valley height
K-D – Krieger-Dougherty	rpm – revolutions per minute
Kg – kilogram	ρ – Resistivity
L – inductance	RFID – radio frequency identification
LAMS – laser ablative mask system	S/m – Siemens per meter (electrical conductivity)
LED – light emitting diode	sq. – square
LF – low frequency	TPU – thermoplastic polyurethane
LPI – per linear inch	μm – micrometre
	UHF – ultra-high frequency

UV(A,C) – ultra-violet light

Vg – viscosity grade

VNA – vector network analyser

VSI – vertical scanning interferometry

wt. – weight

Wt. % – weight percentage

ν – frequency

θ – phase angle

ϕ – phase volume

ϕ_m – maximum packing fraction

$\dot{\gamma}$ – shear rate

Λ – wavelength

$^\circ$ – degrees

$^\circ\text{C}$ – degrees Celsius

τ – shear stress

Chapter 1: Introduction

RFID (Radio Frequency Identification) utilises electromagnetic radiation in the radio frequency range for rapid identification of products. It has many applications including controlled access, personnel tracking, inventory and supply chain management. RFID offers improved processing speed, accuracy, efficiency, and data security. RFID, when compatible with manufacturing printing process, can be integrated with existing technologies and this in turn allows integration into packaging (1). Figure 1-1 shows the reader scans the RFID tag, record data transmitted back and sends this to the computer to log the data.



Figure 1-1 – Interaction between RFID, reader and computer (2).

Since the origins of RFID in 1948, research has continued to expand the applications for RFID and to develop low cost RFID systems (3). The most expensive part of these systems was initially the reader but with tags being fastened to multiple products in mass manufactured applications (millions can be produced), there is a demand to drive down the cost of the chip. Research has reduced the chip costs however, limits in cost reduction remain as the processing of the wafer to attach it to a label remains high regardless of the price of the chip. For a large batch of tags, in the 1 billion region, a predicted minimum cost per RFID tag is approx. 5 cents (4).

RFID is well used in traceability, logistics and access control. It has huge potential in the supply chain, in particular tapping into the Internet of Things through individual tagging. Individual item tagging is highly desirable by all stages of a product's production and distribution lines. The implementation of RFID has benefits in many industries due to its usefulness in product traceability, real-time tracking, product quality assurance and inventory management (5)(6). Further uses of RFID in the future could include, automatic checkout systems, real-time product shelf information including: automatic replenishment and misplaced product alerts and production locations, consequently helping to reduce labour costs (7).

The RFID industry is currently predicted to be worth \$10.7 billion USD (2021) with potential to grow to \$17.4 billion by 2026. Recent growth is due to the uptake of the RFID technology in retail, logistics and supply chain management. Of the three frequency ranges (low, high and ultra-high), UHF RFID tags accounted for the largest percentages of the market in 2020, where applications lie in asset tracking, product part tagging, and supply chain and inventory management. The latter held the largest share in RFID applications (8). UHF is typically chosen for its read ranges (1-100m), which allows for products to be scanned at a distance yet provide enough power for an efficient signal transfer. Examples of UHF RFID tags are shown in Figure 1-2.

Examples of UHF RFID in literature include: inkjet-printed humidity sensor (9); temperature, humidity and amine compound sensing (10)(11)(12); 19-bit chipless RFID tag (13); and a stretchable RFID using a co-polymer ink (14).

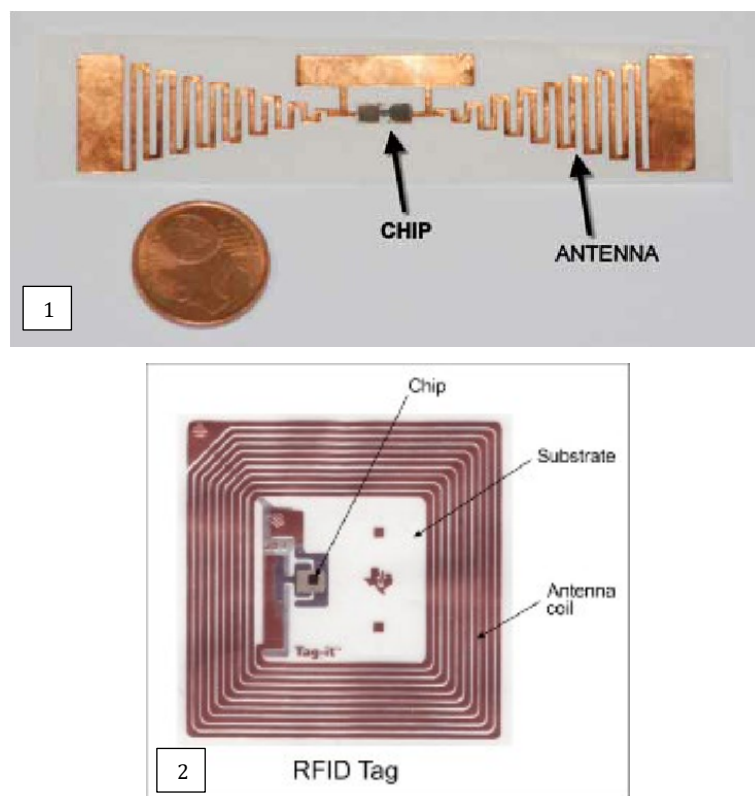


Figure 1-2 – Examples of RFID tags 1) (15), 2) (16).

Passive RFID have no directly connected power supply and obtain their operating power from radio-frequency waves transmitted from the reader. The wireless link between the device and the reader can be classified into two groups, far-field coupling and near-field coupling (17). Far-field coupling enables the device to be read at longer distances than near-field. This means that the device operates at lower voltages and is consequently more susceptible to interference. RFID devices using UHF frequencies use far-field coupling (18). The efficiency of the device in power

harvesting is affected by antenna efficiency, accuracy of pairing antenna to chip, and voltage multiplier efficiency (17). Efficiency of the antenna is directly related to the conductivity of the printed track, which is affected by the quantity of conductive particles and their connectivity once the ink has cured.

In intelligent packaging, systems monitor and display information on freshness. RFID can be used to relay information detected by a sensor on packaging. The main way in which antennas can be deposited onto flexible packaging is by (19) high-volume print processes in which the speed of fabrication is compatible with film converting. Pick and place machines or automated deposition machines are used for adhering the antenna chips to the surface, which is a slow process and turns the package into electronic waste as governed by WEEE regulations.

An RFID antenna, when supplied with a signal, gives a unique response. If this response is altered via a physical change in the antenna, then the antenna would no longer produce the original signal and work as a binary on/off system. This could be achieved by introducing a sensing element in the antenna from which electromagnetic properties change in response to an external stimulus such as temperature. A dedicated reader could determine the change in resonance and this would be an antenna without a chip, i.e., chipless RFID. This would require the printed antenna to be of a consistent quality and performance so changes can be attributed solely to the sensing element.

The objective of this research was to establish the underpinning science to enable the manufacturing process for RFID Antennas to be optimised through a holistic study of the high-volume printing of antenna including ink manufacture, transfer and deposition. This will enable more consistent and better performance, which is essential for the future development of chipless RFID for volume printed smart packaging.

A sensor on packaging could enable a faster information transfer on the quality of the food product than visual inspection but this requires a deeper understanding of antenna printing.

This research will benefit all applications of RFID. The inefficiency of the antenna production also highlights a need to focus on the optimisation of the antenna (20)(21). One of the main costs in the manufacture of RFID is the high value printing ink, typically containing silver. Silver waste is also an issue. Reductions in cost through minimising the use of silver deposited whilst maintaining good conductivity for high antenna performance has the potential to minimise the use of this valuable resource in production.

For printed electronics, the quantity of conductive ink deposited is directly related to the resistance of the conductive track printed. Silver is the most likely conductive component for

printed electronics due to its high electrical conductivity, chemical stability and processability. It has a more stable form when having reacted with atmospheric air, typically to create silver sulphide, and still conducts in this form. Oxidation of copper leads to poor interparticle electrical contact and a reduction in conductivity, hence, copper is not a suitable option for printed electronics. Additionally, copper requires higher levels of post processing, including protective coatings to prevent oxidation, for use in printing (22)(23). Carbon is much more resistive than silver so larger antennas would be required for equivalent performance (24). The use of carbon is not a suitable option for the printed antennas in this work.

1.1 Operating Frequency

The environment in which the RFID tag operates heavily dictates the frequency that is required for operation. RFID tags operate in the low, high, ultrahigh and microwave frequency ranges. There are many restrictions imposed on the ultrahigh range by countries around the world and the full range cannot always be used. RFID ranges and restriction imposed on the ultrahigh range are further outlined in Table 1-1. This is the reading bandwidth of the reader. UHF is the frequency range of focus in this paper however, HF has been used for some testing due to limitations of equipment used in preliminary tests.

Table 1-1 – RFID Frequency Ranges and Typical Applications (1).

Name	Frequency	Read Range	Typical Applications
Low Frequency (LF)	30-300kHz	50cm	Pet Identification
High Frequency (HF)	3-30MHz	3m	Restricted access control
Ultrahigh Frequency (UHF)	300MHz-3GHz	9m	Individual item and pallets
Microwave Frequency	>3GHz	>10m	Vehicle identification

Antenna gain is a measure of the antenna’s power in decibels (dB). Higher antenna gain increases reading range (25). Hence, it is important to increase the response of the system to ensure a good reading.

Read ranges for items within a pallet are assumed to be at least 1m. At this distance, 13.56MHz is required. However, to enable detection of products from a distance, an ultra-high frequency (UHF) of 868-930MHz is required. This enables a passive tag to read at a range of up to 10m. Active UHF tags can read at ranges almost double this. Higher frequency ranges require smaller antenna lengths, which is preferred by manufacturers in twofold: Smaller RFID tags can fit onto

smaller products and cost less. Additionally, higher frequency tags operate better than lower frequency tags for water or metal environments (1).

The next sections present an overview of chipless RFID and printing processes.

1.2 Chipless RFID

Integrating RFID with sensors that interact with the contents of a package could give real-time updates on changes within the packaging. For example, a biosensor interacting with the food contained within, when designed to do so, could give a real-time food status. When a crate of that packaging type is scanned, a real-time understanding of the quality of the packaged foods can be determined. This would aid distributors and manufacturers in identifying weak points in the supply chains. Whilst this may not currently be an option for cheap goods, more valuable products may benefit from this. Additionally, chips can hold much more information about the product such as manufacture, distribution, and retail details, to integrate with other stages of the supply chain.

Printed antenna examples include monopole and dipole (Figure 1-3). Monopole antennas consist of one conducting element, which is connected to a central transmitter that emits or receives the signal. The other end of the conductor is connected to a ground plane. Dipole antennas have two identical conducting elements that are connected to a central transmitter and is the most commonly used class of antenna. Both are commonly used as resonant antennas.

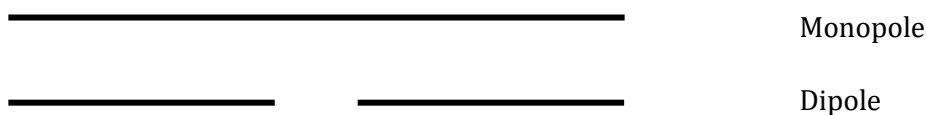


Figure 1-3 – Examples of monopole and dipole antennas.

For a receiving antenna, the emitted signal is accepted by the antenna and converted to an electrical signal which is then passed onto the transmission line. Whether this transmission line is connected to power at both ends or one, is denoted by the shape. Dipole wire antennas can also be described in terms of their relationship with the wavelengths in which they operate: Half-wave dipole, half-wave folded dipole, full-wave dipole, short dipole, and infinitesimal dipole. Monopoles and half-wave dipoles will be further discussed (26).

A half-wave dipole antenna comprises of two conductors feeding into a receiver (Figure 1-4). The electric field (green arrows) of the wave creates a positive and negative charge at either ends of

the conductors by moving electrons in the conductors from one end to the other. This in turn generates a standing wave of voltage (red) and current in the conductors (black arrows). The lengths of each pole are calculated using:

$$c = \lambda v \quad \text{Equation 1-1}$$

where $c = 3 \times 10^8 \text{m/s}$ (speed of light).

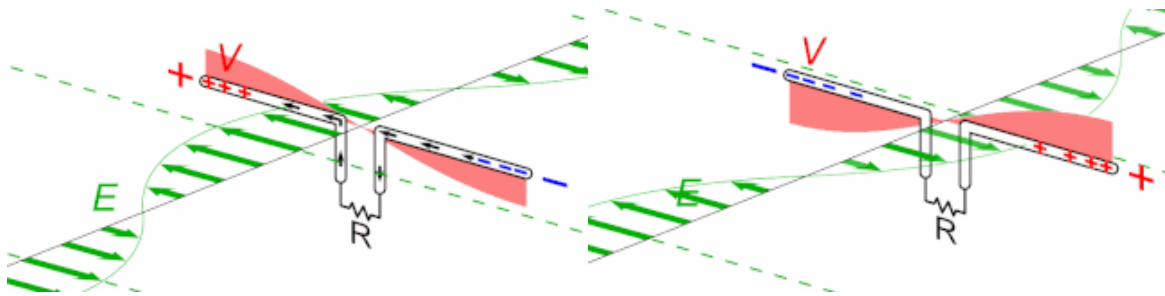


Figure 1-4 – Half-wave dipole antenna: two conductors connected to a central receiver 'R' (27).

1.3 Printed RFID Antennas

The cost of printed antenna is dependent on two key factors: the cost of conductive ink and the volume of ink printed onto substrate. Of the three printing techniques, screen printing, flexography and inkjet, screen deposits the highest film thickness and this decreases respectively for the printing techniques in the order listed (28). For an inkjet printed UHF RFID tag in literature (29), simulation indicated that a high conductivity can still be achieved with a slightly reduced ink volume deposition, however, too small a cross section leads to low antenna efficiency (28). An optimal ink deposition can be reached for cost effective and sufficient performance (29). Printed antennas have slightly lower antenna power gain than copper etched antenna. This could be due to the differences in the internal structure caused by the printing process itself and paste reflowing after deposition on substrate (30).

Resistance is valuable in analysing the performance of a printed RFID antenna tag. Resistivities, which contribute to resistance, are presented in literature (31). Achieved minimum resistivities for RFID include $8.6 \pm 0.8 \mu\Omega\text{cm}$ for inkjet printing of four layers of silver ink onto polyetherimide substrate, and $44 \pm 7 \mu\Omega\text{cm}$ and $39 \pm 4 \mu\Omega\text{cm}$ for screen printing onto polyimide substrate. Despite the lower resistivity achieved by inkjet printing, higher RF losses were found on a coplanar waveguide transmission line. It was the thicker print thickness produced by screen printing that contributed to lower RF losses (31).

Low resistance of printed lines in the RFID tags is of the utmost importance in printed electronics for RFID manufacture. Good print resolution and high film thickness and consistency are key qualities of a print to achieve the desired performance.

Flexography, screen and gravure are scalable technologies and capable of integrating with high speed roll-to-roll, printing films of flexible packaging (1).

Inkjet is also used for the manufacture of discrete antennas. It has a lower throughput than flexography and screen, as well as being restricted rheologically. Gravure is another printing method that has been considered for printing of antenna (32). Screen, gravure and flexographic printing will be discussed further due to their applicability to mass manufacture. The manufacture of chip-based RFID is more complex, with the processes for securing and encoding chips. Manufacture of antennas via printing with a view to improving performance and chipless RFID is the focus of this research.

For printed RFID antenna, the introduction of printing techniques has enabled manufacturing to be conducted at room temperature and ambient conditions for flexible applications. Printing technologies bring the following advantages: high speed and low-cost manufacturing techniques. They are additive technologies and can result in low waste products (1).

The printing technologies currently used to print electronics are compared to each other and the capabilities of each print process are outlined (Table 1-2). This investigation requires a high-speed mass manufacturing printing technique; hence screen printing, gravure and flexography are the most applicable to this requirement. The three techniques are evaluated for the ability to produce a low silver content antenna with good control of ink volume deposition.

Rotary screen, flexographic and gravure are three of the primary printing techniques used in mass manufacture of packaging. To integrate RFID tags with current packaging manufacturing processes, it must be able to be produced on mass printing processes. The objective of this thesis is the development of volume printable antennas to enable this technology.

Flexography and gravure are roll-to-roll processes; scalable to high production rates; use cell engraved rollers to carry ink; and requires relatively low viscosity inks. They primarily differ in the way the image is carried. Flexography makes use of a polymer plate to transfer the image from the engraved cells to the substrate (33). Full scale flexography machines can have 12 inline printing stations and works with a wider range of inks than gravure (34). Due to the initial required ink volume and low-cost polymer plate, initial set-up costs are cheaper for flexography

than gravure and therefore more applicable for smaller runs, especially for laboratory development testing.

Flexography is an appealing technology for printed electronics due to its high-resolution printing and low print thickness, yet it can achieve high print speeds. The understanding of ink transfer from engraved surfaces could be directly relevant to the gravure process (33)(35). Reliability and consistency between a series of prints is critical in printed electronics. The use of the flexible printing plate enables good print quality even on rough substrate surfaces (36) however, flexography is a low film thickness process, which can lead to a high rate of defects in the print, and hence lower conductivity of printed features. Research in increasing print uniformity is required in printed electronics for RFID antennas. A narrow ink viscosity range increases the research requirement to formulate an appropriate ink.

Table 1-2 – Comparison of Printing Techniques.

	Lithography	Flexography	Gravure	Screen	Inkjet
Printing Form	Flat (Al Plate)	Relief (Polymer Plate)	Engraved Cylinder	Stencil Mesh	Digital
Substrate	Papers, boards, polymers	Papers, boards, polymers	Papers, boards, polymers	All	All
Pigment Particle Size (µm)	0.2 – 0.7 (1)(35)	0.001 – 0.5 (37) (1)	0.1 – 0.5 (1)(35)	0.2 – 2.5 (38) (1)	0.05 – 0.2 (39)
Lateral Resolution (µm)	15 (1)	40 (1)	15 (1)	100 (1)	50 (1)
Print Thickness (µm)	0.6-2 (35)(40)	0.005-8 (37)(41)	0.02-12 (42)	3-50 (35)(43)	0.01-20 (35)(39)
Print Speed (m/min)	0.6-900 (44)	5-800 (45)	8-1000 (46)(47)(48)	0.6-100 (49)	1-500 (39)
Req. Solution Viscosity (Pa.s)	0.5 – 2 (50)	0.05 – 0.5 (51)	0.05 – 0.2 (51)	0.5 – 5 (39)	0.01 – 0.03 (39)
R2R Compatibility	Yes	Yes	Yes	Yes	Intermediate
References	(1)(35)	(1)(35)	(1)(35)	(1)(35)	(1)(35)

Despite the promise shown in flat bed laboratory bench systems, gravure relies on the flow of the ink to ensure a continuous line by joining the engraved dots. This leads to internal line defects due to missing dots and edge rippling (52). While sheet fed screen printing has recently been shown to be capable of achieving minimum line widths less than 30µm, rotary screen tends to

lack resolution necessary for antennas, though it would be appropriate for coating with functional materials. As the aim is to integrate chipless RFID with flexible packaging, this research is focused on flexographic printing which is widely used for mass production of food packaging. Therefore, this thesis focuses on the development of flexographically printed antenna for RFID applications that can be integrated into conventional packaging.

Flexography is widely used as a graphics printing process, however, as a method of RFID manufacture, it presents several technical challenges:

- High conductive particle deposition through thick film deposition via flexography, which is typically a low film production process, yet lower silver loading than screen printing (typical 75%-90% loading) is required for good ink transfer via a low viscosity throughout the printer.
- Adequate viscosity to enable:
 - o Low viscosity under shear in printer for sufficient ink transfer to substrate, and ink to printing apparatus.
 - o Increased viscosity when deposited on substrate to prevent high spreading but sufficient spreading of ink to connect dots created by anilox.
- Good resulting contact between conductive particles once print has been dried to ensure a highly conductive track.
- Minimisation of print defects i.e., pin holing and viscous fingering to create a uniform print.

To address these technical challenges, good understanding of the ink, knowledge of changing variables in the printing process, and antenna design are required to increase conductivity through higher silver deposition.

To enable good signal output, sufficient print thickness is required for low resistance and to mitigate skin effects. Skin effect is dependent on cross-sectional area, frequency, permeability and conductivity of the conductor (53)(54). As frequency increases, the skin depth lessens. Increasing the silver content within the ink increases the thickness and conductivity of the line to a point. Limits exist in quantity of silver particles that can be added to a paste as it must still be processible i.e., requires suitable viscosity for the process. As volume fraction of the silver particles increases, the relative viscosity increases (30)(54).

Challenges remain in reducing the quantity of silver used in the printing ink whilst achieving a high-quality print with uniform thickness and surface roughness, which are essential in producing a good print for this application. This highlights the need to have a coherent understanding of the effect of variables in the manufacturing process. With a good understanding of these variables, the print can be optimised for its application and is one of the aims of this thesis.

1.3.1 Basic Principles of Flexographic Printing

Flexographic printing is the one of the fastest printing processes for mass scale production. Flexography is typically used for high-volume production, although smaller capacity printers are frequently used during development. Flexographic printers typically print in the speed range 5-800m/min (35)(55) with narrow webs (<508mm) for high accuracy printing and wide webs (>1016mm) for higher volume productions. Mid-sized webs are used for scaling-up productions (56). It can print up to 12 different inks and onto a wide variety of substrates including flexible and rigid types (57). Industrial scale flexography machines are widely made-to-order and are designed for a specific application. Despite much of the process being automated, setting up an industrial flexographic printer adds time to the production process. Much of the research and development work can be carried out on desktop flexographic proofing printers saving time and resources. There is limited research on flexography as a printing process for RFID, which offers an interesting research opportunity in the printing industry (58)(13)(59).

This typical in line relief printing process is shown in Figure 1-5 (60). The ink is held in an enclosed ink chamber and is picked up by the anilox roller that closes the bath. Doctor blades on the edges of the ink chamber (not shown) are positioned against the anilox and remove excess ink off the anilox surface, and the impression of a plate cylinder extracts the ink onto the raised surfaces, exhibiting extensional forces on the ink. A reel of substrate will run through the flexographic machine on the impression cylinder, which presses the substrate against the plate cylinder.

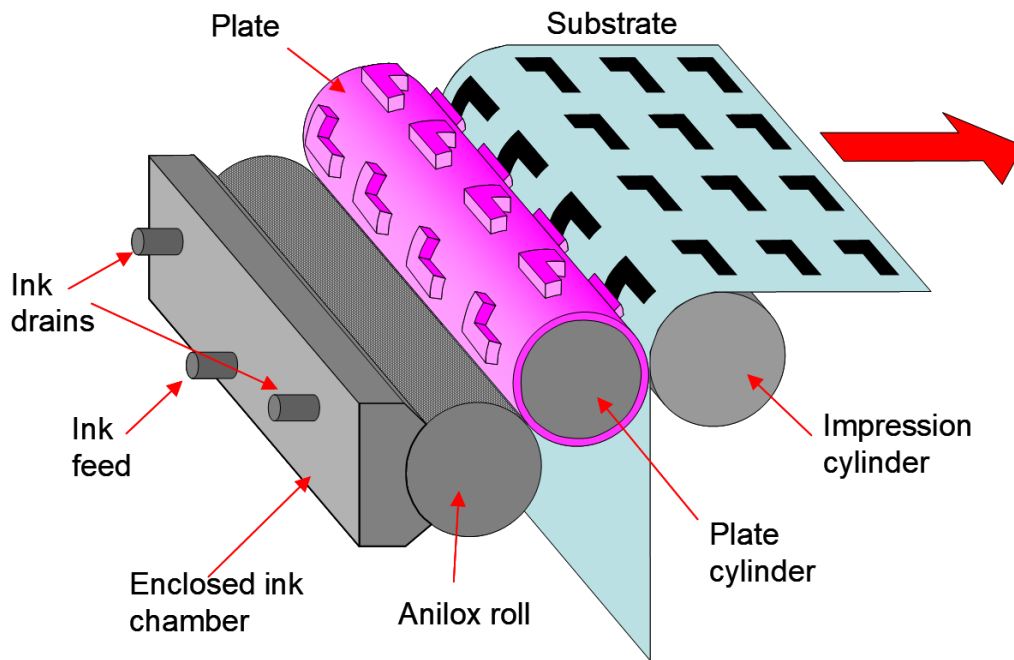


Figure 1-5 – Key components of the flexographic printing process. Image from paper 'Large-scale Roll-to-Roll Fabrication of Organic Solar Cells for Energy Production' (60).

The ink bath tends to be closed chambers as they guarantee a high stability of all inks, reducing the quantity of solvent loss in solvent-based inks. Open chambers are more commonly seen on older printers (61). Additionally, automatic viscosity control units can be used to add solvent throughout, ensuring that a constant viscosity is maintained.

A more extensive list of flexographic printing variables is shown in Figure 1-6, which highlights the complexity of the flexographic printing process. These variables must be optimised to create a printed track with low resistance for an optimised RFID antenna performance.

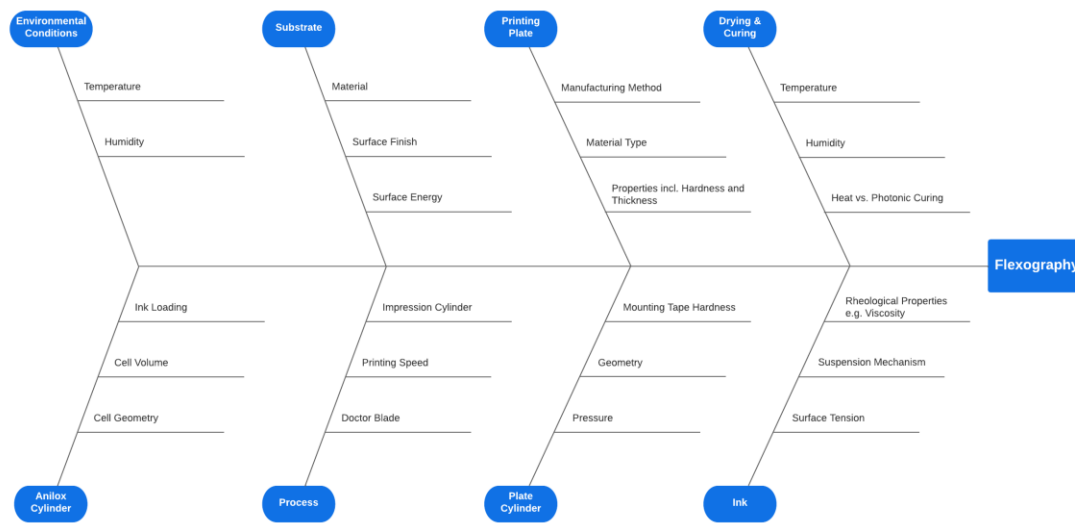


Figure 1-6 – Flexographic Printing considerations for printed electronics (57)(62).

1.3.1.1 Anilox Roller Manufacture, Geometry and Effect on Printing

Anilox rollers are typically made from either ceramic or metal with many laser-engraved cells. Upon filling with ink, the anilox cells are levelled off by the doctor blade. The engagement between the plate cylinder and the anilox roller is manually adjusted, as is the engagement between the plate cylinder and the impression cylinder.

Anilox rollers are laser engraved and coated with a ceramic coating for durability. Laser engraved cells have been found to give a high ink release compared to the roughened surface of the internal cell surface of mechanically engraved cells (63). Three key considerations for anilox choice are the shape and angle of the cells; the cell volume denoted in billions of cubic microns (BCM); and the number of cells per linear inch (lpi). Anilox engravers using laser engraving, define the cell geometry in terms of the ratio of cell depth to cell opening, typically ranging from 0.28:1 to 0.40:1. Figure 1-7 shows some industrially available anilox cell geometries. The top row demonstrates a cross section of three equal cell volumes, varying only in cell shape. Shallow cells are used for more viscous inks as ink release and cleaning are easier than for the thin narrow geometries, whereas deep cells are harder to clean, have rougher cell walls and do not release ink as efficiently. The bottom row has various designs of cell geometries, however, the hexagonal, long cell and GTT designs are used in flexography. Hexagonal geometries with angles between 30° and 60° are the most conventional anilox roll type. Literature (64) has shown cells of comparable volumes, yet different line rulings, transferring varying amounts of ink hence showing the impact of line ruling on ink transfer.

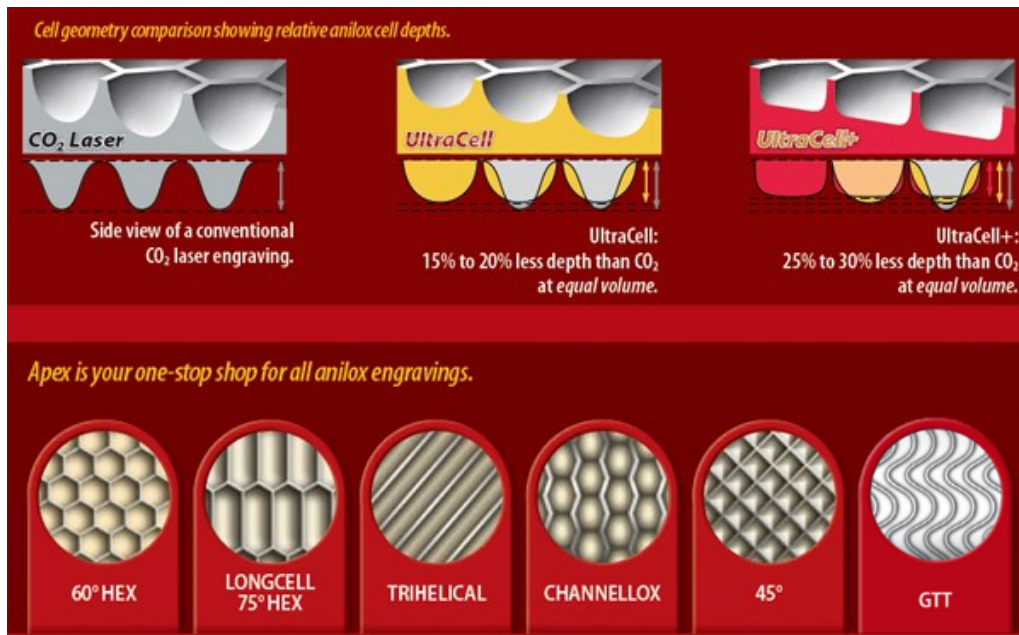


Figure 1-7 – An extract from APEX International demonstrating the various cell structures available. The top row shows a cross section of three cell volumes of the same quantity, varying only in shape and the bottom row shows anilox cell geometries from surface (65).

Higher cell volumes produce a thicker coating, and lower cell volumes deposit thin films, which produce higher print quality. The cell volume directly corresponds to the quantity of ink transferred to the plate (64). Printed electronics for antenna manufacture typically require low resistance conductive tracks, for which a higher volume of ink is required. The volume held by the anilox is determined by the volume and frequency of the engraved cells (33). HARPER, an anilox manufacturer, considers high line screens for a flexographic anilox to be 600-1200 but these values can reach 2000. Higher line screen means more cells on the anilox, thinner cell walls and therefore are more easily damaged, exhibited as an effect called score lines (66).

1.4 Rheology of Printing Inks for RFID Manufacture

Ink development is critical in the production of a low resistance ink for RFID manufacture. In flexography, the ink is typically a shear thinning fluid, able to decrease in viscosity to easily transfer between rollers throughout the printer, and then increase in viscosity to create a solid conductive track on the substrate. The ink must have good adhesion to the substrate; not chemically or physically breaking down the substrate and printing components; and deposit a sufficient volume of silver that has good connectivity between particles once the transfer medium i.e., solvent has evaporated or cures.

Rheology is used in the analysis of inks so that predictions of ink behaviours can be made prior to printing. Rheology is the study of flow in solids and liquids, and defines, through deformation, the relationships between force, time and deformation. Ink viscosity changes with variations in

shear rates that are applied at several points in the printer. It is important to know that the ink will increase in fluidity for better ink transfer during printing and remain solid when deposited on the substrate. Conductive ink formulation has had a lot of focus on material properties of the ink (viscosity, particle size and distribution, resin and additives), however gaps remain when considering the link between rheological properties and printability (67). Inks can be designed for purpose i.e., changing conductive component, using a flexible resin, altering viscosity. Adding particles and additions such as polymers to a fluid introduces new particle interaction forces that must be considered. This must be understood well enough to adjust a fluid to work on specific printing presses.

1.5 Closure

Flexographic printing offers the potential for high-speed manufacture of RFID with integration to existing packaging printing at commensurate speeds. The main challenges that flexography presents are related to sufficient transfer of ink, high conductive particle deposition to increase conductivity of printed track with good resulting contact between conductive particles once print has been dried. Resistance will be the measure of a highly conductive track, and minimisation of print defects. These technical challenges are addressed through experimentation of the effects of print variables, ink rheology, and electrical antenna performance measurements. This will be covered throughout this thesis in the following manner:

Thesis Layout

- Chapter 2 – A literature review on topics related to RFID antenna, mass-manufacture printing technologies, effects of variable print parameters on ink transfer and characterisation of printing inks.
- Chapter 3 – A methodology chapter in which experimental apparatus and techniques are outlined including; Flexographic printing process, surface and electrical characterisation methods; ink formulation and rheological analysis.
- Chapter 4 – This chapter describes an investigation into testing methods of a RFID antenna design to gain benchmarking data for antenna electrical characterisation using a commercial silver ink.
- Chapter 5 – This chapter describes an investigation into the effect of anilox volume, print speed, drying and substrate on printed conductive tracks using commercially available silver inks.

- Chapter 6 – Samples produced via studies reported in Chapter 5 are further analysed to determine the effect of key printer settings on the frequency profile and signal magnitude within the antenna response.
- Chapter 7 – This chapter outlines the development of a silver ink for flexography, with commercial ink benchmarking to gain a better understanding of the relationship between formulation, viscosity and printing. Suspension models for silver particles suspended in a resin are applied to the inks to assess applicability.
- Chapter 8 – This chapter builds upon the work reported in Chapters 4, 5 and 7. An optimal ink was selected for printing of an RFID antenna (Chapter 7) under optimised print conditions (Chapter 5) for antenna design outlined in Chapter 4. Some antenna performance testing was completed.
- Chapter 9 – Discussions.
- Chapter 10 – Conclusions and recommendations for further work.

Chapter 2: Chapter 2 Literature Review

2.1 Introduction

Flexography has been identified as the strongest candidate for high volume R2R printing of antennas directly onto packaging. However, the performance of the antennas is strongly linked to effective uniform ink transfer to create a printed line of desired properties. This review will focus on the impact of various process parameters on the profile of flexographic printed lines. This will include print defects commonly known as “viscous fingering” and “haloing”, which are typical in printed electronics. Viscosity impacts both these behaviours. Functional inks have significant viscoelastic properties which interact with the open channel anilox cell geometries (63). Rheological analysis of the printing inks is critical in the control of ink behaviour throughout the printing process. The percentage of conductive material in these inks greatly contributes to the resistivity and in turn the antenna performance. Hence, the impact of silver weight percentage and viscosity grade of the polymer are discussed. Suspension rheology models are outlined which will later be fitted to experimentally derived rheological data.

2.2 Printed RFID Technology

2.2.1 Factors Affecting Antenna Performance

Performance of antennas is affected by a number of parameters (17):

- Antenna size of both the tag and the reader. Larger antennas increase read range.
- Geometry of line: A meandering dipole has a higher gain than a straight dipole (30).
- Antenna orientation with respect to reader.
- Environmental noise. Noisy environments can reduce read range.
- Antenna Quality factor, which is a ratio between energy received by the antenna and the energy reflected, which indicates system energy loss (typically 30-40 is required). Resistivity of the line greatly contributes to the Quality Factor.

Resistance is dependent on the volume of the printed track i.e., width, length and print thickness. Increasing thickness of the conductive lines increased performance of RFID tags manufactured via inkjet printing (68). Due to a reduction in ohmic losses throughout the conductive elements, the increased performance eventually plateaus with increasing film thickness. The realised gain of the antenna tag was increased through improving radiating efficiency (68). Improvement of antenna performance with film thickness has also been shown to occur using screen printing (69). Screen and flexographic printed track widths over 0.8mm have an RFID read distance of just over half of that achieved with an etched copper antenna. Inkjet printed antenna produced comparable results in terms of read distance to the copper antenna (28). Despite the excellent resolution and

conductivity provided by the inkjet process, thin films of $<1\ \mu\text{m}$ can lead to low antenna efficiency in terms of strength of signal reflected, yet provides a greater reading distance (28).

Increased film thickness increases the peak amplitude in an electromagnetic (EM) signature response of an antenna, and the signal response is very dependent on the choice of substrate (70).

Additionally, substrate roughness influences print quality, ink film thickness and sheet resistivity of conductive tracks. This gives a standardised measurement of ink properties rather than geometry of the line. For paper and cardboard substrates, higher roughness and low surface energy produce low sheet resistivity due to absorption into substrate (41). A study on print parameters is needed to understand the process sufficiently before addressing other issues (41).

Aside from the basic geometry of the lines, there are several factors that affect the inherent resistance. One challenge in printed electronics is uniformity in the print to enable best conductive performance. Imperfections at the surface of the print and within the printed track can hinder conductive performance for example: viscous fingering, print defects such as pinholing and debris on substrate, wetting, and slumping.

Ink structures also play a role in the resistance and resistivity of the track. Figure 2-1 shows SEM images of silver track cross sections, with Figure 2-1 (a) showing a porous print and uneven surface for a silver paste with microparticles, flakes and polymeric binder. Figure 2-1 (b) is a nano-silver paste with no microparticles or flakes and shows good uniformity of print and no imperfections within print layer.

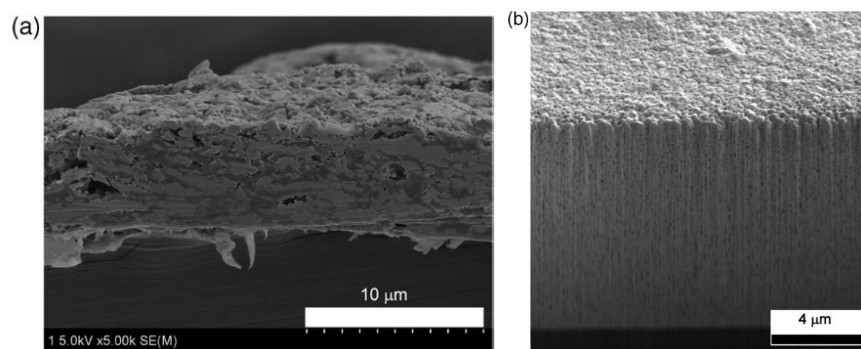


Figure 2-1 – ‘Comparison of sintered microstructures of different types of silver pastes: (a) a conventional silver paste with microparticles, flakes and polymeric binder matrix left after sintering, and (b) the developed silver nano paste, ‘nano Coln E001’ (30).

This screen printed nano-silver paste for RFID demonstrates a low sintering temperature and short time of exposure to heat (120°C for 1min) (30). These are better performance silver inks with microparticles and flake inclusions. Resistivity was $3\ \mu\Omega\text{cm}$ and antenna had comparable radiation performance to copper etched ones, which are regarded as the ‘optimal’. The silver

paste with nanoparticles showed a much more uniform surface roughness and particle alignment, with no large defects in the print (30).

It is most desirable to have a sintering temperature that matches the glass transition temperature of the substrate (80°C for PET). This is not achievable for silver inks and some dimensional changes of PET occur (30), however, PET remains a suitable substrate for printed electronics up to 150°C (71).

Flexography will be discussed in more detail as the chosen print process for its good resolution, good ink deposition for increased conductivity of printed line, and high print speed.

2.2.2 Process Parameters and Their Effects on Ink Transfer in Flexographic Printing

Each of the parameters that can be adjusted in the flexographic printing plays an important role in the quantity of ink deposited on the substrate and the quality of the printed tracks in printed electronics.

The following are key to achieving reliable prints in electronics:

- feature size limits
- accurate control of quantity of ink
- consistent ink film thickness

Process parameters including engagement, printing plate, mounting tape, anilox roller geometries, and substrate can be used to control these. These are discussed further.

In one study, conductive tracks of mean width and thickness 190µm and 1.5µm respectively were achieved through three to five passes on a flexographic printer and 10-minute sinter cycle. This would not be appropriate for high speed R2R as a long sintering tunnel would be needed. Thermal distortion would be an issue if samples heating occurs between prints and this would be an issue for registration. The lowest resistivity achieved in this paper was $2.8 \times 10^{-8} \Omega\text{m}$ for a 190 µm line of ink containing 30% silver and has a 36mPa s viscosity at 1 s^{-1} shear rate. This is close to bulk silver resistivity [$1.59 \times 10^{-8} \Omega\text{m}$ (72)]. The sintering conditions required to achieve this was 850°C for 15 minutes, requiring high temperature resistant ceramic substrate (73).

2.2.2.1 Engagement Distance Between Rollers

Engagement defines the distance between the rollers. There are two sets of engagement settings on a flexography machine: the distance between the anilox roller and the plate cylinder; and the distance between the plate cylinder and the impression cylinder which carries the substrate.

These must be set correctly to transfer the right amount of ink to achieve a high-quality print. Negative engagements can lead to lack of ink transfer between rollers. Positive engagement, that is too high, can lead to inaccurate ink transfer with defects such as halo effects through plate deformation. Figure 2-2 shows initial contact, negative and positive engagements. Increased engagement pressure between the anilox and ink chamber can deliver higher ink density in the print (62). A kiss contact method is typically used to find the optimal engagements between rollers, whereby the rollers are incrementally engaged between test prints to find the point at which the desired image is achieved.

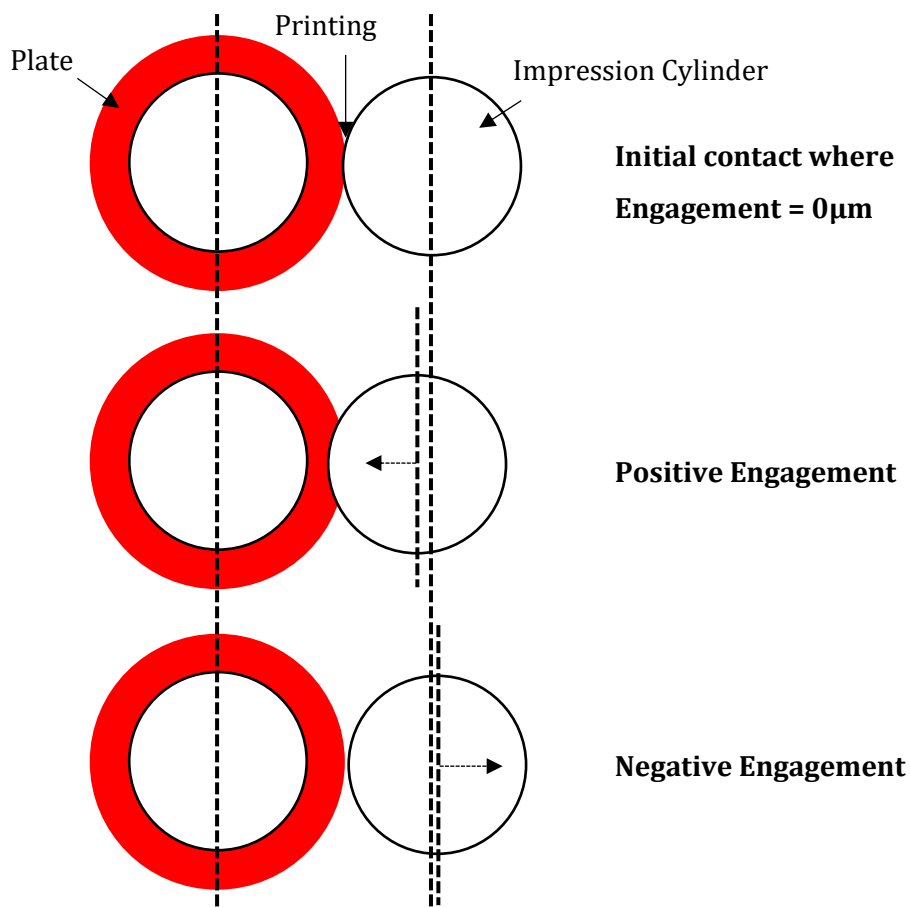


Figure 2-2 – Roller engagement schematic for printing nips.

DeGrace and Mangin observed that for higher engagements, ink film spread further over the substrate surface, creating a more uniform layer (74)(75)(76).

The right engagement is critical in ensuring that the printing plate is not compressed, yet there is enough contact between rollers to efficiently transfer ink (77).

2.2.2.2 Printing Plates

The printing plate is a core component of the flexographic printing process as it carries a thin layer of ink from the anilox to the substrate. The conditions in which the plates are made have a significant impact on the image carried in the process however, this is not covered in the scope of this work. Interactions between the plate and the various printer variables are discussed. Ink transfer variations are thought to be compensated for 'through manipulation of the ink properties and press controls' (74).

The printing plate is also affected by the nip pressures, which distort it temporarily, but can distort permanently and damage the plate. Harder plates resist this deformation but can result in ink being squeezed out of the edges more than softer plates. Low ink gain is achieved through the selection of a plate with a relatively low shoulder angle and an anilox with fine cells (74)(78).

Dot gain can give an impression of line behaviour. The depth of the plate and steepness of the shoulders impact the dot gain however, conflicting evidence is presented in literature (79)(80)(81) as to whether this increases the contact area of the dot and hence dot gain. Ink spreading is the primary contributor to dot gain, whereas the plate deformation is attributed to only a small part of this. For indentation hardness testing, Young's modulus and Poisson's ratio are typical measurables used to determine the plate's structural response, and have been correlated to dot gain (79)(80)(81).

Energy of a surface varies along a hydrophobic to hydrophilic scale, where contact angles above 90° indicate hydrophobic substrate, and below 90° , hydrophilic (82). Regarding the material properties, the impact of plate surface roughness is often overlooked. Additionally, molecule orientation and chemical heterogeneity highly influence the contact angle when it is used as a measure of surface energy (83). Surface roughness can be divided into macro & micro roughness. The former is surface striae, caused by the laser in digital plate imaging production, and has the effect of decreasing surface wetting and ink transfer. Conversely micro-roughness has the opposite effect of increasing surface wetting and ink transfer through increased surface area (78)(79). This increased micro-roughness works for enhancing wettability on hydrophilic surfaces, however, the opposite occurs for hydrophobic surfaces (78)(82).

2.2.2.3 Mounting Tape

Mounting tape is double sided adhesive tape for attaching the flexographic plate to the plate cylinder. The tapes typically range in hardness and thickness. Compressible (softer) tapes act as shock absorbers and reduce over-impression effects on the flexographic plate, whereas harder tapes do not. Harder tapes produce higher uniform ink transfer in solid areas and compressible

tapes are more applicable for small features in the print (57). Ideally a combination of these would be used for a print with both solid areas and small features.

2.2.2.4 Anilox Rolls

Previous studies on water-based ink demonstrated that changes in the depth-to-opening ratio between 0.28:1 and 0.31:1 resulted in no change in the solid density (74). S. Hamblyn found that the anilox volume was the primary contributor to the volume of ink deposited in the roll-to-roll process. For prints produced with a lower anilox volume, there is a decreased reduction in density in comparison to higher anilox volumes. Press speed was found to have no significant effect on transfer of ink from anilox roller to the printing plate, between 80 m/min to 200 m/min (84). Another study using anilox volumes $17.92 \text{ cm}^3/\text{m}^2$ to $36.50 \text{ cm}^3/\text{m}^2$ to print conductive silver tracks of $30 \text{ }\mu\text{m}$, $40 \text{ }\mu\text{m}$ and $50 \text{ }\mu\text{m}$ found an increase in anilox volume to increase line width and significantly increase cross-sectional area. High anilox volumes combined with the smallest track width showed lower consistency and rougher surfaces, however this study highlights the opportunity for the use of high volume aniloxes for printed electronics to increase the volume of ink deposited and in turn reduce the sheet resistance (33).

2.2.2.5 Effect of Substrate on Print Characteristics

Flexographic printing is widely used as a process for printing onto corrugated board, flexible packaging and newspapers (62). Thin flexible substrates were used to contribute to research of printed electronics on flexible packaging. Table 2-1 shows common materials used as substrate for printed electronics and functional surfaces.

Common materials used in packaging (Table 2-1) include paper/paperboard, high density polyethylene (HDPE), polyethylene terephthalate (PET), low density polyethylene (LDP), linear low-density polyethylene (LLDPE), aluminium and glass (85). These are used as primary and secondary packaging to contain, protect and transport food. Aside from glass, many of these materials are lightweight, food safe and can be flexible. Metals are also listed but for RFIDs this can hinder performance and specially designed RFID are required.

Various polymers are used in packaging for their commercial viability, ability to be sealed and in many cases, the fact that they are transparent; allowing the consumer to view the product inside the packaging. Polymers are well-researched, malleable and easily manufactured for a smooth finish. Printing electronics on plastic substrates can be carried out at ambient conditions and can be implemented inline (1). Adhesion to the surface of the substrate, surface roughness and stability of the substrate are to be considered.

Despite their complexities in printed electronics, paper, cardboard and polymer coated paper/cardboard are commonly used as substrates for packaging. Paper and cardboard without coating face challenges with high absorption of ink, which in turn affects the print quality and electrical properties. Cellulose is of growing interest as it is a biodegradable material, made from wood, cotton and vegetable biomass. There is much research on the applicability of these materials in printed electronics (86)(87)(88).

In conclusion, polymers make good substrates for printing onto. Paper substrates can lead to challenges in achieving performance due to ink absorption and metal substrates are challenging to get good performance for RFIDs.

Table 2-1 – List of typically used substrates in printing. Edited from presentation by department of Graphic Arts and Photophysics, Tampere University of Technology at the ActInPak Summer School (2017) (85).

Flexible	Rigid
Paper – uncoated and coated paper, primer	Paper /Paperboard/Fibreboard
Synthetic papers – Pretex (PES/PA), Synaps (PES), Tyvek (HDPE), Teslin (polyolefin)	Cardboard
Glass – 25 to 100µm	Glass – float, quartz
Nanocellulose	Ceramics
Metals	Metals
Polymers – PET, PEN, PI (Kapton, Neopulim) PC, PVC	Thick polymer substrate
Polyolefins – PE, PP	

2.2.3 Process Settings and Their Effects on Ink Transfer in Flexographic Printing

Print speed is a process setting that can be changed for the defined process parameters and it further outlined below.

2.2.3.1 Effects of Print Speed with Respect to Varying Anilox Volume

Effects of print speed on anilox inking in the ink tray, doctor blade wiping, ink transfer between the rollers, still require research.

As the ink is transferred through a flexographic printer, it experiences cycles of rapid high shear rates to short periods of time in which the ink can begin to relax. Kunz (89) discusses fluid relaxation in the cell after the doctor blade levels the surface after the anilox rotates through the ink tray. This process drags the meniscus of ink toward the trailing edge of the cell, after which

the ink relaxes back into the cell. The rheological properties of the ink would determine the relaxation time. This is a likely scenario for a low-speed print, however, at higher speeds, and depending on the rheology of the ink, the ink may not have sufficient time to return to its original position and therefore impact the flow from the cell. The viscous nature of the ink plays a large role in the cell ink release (90). For smooth substrate surfaces, print speed is not found to affect the frequency of viscous fingers (described in Flexographic Printing Defects) for gravure printing (91). Finger instability and cell emptying flows are mutually coupled by localised pressure gradients at a 10µm scale (91).

Several studies have investigated the impact of variations in depth-to-opening ratios (74)(92). Solid density increases with increasing depth-to-opening ratios. This is a non-linear relationship and peaks at 0.35:1. Additionally, anilox cell release characteristics are highly dependent on particle loading, particle size, and binder systems, due to the effect that these have on flow properties (1). Wider opening anilox cells release ink better than narrow cell openings, due to a larger area however, depth plays a stronger role in the amount of ink released. Shallower cells, with a lower depth-to-width ratio, release ink more readily (63).

As printer speed increases, ink release decreases. Reduced engagement time between the anilox roller and the plate roller reduces transfer time of ink. An increase in the x- and y-direction of print because of the shear thinning behaviours required by flexographic inks facilitate high speed ink transfer and higher ink thicknesses (93). Lindholm and Ström showed that an increase in speed did not affect the quantity of ink at a depth-to-opening ratio of 0.3:1. For both anilox volumes 8cm³/m² and 12cm³/m², the quantity of ink transferred to the plate was not affected by an increase in speed (84).

When press speeds are increased, prints exhibit a reduction in solid colour densities. This is thought to be due to ink splitting taking place closer to the substrate (84). Low print speeds resulted in poor ink film quality, indicating there is an optimal print speed to provide good deposition of ink (74)(75)(76).

Higher ambient print temperatures increase ink transfer from anilox cells. The substrate more readily accepts ink at higher temperatures where it was shown to have a lower viscosity (94).

Work has been done on the effects of anilox volume and print speed on the print outcome however, there is little work integrating the combined effects of anilox volume and print speed on the reduction of ink deposition for printed track without reducing the conductive performance. Shallow anilox cells and wide openings deliver the highest volume of ink which is desirable for printed RFID. Ink transfer is critical in high ink deposition on the substrate. The

anilox geometries and print speed heavily affect the outcome. Information available is conflicting around the effects of process parameters and there is not enough research around this for silver ink. There is little work on the effect of process parameters on the outcomes of a print and highlights the need for research in this area. Hence, running print speed and anilox volume tests for the intended process will need to be carried out to determine the optimal settings.

2.2.4 Formulation of Conductive Flexographic Printing Inks

Flexographic printing inks are formulated to align with the printing process and adhere to the substrate (95). Electrically conductive inks have an added function of carrying and evenly distributing conductive particles to enable the movement of electrons through the printed ink (1).

Electrical properties of the ink are primarily defined by the conductive particles within it and the way they are bonded together via a curing process. For electronic networks, inks must have a conductive component, for example: silver, carbon black, copper (96). These are typically in the form of metallic powders from which they are suspended in either water or solvent as the transport medium.

Increasingly, printed electronics are being developed for flexible applications including flexible food packaging and touch screens. In flexible applications, the ink must be as flexible as the substrate (1).

For printed electronics, the quantity of conductive ink deposited is directly related to the resistance of the conductive track printed. If, for example, an application had a tight resistance tolerance, the printing process must produce repeatable results and deposit highly accurate and reliable quantities of ink. In cases where silver ink is used, it is likely that a second coating will be required as a protective layer to prevent reactions with air, altering the conductivity of the track.

2.2.4.1 Silver

Silver is largely used in the printed electronics industry and is a promising metal for RFID applications (97). Silver-based inks are primarily chosen for their high electrical conductivity, however they also possess other important properties including thermal conductivity and chemical stability in comparison to alternatives. Silver has a more stable nature than copper (98)(99). Hence, it is easier to process than copper, which is a highly conductive material commonly used in electronics. This highlights the need to understand the ink formulation further to reduce the filler loading without compromising the conductivity of the printed tracks (1). Silver as a raw material is the more expensive option when compared to its commonly used

alternatives: copper and carbon (28). It is for these reasons outlined that only silver will be used in the work.

Silver particles also have a low sintering point, which aids in formation of conductive thin films under low temperatures. This is useful for printing onto flexible substrates (99)(100)(101). A study on a silver ink and a graphite ink shows that silver produced the best printability property: uniformity of printed layers (96).

Dispersion of silver-fillers is critical in the development of a functional conductive ink. If not sufficiently dispersed, the formation of silver agglomerations take place, reducing the homogeneity of the fluid and affecting the life and performance of the ink (102). Diffusion is significantly influenced by the strength of the electrostatic and van der Waals forces, which is 'controlled by the variation of the ionic strength of the solution' (103). For nanoparticles, these forces have a higher impact on agglomeration than particle size.

Dispersants can be added to formulations to prevent agglomeration of particles, aiding metal colloid stabilisation and increased silver filler. Surfactants and polymers interact with the surface of particles to alter composition. These particle surfaces can then be designed to attract or repel one another (104).

Resin within the ink is a critical component in its adhesion to the substrate and flexibility. The resin is beneficial in the transfer, setting, drying mechanism and rub resistance of the printed tracks. Often a blend of resin components are used to provide a range of properties (95). Particles dispersed within a resin become enclosed within it. The resin then adheres to the surface of the substrate.

Thermoplastic urethanes (TPU) are primarily made of soft segments: polyols, and hard segments: isocyanates and chain extenders. These can be adjusted to alter the overall properties. Covalent bonds present between these cause the formation of block-copolymers. This two phase microstructure of polar hard segments and non-polar soft segments tend toward agglomeration and amorphous formations (105). TPUs possess good mechanical properties including high elasticity, low temperature flexibility and abrasion resistance. It also has good biocompatibility (67)(105)(106). TPU has commonly been used for its flexible nature, which is beneficial in formed packaging and has application in flexible displays, wearable technologies, and sensors. TPU has been used in conjunction with silver particles for strain sensors, wearable sensors and stretchable electronics (107)(108)(109).

There are three primary types of flexographic resins: water-based, organic solvent and UV based inks; each of which is outlined below. They can also assist with surface adhesion and provide key ink properties for transporting the conductive particles through the flexographic printer.

Water-based inks are comprised of water, pigments, surfactants to reduce surface tension, and additives (surfactants, defoamers and waxes) to aid with drying and adhesion to substrates. They typically possess the highest surface tension compared with solvent and UV based inks. Water based inks are becoming more common due to health and safety issues surrounding the evaporation and ease of combustion of solvent-based inks.

Solvent-based inks are primarily comprised of alcohols, acetates, and pigments. They have much lower surface tensions than water-based inks. They are relatively quick drying. They are commonly used on industrial films for their rapid drying and adhesion to non-absorbent substrates.

UV curing inks are also common in flexographic printing and drastically reduce drying time however, these leave behind binders in the cured ink which can inhibit current flow. UV inks commonly include prepolymers, monomers, photo initiators and pigments. These inks only cure under UV light, enabling the ink to be used for longer as it does not dry out. The viscosity of the ink also remains constant throughout the print as there is no solvent or water loss. In contrast, solvent and water-based inks dry over time or in ovens as the solvent evaporates from the ink (110).

Silver particles are typically suspended in either a water or solvent based resin, however, UV resins are also used in some cases. Resins, binders and solvents are used as vehicles to aid the deposition, spreading, adhesion to substrate and drying/curing of the ink, tailoring the ink to the printing process. Depending on the individual boiling points of each ink component, some non-conductive components may remain on the substrate and impede conductivity (111).

Bulk material properties of conducting components have significantly higher conductivity values than printed electronic inks. Printed ink films tend to have between one third to half of the respective bulk conductivities due to lower contact between particles for electrical conduction (100).

2.2.5 Drying, Curing and Sintering of Flexographic Inks

Drying, curing, and sintering of the inks is required to remove the element used as the solvent/water transporting the conductive particles through the flexographic printer. These processes also help to bind the ink to the printed surface and solidify the print.

Drying occurs when solvent or water evaporates from a printed ink, resulting in a solid film. When printing onto substrates, consideration of the drying temperatures of the printing material must be given as the substrate will need to have the thermal budget to withstand heat e.g., hot air, IR.

Curing is a hardening process of the polymer ink matrix. Some further evaporation may take place, but the solid film cannot be redissolved. Treatment processes can perform drying and curing roles at the same time or a secondary process can be used to provide extra curing. Photonic curing is a secondary process utilised within the printing industry to solidify prints after drying. Thus, a high-powered lamp emits flashes of a broad spectrum of light energy, exposing the prints to high energies across short time periods of a few seconds at most. The benefits of this process are that more substrates types are available to the process as low heat tolerate substrates can withstand the short energy impulses over longer exposures to high heat (97).

Sintering refers to a process whereby a powdered metal is subjected to heat and sometimes pressure leaves an essentially solid layer on the substrate. There are many types of sintering: laser induced, flash/photonic and microwave oven sintering (104). The use of softening or partially melting metal powders can strengthen the bond between single particles. Nano-silver particles can be sintered at relatively low temperatures (<150°C) without the need for reducing or protective atmospheric conditions (97). Thermal sintering has been researched as a method of optimising the printed track for the best conductive properties. It has an optimum temperature, which is beneficial to identify in preliminary tests (104).

For printed inks, it is likely that one or more of these post-printing processes (drying, curing, and sintering) will take place to ensure an optimised print.

Metallic inks typically require high sintering temperatures (excluding nano-particle inks), limiting the range of substrates that can be used. Higher sintering temperatures cause solvent evaporation, reducing the conductive print volume. This results in better overlap of particles. Increased contact between particles increases conductivity of the track. For silver particles, literature (14) has shown sintering temperatures (70 °C to 160 °C) to be inversely proportional to resistivity. Low sintering temperature inks have been formulated in more recent years, which makes them more applicable for substrates with lower heat resistance. Particle sizes <20nm significantly reduces required sintering temperatures (112). In addition to this, photonic sintering, near infrared and UV curing can be used to enable the use of substrates with low heat resistance (113).

2.2.6 Design Feature Limits and Effect of Print Outcomes on Conductivity

Printing for electronics requires high levels of control over the process. Key control parameters for an effective print are: feature size tolerances; accurate control of ink deposition quantity; and consistent film thickness on plates. Challenges remain in product design, to make the product as small, efficient, and cheap as possible.

Track geometry in terms of print thickness, print width and surface roughness of a printed sample affect the resistance of a printed line. Low resistance is optimal for RFID printed tracks.

Increased printed ink film thickness is beneficial in terms of conductivity as it increases the cross-sectional area, and increases the electron pathway network, decreasing resistance to flow. Print thickness is linear to Q factor, shown in an experiment using a nano-silver ink via inkjet printing (114). As with print thickness, increased track width gives a large cross-sectional area and increases electron pathways, reducing resistance to flow.

To give an indication of achieved results in literature, a study in 2013 (115), found that increasing the printing speed produced conductive lines with better resolution and uniformity on three substrates, resin coated paper, white polyester film and clear polyester film. At 60m/min and with a 600lpi anilox, widths of 0.1mm with 5% spreading were printed. Thickness was approximately 1 μm . A second layer reduced the sheet resistivity from 4.1 Ω/\square to 0.19 Ω/\square . Due to increased particle-particle interactions creating more paths there was less resistance for electrons in the printed track to flow.

There is limited literature covering the relationship between conductivity and surface roughness. Roughness affects the resistance of printed features and in turn can affect the performance of a sensor.

2.2.7 Flexographic Printing Defects

The following defects (Figure 2-3) will be discussed in greater detail; halo effects (a), viscous fingering (b), dot gain (c), print mottle (d), pin holing (e), filling in/bridging (f), feathering (g), dirty print (h), and chatter (i) (gear marks). Others that more typically affect colour printing include: doughnuts skip out, ghosting and misregistration (116). These are all potential defects that could occur when printing conductive tracks. They can be caused by various factors including print settings, ink formulation, drying/curing settings, or debris on the substrate surface. Defects such as filling in can cause shorting of printed circuits. Viscous fingering and other defects that

distort the surface roughness or create edge effects can impact the resistance of the printed track, which affects antenna performance.

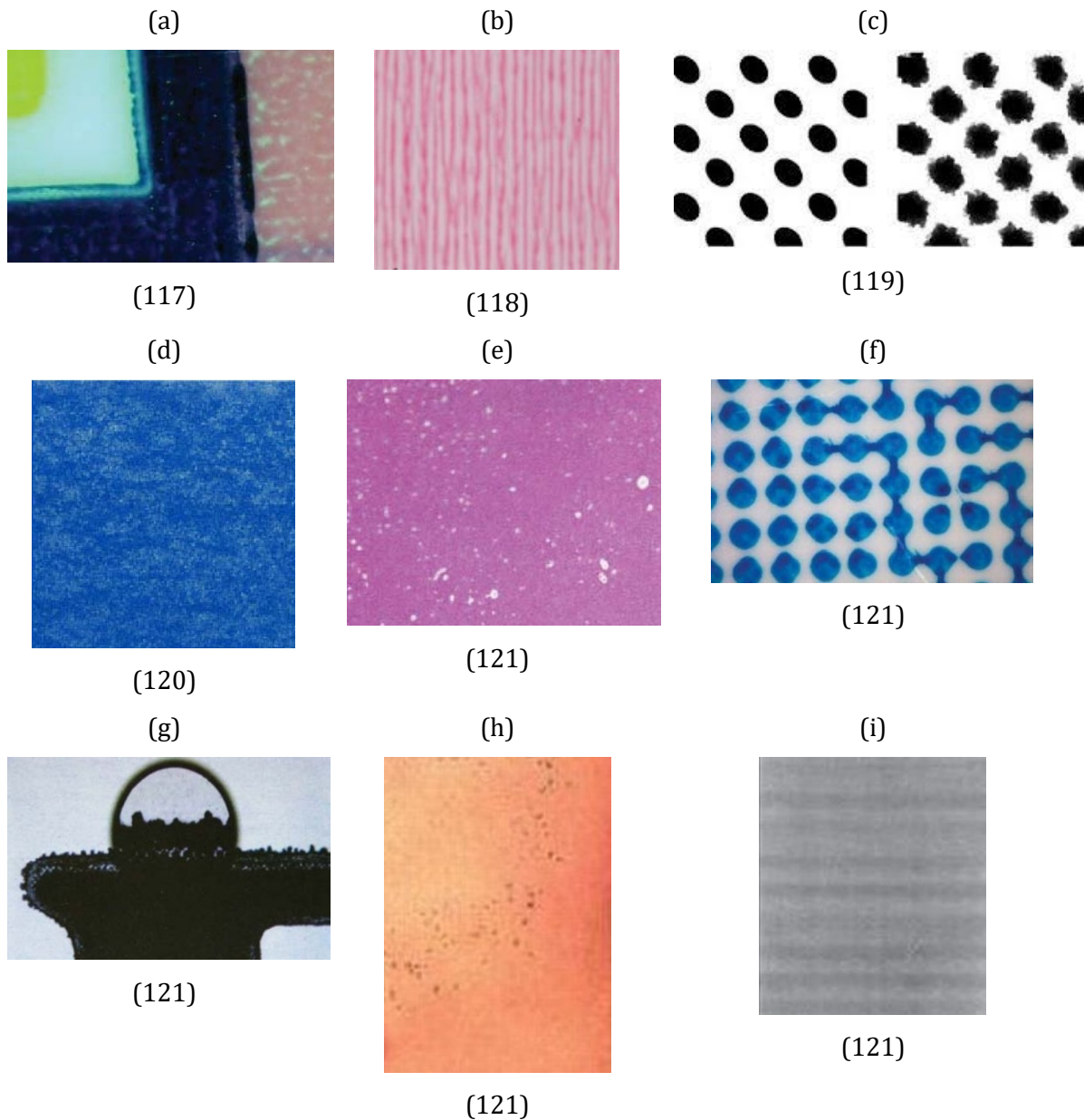


Figure 2-3 – Examples of flexographic print defects. halo effects (a) (117), viscous fingering (b) (118), dot gain (c) (119), print mottle (d) (120), pin holing (e) (121), filling in/bridging (f) (121), feathering (g) (121), dirty print (h) (121), and chatter (i) (gear marks) (121).

Halo effects [Figure 2-3 (a)] (13) and viscous fingering [Figure 2-3 (b)] are common defects. Halo effects occur when the print edges are squeezed and are minimised by reducing the pressure between the plate cylinder and the impression roller. The quantity of ink delivered to the substrate via the anilox and the ink viscosity also contribute to halo effects on the print (122)(118). Viscous fingering is generated in the same region, by the ink splitting between the plate cylinder and the substrate surface. It is characterised by a pattern of small ridges, usually

stemming from one another, printed in the ink surface. As elasticity in inks is increased, effects like viscous fingering become smaller, more frequent and have more breaks in the features (118). One paper shows viscous fingering features to be similar to printed line features and so affect both lines and solid areas (118).

Print mottle is a term used to describe the print uniformity. It is typically a result of uneven ink transfer, incorrect ink viscosity and can also be due to the speed at which the ink dries.

Pin-holing is identified as tiny holes, in the print in solid areas. This could be a result of increased ink viscosity and contamination of the substrate, or ink in the ink tray. The drying speed is also critical in the formation of pin holes. This is affected by the ambient conditions in which printing takes place for example the humidity, and temperature of the room (122).

Bridging and filling-in are similar phenomena. Bridging is when ink connects two parts of an image that are not designed to be so. Filling-in describes areas on the print that have 'over inked', filling-in spaces that should not be. High pressures between rollers or high ink transfer due to incorrect anilox volume use are possible causes for these print defects.

Feathering is identified by its feather like look around the edges of the print. While this may impair the clarity of a graphics print, some correlation between roughness and electrical performance has been determined in literature for printed electronics (123).

Dirty print is more evident on a visual image, however, for printed electronics, the electrical performance will be of greater importance. Dirt entering the printing system is the primary cause, however, ink drying during the process and non-uniform substrate can also contribute to this.

Chatter in the print is distinguishable by bands of higher and lower print thicknesses across the print. This is typically caused by unmaintained flexography equipment, causing gears to wear. This can also be a sign that the cylinders are not centred.

These defects can reduce conductivity and impact antenna performance and are challenges in flexographic printing. Many of these print defects have been found to be closely correlated with viscosity of the ink, highlighting the importance of viscosity in high quality prints. Defects such as halo effects and pinholes can have huge effects on the conductivity of printed lines. Haloing can cause conductive material to be separated from the main body of ink, reducing the overall cross section of a printed track and consequently increasing resistance. It is here where opportunity for research comes in; to produce conductive tracks with minimal defects. Their significance increases in this process as they are more likely to cause a break in a printed track and cause an increase in resistance in thin films.

2.3 Rheology

Rheology is critical in the printing processes to offer a level of predictability in the behaviour of the ink. Varied polymer molecular weights alter the viscosity of the ink through the entanglement of the polymer chains (124). Both viscosity and shear thinning behaviour can be heavily impacted by the addition of dispersant (95).

Suspension rheology is critical within rheology to implement the theory and experimental testing in real-life applications as it is rare to use liquids without suspensions in them. Suspension fluid models and how experimental data are fitted to these models are outlined. The ability to model the effect of a particle on the suspension will guide further developments.

Flexography uses low viscosity liquid ink to produce thinner coatings in comparison to screen printing, which uses highly viscous paste to create thick films.

Ink viscosity has a significant affect on ink transfer. Increased ink viscosity has been shown to increase ink transfer in the flexography printing process (125)(126).

Rheological studies measure ink viscosities and surface tension, which directly influence the ink transfer and ink setting onto a substrate (127). A study analysing viscosity on ink transfer in gravure printing highlighted the requirement for close control of the viscosity as there is a strong relationship between ink transfer, cell geometry and viscosity (89). When the doctor blade removes the excess ink from the cylinder surface, the ink meniscus is dragged backwards in the cell and then the ink relaxes (63). The ink viscosity was found to be a determining factor in the speed of this relaxation. The engraving method of the cylinder also had an impact on the speed of relaxation of the ink (63). Parallels can be drawn from the gravure printing process to flexography in that the anilox collects the ink from the ink tray and is levelled by the doctor blade, therefore the speed of relaxation in flexography will also be dependent on the ink viscosity. Stress relaxation can be measured rheologically by applying a decreasing strain on the fluid. Flexographic inks are shear thinning fluids with operating viscosities range from 0.01-0.5Pa.s. Concentrated solvent and water based flexographic inks tend towards the 0.1-0.25Pa.s range (35)(128). A reduction in ink viscosity via reducing the conductive particle concentration, reduces density and in turn reduces the conductivity of the printed track. The rheological configuration of an ink is a key route to achieving desired printed features (118)(93).

2.3.1 Shear Rheology

At nip junctions between rollers, and between the doctor blade and rollers, high shear rates are exerted on the fluid. The shear rate exerted is rapidly increased at these points. As the ink flows through the flexoprinter, it is repeatedly exposed to these high shear rates [1,000 to 100,000s⁻¹ (129)], with short breaks as the ink is transported to the next nip. When the ink is deposited on the substrate, relaxation of the ink can take place (125)(126).

Shear and viscoelastic rheology are well summarised by Barnes (124)(130). Particle suspension viscosity is highly dependent on: particle volume fraction, particle shape, particle-particle interaction, particle size distribution, suspension structure, surface properties and hydrophilic/hydrophobic nature of individual components of the ink (67)(124)(130) (131)(132)(133).

Brownian, electrostatic and van der Waals forces are important non-hydrodynamic forces for colloidal particle suspensions (67)(132).

- Colloidal force interactions develop attractive van der Waals forces or repulsive electrostatic forces between particles (67)(131).
- Brownian randomising forces are behind particle spatial arrangement and orientation. The magnitude of these forces are particle size dependent and have a greater effect for particles greater than 1µm (67)(134). Brownian forces can affect particles up to mm's in diameter (135).
- Viscous forces exerted on a particle are 'proportional to the viscosity difference between the particles and surrounding fluid' (67).

Electric double layer, steric repulsion (Steric) and van der Waals attractive forces are used in the Derjaguin, Landau, Verwey, Overbeek (DLVO) theory, which states that the net sum of these three forces determines the stability between two surfaces in suspensions (67)(131)(136).

Concentration of particles in the ink greatly affects the viscosity of suspensions, in that a higher concentration causes more disruptions to flow and in turn a higher viscosity. As concentration is increased, a point is reached where the combined viscosity of the particles and the continuous phase is high enough to limit flow alignment under shear and consequently impedes flow.

When analysing particle suspensions, particle volume fraction, particle shape, particle interactions, particle spatial arrangement and bulk flow behaviours are the most critical considerations. For colloid (homogeneous substance dispersed in a second substance) and aqueous systems, the size and shape distributions of the particle suspensions as well as the inter-

particle forces are also of equal importance (137). The shape and size distribution are of particular importance in the packing density of the particles (112). Differently shaped particles hold different thickening effects. Increasingly non-spherical shapes (sphere-shaped particles < cube/grain < plate < rod) are associated with higher viscosity and can ultimately affect the printability of the ink. Also, the packing factor is higher for spherical shaped particles than rod like particles. The fundamentals of non-spherical particle suspension is understood in terms of its relationship to relative viscosity and phase volume (124)(137).

In terms of high concentration suspensions, a particle sheet style model is assumed whereby particles flow over one another (138)(139). The rheology of non-Newtonian suspension fluids for spherical particles has been reported in a number of papers (140)(141). Non-hydrodynamic forces: van der Waals forces, Brownian forces and electrical forces, act on particles in suspension and contribute by causing non-Newtonian behaviour. These are most relevant for particles <1 μ m and increase in importance with decreasing particle size. The presence of these forces combined with the presence of hydrodynamic forces are attributed to increasing the fluid viscosity. This viscosity does not remain constant, and depends on shear and extensional forces (140).

The type of flow plays a part in the rheology of the fluid and many models assume isotropic distribution of particles, which is not always applicable to non-Newtonian fluids. Flow can also cause or inhibit structure formation, and affect the distribution of particles within the fluid (140). Additionally, particles can align with the flow, through a streamlined formation of particles, hence reducing the viscosity.

Shear properties are important in the analysis of non-Newtonian suspensions (shear rate in particular) as fluid microstructure is largely affected by flow. At low concentrations, Brownian motion dominates to create a randomised disordered arrangement of particles. For low applied shear rates on a low aggregated ink, particles must flow over one another. The interaction of particles as they attempt to flow over one another creates a resistance to flow and this is measured as the viscosity. Due to the dominance of Brownian motion in shear flow, distribution of particles remains high and viscosity relatively consistent. For shear thinning fluids, increasing the shear rates begins to alter the particle orientation and overcomes Brownian motion to do so. The new orientations enable flow to move more easily, reducing viscosity (Figure 2-4). Distinct layers are formed as shear rates increase. Orientation and layer formation reach a maximum and at this point, viscosity reaches a minimum (67)(142).

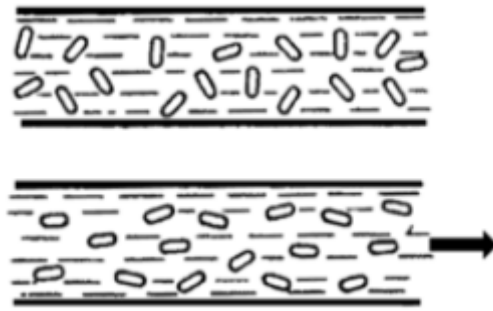


Figure 2-4 – Alignment of particle orientation for a flowing suspension (142).

Phase volume of hard sphere suspensions can occur in varying phase structure from liquid to gel-like with increasing phase volume (Figure 2-5). A fluid suspension state occurs at low concentrations (<0.5) and Newtonian plateaus are visible on the graph. This is where particles diffuse freely in the liquid with little order. Viscosity in these low shear plateau regions is not dependent on particle size, only on volume of particles within the liquid. Increased particle volume causes shear rate and shear thinning to increase. Above 0.5 phase volume crystalline phases become evident and shear thinning behaviours become evident. Hydrodynamic forces become increasingly dominant as the concentration increases (67)(143). Early research assumes volume fraction of particles in a suspension to be the only influential variable in its rheological properties. A review paper by Jeffery and Acrivos demonstrates that particle shape and size, electrical charges and type of flow should also be considered (140).

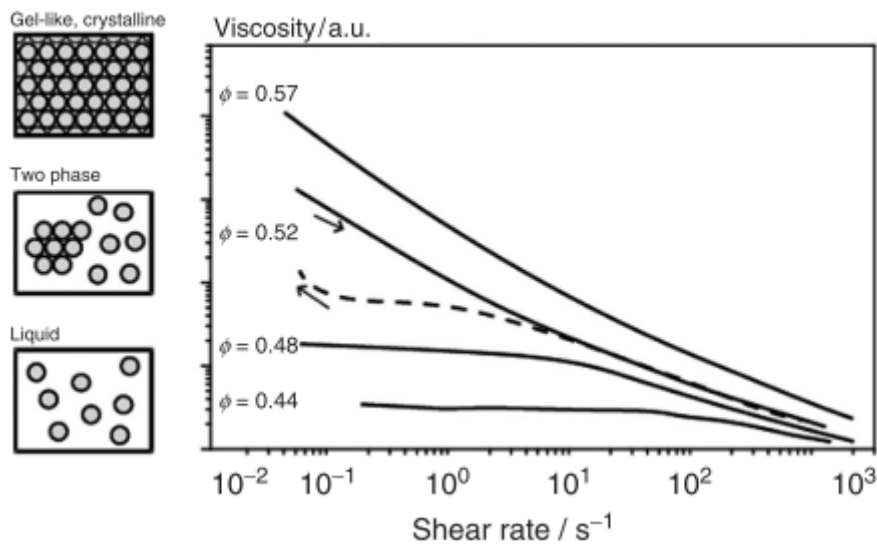


Figure 2-5 – The effect of concentration on shear rate and viscosity (143).

Particle suspension in terms of spherical particles has been well researched. For non-spherical particles there is higher particle interaction when a shear is applied than for spherical particles

and increased flow path deviation when high aspect ratio particles flow over one another. Therefore, particle aspect ratio contributes to the viscosity of the fluid. Orientation of these particles also plays a significant role in the viscosity of the fluid (67)(142).

Interactions between particles and a polymer resin, suspended in the continuous phase occur in four primary ways (67)(144)(145):

- The polymer is neutral and purely a thickening agent for the continuous phase.
- Some types of polymers, i.e., block co-polymers, can adsorb particles on one part of the molecule and interact with the continuous phase on the other part, preventing flocculation and consequent sedimentation/creaming.
- Bridging flocculation by polymer molecules pulling two particles together.
- Depletion flocculation occurs where an osmotic pressure difference is created due to the exclusion of polymer molecules between particles. The osmotic pressure differences pull solvent from the gap between particles, hence forcing particles together.

Due to the high impact of hydrodynamic forces on the particle surfaces, which is mostly unaffected by density, phase volume is used instead of wt.%. Phase volume is the 'volume of a dispersion occupied by a dispersed phase' and particles are considered weightless (124).

Polymer chains can occur as long rods or as coil/strings. Coil and string like polymer chains can be branched or linear. Typically, these coil and string chains are made up of many segments and due to Brownian motion can be constructed of both. Factors that affect polymer rheology are:

- concentration
- Vg distribution
- degree of branching
- temperature
- pressure

At low shear rates, these polymers tend towards spherical shapes. As shear rate is increased, these polymer chains move towards an elliptical shape, slightly aligning with flow. At the highest shear rates, coils of polymers can unwind into strings, further aligning with the fluid flow. At high concentrations of polymer, there is high entanglement between chains. When immersed in a solution, solvent between the polymer chains plays a significant role in influencing the overall rheology. Solvents can also cause polymers to coil or un-coil. Melts and concentrated polymer solutions demonstrate elasticity due to tension between overlapping and entangled polymer chains. As these chains are stretched, entanglements are loosened, and normal viscous

behaviours are exhibited. At these high shear rates, the dependence on V_g decreases significantly until almost negligible effects are present, resulting in viscosity that is almost exclusively dependent on concentration (124).

Electric double layer, steric repulsion (Steric) and van der Waals attractive forces are the forces that impact agglomeration within an ink (143). Agglomeration will occur if the net sum of these forces is attractive. These properties aid in determining the likelihood of flocs occurring in the ink, which can be detrimental in printed electronics. When these forces result in a strongly repulsive net force, the particles repel one another and create a stable suspension. Conversely, when these forces result in an attractive force between particles, agglomeration occurs. As agglomeration develops, particles connect with more and more particles creating larger flocs. Development of the flocs creates heavy clusters of particles and eventually sedimentation occurs (146).

Additives and surfactants can be added to inks to increase the particle – polymer interaction and hence the surface adsorption of one another. They can be added to reduce the effect of van der Waals forces between particles, hence reducing agglomerations/flocs in the ink. Alternatively, mechanical processes can be used for deflocculation to remove large flocs within the ink prior to printing (131)(147).

Aggregation causes a heterogeneous ink solution, which in printing, delivers an uneven print. In printed electronics, this can render the print faulty as there is not an even enough dispersion of conductive particles in the printed track to effectively conduct electricity.

The particle volume fraction ϕ is for non-interacting spheres and will change with particle shape and consequent particle interactions within the fluid. Interactions between these dispersed particles also impact the viscosity of the fluid due to their ability to impact streamlined flow and hence increase or decrease the viscosity (148). Ranges include:

- a) Dilute range is determined to be where the relative viscosity is roughly linear, and it exhibits Newtonian behaviour rheology. $\phi \lesssim 0.01$ (149) and $\phi \lesssim 0.02$ (141).
- b) Semi-dilute range begins to exhibit a stronger dependence on ϕ , and Newtonian behaviour is still prevalent with regards to particle volume fraction. $\phi \lesssim 0.25$
- c) The concentrated range $0.25 \lesssim \phi$ exhibits a high increase in apparent viscosity and the rheology towards more non-Newtonian behaviours (148).

Viscosity increases with the concentration of dispersed particles in a mixture. Shear thinning behaviours are also more prevalent. The continuous phase liquid, which is the resin in terms of printing inks, is the primary control of the viscosity of dispersions. As concentration of particles increases, conductivity of lines also increases however, this increases the viscosity, which can

eventually exceed the viscosity operating window of the printing press and cause print defects (150)(151)(152)(153).

Einstein developed a formula for the viscosity of low concentrations of suspended spherical dispersed particles. Research has investigated the effects of $1.5 \lesssim [\eta] \lesssim 5$, and validated Einstein's theoretical model, however, this equation is limited to very dilute suspensions, no more than a few percent phase volume (150)(151)(152).

Einstein's equation (Equation 2-1) fundamentally states that the viscosity of a dispersion with a low concentration of solid material, η , is dependent on the viscosity and the amount of material in the dispersion according to the equation below, η_0 , and that ink viscosity will increase as the amount of material ϕ increases.

$$\eta = \eta_0(1 + [\eta]\phi) \qquad \text{Equation 2-1}$$

Where:

η = Measured viscosity

η_0 = Newtonian continuous phase viscosity

$[\eta]$ = Intrinsic viscosity (and also known as the Einstein constant), which Einstein calculated to be = 2.5 for spherical particles.

ϕ = Phase volume

This equation assumes that flow diverted around a particle has no influence on the flow of another particle, hence requires a low concentration. Hydrodynamic forces are included; however, inertia is not. Hydrodynamic forces acting on the surface of particles and agglomerates are a highly contributing factor to the phase volume. wt.% is dependent on mass, which describes the quantity of particles without respect to volume fraction. This equation and the next few to be discussed all predict the viscosity of the suspension to be directly proportional to the viscosity of the continuous phase. The shape of these particles is of importance as it dictates the flow profile over one another.

An increase in particle loading increases viscosity. This is due to hydrodynamic changes as there is increased flow divergence around particles. The Einstein-Batchelor equation (Equation 2-2) operates in the semi-dilute range and for hard spheres, it has been validated for $\phi > 0.1$. Particle-particle interactions become more important with higher filler loading. This equation tends to not describe experimental data well for $\phi > 0.25$ and the equation becomes less relevant as the particle volume fraction increases due to the assumption that the finite viscosity value is $\phi \rightarrow 1$.

This is physically not possible as the densest packing factor possible for spherical particles that are monodispersed is $\phi_m \sim 0.74$ (137)(154). Hence, as packing factor is an important variable in the understanding of modelling particle suspensions, the most successful models for validating experimental data include this parameter.

$$\eta = \eta_0(1 + 2.5\phi + 6.2\phi^2) \quad \text{Equation 2-2}$$

Einstein's equation is for low concentrations and assumes that there is no interaction between particles. Empirical equations have been developed which modify the Einstein equations for medium-to-high concentrations of particles in a suspension. Krieger-Dougherty (K-D) equation (Equation 2-3) better represents higher concentrations, where particle-particle interactions are significant. The maximum packing fraction (ϕ_m) provides a limit to concentration viscosity predictions. The maximum packing fraction is the point at which the fluid is considered to be a solid due to the quantity of particles. As it transitions to this point, it goes from acting as a liquid to a gel and to a solid. The maximum packing of any particle in a fluid is 0.74. This value is shape dependant as spherical particles pack better than rod shaped particles.

$$\eta = \eta_0\left(1 - \frac{\phi}{\phi_m}\right)^{-[\eta]\phi_m} \quad \text{Equation 2-3}$$

Where:

η = Measured viscosity

η_0 = Newtonian continuous phase viscosity

$[\eta]$ = Intrinsic viscosity

ϕ = Phase volume

ϕ_m = Maximum packing fraction

Many practical experiments have shown $[\eta]\phi_m$ to equal 2 in many circumstances, reducing this to the Maron-Pierce equation (Equation 2-4).

$$\eta = \eta_0\left(1 - \frac{\phi}{\phi_m}\right)^{-2} \quad \text{Equation 2-4}$$

With all other variables experimentally measured, ϕ_m is a function of particle size distribution, particle deformability, and the flow conditions. It is the point at which a sufficient volume of particles has been included that viscosity appears to have reached its limit. The maximum packing fraction value is higher when particle-size distribution is wider. Wider distribution of particles means both large and small particles will be present, hence in terms of packing, smaller particles

can fill in the gaps created between large particles, increasing the packing factor. Higher aspect ratio particles are associated with lower maximum packing fractions (67)(132)(143).

Zero shear or the intrinsic viscosity $[\eta]$ increases with particle aspect ratio. Higher particle aspect ratios occupy a larger volume within a flow. Increased aspect ratio of particles increases the value of $[\eta]$, and ϕ_m decreases, due to poor packing structure (67). Particularly for higher aspect ratio particles, flow affects the maximum packing fraction (132)(143).

For all the suspension viscosity equations considered, viscosity is directly proportional to that of the continuous phase. Hence if the continuous phase viscosity is altered, it is expected that viscosity of the overall fluid suspension will change proportionally. This is important when considering changes in temperature and concentration (124).

Film splitting describes the phenomenon when wetted surfaces of a fluid, in printing more specifically an ink, are pulled apart. This pulling apart is known as a tensile property, which can often be more prevalent than the inks shearing viscoelastic properties. Figure 2-6 shows the nip junction between rollers. Tensile viscoelastic forces are key to describing the behaviour exhibited in the regions shown in Figure 2-6, particularly for situations such as flexography where it typically uses inks that have high rest viscosities.

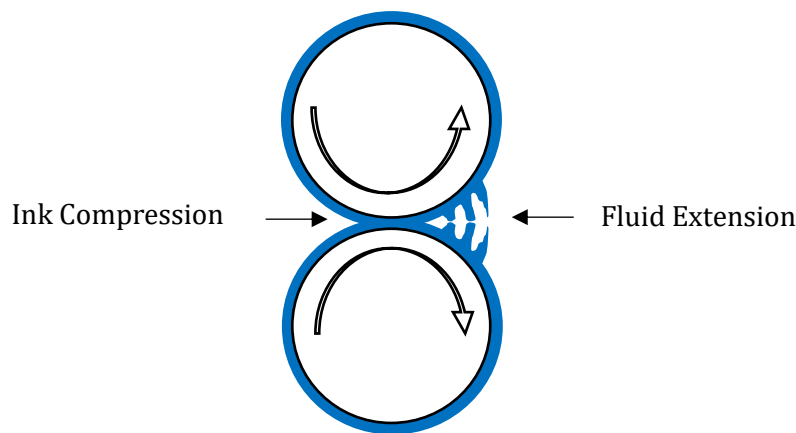


Figure 2-6 – Nip junction schematic where tensile viscoelastic force is important.

Extensional flow is of particular interest when there is an expansion or narrowing of an opening in the printer through which the ink must flow i.e., at the nip junctions. The ink stretches and deforms to do so. If moving from a wide to a narrow opening, the ink experiences compression and a shear is applied. Alignment of particles occurs in the narrowing. Also, as particle concentration increases, particle-particle interaction increases. Greater entanglement of particles creates a higher viscosity. The ink responds by attempting to break these bonds, increasing stress in the fluid. On a flexographic printer, this effect may be seen when ink is rapidly forced into anilox

cell structures and then rapidly drawn back out. An example of uniaxial extensional viscosity as a function of extension rate is shown in Figure 2-7. This is an experiment into purely extensional flow that can characterise these phenomena in isolation. It is distinct from printing where both shear and extensional flow can occur at the same time. Similar behaviours shown in experimental results could indicate the presence of extensional behaviours in the ink (124).

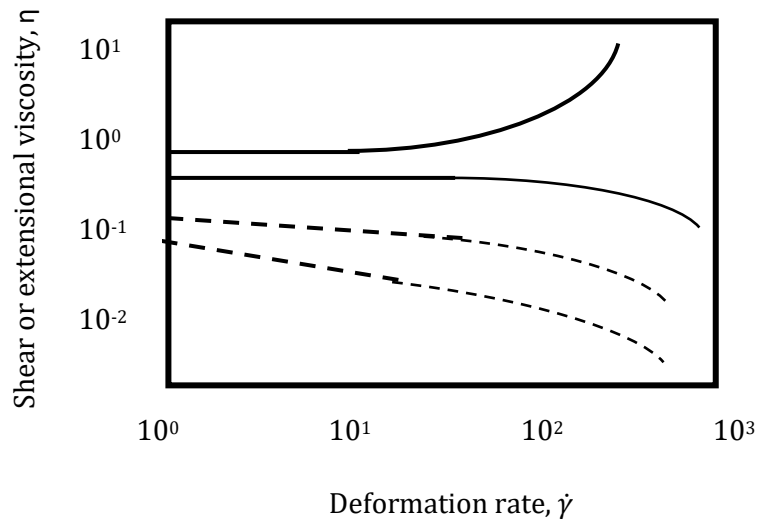


Figure 2-7 – Shear (dotted lines) and extensional flow (solid lines) flow curves for aqueous solutions of polyacrylamide (tension thickening) and collagen (tension thinning) (124).

Increased ink elasticity has been shown to reduce imperfections in the print due to instabilities in the process and are linked to filamentation effects. This is often seen in roller processes and causes continuous stripes, branching and dotting. A study of inks with the same rheological properties under shear but different extensional flow behaviour show a distinct link between orientation of resulting printed patterns in the track and directional electrical performance, with connected inline features creating a higher conductivity (93)(118). Through analysis of the striping effect in viscous fingering of the prints, ink elasticity has been found to have a significant impact on print uniformity. Increasing elasticity was seen to reduce relative feature size. This indicates that rheological tuning can be used to obtain certain features (118).

2.3.2 Silver Ink Rheology in Flexography

Inks of similar shear flow profiles can possess various magnitudes of extensional elasticity. Studies have shown that as the extensional elasticity of an ink and print speed increase, the viscous fingering effect forms in lines aligned with print direction. In this orientation of the

defects, print conductivity was higher than defects orientated perpendicular to print direction. Elasticity of the ink greatly affects the ink flow properties resulting in varying ink transfer (93)(155).

Higher silver loading increases conductivity of the printed ink however (1), there is a threshold beyond which the ink becomes very brittle due to lack of binder content (156) and could demonstrate poor flow between rollers. Silver loading, silver particle size, and binder systems, affect the ink flow properties particularly the anilox cell release characteristics, which is critical in flexography (1). Solvent based inks for silver typically require a viscosity of 0.1-0.25Pa.s (51). This range shows that a single viscosity value is not indicative of a shear thinning ink.

Too much silver can make the ink too viscous and ineffective as an ink in the printing process. Phase volume is important in the formulation of a silver ink to understand the quantity of silver particles required to achieve the appropriate range for the print process. Silver is particularly susceptible to forming large flocs and sedimentation occurring within a liquid (146). The effect of charge at the surface of silver nanoparticles is capitalised on for its antimicrobial activity but in fluids, extra energy is dissipated due to flow effects on the distortion of the surrounding charge cloud. As a face-centred cubic structure, silver has a maximum atomic packing factor of 0.74, meaning the packing factor cannot be higher than this. Typical commercial silver inks for flexography have concentrations of 12.5-18.2 vol.% silver and some papers have demonstrated a 3.9 vol.% loading (73). If there is a high amount of particle-particle interaction within the ink, then it must be pre-processed prior to printing in order to remove agglomerates and create the highest dispersion of silver particles within the ink (131).

The lack of literature on the link between rheology of silver inks to the flexographic printing process highlights the need for investigation. In a conductive silver ink, there must be enough silver particles to create a conductive track, and these must dry/cure to create connections between particles to allow current to flow. This differs from pigmented inks in that we are looking at performance over the visual image.

2.4 Chapter Closure

Flexographic printing has been shown to be a promising technology for RFID due to its good ink volume deposition, high print speed and accuracy of deposition. The research on the application of flexography to printed electronics has tended to focus on the impact of process parameters. These studies have used commercially available conductive inks. This has not allowed the investigation of a systematic variation of rheology and ink loading, despite its impact on ink transfer, line profile, defects such as viscous fingering and bulk resistivity. However, it has

highlighted that these more structured inks can have viscoelastic properties which interact with the anilox cell geometry.

There is a need for analysis on the effects of varying the anilox volume and process variables such as print speed and engagement while simultaneously varying the physical properties of the functional ink.

Rheology has long since been used as an aid for formulating and developing inks for many printing processes, however gaps exist in correlating viscosity, print parameters such as print speed and anilox volume and quality of print. Understanding the rheological properties and the ability to alter them are key in the characterisation of the microstructure and flow properties of dispersion (67). Dispersion rheology is critical in the optimisation of ink formulations through the adjustment of flow properties.

Understanding the impact of ink formulation on the rheological properties and subsequent impact on printability would assist in the future development of inks for printing of antenna.

Particle suspension models can aid the understanding of the ink behaviour at a micro and nano level. However, there is a lack of literature for silver ink. With further understanding of silver inks, processing reliability can be improved.

Gaps lie in research in the relationship between flexography and the variation of rheology and ink loading; further exploration of the anilox and print speed relationship; and understanding the rheology of the printed inks to see if alterations to rheology can control print features and consequently be used to improve function.

Rheology is an important factor in printing but has not been looked at extensively for silver ink in flexography and in particular, silver flake rheology in printing. Focus is required on the relationship between print parameters and printed outcomes with antenna performance. The continuity of prints using the flexography process will also be investigated. The following chapter will outline the methods and materials used.

Chapter 3: Methodology

3.1 Introduction

In this chapter, experimental and analytical procedures are described as well as the antenna design and analysis software.

The procedure for the manufacture of the model inks is also described together with the methods used for the rheological characterisation.

3.2 Overview of the Antenna Design and Manufacture

This section will give an overview of the software and equipment used to simulate the antennas and to test them. Firstly, a chipped antenna designed to work in the ultra-high frequency range (868-930MHz) was manufactured by printing and proof of concept was realised. The chip was later removed from the design and a series of tests were undertaken to determine an appropriate physical test method for a 'chip-less' antenna. Several methods were used to measure the printed chip-less antenna: firstly, a spectrum analyser and arbitrary generator system; secondly, a vector network analyser.

Testing was undertaken to select an appropriate simulation software for further design development. MultiSim by National Instruments and CST Studio Suite by Dassault Systems were both assessed for their applicability in simulating the chip-less antenna system.

The testing and simulation of the chip-less antenna system proved to be challenging. A vector network analyser provided the most consistent and comparable results to simulations created on CST Studio Suite. Hence, it was these two methods that were carried forward for further simulation and test work.

3.3 RFID Antenna Measurement

3.3.1 RFID Antenna Measurement

This reader is used as a preliminary test of the antenna design to ensure that it is suitable for further testing. Signals were read using a PC desktop model, USB powered, UHF reader (09CSHarp V1.5) with computer plug-in. The antennas with an NXP chip were measured using a PC USB connected handheld reader (Figure 3-1) that is compatible with CF-RU5102 UHF RFID software. The software was used to control the signal sent by the device and to display the signal received by the reader.



Figure 3-1 – UHF RFID computer plugin reader.

Antenna designs are presented more in depth later in this thesis (Antenna Design). They consist of a printed track and are paired with an NXP processing chip. The number of successful applications of the chips to the antenna were low however, working designs were found to have reading ranges of between 1cm and 15cm. The use of transparent PET substrate assisted in increasing the number of successful applications as the process could be viewed from both sides of the substrate.

Using the UHFReader09CSHarp V1.5 software, a response from the reader could be detected. What was not apparent from this software was any detail about the response signal. To understand the effect of the printing process and ink formulation on the response of the antenna, a new measurement technique was required.

3.3.2 Fundamentals of Complex Measurement of RFID Antenna

A number of papers have discussed the use of a vector network analyser to obtain results from an antenna construction that contains no chip, isolating the printed track and analysing the performance (157)(158)(159). These papers analyse the natural response of the conductive track and identify resonance in the response frequency. These unique response signals can be characterised to a particular antenna. Any changes in the design will have an impact on the response signal, hence this method was used to characterise the prints from an antenna response scenario.

The impact of values of the resistance, inductance and capacitance are well researched and their impact on the quality factor (Q factor) however, the effect of variables of a flexographic printing process on these parameters is not well researched (160).

In practice, these antennas are made of metallic particles suspended in a polymer resin and diacetone alcohol solvent. When printed and dried, solvent evaporates, and the silver flake and

polymer remain. It is how these particles dry amongst the polymer that creates fluctuations in the deposition.

3.3.2.1 Quality Factor

The Q factor is a ratio to describe how much energy is lost between receiving a signal and transmitting it back. It is a dimensionless indicator of the energy losses in a resonating system. A higher value of Q would indicate a lower rate of energy loss relative to the energy stored in the system and therefore a slower release of energy. The Q factor is dependent on resistance, capacitance, and inductance for the frequency range in which the resonant condition occurs (160)(161).

An LCR bridge has been used to measure the Q factor. The following equations (Equation 3-1 and Equation 3-2) are those which define the Q factor from LCR bridge measurements.

The equation for Q is:

$$Q = \frac{E_{Stored}}{E_{Lost /cycle}} \quad \text{Equation 3-1}$$

Where:

E_{Stored} = Energy stored in system

$E_{Lost /cycle}$ = Energy lost per cycle

And Q for a RLC circuit is (162)(163):

$$Q = \frac{f_{\max (resonant)} L}{R} \quad \text{Equation 3-2}$$

Where:

$f_{\max (resonant)}$ = Frequency at resonance

L = Inductance

R = Resistance

It is important to understand the relationship between Q factor, resistance, inductance, and capacitance. Resistance is a measure of the opposition to current flow. Resistance will be directly influenced by the quantity of ink deposited. It can be controlled by varying the printing process or by changing to a more conductive ink. Inductance is the resistance to changes in the current, allowing only direct current (DC) and resisting alternating current (AC). Typically, an inductor is a coiled wire through which an electrical current flows and causes a magnetic flux to develop

around the coil of wire. This magnetic flux is proportional to the electrical current flow. However, the printed tracks that are to be measured have wide meanders and so it is expected that the inductance will be weak and hence small inductance will be detected by the LCR bridge. A capacitance can occur when two conductors are separated by a dielectric, and it is typically used to filter out DC or low frequencies, which is useful in this application. When current flows, the voltage changes in a capacitor and vice versa. Micro capacitances can build between peaks in a surface roughness. Printing methods such as flexography can cause large variations in the surface roughness. Increased surface roughness has been shown to increase the capacitance. A rough and disordered surface is the cause of an inhomogeneous electric field distribution, and geometrical patterns leads to non-linear changes in the capacitance (121).

3.3.3 Antenna Reading Equipment

3.3.3.1 Digital oscilloscope and Arbitrary Generator

A Rohde and Schwarz RTm 2024 Digital Oscilloscope and a Rohde and Schwarz HMF 2525 Arbitrary Function Generator, that operates up to 25MHz, were used to apply the frequency and measure the frequency response to and from the discrete component resistor-inductor-capacitor (RLC) circuit shown in Figure 3-2. The oscilloscope is linked to a high specification computer which can record data and send data sets to documents on the computer.

Connection to Arbitrary Generator and
Spectrum Analyser

Resistor, Capacitor and Inductor

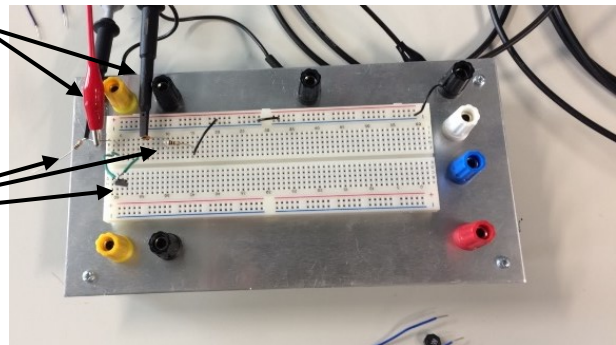


Figure 3-2 – An RLC circuit on a Tic-Tac® Box

3.3.3.2 Spectrum Analyser and Arbitrary Generator

A Rohde and Schwarz HMF2525 arbitrary generator was used for generating the input signal for the printed monopole. It has a waveform frequency range of 10 μ Hz to 25MHz, which does not reach the intended working range of the chipped antenna. However, it was used to investigate the

potential behaviours of the antenna in this range. It has an output impedance requirement of 50Ω , which dictated the connection component required.

A Rohde and Schwarz FSL spectrum analyser was used to display the output signal. Testing is shown in Monopole Design Test Using a Spectrum Analyser and Arbitrary Generator. It has the capability to process signals from 9kHz to 7GHz and has a typical average noise level of 1Hz in the results.

A circuit diagram and experimental set-up of the antenna, spectrum analyser and arbitrary generator are shown in Figure 3-3 and Figure 3-4, respectively. In Figure 3-4, the two probes shown were also replaced by a coiled wire, acting as an inductor, to determine if a response was achievable from an external source. The method of using the point probes used did not produce distinct differences between samples hence the use of vector network analyser was implemented and is shown in Monopole Design Test Using a Spectrum Analyser and Arbitrary Generator.

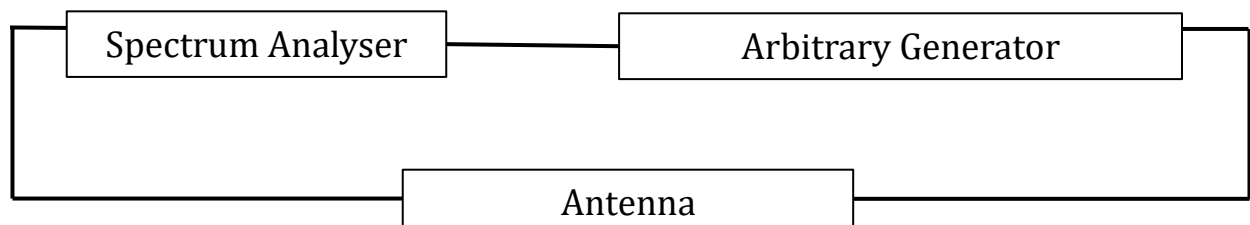


Figure 3-3 – Simple circuit diagram for chip-less antenna tests using a spectrum analyser and arbitrary generator.

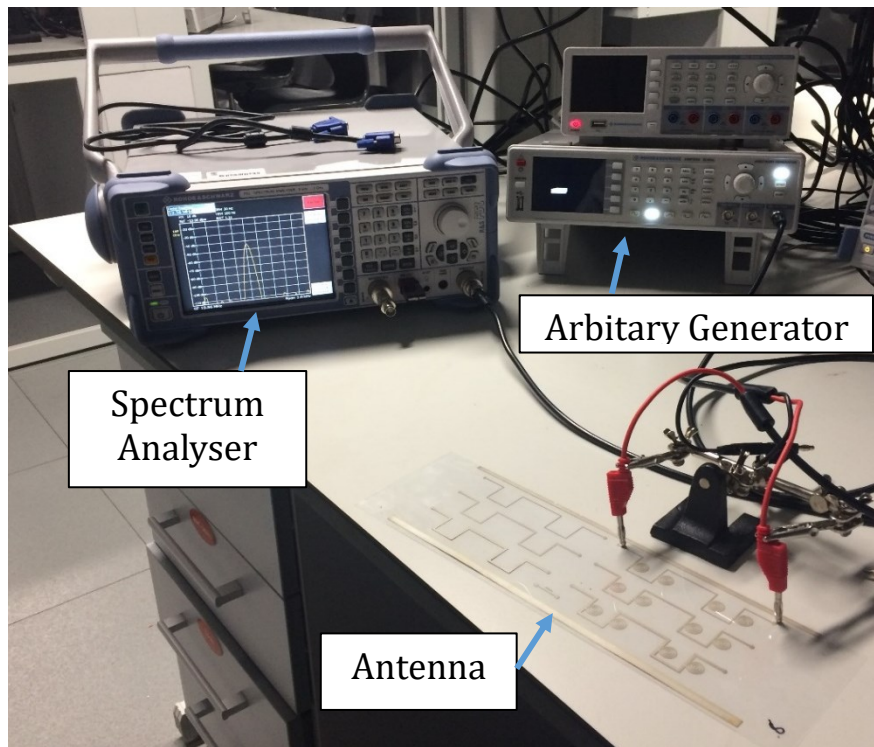


Figure 3-4 – Physical spectrum analyser, arbitrary generator and antenna set up.

3.3.3.3 Vector Network Analyser

In response to the inadequate readings from the spectrum analyser-arbitrary generator measuring system, a vector network analyser was implemented. A Keysight Technologies N9923A FieldFox handheld RF Vector Network Analyser (Figure 3-5) was selected for its capability to make accurate spectrum analyser measurements ($\pm 0.5\text{dB}$), measure up to 6.5GHz and be easily used with an anechoic chamber in future testing of the samples (164). A two-point probe is connected to the vector network analyser (VNA) and each point is placed at either end of the printed antenna. S-parameters were measured on the VNA and specifically, the S22 parameter was measured which is the output reflection coefficient.

As shown on the screen of the VNA in Figure 3-5, several resonant troughs occurred as a frequency sweep was applied through the printed antenna by the VNA. A typical plot is shown in tests presented in Testing Using a Vector Network Analyser. At the highest occurring resonant trough measured within the frequency sweep, the inductance, resistance, and capacitance were recorded, as well as the frequency and magnitude of that resonant trough. To achieve results with minimal noise in the data, an anechoic chamber and antenna horns to transmit the signal through the air are required. However, the method initially used gave a useful indication of the antenna

behaviour and had helped to characterise changes between samples when print parameters and antenna designs were altered.



Figure 3-5 – Keysight Technologies N9923A FieldFox handheld RF Vector Network Analyser and printed sample.

3.3.3.4 LCR Analysis

A Thurlby Thandar instruments LCR400 LCR bridge with a 0.1% accuracy, as shown in Figure 3-6, was used to obtain separate inductance, capacitance, resistance and Q factor values for each sample with an applied 10kHz frequency. Wiring was used to extend the contact points to the samples as shown.

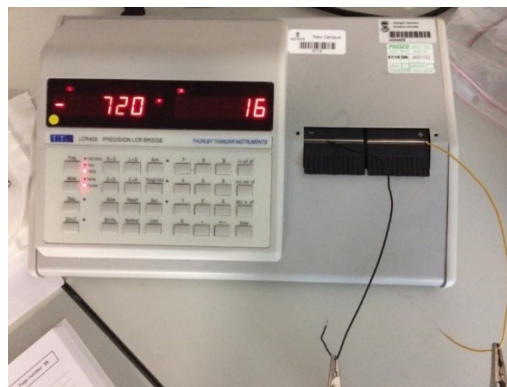


Figure 3-6 – Inductance, capacitance, resistance (LCR) bridge with wires for measuring antenna samples.

3.4 Antenna Design Software

Initially, National Instruments MultiSim was used to create a simplified model of the printed antenna, however, after several short tests it was demonstrated that the system did not align well with the simplified LCR model. Instead, a programme called CST Studio Suite 2019 was implemented to simulate the antenna.

3.4.1 CST Studio Suite 2019

CST Studio Suite is used in designing, analysing and optimising 3D electromagnetic models. It has the propensity to incorporate several models. It can analyse the performance and efficiency of ‘antennas and filters, electromagnetic compatibility and interference, exposure of the human body to EM fields, electro-mechanical effects in motor and generator, and thermal effects in high-power devices’ (165).

Typical graphs are modelled in Figure 3-7.

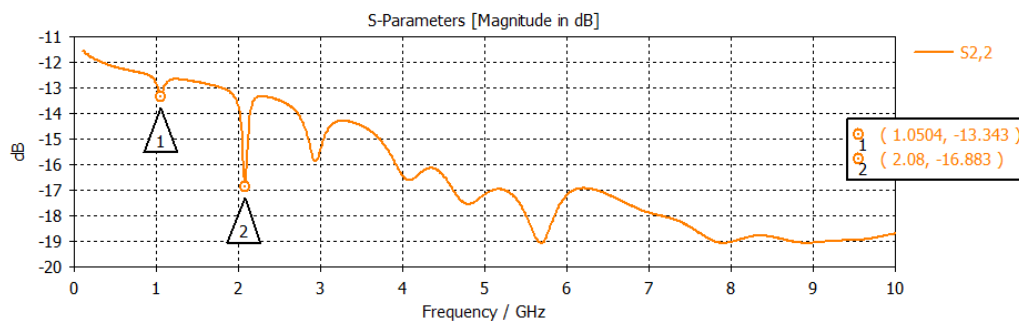


Figure 3-7 – Typical Frequency – S₂₂ graph from CST Studio Suite

Each antenna design was modelled on CST Studio Suite with substrate material included. The properties input to the software to represent the materials used are shown in Table 3-1 and Table 3-2. Surface roughness and electrical conductivity were measured from the printed samples and inputted into the model. Larger frequency sweeps were achievable on the software in comparison to real life testing, hence the largest resonant frequency troughs were found to be at a different frequency than previously tested.

Table 3-1 – Modelled Silver ink properties

Property	Value
Surface Roughness	7e-5 mm
Electric Conductivity	1.46×10^6 S/m
Mu	1
Density of Printed Silver	2200kg/m ³

Table 3-2 –Modelled PET substrate properties

Property	Value
Epsilon	3.5 Fm ⁻¹
Mu	1 N/A ²
Material density	1370 kg/m ³

A summary of the signal outputs for each method is presented in Figure 3-8. As described, the frequency traces produce similar outputs to one another whereas the trace produced by the spectrum analyser set up is not comparable.

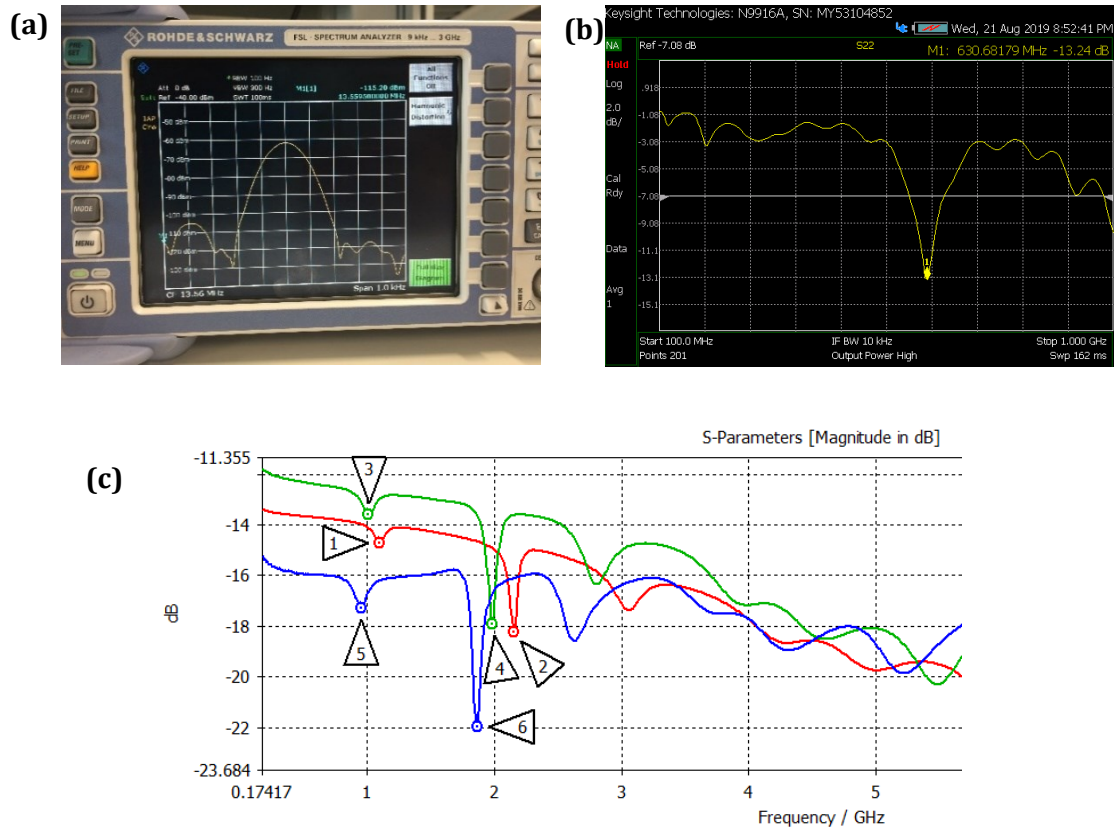


Figure 3-8 – Frequency responses on: (a) spectrum analyser (b) vector network analyser and (c) CST Studio Suite 2019 simulations.

3.5 Closure

The testing and simulation of the chip-less antenna system proved to be challenging. A vector network analyser provided graphs that resembled those in simulations created on CST Studio Suite (Figure 3-8). Hence, it was these two methods that were carried forward to do further simulation and test work.

3.6 Printing for RFID Manufacture

3.6.1 RK Control Coater (Bar Coater)

Prior to being subjected to any other print tests, all inks were tested on the RK Control Coater for adhesion to the substrate.

Thus, the coating bar was placed under the hinges as shown in Figure 3-9. The ink was deposited on the substrate in front of the bar and at a steady rate, the bar was drawn across the substrate pushing the Sheen multifilm applicator in front of it, spreading the ink in a linear direction perpendicular to the bar. A Sheen multifilm applicator, with gaps sizes at each edge (25 μ m, 50 μ m,

75 μ m, 100 μ m, 125 μ m, 150 μ m, 175 μ m and 200 μ m), can be used to set a print thickness. For the samples, a 25 μ m setting was used and assembled as shown in Figure 3-9.

Samples were dried and visually inspected for signs of peeling and excessive ink spreading to ensure compatibility between substrate and ink.

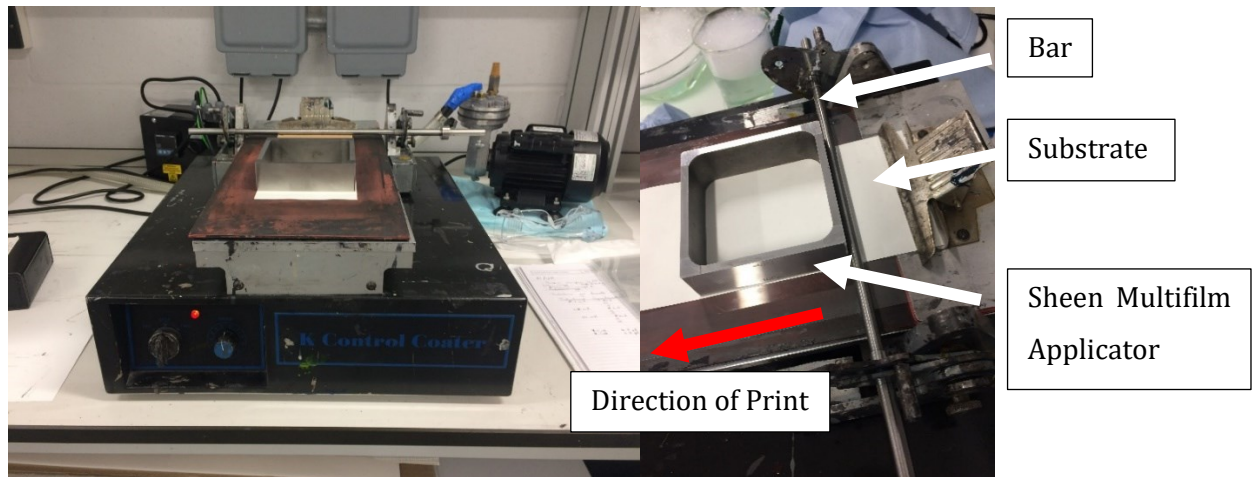


Figure 3-9 – RK Control Coater.

3.6.2 Flexographic Printing

A laboratory printing press, RK Flexiproof 100 (166), was used to print all conductive tracks (Figure 3-10). Its print area of 240 × 75mm allows for several designs to be printed simultaneously.

This printer operates at much slower speeds than industrial scale models. It is primarily used for conducting feasibility trials, optimise the print process including colour matching, research and development purposes, and monitoring ink and substrate interaction before upscale. At the nip points between rollers, the ink experiences a shear. The shear rates for a full scale flexographic printer range between 1,000 to 100,000s⁻¹ (129) however, the shear rates for a desktop flexographic printer will likely be at the lower range of this.

The anilox roller is connected to the plate cylinder, which is connected to the impression cylinder. The anilox roller has a doctor blade to remove excess ink from the surface. Ink from the cells in the anilox roller transfer onto the plate cylinder, which has a flexographic plate that can be replaced for a different pattern.

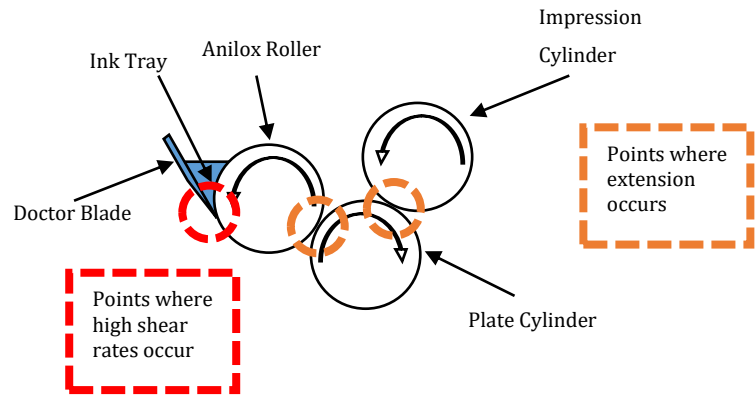
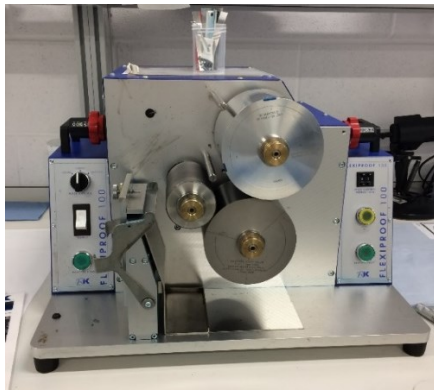


Figure 3-10 - Flexiproof 100 and a schematic of the rollers.

The speed of print, engagement distance between rollers, the hardness rating of the mounting tape, and the anilox cell geometries can all be changed. The print speed can be varied between 1 and 99 m/min. Engagements between the anilox roller and the plate cylinder, and between the plate cylinder and the impression cylinder can be changed in steps of 4µm.

For each print trial Samples 1-6 were disposed of due to settling of the printer i.e. sufficient coating of printer components and is good lab practice. Measurements were taken from samples printed thereafter.

A 3M medium hardness (E1120) tape was used for fine features as well as for larger areas, present in the designs. LUX ITP 60 photopolymer plates manufactured by MacDermid SGS were used. These are designed to be compatible with water and alcohol-based inks up to 20% acetate. The ITP 60 technology defines the flat-top dot specification rather than curved tops and achieves a sharper image, compared to traditionally manufactured plates, through applying a laminate to the surface after imaging but before UV exposure to exclude oxygen from the polymerisation process.

3.6.2.1 Plate Design

The plate design in Figure 3-11 has three main sections: the design placed centrally on the flexographic plate with annotations for clarity when printing; the support bars around the edge; and the 400-micrometer bar. The support bars provide support for the image carried, and the arrowhead provides stability upon entry into the printing nips. The antenna designs go in the central space. The 400-micrometer bars were to be measured for their resistance to enable prints to be compared between tests. This would enable the detection of consistent printing between plates of different designs.

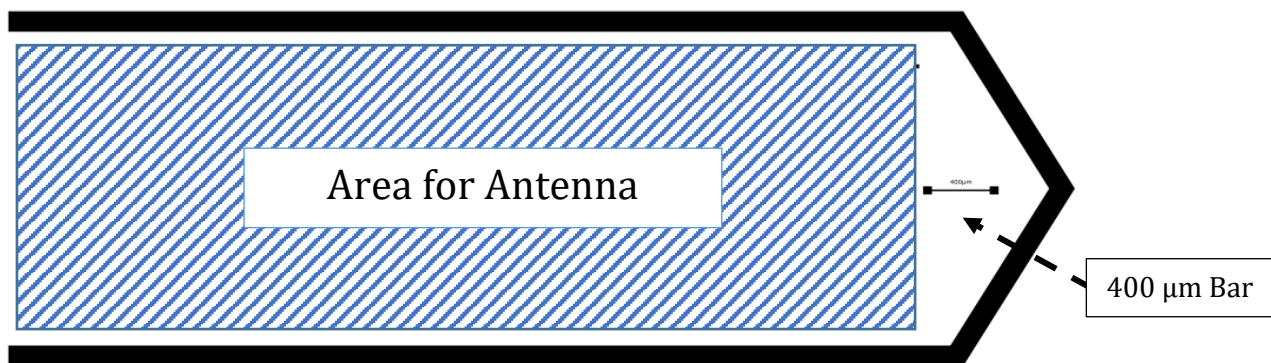


Figure 3-11 – Standard flexography plate design.

3.6.2.2 3.5.2.2. Anilox Rollers

The anilox volumes used are shown in Table 3-3. These were chosen to give a good range of volumes for testing.

Table 3-3 – Anilox cell volume and screen line ruling.

	Anilox 1	Anilox 2	Anilox 3
Screen Ruling (lpcm)	140	80	30
Cell Volume (cm³/m²)	8	14	24
Cell Degree Angle (°)	60	60	60

3.6.3 Drying and Curing of Silver Ink

A Vötsch VTL 60/90 Oven by Heraeus was used to dry and cure samples of silver ink on flexible substrate. The oven reaches up to 250°C and has an air fan for homogenous temperature distribution (167).

3.7 Surface Characterisation of Flexographic Printed Silver Ink

There are two phenomena present within the surface topography of a flexographic printed sample, roughness, and waviness. The roughness is determined when the long wave component is suppressed. The waviness describes the overarching undulations in the sample, whereas the roughness represents each peak and trough presented in the measured sample. The waviness will be noted however, it is the surface roughness that is of importance when comparing samples. A white light interferometer Veeco NT9300 was used to measure the surface roughness. An Alicona Infinite Focus microscope was used to measure the printed track widths. Higher magnification leads to analysis of a smaller area and a higher std. There is a compromise between magnification and these factors.

3.7.1 White light Interferometer: Veeco NT9300

The Veeco NT9300 is a wide area white light interferometer optical microscope. It is a non-destructive and non-contact surface optical profiling machine for obtaining a grey-scale high-resolution 3D profile of the surface of the sample. No sample preparation is required for this method and the advantage of using this type of interferometer as opposed to others is its ability to scan a field rather than simply from point to point (168).

The scan generates a three-dimensional surface profile using fields of views ranging from 0.55× to 2× (0.75, 1 and 1.5 inclusive). It has a vertical measurement range of 0.1nm to 10mm and a resolution of <0.1nm (169). The machine is used to obtain print heights, print widths and several variations of roughness including roughness average (R_a), root mean square roughness (R_q), mean peak-to-valley height (R_z) and maximum peak-to-valley height (R_t). R_a was used for surface roughness, as it considers any defects and gives an average of the results. It does not however indicate the spread of ink.

For the experiments in this thesis, a 5.1× field of view in VSI mode was used. Roughness values R_a were used for comparisons. Figure 3-12 and Figure 3-13 show how print thicknesses and surface roughness were obtained from the WYKO Vision 32 software.

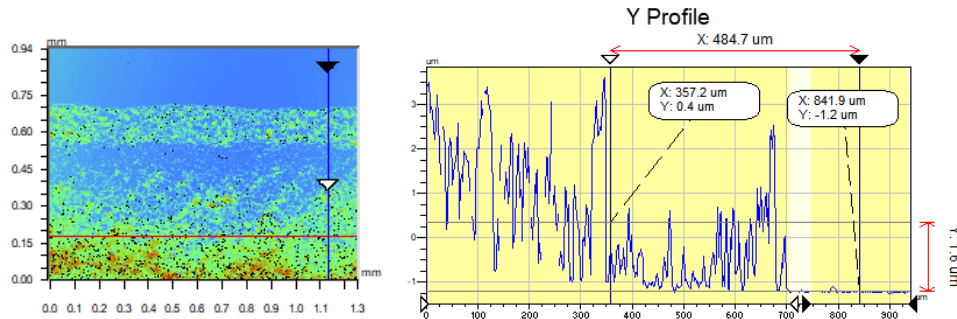


Figure 3-12 - Analysis of average print thickness of printed track.

Surface Statistics:

Ra: 1.20 μm
Rq: 1.47 μm
Rz: 9.02 μm
Rt: 12.15 μm

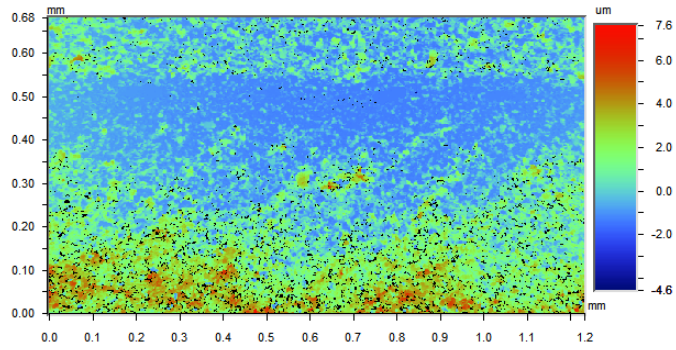


Figure 3-13 – Surface roughness example from WYKO Vision 32 software for a printed track.

3.7.2 Focus Variation Microscopy: Alicona Infinite Focus Microscope

The Alicona Infinite Focus microscope (a type of focus variation microscope) (Figure 3-14) is a well-established non-contact, optical, surface profiling machine. This can be used to gather surface roughness data and obtain 3D images of a surface. It was used to measure variations in the width of the printed lines.

It has an objective magnification of 2.5 \times , 10 \times , 20 \times , 50 \times and 100 \times and vertical resolutions of 2300nm, 100nm, 50nm, 20nm and 10nm respectively (170). A 2.5 \times magnification was used in these experiments.

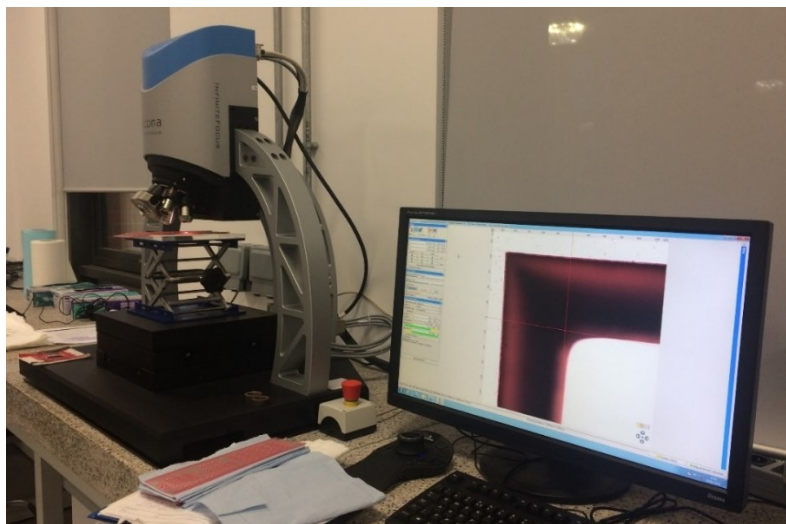


Figure 3-14 – Alicona microscope in the Welsh Centre of Printing and Coatings laboratories. A flexographic printing plate is on the bed and shown on the screen.

Within the microscope view in Figure 3-14, 10 measurements were made across the line to determine line width at each of the three locations circled in Figure 3-15.



Figure 3-15 – Locations of the readings taken on the Alicona Infinite Focus Microscope

Figure 3-16 and Figure 3-17 show how the line widths were measured on the Alicona MeasureSuite 5.3.5 software. For printed lines with relatively straight edges, two lines were drawn along either edge and the distance between the two lines was measured by the software (Figure 3-16). If the printed line did not have straight edges or after using the first technique it was evident that the edges were not parallel, the technique shown in Figure 3-17 was applied. This entailed ten vertical lines being drawn, connecting either edge of the printed line. The software worked out the average distance from the lines drawn.

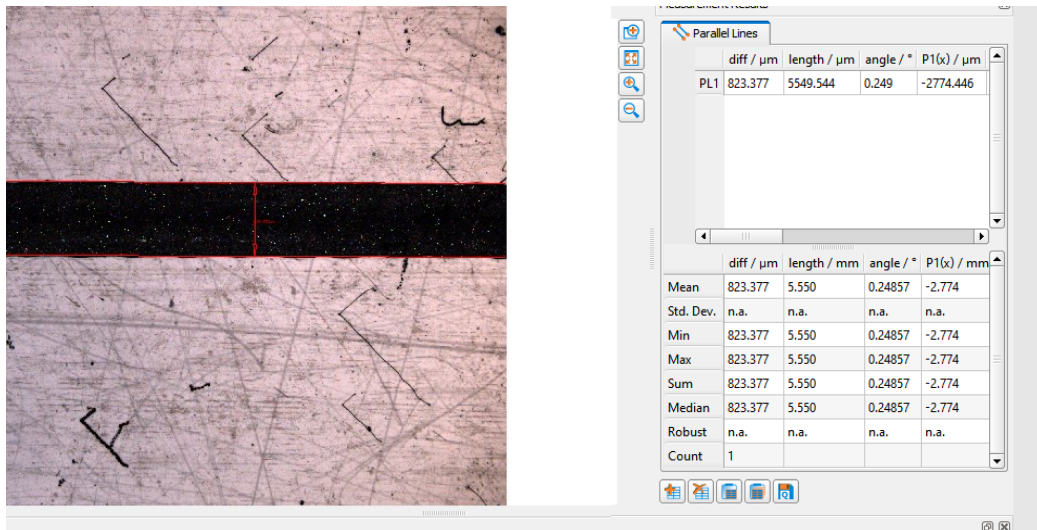


Figure 3-16 – Line width Measurements on Alicona MeasureSuite 5.3.5 software.

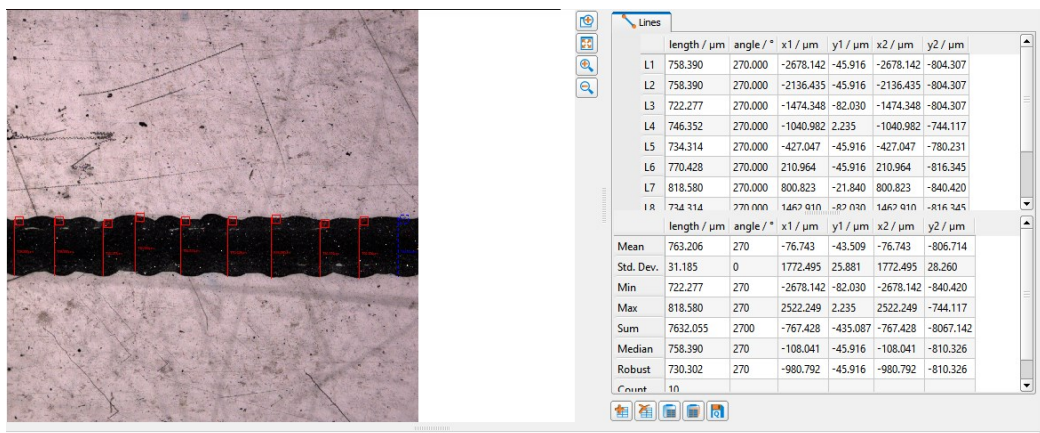


Figure 3-17 – Line width Measurements on Alicona MeasureSuite 5.3.5 software.

The Alicona microscope was also used to obtain the anilox cell diameters for an overlay on the printed tracks in analysis. The 24cm³/m² volume anilox is shown in Figure 3-18.

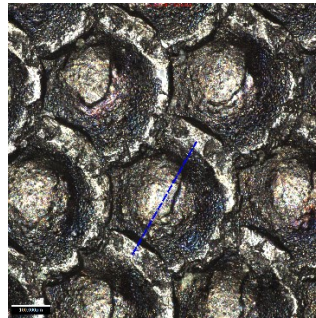


Figure 3-18 – Alicona microscope image of 24cm³/m² anilox cell surface with blue measurement line.

3.8 Electrical Characterisation of Flexographic Printed Silver Lines

A two-point multimeter was used to measure resistance of the printed silver ink. The probes were placed at either end of the printed line indicated by black arrows in Figure 3-19. A two-point probe was used over a four-point probe due to the sensitivity of the equipment being appropriate for the measurements taken. A two-point probe is sufficient since contact resistance is small in comparison to printed feature resistance.



Figure 3-19 – Multimeter probe locations.

Resistance of the prints is a key measurable for analysis and comparison. Resistances on different designs are only comparable if the printed image is of the same dimensions each time. Resistivity defines resistance over a given area and can be compared between prints of different sizes. It is a property that characterises a printed line.

In combination with line width and length measurements, the resistivity can be calculated using Equation 3-3.

$$\rho = \frac{RA}{L}$$

Equation 3-3

Where:

ρ = Resistivity (ohm m)

R = Resistance (ohms)

A = Cross-sectional area (m^2) = average print width x average print thickness

L = Length (m)

3.9 Manufacture of Inks for Flexographic Printing

The selection of the functional component, solvent and polymer is outlined in this section, as is the ink manufacture procedure. Resins of various polymer weights were dispersed in the solvent. The silver flake was then mixed into the resin and solvent. Silver tends to agglomerate so the inks were three-roll milled to break up any agglomerates and evenly distribute silver particles within the resin. These inks were benchmarked against a commercial ink and ratios of solvent, polymer and silver were readjusted. The methods and machinery used are further outlined below.

3.9.1 Selection of Conductive Component

3.9.1.1 Silver Flake

Technic Inc. Engineered Powders Division Silver Flake 164 was selected as the conductive component of the manufactured inks owing to its high conductivity, chemical stability, and ease of manufacturability in ink making. Manufacturer particle size distribution states that 95% of particles are below $13.2\mu m$ (Table 3-4).

Table 3-4 outlines break down of the particle size distribution as provided by the manufacturer.

Table 3-4 – Technic Inc. Engineered Powders Division particle size distributions as provided by manufacturer.

Test	Result	Value
Particle Size Distribution	D5<	<1.2
	D10<	<1.7
	D50<	<4.8
	D90<	<10.6
	D95<	<13.2
Specific Surface Area		0.5 m^2/g

3.9.2 Resin Manufacture

To manufacture the resin, two primary techniques were used; overhead mixing to achieve sufficient mixing of polymer within the solvent, and three-roll milling to achieve an even distribution of silver particles within the resin-solvent prior to printing and rheological testing. The selection of the two materials for the resin are outlined and following that, the mixing techniques.

3.9.2.1 Overhead Mixer in Resin-Solvent Formulation

A Heidolph RZR 2041 mixer (Figure 3-20), is used to aid the dissolution of TPU and DAA. The rotary blade is typically used for viscous fluids, and magnetic stirrers are used in thinner fluids. Due to the high viscosities involved in the manufactured inks, the rotary blade was used for all experiments for consistency.

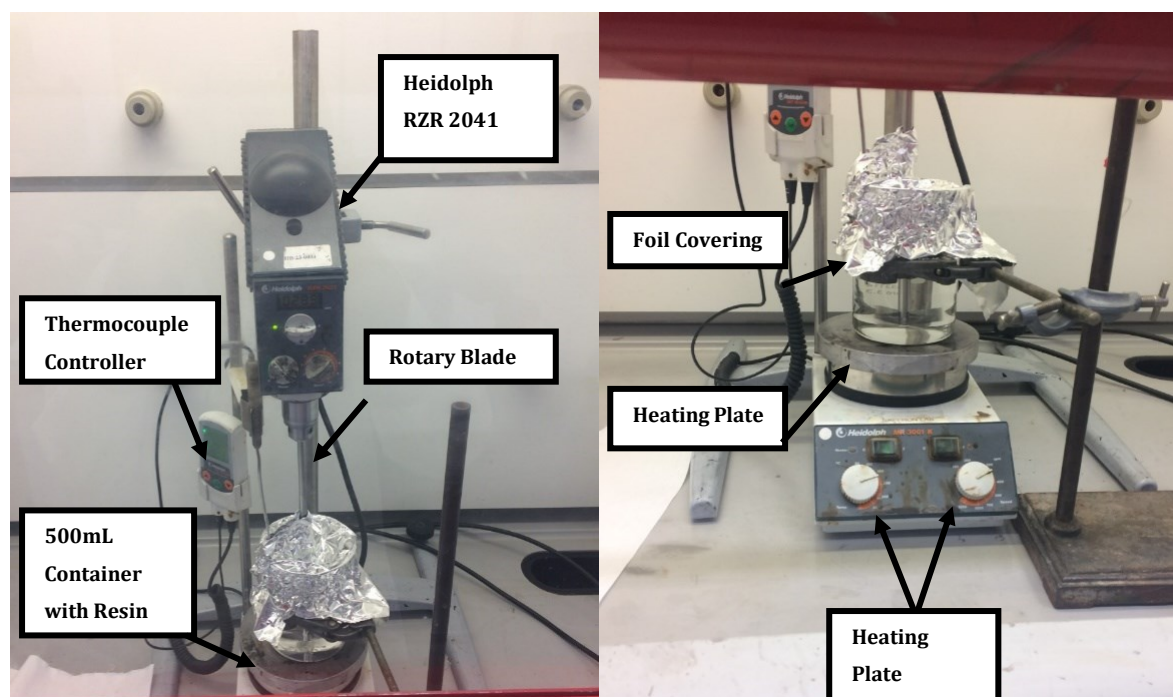


Figure 3-20 – Overhead mixer used for ink formulations.

A beaker was cleaned with solvent and dried. This was weighed with the stirrer. The desired quantity of polymer pellets was weighed out separately. For the initial ink formulation experiments ratios of 1:7 TPU:DAA were weighed out. The polymer was warmed in a convection oven for 1 hour at 50°C to bring the polymer to a closer temperature to the solvent. The solvent was measured out into a 500mL beaker, clamped into place on the hot plate and then stirred using the overhead mixer whilst being warmed to 80°C. The setup was within a fume cupboard (Figure 3-20). A thermostat was used to control the temperature at 80°C within the beaker and once reached, approximately 1/3 of the polymer pellets were poured into the solvent. The top of the beaker was covered with tinfoil to reduce solvent losses during mixing. Once the polymer was mixed and there were no longer polymer pellets visible, the next third was added. This process was repeated for the final third and inspected visually. Finally, the beaker, stirrer and solution were weighed, and then the weight was compared to the original measured values. Any discrepancies are assumed to be solvent losses and so additional solvent was added at this stage to rebalance the ratios. The solutions were then transferred to an airtight container.

Silver was weighed out and stirred in. Overhead mixing alone was unable to fully disperse the silver particles. The silver-resin-solvent suspension was weighed out in a separate container, then three-roll milled to disperse silver particles within the resin.

3.9.2.2 Three-roll Milling for Silver Particle Dispersion

An EXAKT 50 I compact bench top three roll mill unit, manufactured by EXAKT Advanced Technologies GmbH (Figure 3-21), was used in these experiments for breaking down agglomerates to produce inks with a fine particle dispersion.



Figure 3-21 – EXAKT Advanced Technologies GmbH three-roll mill (171).

Available gap sizes between rollers are 5 μ m-153 μ m and roller speed for the front roller ranges between 30-600 rpm. The other two rollers are on a gearing system so have different rpm. Two passes were required to fully disperse the silver flake (Table 3-5). This was assessed visually for evidence of any large agglomerates.

Table 3-5 – Triple Roll Mill settings for two passes of silver ink.

Pass	Roller Engagement Back Gap, Front Gap (μ m)	Roller Speed (rpm)
1 st Pass	60, 15	80
2 nd Pass	20, 5	200

3.10 Rheological Analysis

Rheological analysis was performed using two rheometers; both manufactured by Malvern Panalytical. A Bohlin Gemini was used to gather preliminary data on the PFI-722 Novacentrix ink as a benchmark. A Malvern Kinexus Pro Rheometer was used to do more detailed analysis of formulated inks. It enabled the measurement of the viscoelastic components [Novacentrix PFI-722 and Gwent Group UV Ink (Product number: C2140326D1)] and subsequent ink formulations to gain characteristics of the ink.

3.10.1 Rotational Rheometry

A smooth parallel plate configuration of diameters upper plate: 40mm and lower plate: 61mm was used in rheological testing. Wall slip tests were conducted to determine a gap size of 0.5mm to ensure minimal slip is present in experiments.

3.10.2 Bohlin Gemini

Malvern's Bohlin Gemini is a rotational rheometer as shown with cone and plate geometry in Figure 3-22, used for preliminary rheometric testing. It is designed to work best with low viscosity, low volume and weakly structured systems (172).



Figure 3-22 – Malvern Bohlin Gemini Rheometer at Swansea University with cone and plate set up.

3.10.3 Kinexus Testing

The Netzsch (formerly Malvern) Kinexus Pro Rheometer (173) is used for more advanced analysis (Figure 3-23).



Figure 3-23 – Malvern Kinexus Pro Rheometer (174).

A sample of the ink is held between a stationary plate and a parallel plate. The WCPC test sequence produces dynamic viscosity based on constant shear and visco-elastic properties using small amplitude oscillatory shear (SAOS) (175). SAOS is used to understand the viscous and elastic components of the fluid which gives understanding of how the ink will likely perform in the printer (175).

3.10.4 Krieger-Dougherty, Maron-Pierce and Einstein-Batchelor Equations

The Krieger-Dougherty, Maron-Pierce and Einstein-Batchelor equations were evaluated for the prediction of relative viscosity when varying silver loading and polymer viscosity grades. An example ink was used to demonstrate how the viscosity values were obtained for the three equations previously mentioned. The viscosity values were obtained from a shear viscosity vs. shear rate graph. Shear viscosity values were taken at a shear rate of 1s^{-1} . Table 3-6 shows the densities for each component of the ink in calculating each volume using mass/density. Phase volume was then calculated through a ratio of the volume of each component by the total volume of all three components.

Table 3-6 – Densities used in calculations for volume.

Density (g/cm ³)		
Ag	TPU	DAA
10.49	1.2	0.931

To solve for the unknowns for the three equations (presented in Shear Rheology): intrinsic viscosity and maximum packing fraction of the fluid, the Excel solver feature was used. Relative

viscosity and phase volume were plotted against one another to demonstrate alignment of the silver-polymer-solvent ink to the equations. Examples of the graphs can be seen in Appendix E: Modelling of Polymer Viscosity Grade and Silver Loading Suspension Behaviours for Viscosity and Phase Volume (Section 7.5.).

3.11 Chapter Closure

This chapter has detailed the material, apparatus and procedures used in the experimental work. Chapter 4 explores various test methods for RFID antenna designs using commercially available ink.

Chapter 4: Preliminary Evaluation of Techniques for Measurement of Printed Antenna Electromagnetic Response

4.1 Introduction

Chipped dipole and monopole antennas were printed using a silver ink (Novacentrix PFI-722) and their performance compared with a theoretical model. This gave a baseline to which further developments were compared. In this section, a range of techniques to measure antenna behaviour are assessed for applicability.

A dipole design (Figure 4-1) was then adapted to create a monopole (Figure 4-2) of the same operating frequency, by closing the gap between both dipoles to create a single continuous 1.5mm wide conductive track. Due to the lack of the chip, this conductive track was read using an LCR bridge to obtain the resistances, capacitances, and inductances when a frequency was applied to the system.

With a model for a printed antenna, the design has potential to be modified and tested virtually before conducting a lengthy physical testing process. An equivalent discrete RLC model was designed. The simple RLC circuit, typically used to describe the behaviours within antenna, was tested on a breadboard (Tic-Tac). The response measured on this did not align with the results previously obtained by using the VNA machine of the printed transmission line. Hence, more complex modelling techniques were required for modelling of the printed transmission line.

Models were then generated using CST Studio Suite 2019 to analyse response. The response of simulation models was compared with physical test results to determine the degree of correlation.

4.2 Antenna Design

Dipole antennas are easily printed as they have no overlapping printed tracks. One of the more common types is the half-wave dipole, where each of the poles (Figure 4-1) are approximately $\frac{1}{4}$ of the wavelength in length (Equation 1-1). When the chosen operating frequency is 866.8MHz, λ is calculated to be 0.34m. Each pole in the dipole antenna is $\frac{1}{4}$ of the λ , hence the lengths are 8.65cm.

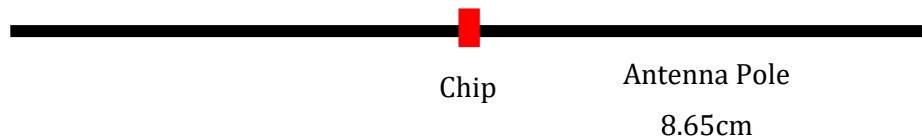


Figure 4-1 – Layout of chip and antenna poles for a dipole antenna.

Three basic designs were tested (Figure 4-2): One complex design that has a compacted shape; the second a straight-line dipole; and the third a meandering dipole.

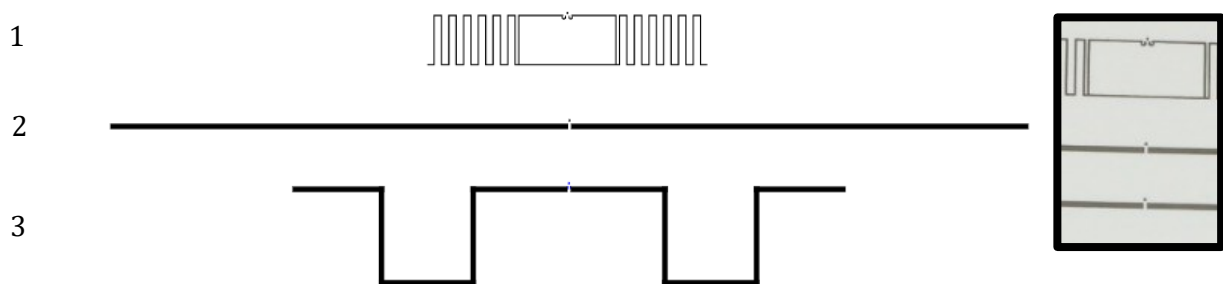


Figure 4-2 – 1. Compact design dipole; 2. Straight-line dipole; 3. Meandering dipole. Insert: Contacts for chip placement.

The dipole antenna design was printed onto transparent 175 μ m thick PET using a Novacentrix PFI -722 silver ink to test viability in the replication of the design. These designs work with resistances as low as 1-4 Ω .

G2X NXP Semiconductors MPN:SL3S1002FTB1, 115 chip (176), were impedance matched to the antenna design and applied manually using a silver paste to contact points.

The chip application process using a silver paste, which is done by hand, had less than a 50% success rate. In the testing of 20 samples of design 2, resistances of the printed tracks ranged from 4 – 13 Ω , line widths varied between 0.98 – 1.24mm and roughness ranged from 415 – 512nm. Using the transparent PET, the underneath of the chip in contact with the conductive track could be seen and any over spill of the silver paste, which would effectively short circuit was visible.

4.2.1 Monopole Antenna Design

As the response was likely to be influenced by the consistency of attaching the chip, it was more reliable to use LCR testing to evaluate printing of antennas. Using a breadboard, discrete component models were tested as part of the process to develop the test method for the printed sample [Appendix A: Discrete Component Model (Section 4.2.1.)].

The frequency response of the discrete component set up is a regularly oscillating sine wave. Varying the values of capacitance, resistance and inductance show variations in the peak voltages achieved. Higher capacitance values showed a lower output voltage at a lower frequency. The voltage peaks become more prominent as the input frequency increase. Higher inductance values used in the system produced higher output voltage peaks and at a lower frequency. Results could not be obtained for resistor value 4.7Ω , however, for those tested, troughs occurred at the upper end of the frequency range tested. The system will change with changes in resistance, capacitance, and inductance, highlighting the requirement for control over these parameters in a printed system in order to achieve consistency in print and readability as an antenna.

The dipole was redesigned as a monopole of dimensions 1mm wide and 164mm in length (Figure 4-3).

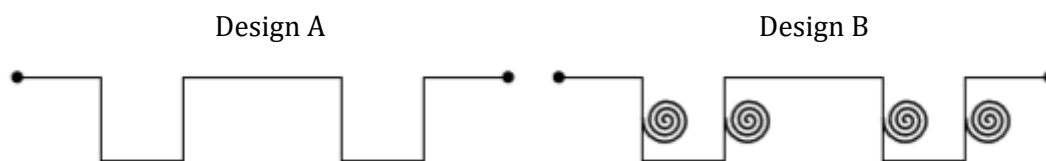


Figure 4-3 – Left: Design A - meandering monopole. Right: Design B - meandering monopole with four spiral resonators.

4.2.2 Monopole Design Test Using a Spectrum Analyser and Arbitrary Generator

Initially, the track frequency response was measured using an arbitrary generator and spectrum analyser. An input frequency of 13.56 MHz was programmed. The arbitrary generator was connected to a coiled wire for a solenoid, shown in Figure 4-4, which was held over the antenna attached to the spectrum analyser as shown in Figure 4-5.



Figure 4-4 – Solenoid and spectrum analyser.

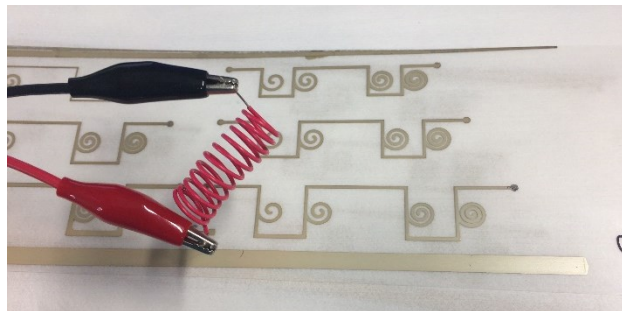


Figure 4-5 – Solenoid and printed antenna

When the solenoid was held over the printed antenna, a resulting frequency response was detected in the spectrum analyser. A typical example is shown in Figure 4-6. As the solenoid was held closer to the antenna, the response increased. This experiment demonstrated the feasibility of obtaining a resonant peak from the system.

An array of antenna of various widths and lengths were on the printed substrate. The response was of the same order of magnitude for the antennas tested. There was no apparent difference in measured response. Other test methods would be required to detect variations in the frequency response. However, the measurements were inconsistent, and values did not correlate with the simulations.

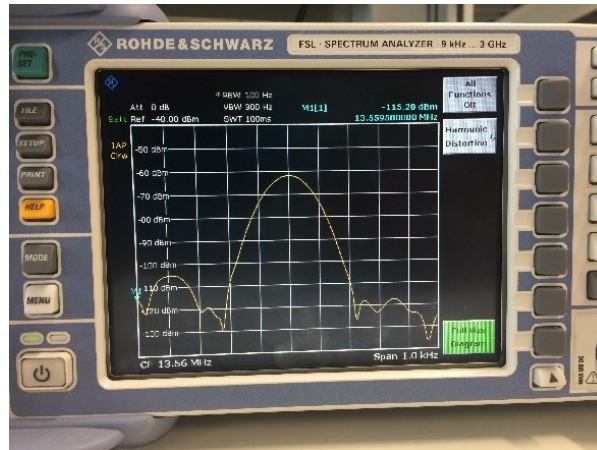


Figure 4-6 – Frequency response shown on the spectrum analyser.

4.2.3 Testing Using a Vector Network Analyser

Inductance, resistance, and capacitance are important parameters in determining the behaviour of the printed track as an antenna. To obtain a wider range of parameters a vector network analyser (VNA) has previously been used to obtain the electrical characteristics of the printed track (177)(178)(114). The samples were connected to the VNA using direct contact 2-point probes, one at either end of the line. This test was to obtain an idea of the behaviours and is not a set up for fully testing the chip-less design. Full tests require anechoic chambers, simulations, and antenna horns to be connected to either end of the track.

As the VNA sweeps a range of frequencies through the track, a trough is seen (Figure 4-7). The most prominent trough will be at a characteristic frequency. Although the inductance and capacitance can be analysed, this work focuses on the magnitude and frequency at which these troughs occur.

The VNA was also used to evaluate the samples printed in the full-factorial study in Chapter 6.

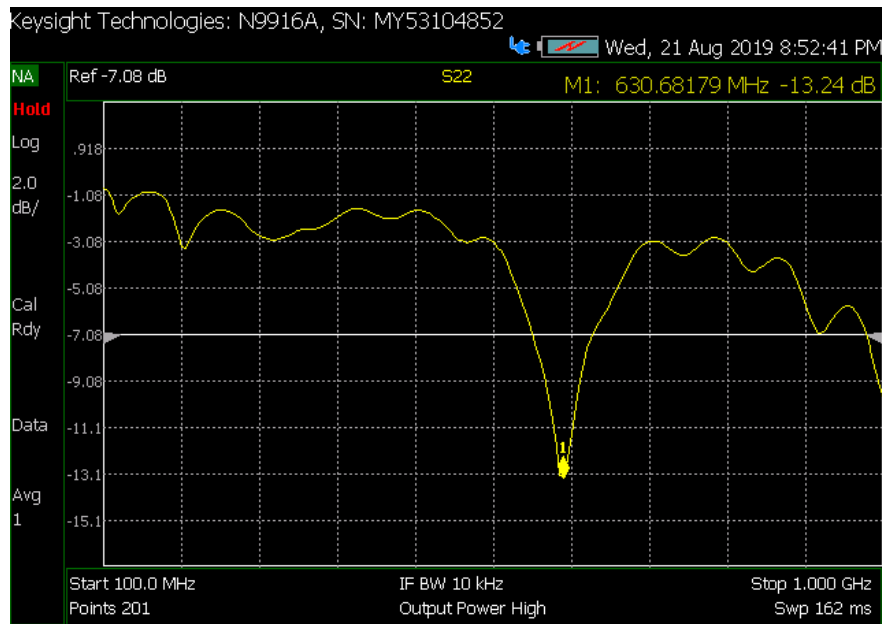


Figure 4-7 – Screen grab of VNA screen when analysing a 0.5mm wide printed Novacentrix PFI 722 silver ink track.

4.3 Simulation of Design

A printed monopole design A, as shown in Figure 4-3, was modelled on CST Studio Suite 2019 to attempt to make a model that aligned well with testing and could be used to evaluate changes in the design before printing.

Properties inputted for the silver ink and PET substrate are outlined in the methodology (CST Studio Suite 2019). Figure 4-8 and Figure 4-9 show the responses for the designs (outlined in Revised Monopole Antenna Design for Testing Print Variation) for an increase in both track length and width, and an increase in track length, respectively. Resonant troughs were present in the simulation responses. These were sharp troughs along the wave response and were the points at which the applied frequency is equal or close to the natural frequency of the printed track. These troughs were individual characteristics of the system and if they can be matched to physical testing, they can be utilised within an application to transfer data. The studio simulation shows the resonant frequency increases with decreasing line lengths (69, 67.5, 63, 58.5, 57, 51 mm) and with decreasing line widths (1.5, 1, 0.5 mm), as expected from theory. These graphs are used for comparison later in this thesis (Antenna Performance Testing for Optimised Silver Ink).

Table 4-1 – Printed tracks of various lengths and widths that are simulated on CST Studio Suite 2019

Antenna Design	Number denoted on simulations in Figure 4-8 and Figure 4-9	Line width (mm)	Line Length (mm)
A	1	0.5	58.5
B	2	1	51
C	3	1	63
D	4	1	57
E	5	1.5	67.5
F	6	1	69

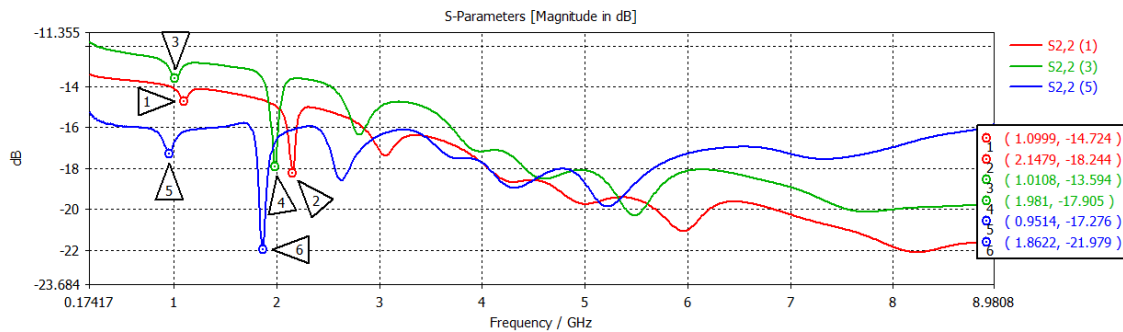


Figure 4-8 - CST Studio Suite 2019 simulations of printed tracks of increasing track lengths and widths.

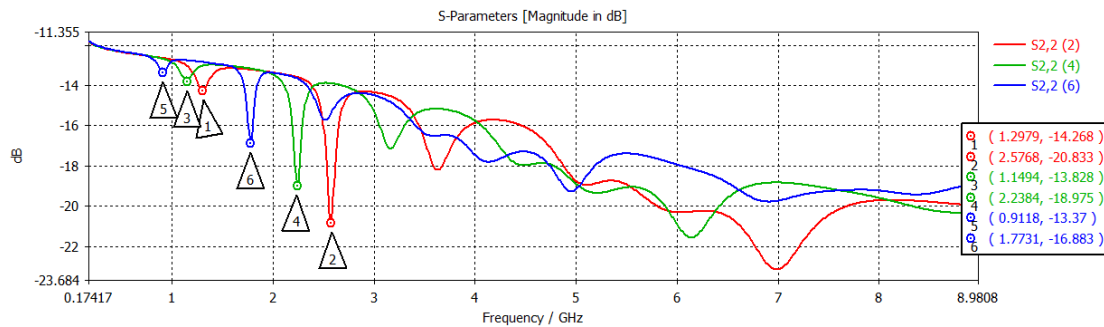


Figure 4-9 - CST Studio Suite 2019 simulations of printed tracks of increasing track lengths.

Further simulations were carried out using measured values for surface roughness and print thickness to detect the impact on frequency response. These measurables are averages achieved by altering print settings used in the full factorial print trial (presented later), where print speed and anilox volume are altered. There was no significant change in resonant frequency or trough magnitude as a result of any changes in surface roughness or print thickness [Full results are in

Appendix B: Simulation Array for Theoretical Impact of Surface Roughness on Frequency Response (Section 4.3)].

4.4 Chapter Closure

The simulation models show distinct variations between each design in terms of its frequency response. It has been established that the vector network analyser produces a response signal similar to that of the simulations, however extensive test data will be conducted later in the thesis, to which, the simulations will be compared to.

The next chapter (Chapter 5) investigates the impact of anilox volume, print speed, drying and substrate on the printed designs outlined in this chapter in terms of electrical conductivity. Chapter 6 investigates the impact of these parameters on the performance of the antenna design in this chapter. This is to understand how variations in the manufacturing process can affect antenna performance and to what degree this affects performance.

Chapter 5: Assessment of Flexographic Process Parameters

5.1 Introduction

Print trials using silver ink were conducted to analyse the effects of anilox volume, speed, substrate and drying conditions on line widths, film thickness, surface roughness, resistance, and resistivity. Nuances of the printer and print defects, such as alignment and viscous fingering are also discussed.

A proof of concept for a chipped antenna design was printed using two inks: Novacentrix PFI-722 and Inktec TEC-PR30. The ink, producing the lowest resistance and most consistent printing results, was chosen for further testing (PFI-722). Manufacturer recommendations for drying times and temperatures were used.

Six variations of a monopole meandering line (Figure 5-6) were then created: varying in length and width of track. These designs were printed with Novacentrix PFI-722. A study of the effects of changing anilox volumes and print speeds on the print outcomes on the measurable parameters of resistivity, resistance, surface roughness, film thickness and print width data were collected and compared with the variations in design.

Increased exposure to temperature and extend heat duration was shown to improve conductivity of printed tracks in a study on drying temperature and duration, which is presented in this chapter.

5.2 Benchmarking of Antenna for Different Substrates

5.2.1 Benchmarking of Commercial Inks for Print Quality

The properties provided by the manufacturers, of the nano-silver inks used are displayed in Table 5-1. These inks have been selected for their low resistivity and range of compositions.

In these experiments, silver ink, PFI-722, manufactured by Novacentrix, and an InkTec TEC-PR30 were used. The PFI-722 ink is a 60wt.% silver content water-based flexographic ink. Data specifications are obtained from the company website and are shown in Table 5-1. Novacentrix flexographic inks are typically used for capacitive touch sensors, RFID tags and printed batteries due to their medium level viscosity relative to other print processes that use silver inks. It can achieve print thicknesses of 0.5 to 2 microns; has fast drying and curing capabilities; and an ability to print fine features, all on the flexographic roll to roll process (179). The PR-30 by InkTec is a lower silver content ink ~40wt.%. Both are suitable for printed electronics and are used in the following test to determine a suitable ink to complete further testing.

The data for the inks are limited regarding resistivities and viscosities, which is a contributing factor in the requirement for a known ink formulation. Working with a known formulation allows for small changes to be made, tailoring it to a specific application.

Table 5-1 – Commercial ink specifications.

Property	Novacentrix PFI-722 (180)	InkTec TEC-PR30 (181)
Silver Content	60% ±2%	~40wt.%
Viscosity	0.55 Pa.s (550 cP) @10s ⁻¹	Unavailable
Volume resistivity	2-2.8 mΩ/□/mil	5 x 10 ⁻⁶ Ωcm
Printed Sheet Resistance	50-350 mΩ/□	Unavailable
Curing Temperature	140°C	120-170°C (2-5min)
Coverage	100 – 600 m ² / kg	Unavailable
Shelf Life	> 8 Months if kept refrigerated between 2-9°C	Unavailable

Two conductive tracks both 1mm in width and 172mm in length and differing only in meandering pattern, were printed (Figure 5-1). Design 1 is a straight line and design 2 is a meandering line, which is more compact, occupying a space of 103mm × 20mm. The aims of this experiment were to develop a good understanding the effects of a range of parameters in the print process. The two silver inks; Novacentrix PFI-722 and Inktec TEC-PR30, were printed and compared to establish a baseline for ink development tests. Printer settings are shown in Table 5-2. Roller engagements were determined via the kiss contact method. The Innovia film was used as to evaluate how these inks worked on thin packaging film.

Table 5-2 – RK Flexiproof 100 print settings for print trials using Novacentrix PFI-722 and Inktec TEC-PR30

Printer	RK Flexiproof 100
Anilox Volume	24 cm ³ /m ²
Engagements (Anilox-Plate, Plate-Impression)	260µm, 268µm
Print Speed	90 m/min
Substrate	Innovia Film non-porous WPA59
Mounting Tape	3M E1120
Drying in a Conveyor Dryer	90s @120°C

Printed samples were dried using a conveyor belt heater, and resistance measurements were taken using a 2-probe multimeter. Each design has two conductive tracks and probes were placed at either end of each of these.

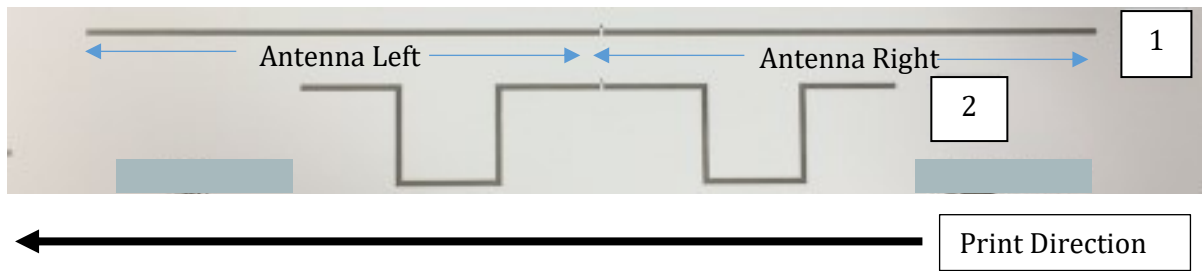


Figure 5-1 – Design of the two sets of silver printed conductive lines labelled 1 and 2.

5.2.2 Benchmarking of Resistance for Antenna Printed Tracks for Commercial Ink Selection

Figure 5-2 shows the average resistances of the two inks (20 samples of each ink printed – not including the initial prints while the RK100 stabilised). Novacentrix PFI 722 silver ink has a significantly lower resistance and lower standard deviations meaning more consistent results across all prints than the InkTec TEC-PR30. Therefore, it was selected for use throughout this thesis. The meandering line (#2) has a higher resistance for both inks, due to higher resistance in the corners of the line. This effect is much less pronounced on the Novacentrix ink printed samples, but variability is greater in design 2 (Figure 5-3). This is likely due to the higher silver content in the Novacentrix ink (Table 5-1).

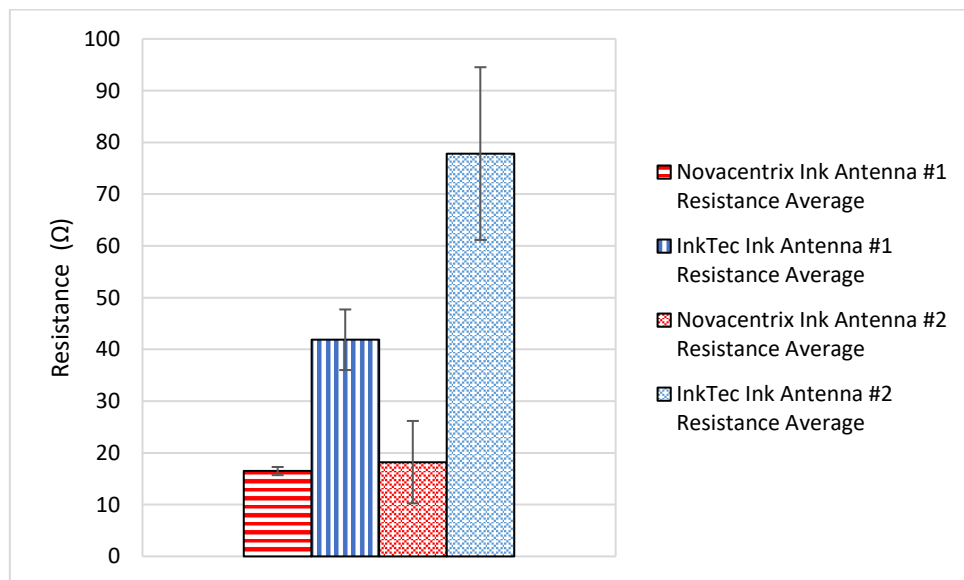


Figure 5-2 – Comparison of the general trend of resistances between flexographic prints of the Novacentrix ink and the Inktec ink for antenna 3 design. 20 samples for each ink measured. Error bars show 1 standard deviations.

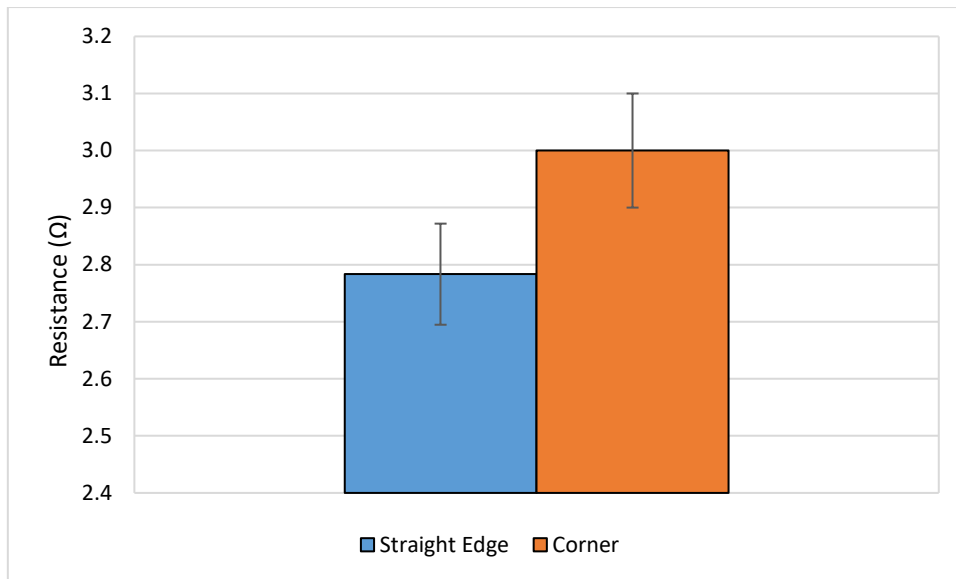


Figure 5-3 – Average resistances for Novacentrix ink antenna #1 18mm in a straight line and 18mm with a corner. Error bars show 1 standard deviations.

Resistances for Novacentrix PFI 722 and InkTec TEC-PR30 inks are shown in Figure 5-4 and Figure 5-5 respectively. There is inconsistency of resistance along the print direction. For both designs, 1 and 2, and both inks, the right-hand side of the print has a higher resistance consistently throughout the print and was printed after the left-hand side. The peaks in the graphs could be due to rewetting of the anilox cells during the print cycle (i.e., new ink being added to the ink tray for further printing), resulting in less ink transferred to the printing plate to the substrate. Hence, this is not a continuous process and there could be some deviation along the print run. Between prints, the anilox roller rotates several times, through the ink tray, allowing more time for the cells to fully refill. For a new print, the anilox cells are sufficiently filled at the start but cell replenishment may not be complete due to the higher roller speed during printing.

The roller could also be applying more pressure on one side of the print than the other due to rollers not centralised on the rotating axis. This would affect the quantity of ink deposited due to a squeezing effect between the substrate and the flexographic plate design. Nevertheless, data collection going forth will include reading from several points along the printed tracks to incorporate all these variations in the print consistency. There is a need to manually reload ink as required and this may give variation print to print i.e., the peaks in the graphs.

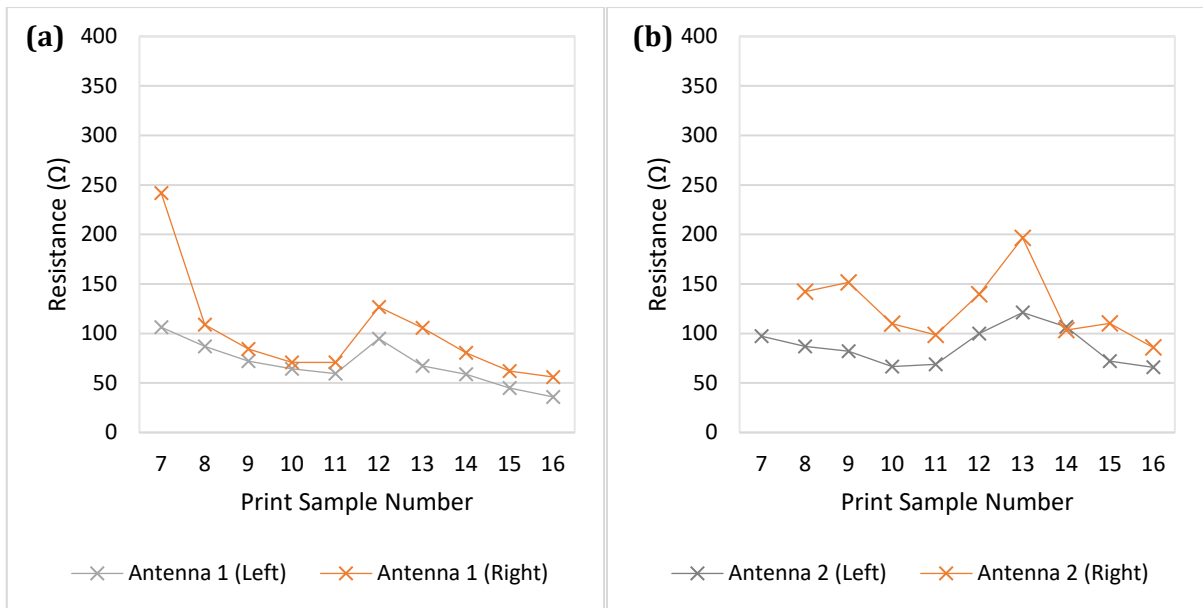


Figure 5-4 – Conductive silver track resistances for flexographic printed samples of the Novacentrix PFI-722 silver-based ink (a) antenna 1, (b) antenna 2.

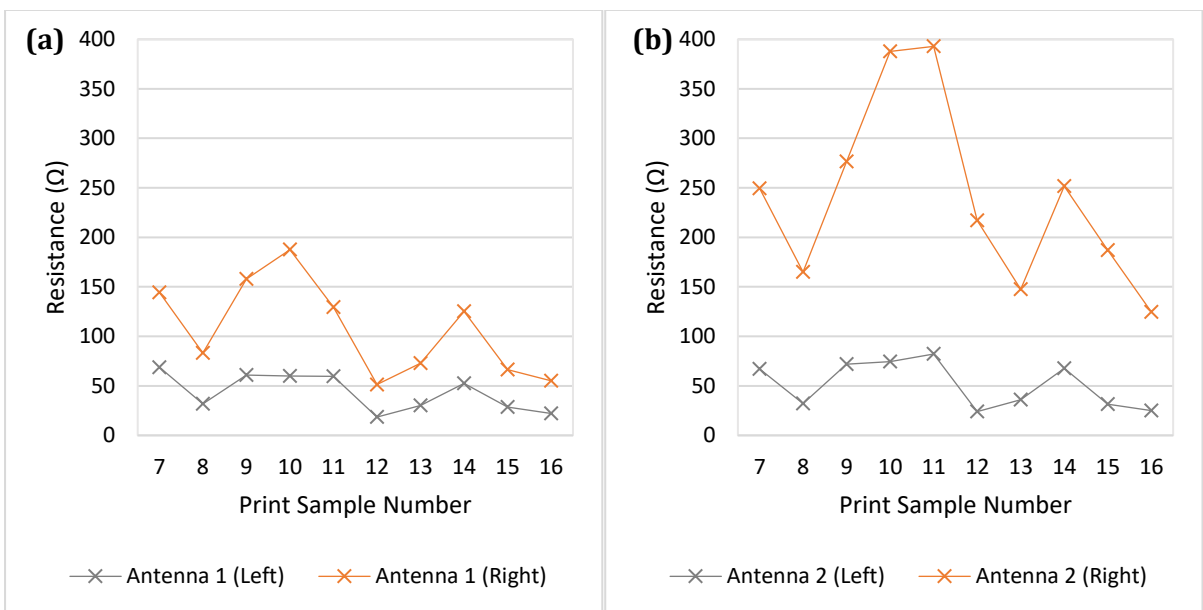


Figure 5-5 – Conductive silver track resistances for flexographic printed samples of the Inktec TEC-PR30 silver-based ink (a) antenna 1, (b) antenna 2.

5.2.3 Substrate Selection

A heating experiment in which three substrates were tested to identify a suitable substrate for further testing. The Innovia film demonstrated slight warping at higher temperatures. Hence, a thicker substrate was chosen to test. Two cellulose substrates were also chosen for this trial.

- HiFi Industrial Film SU320 Polyethylene Terephthalate (PET) 175µm
- Vegware
- Eco Craft

Substrates were held at a range of temperatures (70-160°C) in the Vötsch VTL 60/90 Oven by Heraeus, and inspected for structural integrity, to determine whether substrates could withstand the 140°C curing temperature of the PFI-722 silver ink. The temperatures were raised at 5-minute intervals in 10°C steps from 70°C to 160°C.

The HiFi Industrial Film SU320 Polyethylene Terephthalate (PET) 175µm, demonstrated stability at higher temperatures. It is a heat stabilised polyester film for which the manufacturer claimed it to be dimensionally stable up to 150°C. It remained stable in these tests up to 160°C. The glass transition is between 340K to 353K (67°C to 80°C) and a T_m of 540K (267°C), meaning that there may be some breakdown of structure within the substrate (182). The PET has an adhesion promoting coating on both sides to increase the amount of silver that has adhered to the surface of the substrate.

The biodegradable substrates could not withstand the elevated temperatures, Vegware distorted at 70°C while Eco Craft became tacky and discoloured at 150°C. Eco Craft remained functional for moderate temperatures, demonstrating that it is potentially a bio-substrate compatible with silver printed electronics.

5.3 Revised Monopole Antenna Design for Testing Print Variation

After this initial testing, Design 2 was taken forward for its compactness and edited to create six meandering lines of varying widths (Figure 5-6 and Table 5-3 with Figure 5-7). Table 5-3 and Figure 5-7 show the digital target widths and lengths of the lines. This is to investigate the impact of line width and length for a meandering line on the print outcomes: resistance, surface roughness, film thickness and print width.

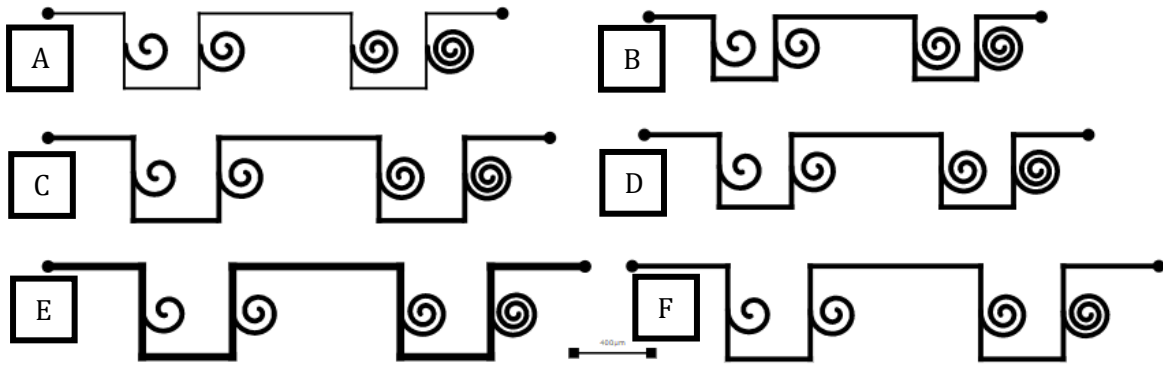


Figure 5-6 – Printed antenna designs A, B C D E and F.

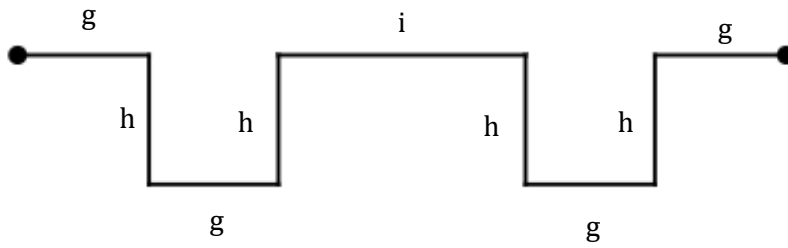


Figure 5-7 – Design for printed antennas with annotations outlined in Table 5-3.

Table 5-3 – Design parameters of a plate with lines of various widths and lengths.

Antenna Design	g (mm)	h (mm)	i (mm)	Track Width (mm)
A	15	15	30	0.5
B	13	13	28	1
C	17	17	32	1
D	15	15	30	1
E	19	19	34	1.5
F	19	17	34	1

Resistances were obtained for all designs. However, for print widths, only designs A, C and E were compared for variations in line width as line width does not change for the other designs. To isolate the changes in both line length and line width, design C was also compared to design D. Hence, only these four designs were analysed for determining resistivities. Average film thickness and surface roughness were found for all samples and presented in this section. The designs have spiral resonators present for testing in 'Effect of Printer Parameters: Anilox Volume and Print Speed on Frequency and Magnitude of Resonant Troughs'.

5.3.1 Line Widths of Monopole Antenna Design

Line widths for line lengths A, C, D and E were measured (Figure 5-7 and Table 5-3) in locations shown in Figure 5-8. B and F were omitted as C to D provides data in terms of consistency along print direction and isolate differences in line width due to change in length of line. A to E provides the consistency data across the roller and design line widths increase from A to E. Figure 5-9 (a) shows the line widths of four printed track designs from Figure 5-7. Figure 5-9 (b) shows the variation in line width along the printed track. Points 1, 2 and 3 were taken as representative results of the line width in the locations shown in Figure 5-8.

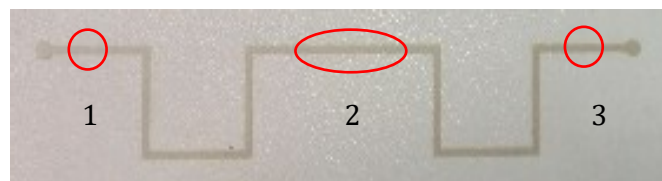


Figure 5-8 – Locations of the readings, 1, 2 and 3, taken on the Alicona Infinite Focus Microscope.

Figure 5-9 (a) shows the thinnest lines to have the highest % increase from designed print width. All print lines are over the designed line width.

Design C showed a marginal increase in line width along the printed line [Figure 5-9 (b) points 3,2,1]. As previously discussed, extraction of ink from the anilox roller during the print is a likely cause.

The spreading exhibited could be compensated for in the design if line width was of critical importance to the design. Line widths are known to be affected by several factors including printer engagement settings and ink rheology. More investigation is required to understand the impact of other factors on the line width for silver inks.

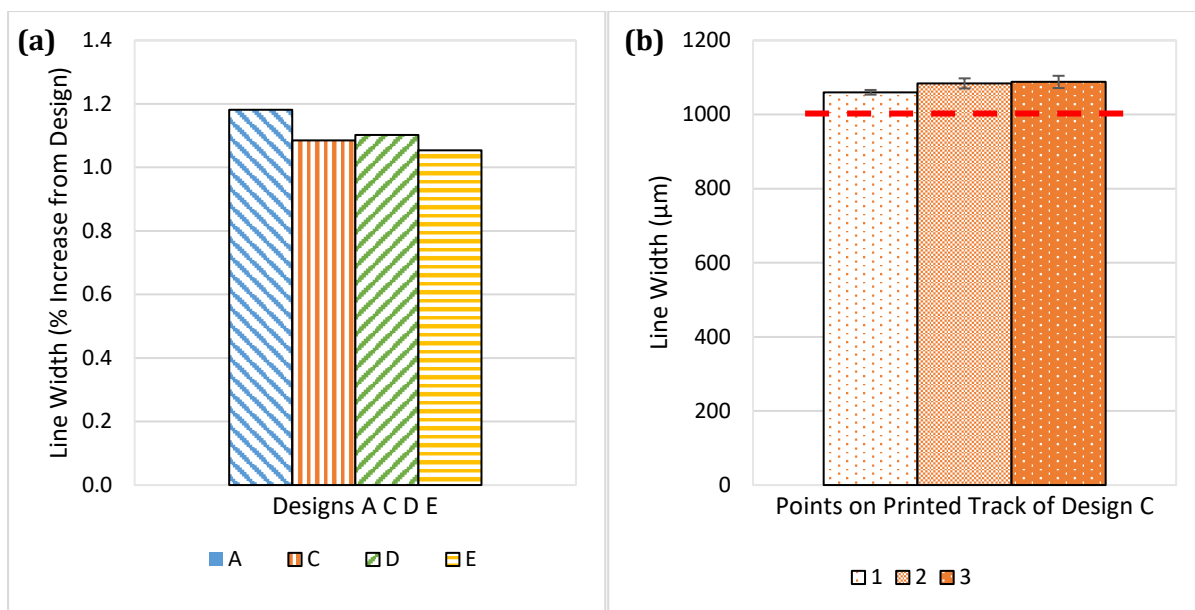


Figure 5-9 – **(a)** Line width % increase for designs A, C, D and E printed with a Novacentrix PFI-722 nano-silver ink. **(b)** Printed line widths at three points along the print direction for the design shown in Figure 5-8. Intended line width is shown via a red dashed line.

5.3.2 Film Thickness

Average film thickness for design C was $0.41\mu\text{m}$ with a standard deviation of ± 0.07 . Figure 5-10 shows film thickness over print sequence. White light interferometry was used to measure film thickness and surface roughness of the printed silver ink. The average film thickness was $0.41\mu\text{m}$. The peak in the graph may correlate with ink addition into the printer ink tray as it was at this point ink was added to the tray. The doctor blade should prevent this, but the ink used visually changes in viscosity so as the ink runs low in an open top ink tray, there could be changes in the film thickness deposited.

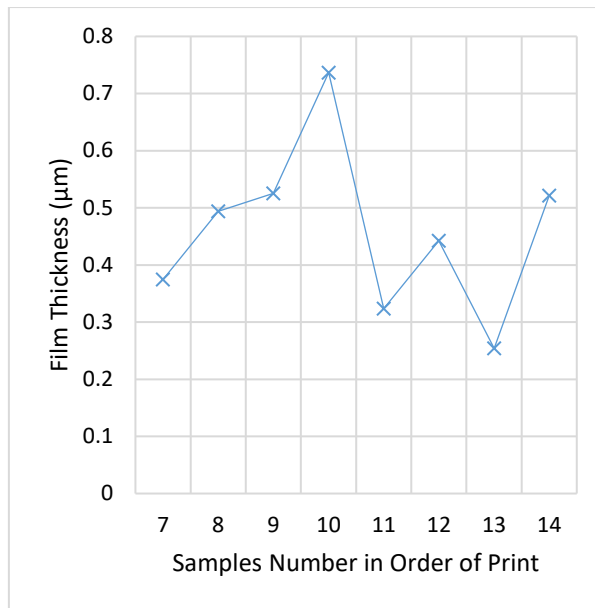


Figure 5-10 – Film thickness for each print sample over the print sequence.

5.3.3 Surface Roughness of Monopole Antenna Design

White light interferometry was used to obtain the average surface roughness of prints, which is $256\text{nm} \pm 35.66$ (Figure 5-11). An increase in surface roughness over print duration is observed likely due to solvent evaporation in the open top ink tray creating a more viscous ink, which means that ink relaxation once deposited on the substrate will be lower. The ink may be holding its roughness created in the anilox and interaction with the rollers more so as solvent decreases. The peak is likely due to ink added to the printer ink tray.

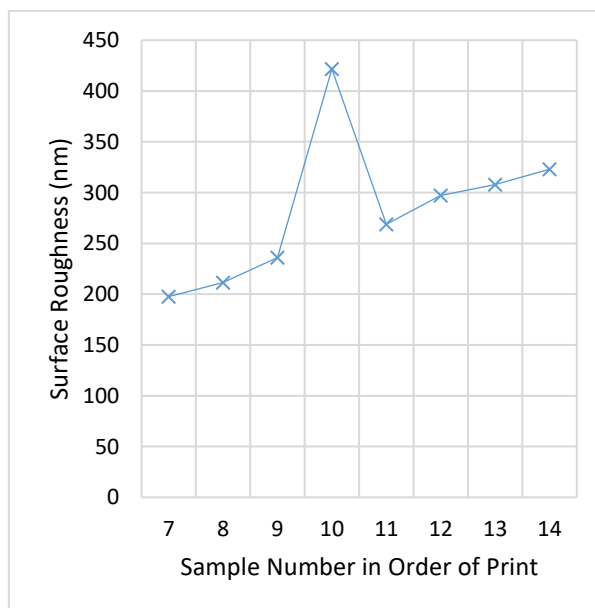


Figure 5-11 – Surface roughness, Ra, of each print sample over the print sequence.

The Y-profile in Figure 5-12 shows multiple peaks, which is indicative of viscous fingering. The intensity of the viscous fingering was determined by the average distance between peaks of the ridge lines. The yellow bar on the 'Y-Profile' was expanded to the width between the two peaks along the cross section. Readings are taken along this cross-section and again for another two cross-sections in the sample.

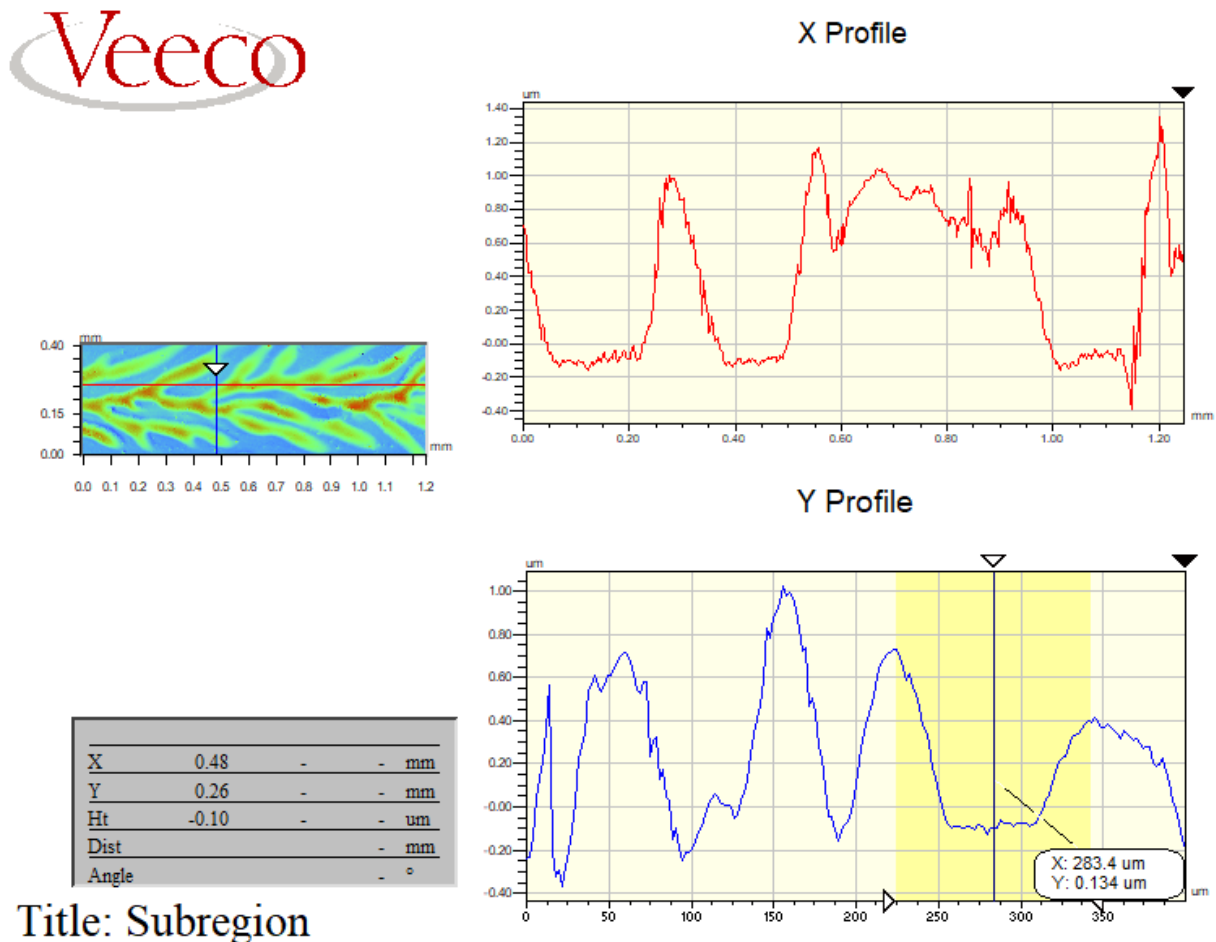


Figure 5-12 – View of a sample of the printed track on the Veeco White Light Interferometer software.

The measured peak-to-peak distances are shown in a scatter plot compared to film thickness in Figure 5-13 (a) and (b). There is a general increase in both film thickness and surface roughness with an increase in distance between peaks, meaning that the viscous fingering effect became more infrequent in higher film thickness. No correlation was found in this experiment between film thickness and surface roughness for this ink and particular setup. Roughness is dominated by large features of viscous fingering rather than features due to topography of particles.

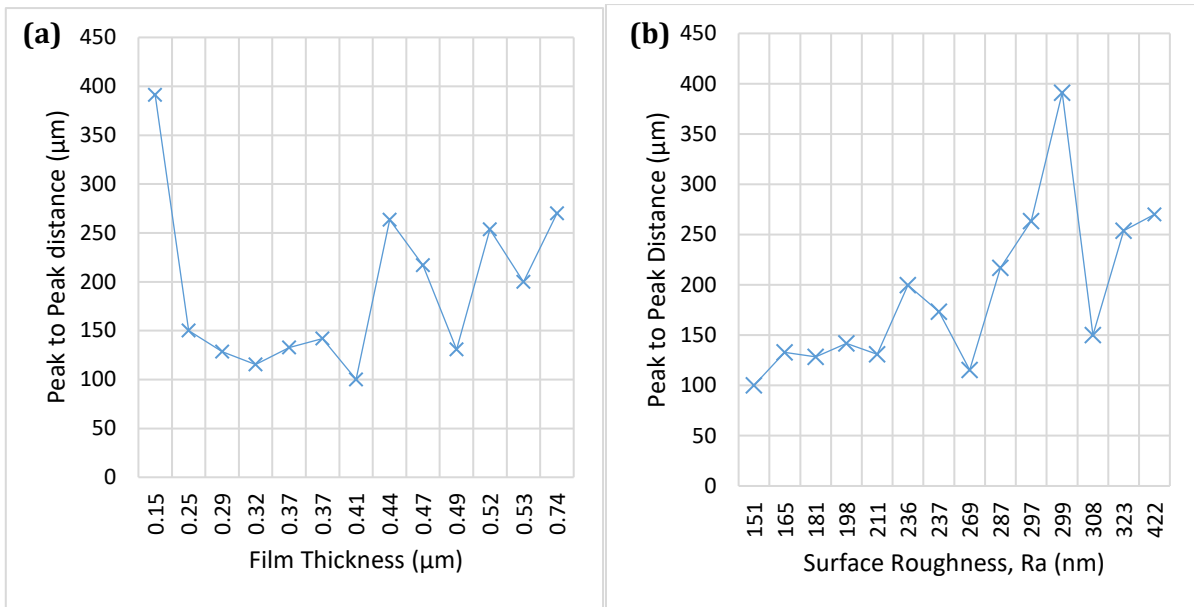


Figure 5-13 – Film thickness against peak-to-peak distance for Novacentrix PFI-722 nano-silver ink.

Figure 5-14 shows film thickness plotted against surface roughness, Ra, for the printed samples. These two do not have a correlation, and surface roughness is inclusive of waviness of the print which means that at least two types of surface roughness are contributing to this.

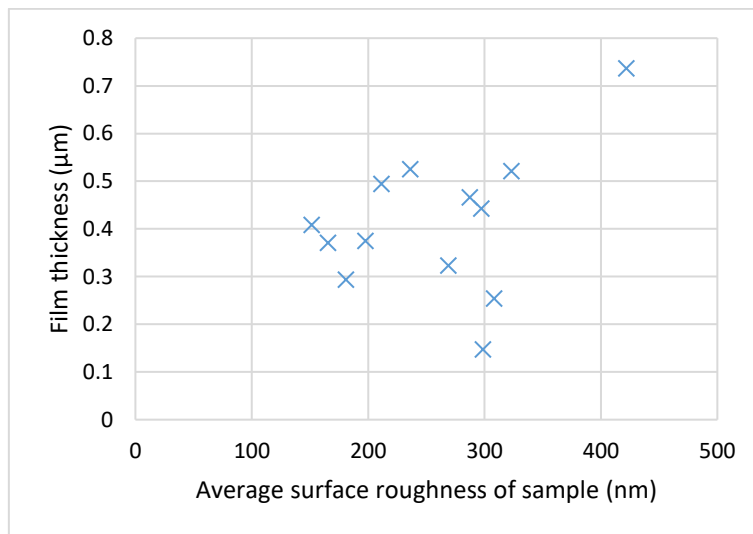


Figure 5-14 – The average surface roughness across each printed antenna against the average film thickness for each antenna.

5.3.4 Resistances

Average resistances for these prints were measured [Figure 5-15 (a)]. B, D and F have the same designed line width and the line increases in length only. As the line length increases, the resistance increases. For designs A, C and E, the line width increases as does the line length as

expected. The line width has a substantial effect on the measured resistance. The resistance decreases as the line widths increase. This effect is still prominent, despite the increase in resistance due to the increase in line length. There is a greater effect on the reduction of resistance from a change in width from 0.5mm to 1mm, than a change from 1mm to 1.5mm.

Figure 5-15 (b) shows the resistance for each design over print time. The track of 0.5mm in width shows high variability. There is a marginal decrease in resistance over the print time for all designs.

In increasing order of line length, the line references are: B, D, A, C, E, F and the increasing order of line widths are A; B, C, D, F; E. Figure 5-15 (b) shows the widest line of 1.5mm to have the lowest resistance and the thinnest line of 0.5mm to have the highest resistance due to their relative cross sectional areas. On the figure, lines BCF are clustered together, and variability is too large for a deduction to be determined regarding the impact of line length. However, line B is of a lower resistance than other line widths of 1mm for a shorter line length.

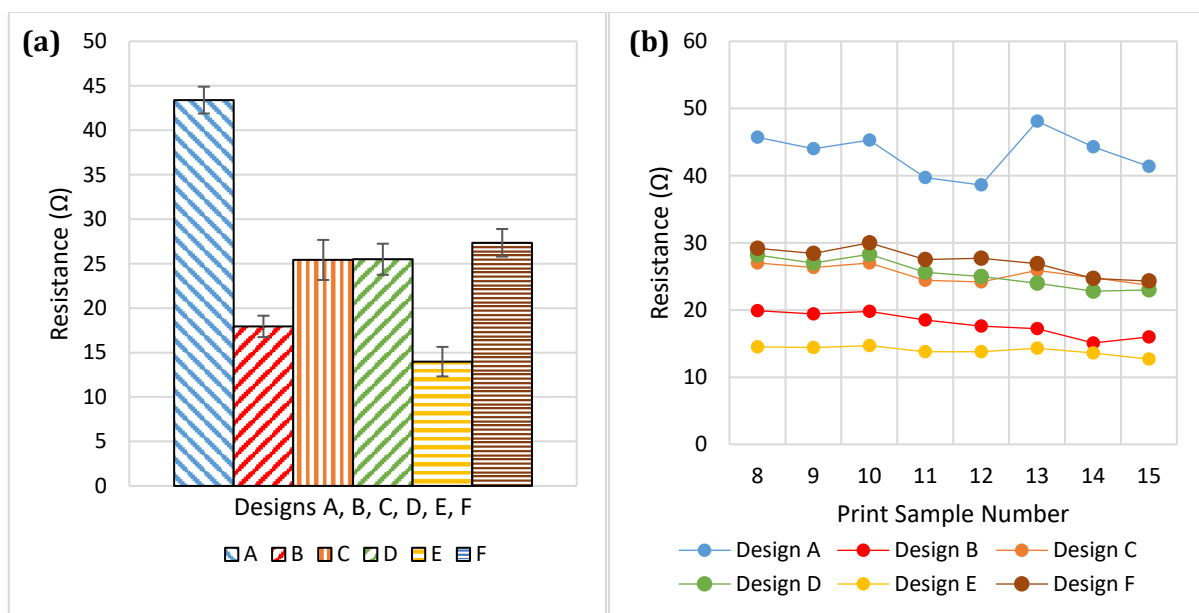


Figure 5-15 – (a): Resistances over print time for six designs of different line widths and line lengths. Error bars show 1 standard deviations. (b): Resistance changes over print time for six designs of different line widths and line lengths.

5.3.4.1 Resistivity

The ink manufacturer, Novacentrix, states achievable volume resistivity as 5-7nΩm. The volume resistivity, which is the resistance to current through the body of the material as opposed to the surface, in this experiment will be higher as the track is thinner yet much longer than the typical commercial test area. Figure 5-16 shows the resistivity values calculated for designs A, C, D and

E. Although lines increase in width from A, C and E, the resistivity does not follow the expected pattern of decreasing as the line increases. Design C increases in resistivity.

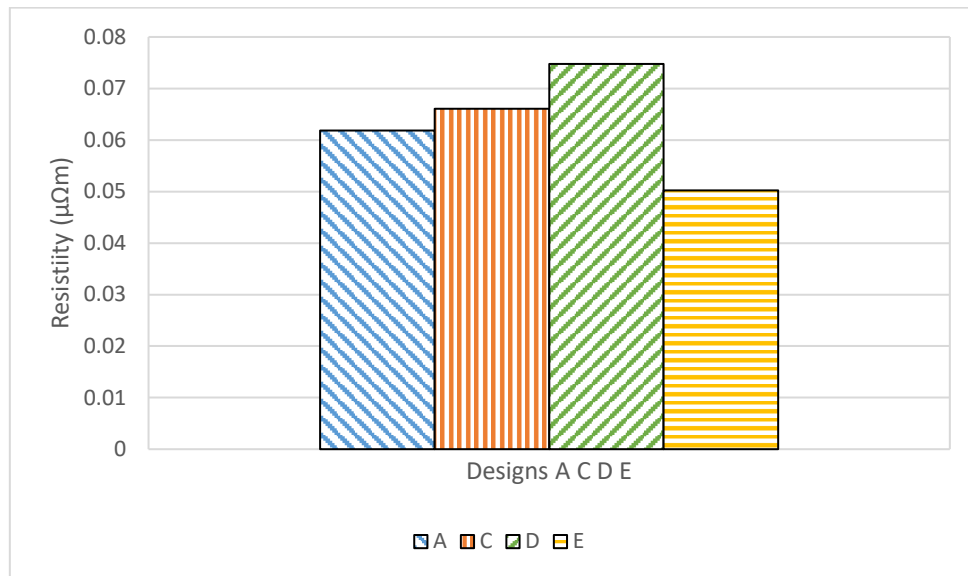


Figure 5-16 – Resistivities for four designs: A, C, D and E.

A rheological study of the degradation of the ink was carried out by measuring the viscosity of batches of the PFI-722 ink: one of approximately 1 year old, and one newly purchased batch (Figure 5-17). Throughout initial print trials, the Novacentrix PFI 722 ink visually showed a significant increase in viscosity over time. The manufacturers data is in Table 5-1. The older ink was found to have a much higher viscosity due to solvent loss after each use of the pot. This test demonstrated the importance of having a newly manufactured ink. This could also be compounded by batch-to-batch variation caused by variations in the raw materials and the manufacturing tolerances.

For both inks, viscosity is lower on the return sweep due to structural formations in the ink as a shear is applied by the rheometer. A second frequency sweep followed the same forward and return path on the graph. This signifies flow alignment after a single viscosity sweep from a shear rate of 0.01 to 1000s⁻¹.

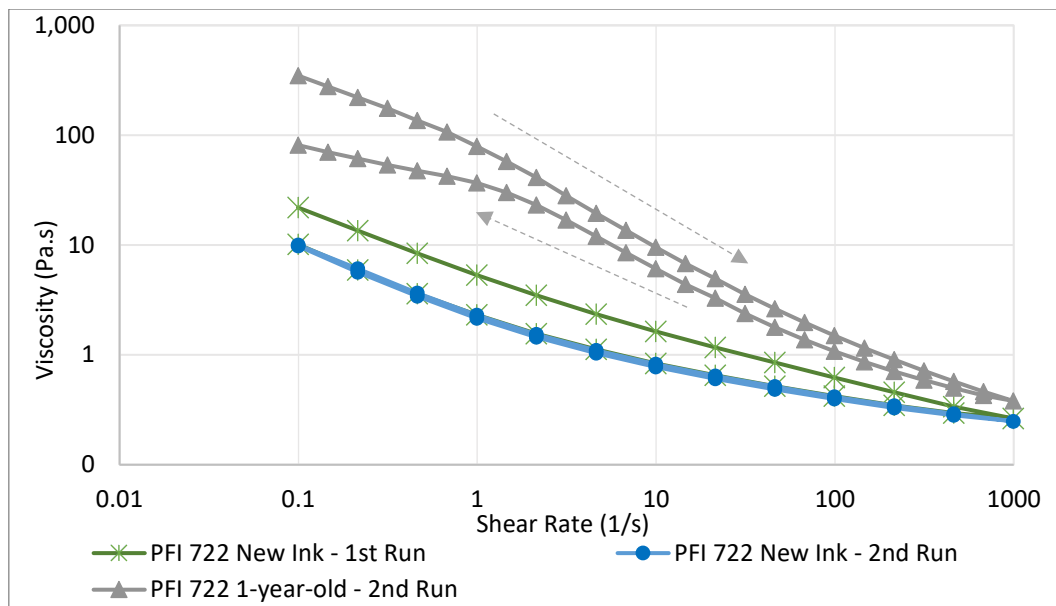


Figure 5-17 – Log-log graph of viscosity against shear rate for a newly manufactured and a 1-year-old Novacentrix PFI 722 ink. Grey arrows indicate direction of 1- year old ink.

5.4 Effect of Print Process Parameters on Print Quality

The effects of anilox volume, print speed and drying conditions on the resistance and geometry of a print track were investigated. Through control of the print variables, print defects such as line gain, pin holing and filling-in can be minimised to lower resistance and produce prints with clean and defined features.

5.4.1 Effect of Anilox Roll Volume and Print Speed on Print Outcomes

A series of prints were analysed to determine the effect of anilox volume and print speed for a 0.5mm line width. A full factorial study using anilox volumes between 8, 14 and 24 cm³/m², and print speeds between 20, 50 and 80m/min was carried out.

The meandering track shown in Figure 5-18 was used.

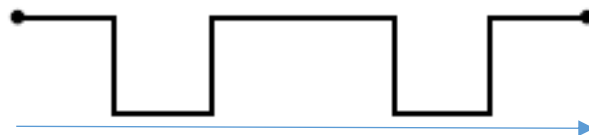


Figure 5-18 – Print design with arrow labelling print direction. Arrow will enter printer last.

It was observed that print width decreases for increasing print speed [Figure 5-20 (a)] for all anilox cell volumes. For each increase in anilox volume, there was an increase in line width. The smaller anilox size means that there are more cells on the surface of the anilox. More cells mean

that there is less ink extracted. Figure 5-19 shows an illustration of the cross-over of raised printing plate images and the anilox cells. Wide cell openings allow more ink to adhere to the print plate and transfer to the substrate.

Finer plate features cover fewer anilox cells. When the line only partially covers an anilox, the viscous forces can hold the ink within the anilox if there is not enough printing plate area covering the cell. This effect is reduced when using a higher anilox line count (Figure 5-19). Wider lines fully cover more anilox cells and have a stronger ink extraction from these, causing rougher line edges. Good surface adhesion to the printing plate can enable the printed tracks to draw ink from cells that are only partially covered. Strong inter-particle forces within the ink can assist in drawing more ink from these partially covered cells. This excess ink is then squeezed out when the printing plate track connects with the substrate. The larger the anilox openings are, the more ink transferred to the printed track and hence more ink squeezed out, creating larger line widths.

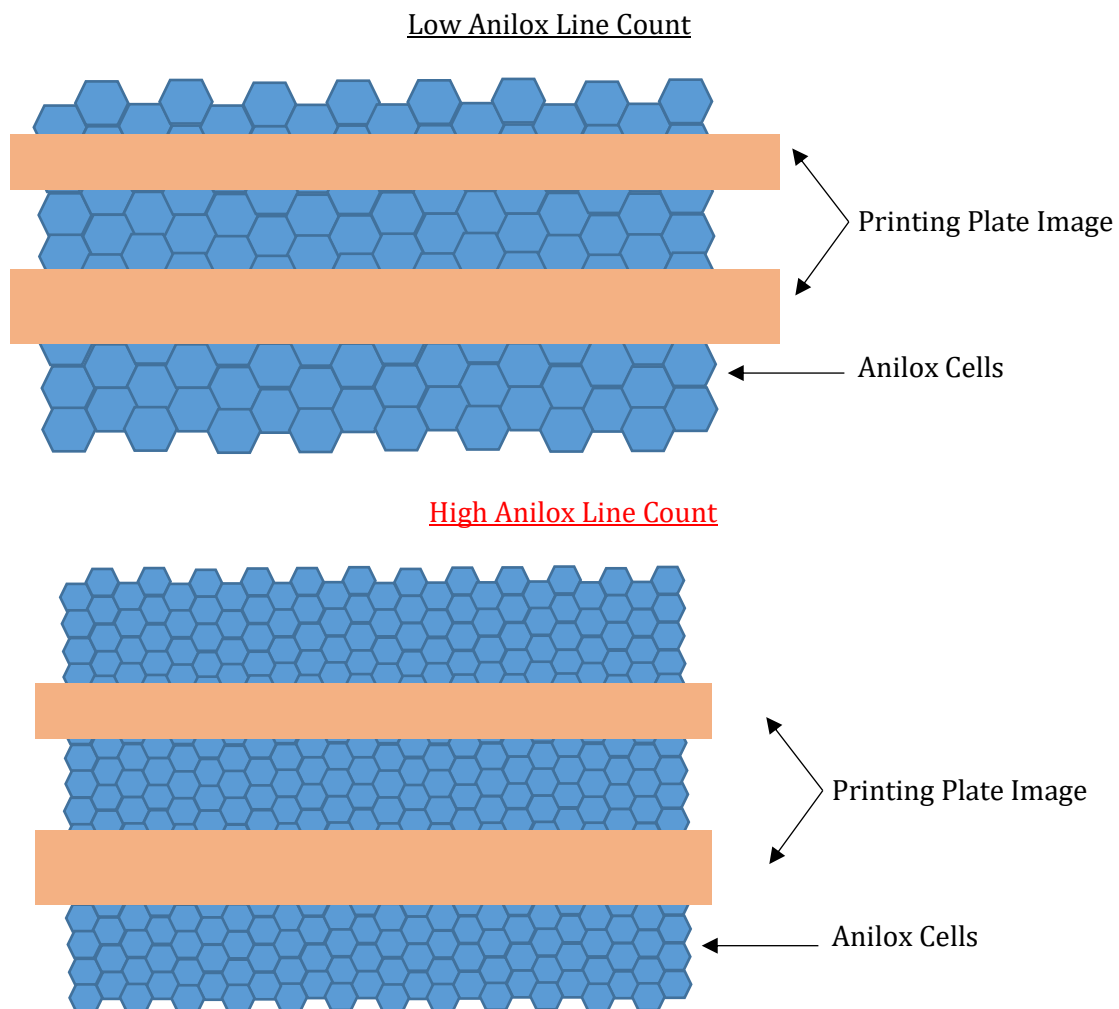


Figure 5-19 – Image of raise printing plate image overlaid on anilox surface.

The tests performed for each of the tested factors are outlined in Table 5-4.

Table 5-4 – Measured data for factors tested.

	Anilox Volume 8 cm³/m²	Anilox Volume 14 cm³/m²	Anilox Volume 24 cm³/m²
Print Speed 20m/min	Print Widths Print Thickness Roughness Resistance	Print Widths Print Thickness Roughness Resistance	Print Widths Print Thickness Roughness Resistance
Print Speed 50m/min	Print Widths Print Thickness Roughness Resistance	Print Widths Print Thickness Roughness Resistance	Print Widths Print Thickness Roughness Resistance
Print Speed 80m/min	Print Widths Print Thickness Roughness Resistance	Print Widths Print Thickness Roughness Resistance	Print Widths Print Thickness Roughness Resistance

speeds. Literature found increased anilox volume to produce tracks with larger thickness but not necessarily larger track width, and consequently increasing conductivity (33).

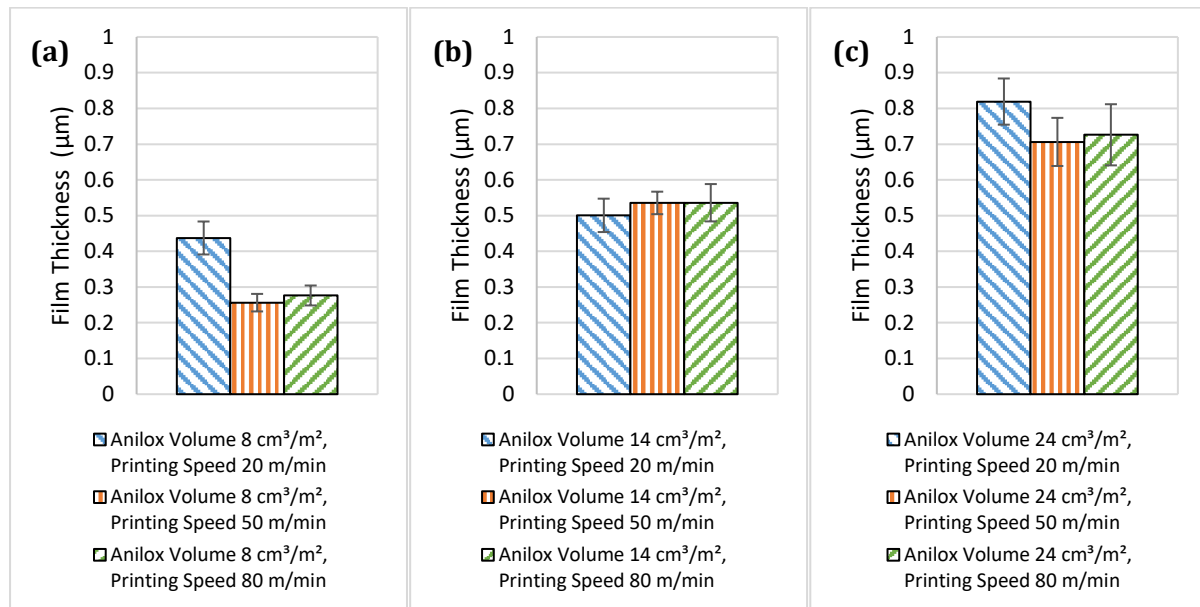


Figure 5-22 – Average film thickness of Novacentrix PFI-722 ink for: (a) anilox volume 8cm³/m² and print speeds; (b) anilox volume 14cm³/m² and print speeds; (c) anilox volume 24cm³/m² and print speeds. Error bars show 1 standard deviations.

A check on side to side variation, in support of the thickness study, is presented. Large standard deviation demonstrates large fluctuations in film thickness along the track (Figure 5-23). There is not deemed to be a statistical difference due to the large standard deviation overlap.

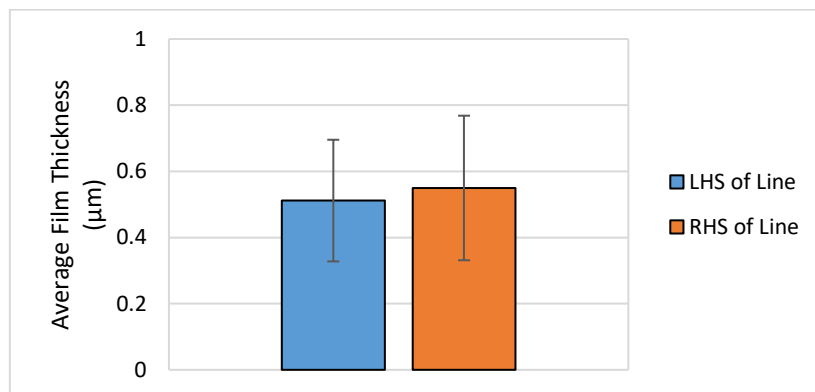


Figure 5-23 – Comparison of film thickness along print direction by taking measurements from the left (LHS) and the right (RHS) of the print. Error bars show 1 standard deviations.

For print speeds 50m/min and 80 m/min, the surface roughness increases with increased anilox volume (Figure 5-24). However, at the lowest tested speed, 20m/min, the peak surface roughness, of 479 µm, is at the middle anilox volume. For the two largest anilox volumes, the surface roughness is very similar for the lowest speed. The lowest surface roughness for the

variable tested in this print trial can be achieved using an 8 cm³/m² volume anilox at a print speed of 50 m/min. The highest surface roughness of 609 μm is achieved by using a 24 cm³/m² anilox volume and a print speed of 80 m/min. The highest surface roughness is 193.578 nm away from the average, whereas the lowest surface roughness is only 111.7 μm from the average of all results. The highest surface roughness achieved is approximately double of the lowest value produced by the settings using the highest speed and largest anilox volume.

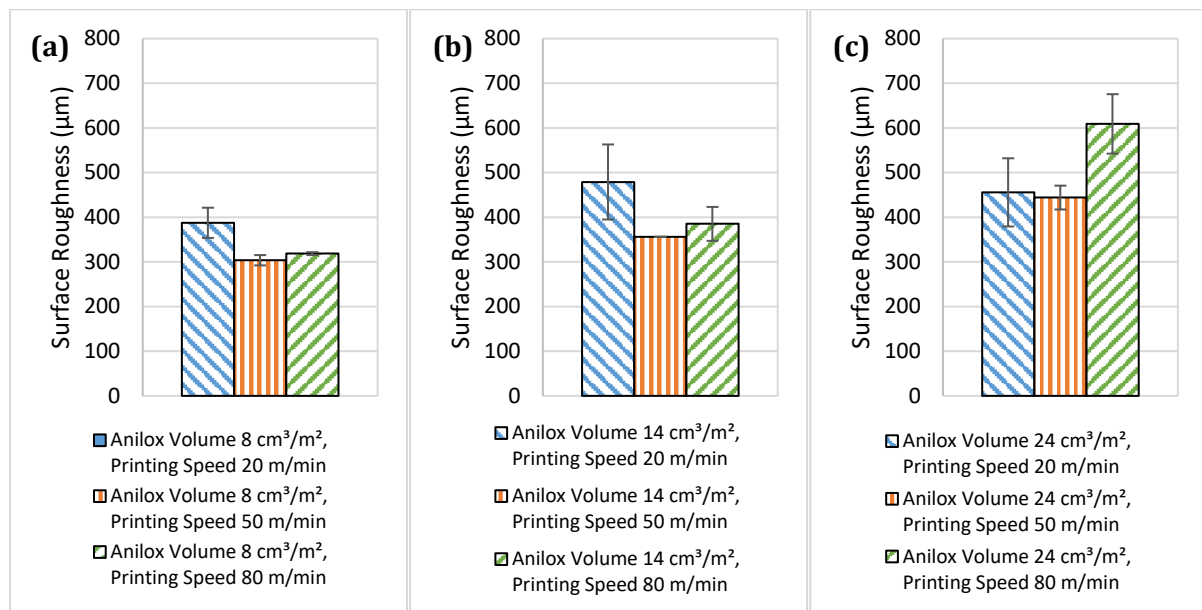


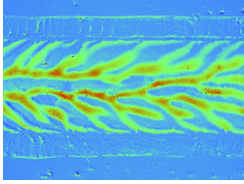
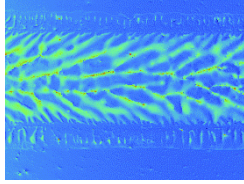
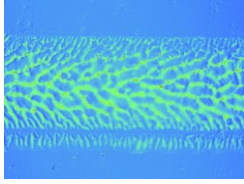
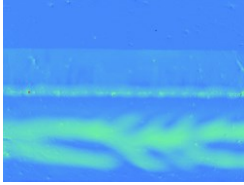
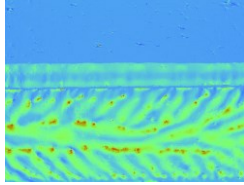
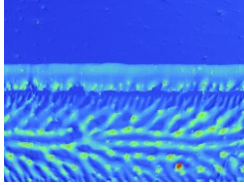
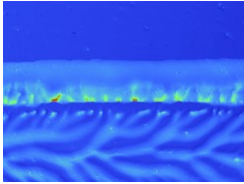
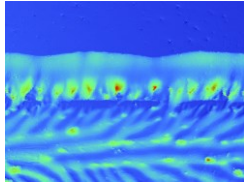
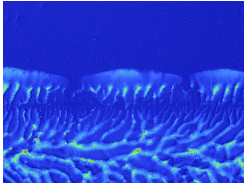
Figure 5-24 – Average surface roughness of Novacentrix PFI-722 ink for: (a) anilox volume 8cm³/m² for print speeds 20m/min, 50m/min and 80m/min; (b) anilox volume 14cm³/m² for print speeds 20m/min, 50m/min and 80m/min; (c) anilox volume 24cm³/m² for print speeds 20m/min, 50m/min and 80m/min. Error bars show 1 standard deviations.

Surface topography plots were taken using the white light interferometer to show the viscous fingering effects (Table 5-5). The images were taken on the same magnification (X 5.1) to include edge effects and hence, wider line widths produced by the larger anilox volumes are not capable of being captured in the array size. An increase in print speed results in more frequently occurring viscous fingers. Whereas an increase in anilox volume has a minimal impact but does slightly increase the density of the viscous fingers.

Peak-to-peak distances was earlier found to increase with film thickness. The relationship between film thickness and peak-to-peak distances of these features exists for that particular printer set-up. However, in these prints increasing print speed causes a decrease the peak-to-peak distances of the viscous finger effects (Table 5-5).

The edges of the print increase in width as anilox volume increases. Waviness of the edges of the print are also more prominent with higher print speeds for the 24 cm³/m² volume anilox.

Table 5-5 – Array of white light interferometry images of viscous finger effects from a print trial varying anilox volumes and print speeds.

Anilox Vol.(cm ³ /m ²)	Printing Speed (m/min)		
	20	50	80
8			
14			
24			

Scale: 1mm



Figure 5-25 shows the relationship between resistance and print speed for the three anilox volumes tested. Consistency is similar for 14 cm³/m² and 24 cm³/m² but lower for 8 cm³/m² which is likely due to a greater number of defects in the printed tracks. For the lowest anilox volume sizes, an increase in print speed causes a rise and then a decrease in resistance. There is little variation for print speed when the largest anilox volume is used. For all print speeds, the resistances decrease with increasing anilox volumes. These are distinct changes as the standard deviations do not overlap.

More silver particles create more pathways for electricity to pass through assuming that silver particles are evenly distributed throughout the ink. If more ink is being deposited, the resistance will decrease. Hence, a lower resistance will be indicative of a higher volume of ink, albeit not the only possible cause. This correlates with what has been found in these experiments. Print widths and print thickness increase with anilox volume, hence more ink being deposited. This correlates with results found in literature (33). This translates into lower resistance (Figure 5-25).

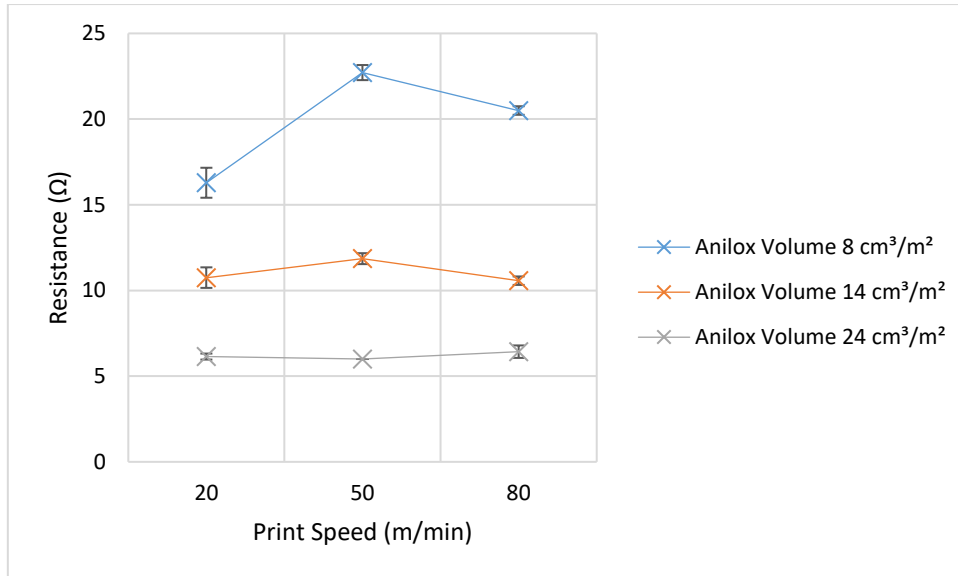


Figure 5-25 – Average print resistance of Novacentrix PFI-722 ink for anilox volumes 8, 14 and 24cm³/m² at print speeds 20m/min, 50m/min and 80m/min. Error bars show standard deviations.

Resistivity is highly reliant on the extent of change in each of the three components that contribute to the resistivity value: resistance, cross sectional area, and line length. These have been presented.

The calculated resistivity values are presented in Figure 5-26. Consistent trends cannot be drawn from the graphs between resistivity to print speed and anilox volume. Results all lie between 0.24 and 0.32μΩm, which shows good consistency for the process.

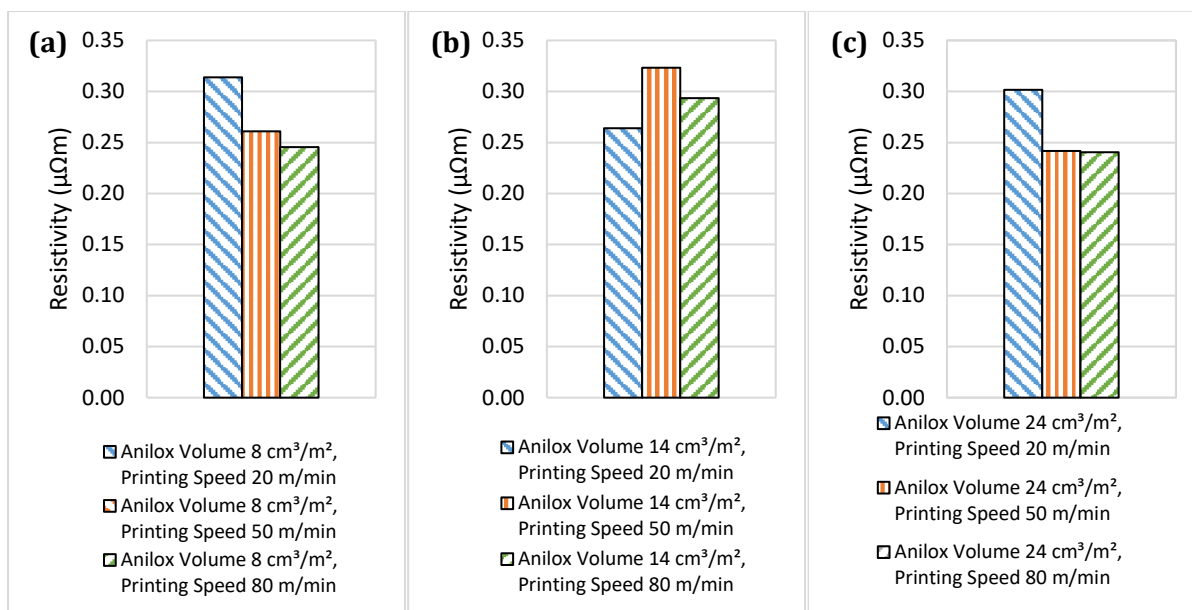


Figure 5-26 – Average print resistivity of Novacentrix PFI-722 ink for: **(a)** anilox volume 8cm³/m² for print speeds 20m/min, 50m/min and 80m/min; **(b)** anilox volume 14cm³/m² for print speeds 20m/min, 50m/min and 80m/min; **(c)** anilox volume 24cm³/m² for print speeds 20m/min, 50m/min and 80m/min.

5.4.2 Discussion

Experiments in the first section of this chapter have provided benchmark values for a commercial, nano-silver, water-based flexographic ink, selected from preliminary testing of two commercially available silver inks. The second section presents a full factorial anilox volume and print speed experiment.

Resistivities achieved were three orders of magnitude higher than stated on the manufacturers data sheet for the ink. It is likely that this is due to the ink having deteriorated in its container over time. Ink making is a small volume process compared to other chemical manufacturing and frequently has to purchase materials such as resins and nano silver on the spot market where there can be significant batch to batch variation. Additives are also used to adjust performance. Therefore, more control is required to get a better understanding of the relationship between ink physical characteristics and printability.

Resistivity decreased between the 0.5 and 1.5mm width lines. The lowest resistivity of $5 \times 10^{-7} \Omega m$ occurred for the widest line width, which is an order of magnitude higher than the commercial ink specifications. Average resistance values for designs A (0.5mm track width), C (1mm track width), and E (1.5mm track width) are 43Ω, 25Ω and 14Ω, respectively. This is roughly proportional to the change in width. Designs B (128mm track length), D (142mm track length), and F (182mm track length) have average resistances of 18Ω, 26Ω and 27Ω, respectively. Tests were repeated but there may be an anomaly in these results, which could be due to a defect

in the prints. The change in length after 142mm has a minimal impact on the change in resistance in comparison to the change between designs B and D. Line width has a higher impact on the resistance than the line length within the range used because the relative change in length was far smaller than the relative change in width. This is an important factor to consider when printing onto small areas. Small standard deviations are shown for both line widths and film thicknesses. The impact of changes in track length and width are shown to increase volume and hence reduce resistance for longer and wider tracks.

5.4.2.1 Effect of Print Process Parameters on Print Quality Discussion

There is a slight increase in film thickness and surface roughness during the print run, which could be due to the open ink tray in the flexographic printer, leading to loss of solvent and, hence increasing the viscosity. This could affect ink relaxation once ink has been transferred to the substrate with ink holding its form once deposited. As a result of measuring the distances between peaks in the viscous finger effect, the effect was more spatially frequent for lower film thickness and sparser for high film thickness and surface roughness.

For tracks in line with print direction, line widths increase marginally over the length of the printed track. Variations across the print for line widths will shape the readings taken in future experiments, meaning that three readings across the printed tracks will be averaged to account for any variations. Spreading can be included in the design if it is an important parameter.

Volume of ink is highly correlated to the resistance, and spreading is demonstrated in the widths measured. Figure 5-27 shows resistance against film thickness for design C and there is no correlation between film thickness and resistance. This does not align with other published data and requires further work.

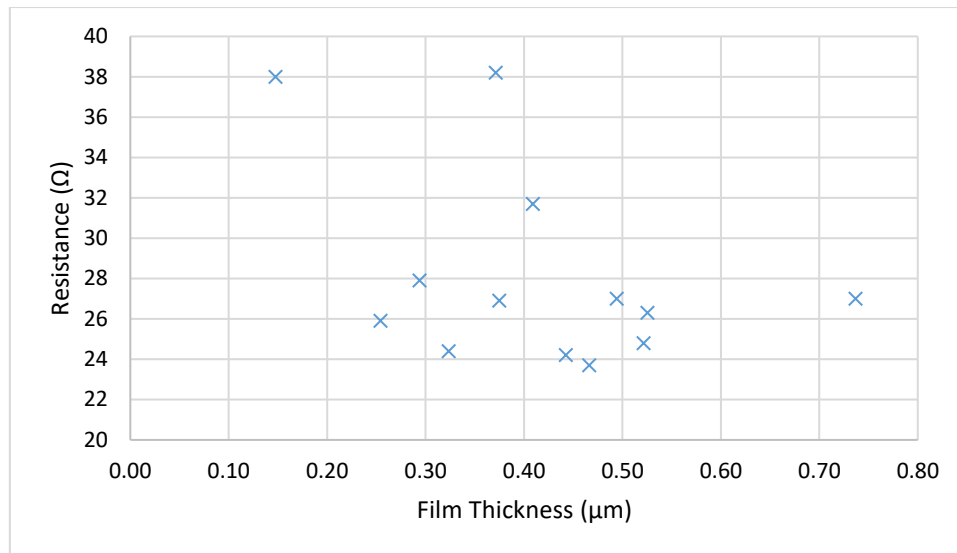


Figure 5-27 – Resistance against film thickness for design C.

Volume of ink transferred through the printing process is highly dependent on several factors, already outlined in the literature review including roller engagements. This is a critical parameter to control for sufficient ink transfer. Roller engagements were initially determined by a kiss-contact method whereby the rollers are engaged to the point at which a complete print is produced. However, the rollers will not be engaged any further than this point. An investigation is later conducted in 8.2 Effect of Press Engagement to verify this method or identify the best engagement settings. However, the pressure was maintained constant as the speed was increased for a given anilox volume so the impact of speed can be observed.

The full factorial experiment in the second section found optimal printer settings and developed fundamental understanding of the underpinning science. The ink achieved a resistivity of $619\text{n}\Omega\text{m}$ in the initial experiment and through optimisation of print speed and anilox volume, the resistivity of the same line length and width was reduced to $240\text{n}\Omega\text{m}$.

The expectation was that as print speed increased, volume of ink transferred to the substrate decreased and hence resistance increases (63)(183). However, lowest resistivities are achieved using higher print speeds of 50 and 80 m/min and using the largest anilox size of $24\text{cm}^3/\text{m}^2$. This could be because of the large anilox cell volume and that it is easier to withdraw ink from large cells as smaller cells provide more resistance to extraction (78). The lowest resistances are achieved by using the largest anilox cell volume. For the smallest anilox volume there is an increase in resistance with increased print speed. A. Hamblyn theorised that the doctor blade is being deflected during anilox cylinder rotation and this effect increases with print speed, causing a gap change. This could cause more ink to pass under (78). Additionally, high print speeds were expected to reduce ink transfer due to reduced dwell time. Results in this thesis do not align with

this theory as more ink is not deposited (in terms of print width and thickness) with increased print speed. This could be due to different inks being used, different anilox volumes or perhaps a large sample size is required.

With increasing anilox volume, the resistance is less affected by print speed of the flexographic printer. Larger anilox cell volumes hold more ink than smaller volumes and more ink can be drawn from the cells, as with larger cells, the area of the cell opening expands beyond the line image (Figure 5-19). The ink is drawn out due to tensile forces within the ink and transferred to the plate, resulting in greater film thickness and widths. Some excess ink is shown to be outside of the printed tracks. The lowest surface roughness was produced using $8\text{cm}^3/\text{m}^2$, however, the highest surface roughness was produced by the $24\text{cm}^3/\text{m}^2$ anilox cell volume.

There is significant discrepancy between designed plate track width and achieved printed track width. White light interferometer images show spreading effects that show a minimum of $200\mu\text{m}$ of spreading for all anilox volumes and speeds. Increased anilox volumes increase line widths and have a significant impact on the line widths. Larger anilox volumes have larger surface openings, from which more ink is drawn from the anilox cell by the printing plate. Excess ink from over extraction from the printing plate partially covering cells delivers higher amounts of ink to the substrate and hence increases line width.

Regarding printing defects, the density of the viscous fingering effect, described by its peak-to-peak distance (lower peak-to-peak distances meaning higher density of effect), was seen to decrease with increased film thickness and decrease in density for a lower print speed. The relationship between decreasing viscous fingering density for increased film thickness was not found, indicating that this is print parameter dependent. If the printer parameters are changed, these could have an overriding effect on this print defect. When comparing the range of viscous fingering densities against resistance of the track, there appears to be little effect of viscous fingering density on resistance, meaning that this defect is not significantly impacting on the conductivity of the sample. This implies there is sufficient ink deposited below the viscous fingering effects to mitigate against it and/or current is able to flow through these viscous fingers and they cause little hinderance to flow.

The values obtained in these tests will be used as a benchmark for the model inks.

It is important that these correlations between print parameters and print outcomes are linked with the application performance. The points at which the antenna resonates are important in terms of the strength of the signal. As discussed in Factors Affecting Antenna Performance there are numerous contributing factors in producing a good antenna. Deposition of ink is one key

factor; hence links will be analysed between print outcomes and antenna performance later in this thesis.

As the viscosity is critical for the ink release process, this is investigated further in Chapter 7 where a model ink is developed and then printed in Chapter 8.

5.5 Substrate Optimisation

The effect of substrate on print quality has been analysed.

In one study, the effect of time on resistance of the printed track for a transparent, biodegradable Eco Craft cellulose 30 μ m film (184) and a HiFi Industrial Film SU 320 PET 175 μ m thick (185) has been analysed. These were chosen for their flexibility, smooth surface and chemical stability. The HiFi film was chosen for its thermal stability also.

5.5.1 Effect of Substrate on Track Conductivity and Ageing

Preliminary experiments indicated that printed silver tracks changed over time. An investigation into this effect is presented. Resistances were measured for printed tracks of the Novacentrix PFI-722 silver ink at three points during a 12-week period for two different substrates to determine whether there are any longer-term changes in the performance of the printed track. Resistance readings were taken a day after printing, then at 6-week intervals for 12 weeks. Results are shown in Figure 5-28.

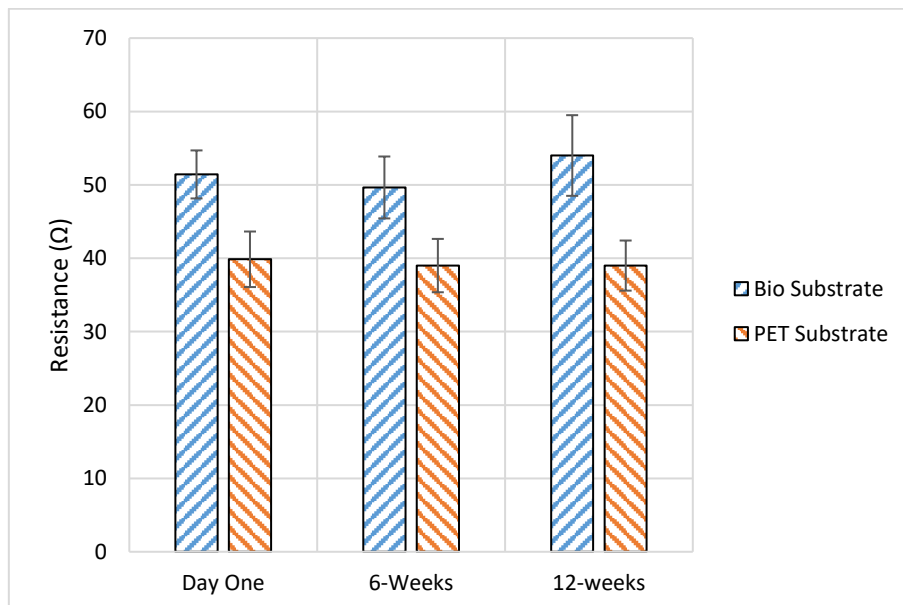


Figure 5-28 – Resistance changes over print time for Novacentrix PFI722 silver onto bio substrate and PET substrate. Error bars show 1 standard deviations.

5.5.2 Discussion

PET substrate showed higher consistency over time in terms of resistance than the bio substrate. There is a higher resistance overall in the printed track on the bio-substrate than the PET, however, there is no significant change over time. The changes that do exist are smaller than the inherent variability (standard deviation) so are not statistically significant. Differences between the PET and bio-substrates could be due to porosity, surface roughness or additives in substrates, which would require further testing but not covered in this thesis.

5.6 Effect of Ink Drying Temperature and Duration on Printed Silver Tracks

The heating cycle selected for experiments thus far was as per the manufacturer's recommendations. The effects of temperature and duration of heating were investigated to establish whether the manufacturers recommendations are most appropriate.

A heating study was conducted, analysing four temperature intervals from 90 to 180°C, and four time intervals from 5 to 20 minutes for the adapted monopole design C in Figure 5-6. The Vötsch VTL 60/90 Oven was used due to its higher temperature range and good environmental control. All designs from Figure 5-6 were printed, although only design C were measured. Experimental setup is outlined in Table 5-6. Higher temperatures than 180°C were not used due to the limits of the substrate stability. The impact on resistivity, resistance, line width, surface roughness and film thickness were investigated.

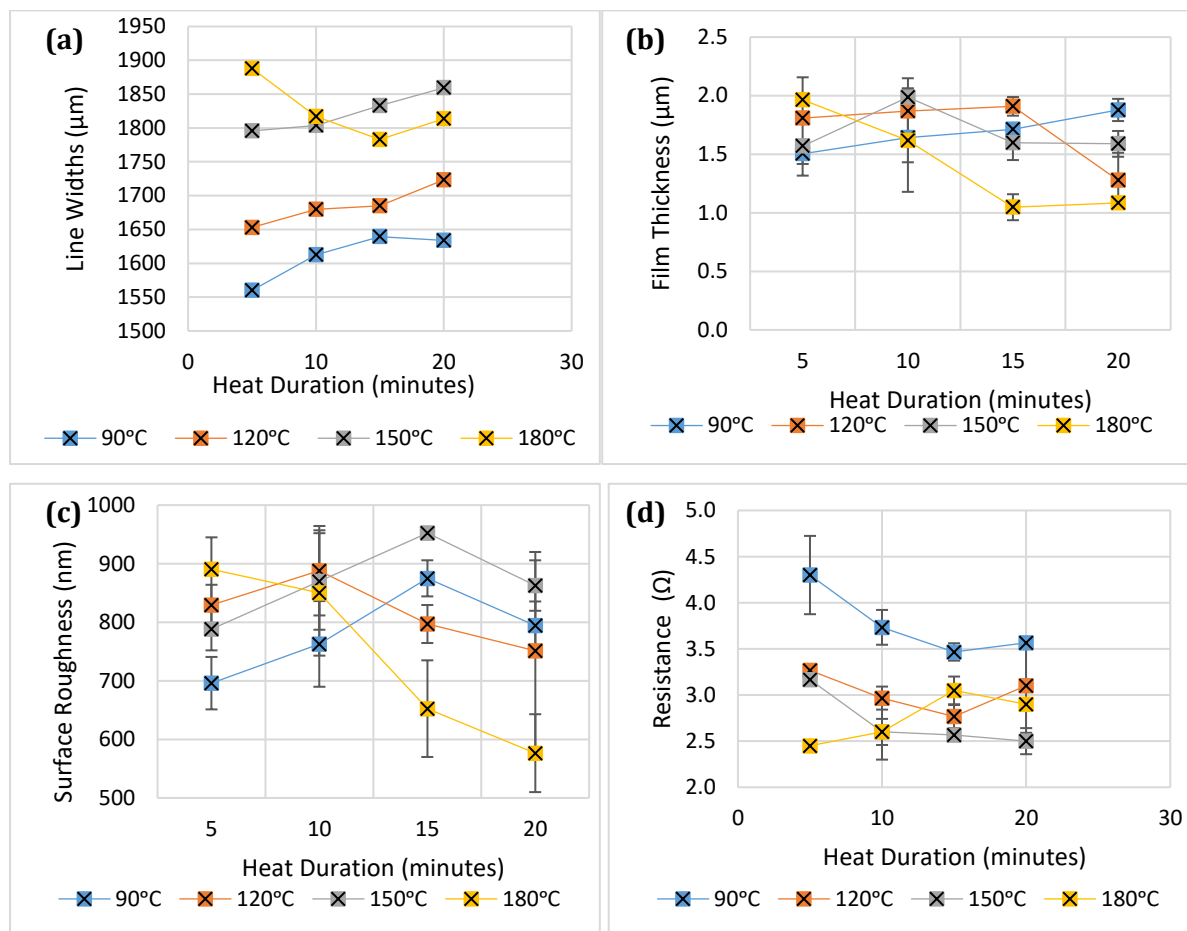
Table 5-6 – Print and oven settings used for the heat study.

Printer	RK Flexiproof 100
Ink	Novacentrix PFI 722
Substrate	175µm PET
Anilox Volume	24 cm ³ /m ²
Backing Tape	E1120
Print Speed	50 m/s
Engagement Setting	260µm, 320µm
Drying Method	Vötsch VTL 60/90 Oven

There is a general trend in Figure 5-29 (a) that line widths increase with increasing temperatures up to 300 µm. There is a slight fluctuation with time in the samples heated at 180°C as they decrease before increasing after 15 minutes. The other three temperatures tested show an

increase in line width for length of time heated. Increased time and magnitude of temperature increase the energy within the printed track. Increased energy leads to increased particle interactions and movement, and decreased viscosity, causing spreading of the ink on the substrate. If there is spreading, the printed track profile would change, causing loss in print height. This is only the case for two of the temperatures tested.

After 1 minute of heating, the sample demonstrated a heating pattern (Figure 5-30). There are bands across the image, signified by arrows that show a pattern in which the sample dries. The sample is placed on racking within the oven, and it is in these locations that the ink begins to dry initially. The pattern in which these samples have dried could lead to added waviness of the sample. A flat tray could be used to mitigate this effect. Some variation in line widths could be due to distortions in PET substrate at high temperatures and drying effects on the ink.



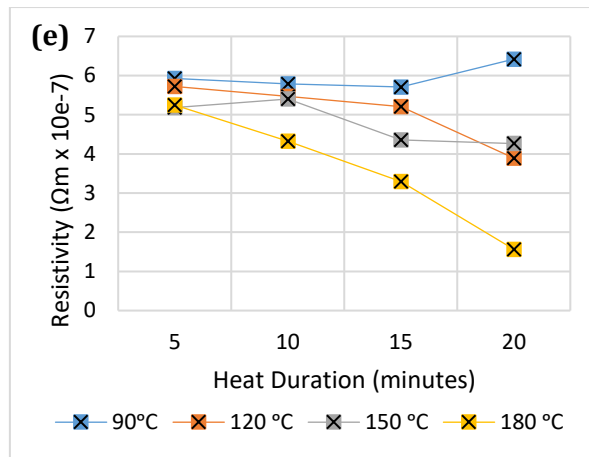


Figure 5-29 – (a) Track width measurements for four temperatures at four distinct heating intervals. (b) Film thickness measurements for four temperatures at four distinct heating intervals. (c) Surface roughness measurements for four temperatures at four distinct heating intervals. (d) Resistance measurements for four temperatures at four distinct heating intervals. (e) Resistivity measurements for four temperatures at four distinct heating intervals.

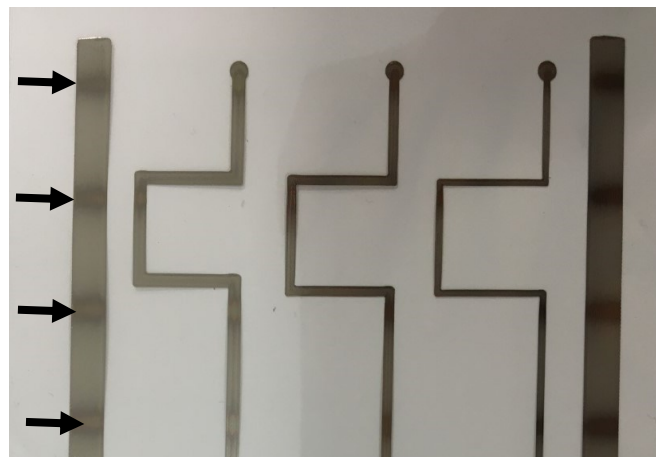


Figure 5-30 – Drying pattern after one minute.

Figure 5-29 (b) shows print thickness against heat duration for four drying temperatures. At a time interval of 5 minutes, increased heating temperature demonstrated a higher film thickness. However, as heat duration was increased to 20 minutes, increased temperature generally reduced film thickness. Longer heat duration encourages more solvent to leave the printed track and particles to fill gaps where solvent has left thus reducing overall thickness of print.

For a heat cycle of 5 minutes at 90°C, film thickness is at its lowest measured value of 1.5 μm. For the highest temperature, 180°C, used at this time interval, the film thickness was at a maximum of 2 μm. For increasing heating time, the reverse occurs. The lowest temperature, 90°C, achieves the highest film thickness and the highest temperature, 180°C, achieves the lowest film thickness.

Measurements for 120°C and 150°C over time do not show the same distinct pattern and film thickness did not change appreciably with heating duration. The reduction in film thickness for high temperature (180°C) at increasing heat duration could be due to the initiation of sintering. As sintering occurs, particles begin to deform and bond, which increases packing of the particles and film thickness reduces. There could also be substrate deformation at higher temperatures.

Up to 120°C, surface roughness peaks at 15 minutes before decreasing. This trend of increasing and then decreasing surface roughness occurs earlier in heat duration for higher temperatures [Figure 5-29 (c)]. For a heat cycle of 5 minutes at 90°C, surface roughness is at its lowest measured value of 700 nm. For the highest temperature, 180°C, used at this time interval, the surface roughness was measured to be at its highest point at 900 nm. Temperatures 90°C and 150°C show an increase in surface roughness between heating of 5 minutes to 20 minutes, whereas temperatures of 90°C and 120°C show a decline. The reduction in surface roughness for high temperature (180°C) at increasing heat duration is likely due to the initiation of sintering and would require SEM studies to confirm. If sintering occurs, particles begin to deform and bond, which increases packing of the particles and surface roughness reduces. This effect can also be seen for 120°C above 5 min heating duration. Deformation of the substrate could also be contributing to increases in surface roughness at higher temperatures.

All measured resistances reduce with temperature [Figure 5-29 (d)] apart from the print cured at 180°C for longer than 5 minutes. This decrease could be due to deformation in the substrate with long exposure to high temperatures. Print resistance decreases with increasing heat time until the 15-minute interval. There is no benefit in heating for more than 10 minutes for temperatures above 90°C. However, at 90°C there is continued benefit with longer heating duration.

The resistivities are generally lower for higher temperatures used [Figure 5-29 (e)]. For samples heated to 180°C, there is a significant decrease in resistivity with increased time in the oven. 180°C for 20 minutes, are the conditions that produce the lowest resistivity due to sintering. An SEM could be used to verify changes in silver flake interactions over the heat duration and intensity tests.

Increased heat and length of heat treatment significantly reduces resistivity of the printed tracks, which could be due to solvent further evaporated from the prints. As these are increased, the silver particles are reaching sintering temperatures, softening particles to create bonds with neighbouring particles. Solid bonds with other silver particles in the track increases electron pathways for good conductivity. Generally, higher temperatures of 150°C and 180°C achieve the

lowest resistance and resistivities due to likely sintering effects taking place. 15 minutes is the optimal temperature for achieving the lowest values. Increased temperatures cause an increase in print widths and a reduction in film thickness. High film thickness is important for good antenna signal transfer, therefore, a 150°C setting with a duration of 15 minutes is optimal for these printed samples. Longer heat durations did not provide a significant improvement in resistivity.

Longer heat cycles and increased temperatures bring the silver particles closer to the required sintering temperature. Lower resistances indicate that particles are making better connections with neighbouring particles.

5.7 Closure

The high anilox volume size, 24cm³/m², increased the volume of ink transferred to the substrate, causing greater line widths, film thickness and significant line spreading. Due to the high deposition of ink using this anilox volume, the lowest resistivities and resistances were measured.

Variations in print speed did not show any strong correlations with track width, film thickness, surface roughness or resistance. There was some decrease in print widths and print thickness for higher print speeds however, not distinct enough to agree with literature (63), where a relationship has been observed for UV inks. UV inks may not provide a good comparison but they can be indicative of behaviours present in silver inks. High print speeds of 50 and 80 m/min did produce the lowest resistivities for anilox volumes 8cm³/m² and 24cm³/m². Despite the print speed not showing any significant correlation with any of the print outcomes, it did increase the flexographic printing defect, viscous fingering.

Hence, due to their high deposition of ink for lowest resistance and resistivity, which are critical for printed track performance in antenna applications, 24cm³/m² and 50m/min are used in the following chapters.

Increased heat and duration of heating significantly reduce resistivity of print tracks. Up to 120°C surface roughness peaks at 15 minutes before decreasing. This trend of increasing and then decreasing surface roughness occurs earlier in heat duration for higher temperatures. A temperature of 150°C for 15 minutes provides an optimal heat cycle (0.43μΩm). Up to a heat duration of 10 minutes, there is little differentiation between temperatures up to 150°C. Longer heating times provide a further reduction in resistivity, however this provides little extra benefit. Temperatures beyond this value do not provide any significant improvement.

PET substrate performed best in terms of heat resistance, stability over time, and resistance of sample.

These learnings are carried forward and used to define optimal experimental parameters that provide prints with the lowest resistivity. Chapter 6 looks at how the variations in these parameters affect antenna performance and if any correlations exist to highlight areas of focus in the manufacturing process of RFID tags. Chapter 8 looks at model inks to address some of the issues of using a commercial ink including the inability to control spreading of the ink when using large anilox volumes for high ink volume deposition in flexography.

Chapter 6: Effect of Printer Parameters: Anilox Volume and Print Speed on Frequency and Magnitude of Resonant Troughs

6.1 Introduction

Chapter 5 investigated the impact of print process parameters on physical print attributes (line width, film thickness, surface roughness, resistance, resistivity). This section investigates the effect of these attributes on antenna response.

At the point of resonance, there are only resistive properties present. Print outcomes: surface roughness, print thickness and print width are critical in contributing to the resistance of a printed track and therefore have been analysed for their impact on the resonant frequency and trough magnitude.

Samples tested on the VNA machine were printed as part of the full factorial flexographic printing study in Assessment of Flexographic Process Parameters, whereby the anilox volumes and print speeds on the printer were varied. The results from testing with the VNA is shown compared with printing characterisation of the samples (print thickness, resistances, surface roughness and print width).

Resistance of printed features changed over time; hence a series of prints were measured for inductance, resistance, and capacitance, over a 12-week period.

6.2 Trough Magnitude and Corresponding Frequency for Print Parameters

Designs A and B (Figure 5-6) were tested for their antenna performance. A two-point probe, connected to a VNA, was used to measure the trough magnitudes and frequencies at which the largest trough magnitude occurred in a frequency sweep (Figure 6-1 and Figure 6-2 respectively). Three samples were measured for each print setting. In the previous chapter, inputs (machine settings) and outputs (film thickness, roughness, and resistance) were compared. The results were analysed to identify the impact from print process parameters; print speed and anilox volume. The graphs in Figure 6-1 and Figure 6-2 depict the resonant troughs. If the spiral resonators were to be detected, they would have individual resonant troughs correlating to each resonator. The profile of the frequency response did not change between antennas with and without spiral resonators and therefore they are not detectable in this method of measurement. For the design A, the frequencies are generally within small standard deviations and occur around the 600MHz point regardless of the anilox volume used. The highest print speed of 80m/min has a significant impact on the range of frequencies recorded and also the standard deviation. When

comparing these with Table 5-5, higher print speeds produce more viscous fingers correlating with a lower resonant frequency.

Design B showed low standard deviations across the graph and the lowest print speed provided the most consistent results for changing anilox volumes. Many of the settings used produce antennas resonating around 600MHz. However, there is more variability in the results compared with design A. This could be due to a higher volume of ink deposited or the corners in the design are not printed consistently, and hence more scope of variability in the results.

For the smaller line width, design A [Figure 6-1 (a)] increasing to the highest tested print speed caused a decrease in the frequency at which the highest magnitude trough. This behaviour was not repeated for the larger line width tested, design B [Figure 6-1 (b)]. The lowest anilox volume combined with the lowest print speed provide the most reliable results of all parameters tested and has low standard deviations.

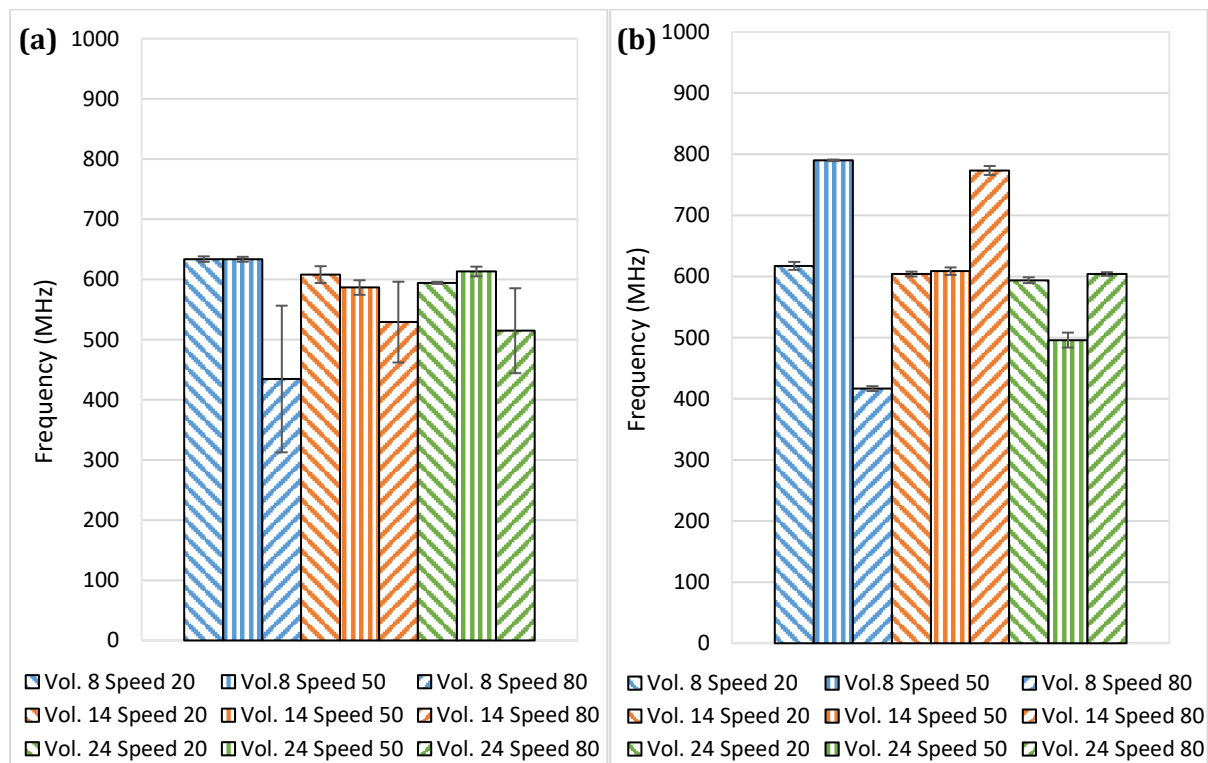


Figure 6-1 – Frequencies at the point of largest trough magnitude for design A at anilox volumes 8cm²/m², 14cm²/m², 24cm²/m², and print speeds 20m/min, 50m/min and 80 m/min. Measured using a vector network analyser. Standard deviations are shown. (a): Design A, (b): Design B.

The corresponding trough magnitudes are shown in Figure 6-2. Overall, for both graphs, the magnitudes have high standard deviation values and there is little correlation to be drawn. These are the printer settings. The lack of correlation with process parameters shows these are not a reliable way of changing the antenna signal. High standard deviation could be due to external

factors providing undesirable noise to the measurements or perhaps variability in the print itself could account for this. Print parameters may affect the magnitude of the resonant troughs however, it is not a consistent effect for any print parameter. For both designs, the low anilox volume of 8 cm³/m² and print speeds of 20 and 50 m/min produce similar results, with design B having a slightly larger magnitude. All four of these set-ups produce a magnitude with a similar frequency also, excluding the middle speed of 50m/min for design B. Design B generally sees higher magnitudes for all parameters however, errors are high for most of the results collected and hence, do not show distinct variation between many of the results.

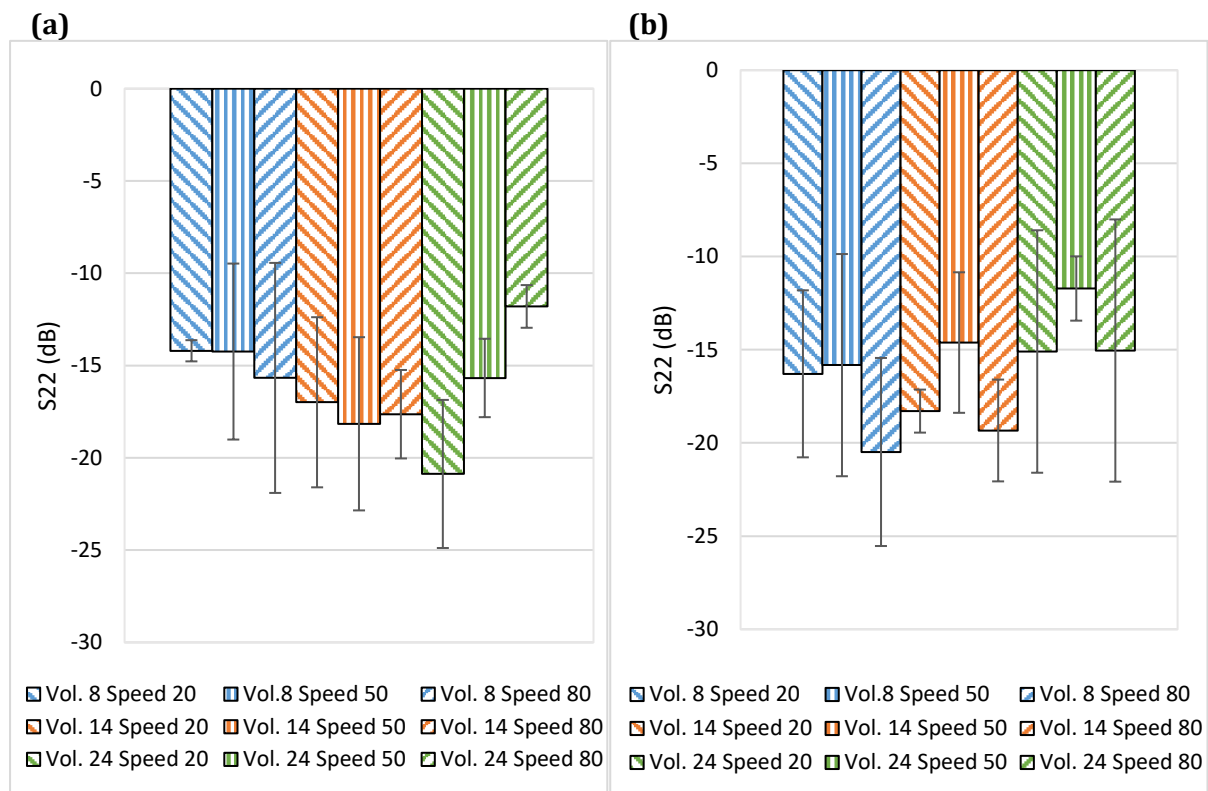


Figure 6-2 – Highest magnitude troughs recorded in the frequency sweep of 100 MHz to 1 GHz at anilox volumes 8cm²/m², 14cm²/m², 24cm²/m², and print speeds 20m/min, 50m/min and 80 m/min. Measured using a vector network analyser. Standard deviations are shown. (a): Design A, (b): Design B.

All the troughs occur at roughly the same frequency and are a function of the line length, while the variation in amplitude reflects the impact of print defects and surface effects such as viscous fingering. As induced currents start at the surface, then the latter would have most impact on the amplitude as it would create a more tortuous surface path. The performance of the largest anilox at the lowest speed reflects the additional material (thicker layer and less resistance) with reduced surface effects. This has the best and most consistent performance, the frequency remains constant, and the amplitude has a small variability. Even at 50m/min, the amplitude is still higher than most of the other anilox volumes.

The trough magnitudes and corresponding frequencies for design A previously shown in Figure 6-1 (a) and Figure 6-2 (a), are shown against one another in Figure 6-3. Outliers in these results have been removed if an inconsistent feature was observed. This graph demonstrates the operating bands in which this design works for all printer settings used. All results lie within the 570-640MHz range and -8 to -16dB, excluding the results produced by the largest anilox volume at the lowest speed.

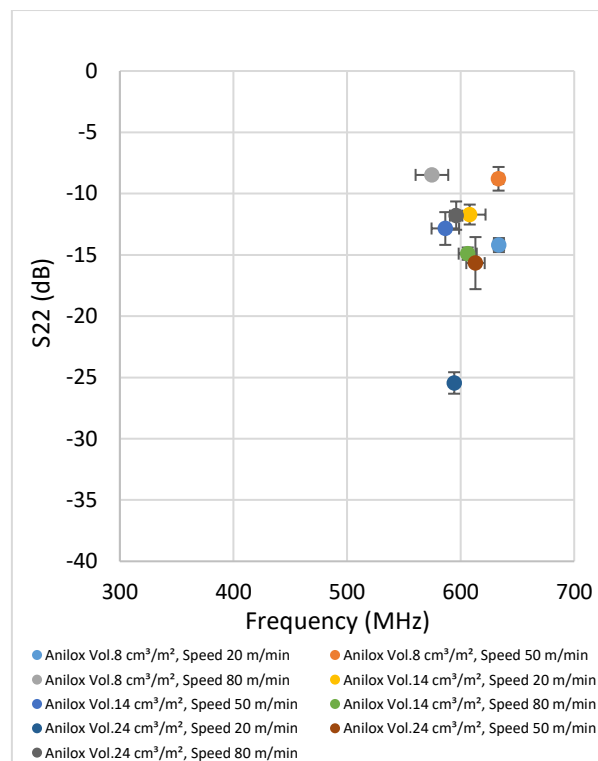


Figure 6-3 – Effect of print speed on an amplitude – frequency graph for design A at anilox volumes 8cm²/m², 14cm²/m², 24cm²/m², and print speeds 20m/min, 50m/min and 80 m/min with outliers removed. Measured using a vector network analyser. Error bars represent standard deviation.

The following graphs show frequency and amplitude against print outcomes to determine if they can have an impact on the electrical outcome of the print with reference to antenna performance. If print parameters can be used to control the outcome, then the antenna can be characterised. Characterisation of antenna behaviour can be used to encode information and consequently be used to transfer data.

6.3 Frequency at Highest Magnitude Resonant Trough Against Print Outcomes

As shown in, Figure 6-4, the average frequency obtained for each anilox volume used at each print speed ranged from 434MHz to 634MHz. There is small standard deviation error in frequency for most values, except for those at print speeds 20m/min and 50m/min for the middle anilox volumes tested.

The resonant frequencies show an increase in value as the surface roughness of the print increases and aside from one anomaly, the relationship appears to plateau after a surface roughness of 430nm [Figure 6-4 (a)]. Aside from one anomaly (8 cm³/m², 80m/min), frequency increases with an increase in resistance [Figure 6-4 (b)].

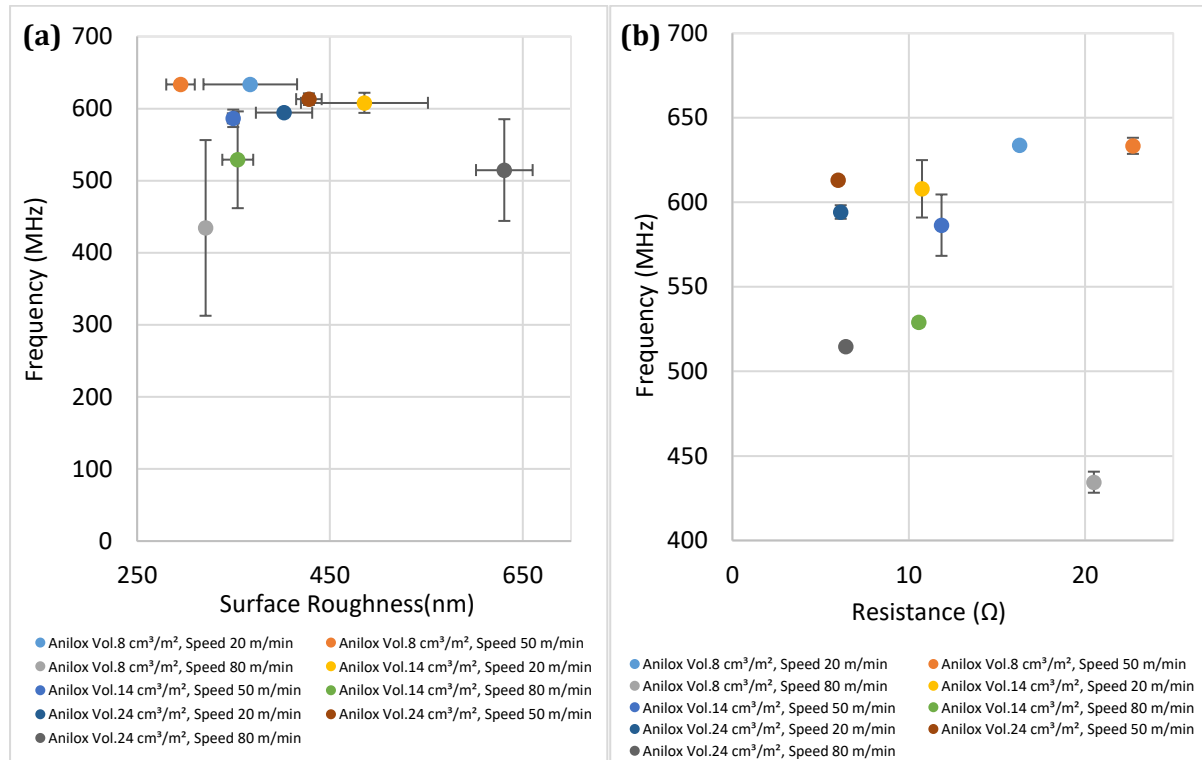


Figure 6-4 – For anilox volumes 8cm²/m², 14cm²/m², 24cm²/m², and print speeds 20m/min, 50m/min and 80 m/min, and measured using a vector network analyser: **(a)** Frequency against surface roughness **(b)** Frequency against resistance. Error bars represent standard deviation.

6.4 Highest Magnitude Resonant Trough Against Print Outcomes

Figure 6-5 demonstrates relationships between trough magnitude and print thickness, surface roughness, and surface roughness/print thickness (thin lines with high roughness highlights defects in line). Outliers were removed based on being outside of the expected range of frequency of approximately 580 to 700Hz, low signal trough magnitude and where surface roughness was larger than the thickness, indicating the track had defects.

Magnitude of the signal marginally increases with increased print thickness but increases significantly with increased surface roughness.

Straight correlations between signal magnitude and frequency with print outcomes are challenging as many parameters are changing including print thickness and surface roughness.

Samples with high roughness may be demonstrating that the lines are not fully printed and consistent. The slight decrease in S_{22} for increased surface roughness correlates with literature (186). High micro-capacitances are formed due to the nature of the printing process and particles not always touching one another, which may create anomalies in results.

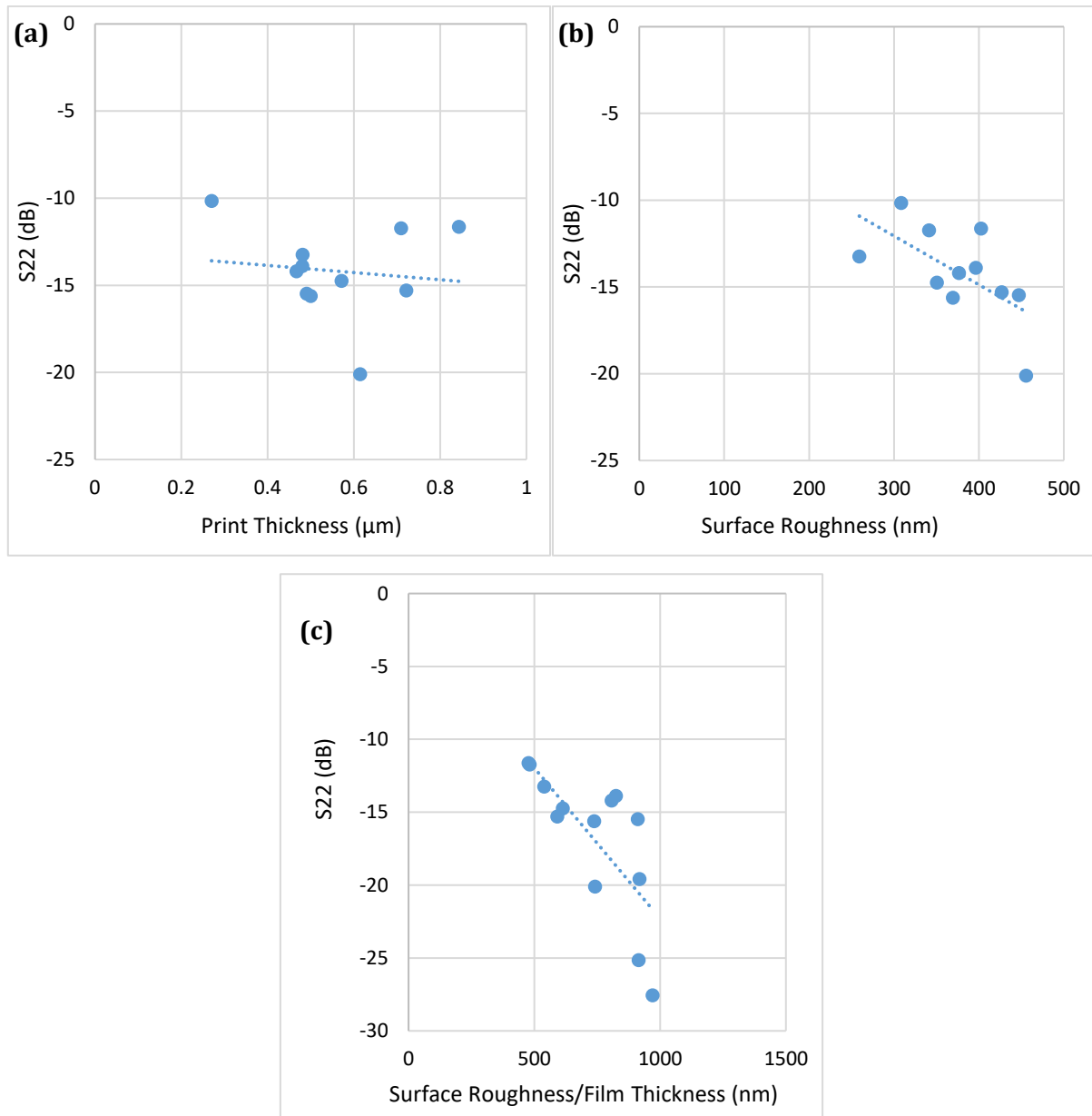


Figure 6-5 – For antenna A, S_{22} against (a) Print thickness (b) Surface roughness (c) Surface roughness/ film thickness.

Merilampi et al (69) showed that antenna performance characteristics declined as the thickness of the screen printed antenna was reduced. As the thickness of the layer decreases, the power loss increases. Despite this, thinner ink layers offer potential for cost savings where lower performance is acceptable. It should be noted that the thin ink films produced by flexographic printing make it much more sensitive to variation and print quality issues when compared to

screen printing. Unevenness in conductive layers result in high current density regions, which worsens tag performance.

6.5 Effect of Line Width and Length on S22 at Resonant Frequency

A comparison between printed line widths and lengths, and the measured peak magnitudes and frequencies was conducted to identify any correlations.

S22 values for designs, of dimensions shown in Figure 6-6 and Table 6-1, were found and presented in Figure 6-7. For an increase in antenna design length and width, there was a distinct increase in magnitude. Standard deviations demonstrate that the three designs show distinct regions in which they operate. As previously discussed, increased resistance causes a slight increase in the trough magnitude and frequency. There is a lack of correlation with print thickness and a strong correlation with increased print width. This effect is likely due to the relative increase of conductive material deposited by an increase in line width. Through the characterisation of each of the designs, some level of information can be transmitted.

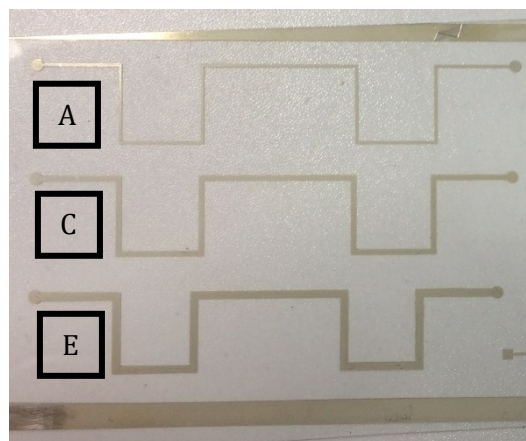


Figure 6-6 – Printed antenna designs A, C and E.

Table 6-1 – Design parameters of a plate with lines of various widths and lengths.

Line Reference	Line Width (mm)	Line Length (mm)
A	0.5	147
C	1	164
E	1.5	181

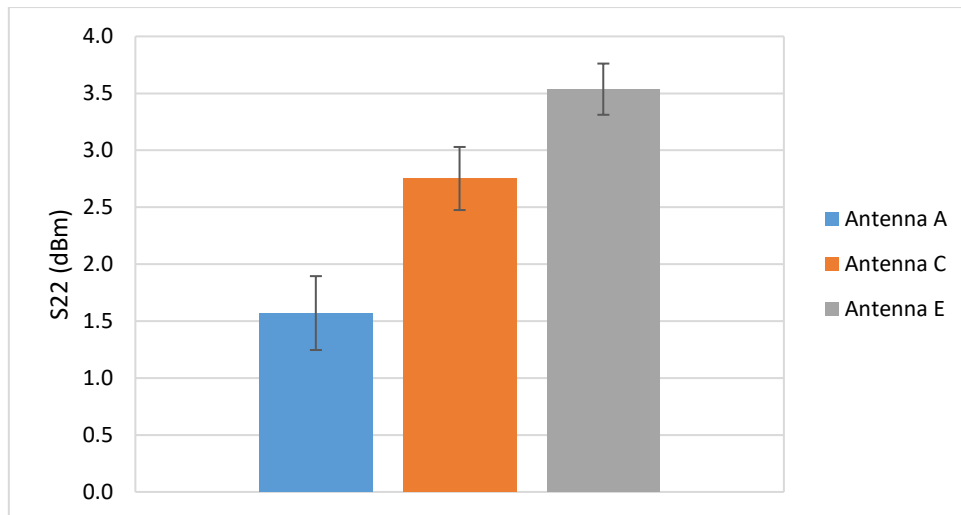


Figure 6-7 – S22 for three track designs of varying length and width. One standard deviation is shown.

6.6 Changes in Printed Line Performance on Biodegradable and PET Substrates Due to Environmental Exposure

When repeat experiments were made on the various substrates tested, it was noticed that resistances changed over time. Despite the cellulose substrates not being suitable for the silver ink, some valuable results that give more insight were demonstrated and are presented. Further investigation into electrical changes in the printed line are presented below.

Long Term Testing on PET Substrates

Using an LCR bridge, inductance, capacitance, resistance, and Q factor were all measured over a 12-week period. Resistance remains consistent over the period, however; capacitance and inductance values decrease and increase respectively. The overall effect reduces the Q factor from 0.00193 to 0.00086, both of which are incredibly small values for a high-performance antenna. Continual solvent evaporation and some additional sintering could also contribute to this change in value. Graphical representation of the results and further discussion is presented in Effect of Line Degradation on Resistance, Capacitance, and Inductance due to Environmental Exposure.

Resistance, Capacitance, and Inductance Testing on Biodegradable Substrates for Comparison with PET

PET substrate has been used throughout this work; however, a study was conducted on the effect of a cellulose-based flexible biodegradable substrate Eco Craft 30 μ m thick on the performance of the ink with regards to antenna performance. The PET substrate measured a resistance 15 Ω lower than the bio-substrate. There were significant differences between capacitance and inductance. Overall, the Q factor was higher for the PET substrate implying better antenna

performance is achieved on the PET substrate. Despite the PET having a higher Q-factor and a lower resistance, the Q-factor is still extremely low for this application and the resistance is relatively high.

6.6.1 Effect of Line Degradation on Resistance, Capacitance, and Inductance due to Environmental Exposure

An investigation was conducted into the changes in resistance, capacitance, and inductance over a 12-week period.

Initially, resistance and Q factor were measured using an LCR bridge, as they give an indication of the print quality and antenna performance, respectively. An applied frequency of 10kHz was used as the LCR and Q factor values are of different values when AC are used. After the initial six weeks of atmospheric exposure, a second set of measurements were taken. These showed a decrease in the average Q factor values whereas, the resistances varied marginally in comparison. The reduction in resistance could be due to oxidation of the silver ink.

This led to further investigation of the three parameters that construct the Q factor value: resistance, capacitance and inductance. The capacitance and inductance were measured and then, after another six weeks period had elapsed, all four variables were measured. The results are shown in Figure 6-8 and Figure 6-9.

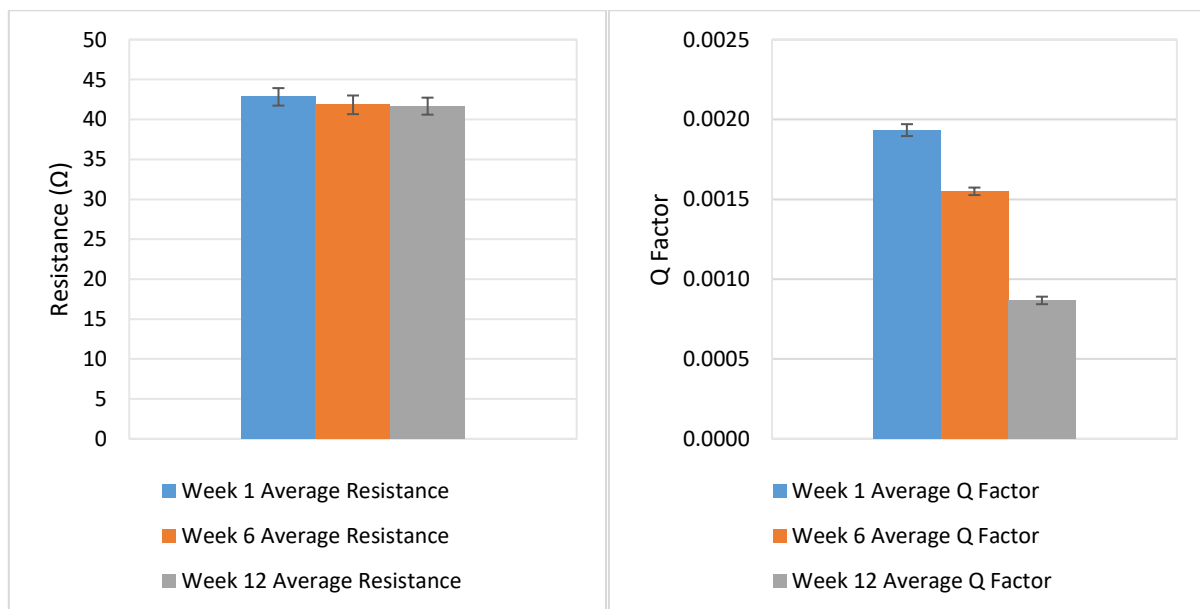


Figure 6-8 – Average resistances and Q-factors measured over 6-week intervals for printed Novacentrix PFI722 nano-silver ink onto PET substrate.

It is evident that there are changes occurring in the printed samples from looking at Figure 6-8, although the resistance values remain consistent over the 12-week period. The capacitance and inductance changes for the second 6-week period are shown in Figure 6-9.

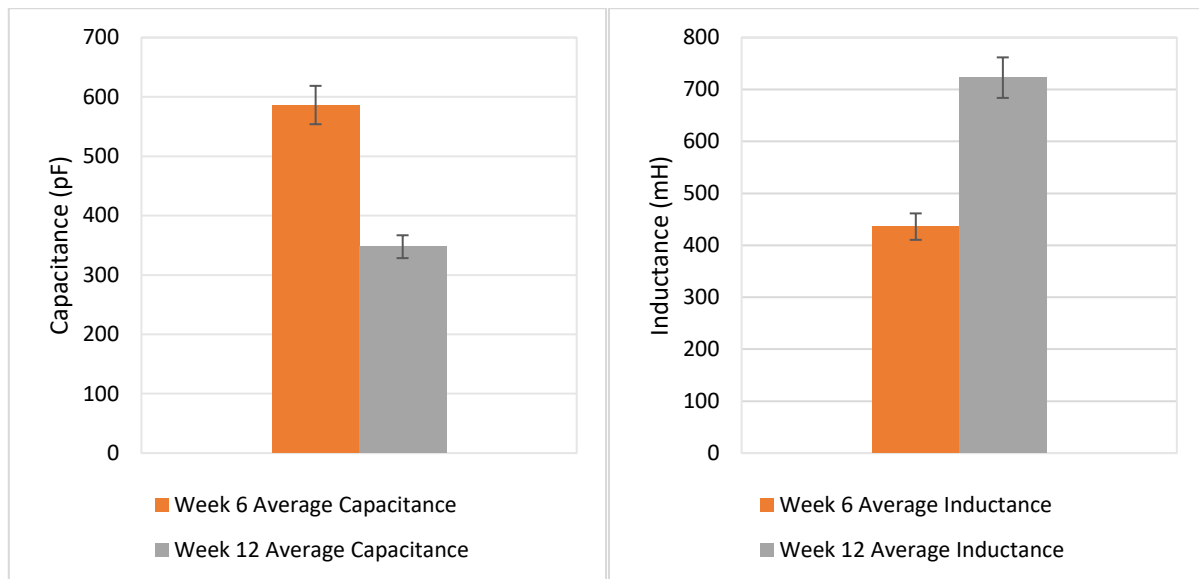


Figure 6-9 – Average capacitance and inductance measured over 6-week intervals for printed Novacentrix PFI722 nano-silver ink onto PET substrate.

The degradation in the ink over time is evident and aligns with literature (187) regarding the tarnishing nature of silver, proving the requirement for coating the printed tracks to hold consistency in the print over time.

For the PET substrate, capacitance dropped by 41% between six and twelve weeks of being exposed to the atmosphere after printing, and the bio substrate print had a greater drop of 47%.

For the PET substrate, inductance increased by 69% between six and twelve weeks of being exposed to the atmosphere after printing, and the bio substrate print had a higher increase of 96%. The overall effect of the increase in inductance and decrease in capacitance, results in 43% drop in Q factor for PET and a 50% drop in Q factor for the bio substrate. Comparisons of the changes, by percentage, for the resistances and Q Factors are shown in Table 6-2.

Table 6-2 – Comparisons of resistance and Q Factors over a 12-week period for two substrate types.

	PET Substrate		Bio Substrate	
	Resistance	Q-Factor	Resistance	Q-Factor
Week 1 atmospheric exposure	- 2.0%	- 19.8%	- 7.3%	- 15.8%
12-week atmospheric exposure	- 1.7%	- 54.7%	- 3.9%	- 60.4%

There are greater changes in resistance for the biodegradable substrate, meaning it is less stable. The Q-factor significantly decreased by over 50% for both substrates. This indicates a coating is required for printed silver ink.

6.6.2 Effect of Biodegradable Substrate on Printed Track Electrical Characteristics

PET 175 μ m and Eco Craft 30 μ m thick flexible cellulose substrate, were tested for electrical characteristics. Measured resistance, Q factor, capacitance and inductance average values are shown for both materials in Figure 6-9.

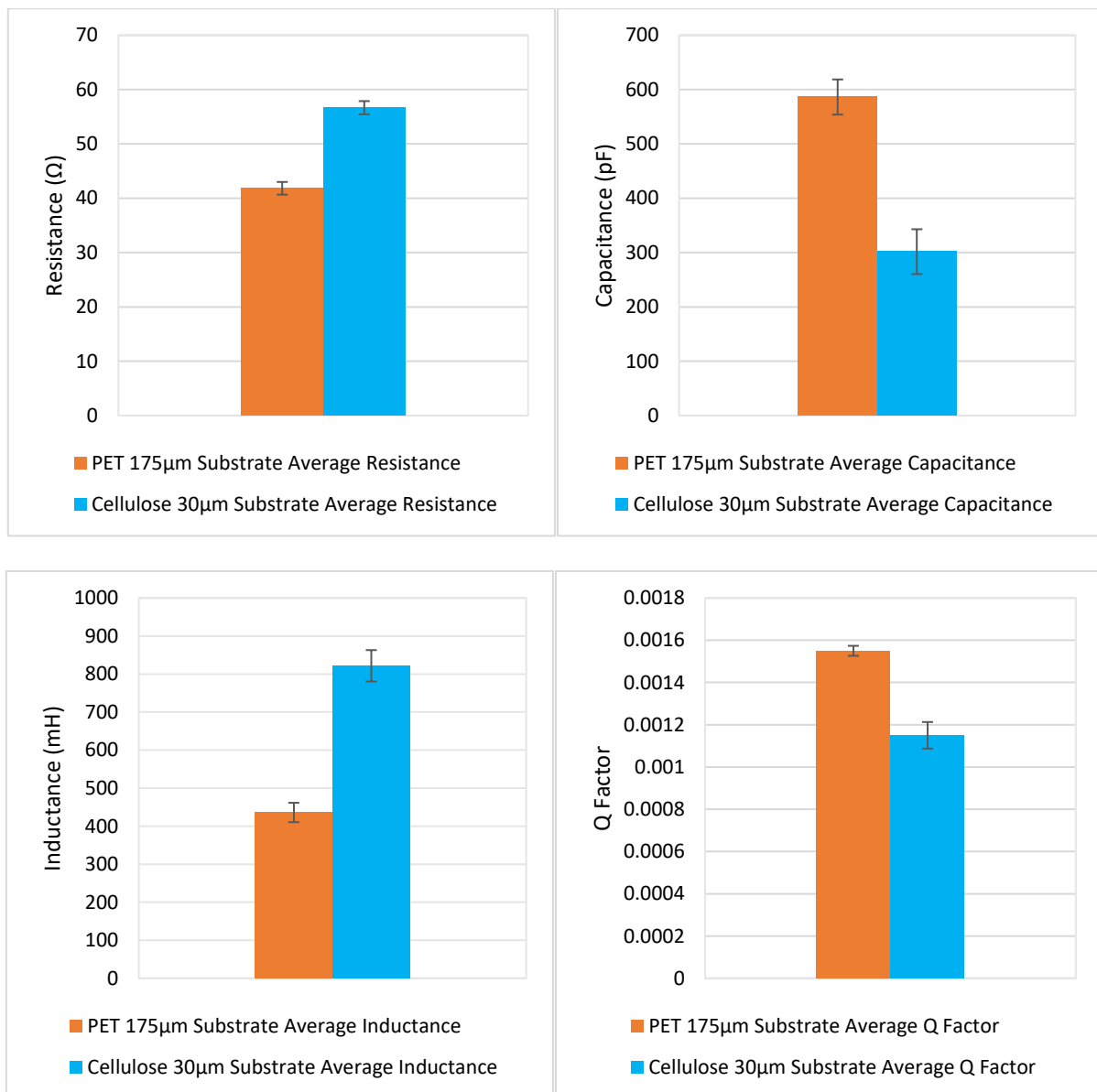


Figure 6-10 – Average resistance, capacitance, inductance, and Q-factor measured on an LCR bridge for printed Novacentrix PFI722 nano-silver ink on HiFi Industrial Film 175 μ m thick PET substrate and on Eco Craft 30 μ m thick cellulose substrate.

The PET substrate demonstrated the highest Q factor, indicating that the best results will come from a printed antenna on PET substrate over biodegradable substrate. For the PET substrate, inductance and resistance are both the lower of the two and the capacitance is higher. A low resistance is essential for good conductivity in this application. Inductance and capacitance are inherent traits in the print and are challenging to control through the print process, whereas resistance can be improved by altering the design to include more ink. Lowering the resistance will improve the Q factor at resonant troughs as it allows more current to flow.

6.7 Closure

S22 and frequency were measured for antennas printed using a range of anilox volumes and print speeds. Tests using a spectrum analyser to measure frequency and S22 determined that the printed samples were acting as an antenna. A VNA was used to characterise the response of the signal with regards to the various flexographic print parameters used; anilox volumes of 8, 14 and 24 cm³/m² and print speeds 20, 50 and 80 m/min.

In the previous chapter, parameters of high interest were largest anilox volume, 24cm³/m², and a high print speed of 50 and 80m/min as they produced the lowest resistivities. At this anilox volume, the print speed did not greatly affect the resistance. For these settings, print width, film thickness and surface roughness were all at their maximums.

This chapter compared both print parameters studied in the previous chapter and their outcomes with the recorded peak S22 values and correlating frequencies. There was no correlation between peak S22 values and print outcomes. High peak S22 values are important in antenna performance to provide a strong response signal. Antennas with strong response signals are desired for RFID applications. Further work needs to be done to collect more data to draw any reliable correlation.

Frequency had no correlation with film thickness. The resonant frequencies show an increase in value as the surface roughness of the print increases and aside from one anomaly, the relationship plateaus after a surface roughness of 430nm. Aside from one anomaly, frequency increases with an increase in resistance. Changes in frequency of the signal indicates that through changing print parameters to achieve these outcomes that information can be stored in these signals. Changes to the resistance of the printed track will shift the frequency higher or lower and this can be utilised in sensors that are integrated into the antenna.

There were no correlations found between print parameters and S22, and only an increase to the fastest print speed, 80 m/min, decreased the frequency. This decrease also came with an increase in variation in the results. This signifies that there is no ability to use the printer settings tested in this work to control the antenna outcome.

Over a 12-week period, track resistance decreased by 1.7% and 3.9% for the PET substrate and the bio substrate respectively. Changes in inductance and capacitance were also shown. Collective changes in these three measurables caused the Q-factor to decrease in value by 54.7% and 60.4% for the PET substrate and the bio substrate respectively, meaning that the quality of the antenna signal response deteriorates faster.

The Q factor for silver ink on PET substrate loses value over time, which is likely due to silver tarnish as this is a common phenomenon for silver inks. Some of the ink may be being absorbed by the biosubstrate or alternatively it is not as good a barrier as PET and releases solvent through the substrate. A more protective coating is required to be able to use biosubstrate in printed electronics. Additionally, for a comparison between a PET substrate and a cellulose-based biosubstrate, the PET demonstrated the highest Q factor, meaning it will yield the best results.

Flexography has proven to be a method of producing antennas and has potential as a manufacturing process. When analysing the track as a monopole, there is large variation in the response due to inherent variation in the process. Due to the link between resistance and frequency, there is viability to tune the antenna through design and changes in the process to achieve varying responses. Consistency in terms of signal response is low and there are weak/non-existent correlations between print outcomes with measured S22 values and frequency. However, knowing that changes in track resistance can alter the frequency, then each antenna can be used as manufactured, and a secondary system can be integrated to alter the resistance in response to changes on a product for example. This would demonstrate a binary on/off system where the frequency would appear in the initial test region at first and as changes occurred in the track resistance, the frequency would shift out of this region. Increases in line width of 0.5mm have shown to increase the signal response of the antenna. A line width of 1.5mm (Design E) and lowest resistance, gives the strongest response to a signal. As mentioned, there is some inherent variability in the prints, which needs to be accounted for.

A further study would be interesting to note the rate of degradation of the silver ink on this substrate due to its higher substrate porosity than PET. This could allow degradation of the ink on both sides and speed the rate at which the Q factor decreases, in turn influencing the requirements for a preventative coating. Additional print analysis would also need to be done to compare print quality on biodegradable substrates and PET substrates. Encapsulation methods could be used to protect the printed tracks. This may be appropriate for nano inks as the binder provides a degree of encapsulation for particulate inks.

Chapter 7: The Effect of Polymer Viscosity and Silver Loading on Ink Rheology and Printability

7.1 Introduction

In the previous chapters, the print process parameters were changed to study the effect on the print quality and hence the antenna performance. However, some of the flexographic print defects cannot be resolved through altering print parameters alone, as they are dependent on the ink rheology. Commercial inks are provided with limited information regarding weight percentage of silver, silver shape, resin blend and solvents. They also contain additives and surfactants to alter the viscosity while speeding recovery of viscosity to minimise ink spreading. A series of model inks without additives were created so the impact of silver loading and carrier viscosity could be studied. For the newly formulated inks, the effect on rheology was studied by varying:

- Viscosity of the carrier by use of different viscosity grade of polymer resins
- Silver flake loading

The inks were made of silver particles, varying grades of Huntsman's Irostick TPU and diacetone alcohol.

The validity of the Krieger-Dougherty, Maron-Pierce and Einstein-Batchelor equations for predicting the influence of particles on suspension rheology was assessed for this ink system.

7.2 Development of Optimised Carrier Ratio

The rheology of two commercial inks: water based Novacentrix PFI-722 and UV curing Gwent Group (Product number: C2140326D1) silver inks were established to provide a comparison.

The Gwent Group silver ink is a UV cure ink and the Novacentrix PFI-722 is a water-based silver ink. Testing of the inks was to determine an infinite shear operating range of commercially available flexographic inks as a benchmark for polymer resin rheology. Ink properties of these two inks are shown in Table 7-1.

Table 7-1 – Commercial ink specifications.

Property	Novacentrix PFI-722 (180)	Gwent UV Ink
Silver Content	60% ±2%	~72%
Viscosity	0.55 Pa.s (550 cP) @10s ⁻¹	1.0 - 3.0 Pa s @25s ⁻¹ at 25°C
Volume resistivity	2-2.8 mΩ/□/mil	2.0 - 5.0 Ω/□
Printed Sheet Resistance	50-350 mΩ/□	Unavailable
Curing Temperature	140°C	UV Curing
Coverage	100 – 600 m ² / kg	Unavailable
Shelf Life	> 8 Months if kept refrigerated between 2-9°C	6 Months

The shear viscosity – shear rate profile for the commercial inks were first measured (Figure 7-1) to determine a working range of flexographic inks. The inks were measured from 0.1 to 200 s⁻¹ to show an operational range of 75 Pa.s at 0.1 s⁻¹ and 0.25 at 200 s⁻¹. The shear viscosity value drops with shear rate, as expected from manufacturers data. The measured shear viscosity of the Novacentrix ink at 10s⁻¹ was 0.24 Pa.s, whereas the manufacturing data sheet states this to be 0.55Pa.s. Both commercial inks are shear thinning and tend towards a plateau at high shear rates, which is referred to as the infinite shear viscosity.

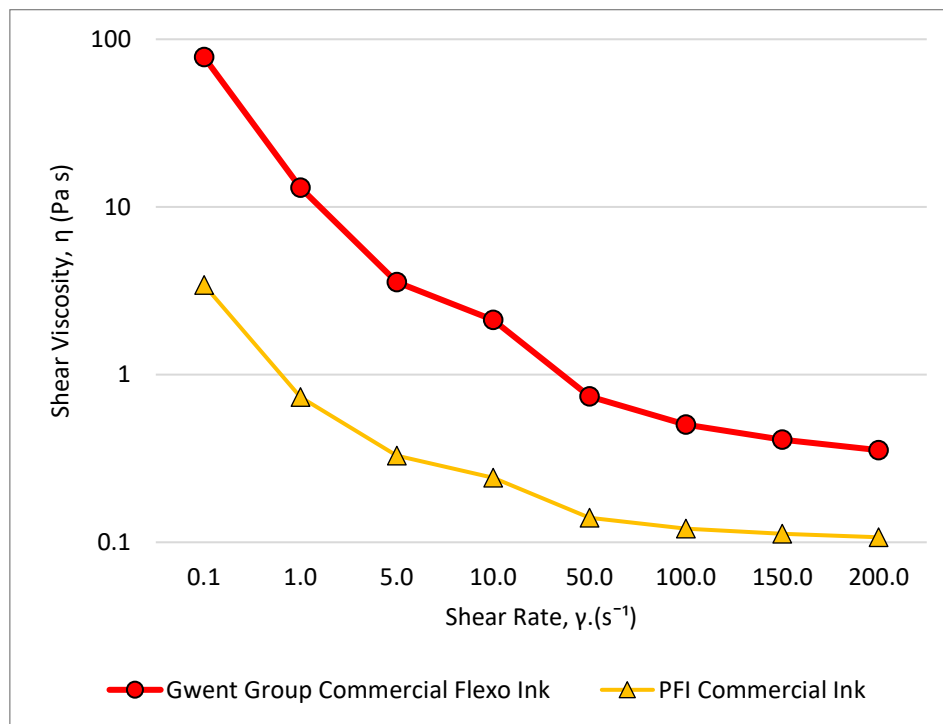


Figure 7-1 – Shear viscosity – shear rate graph for two commercial inks.

7.3 Polymer Resin and Solvent

Five resins of wt.% ratio 87.5:12.5, DAA solvent:TPU polymer are formulated. Thermoplastic polyurethane (TPU) was selected as the polymer component of the resin. TPU has been shown to work well for carbon formulations (67), in particular, Huntsman's Irostick linear TPU. The five variations of the Huntsman's Irostick TPU's S7614-1.5, S7614-08, S7614-12, S7614-19 and S7614-25 were used for their good elasticity properties (applicable for flexible packaging), its heat resistance, and adhesion to a wide range of substrates. It has specifically been designed for use in solvent-based applications (188). The suffixes to the part numbers (1.5, 8, 12, 19 and 25) denote the 'viscosity grade' of the TPU polymer. Outlined on the manufacturing datasheet (188), the suffixes are the viscosity at 15% solids in methyl-ethyl-ketone. The viscosity units are mPa.s, with seconds in hundreds so, for example, S7614-1.5 has a viscosity of 150mPa.s at 15% in MEK and S7614-08 has a viscosity of 800mPa.s. These viscosity grades are analogous to molecular weight. Sigma Aldrich Diacetone Alcohol (DAA) (product number: H41544) was used as the solvent due to its slow evaporation rate and good flow characteristics for printing (189,190).

The five resins of wt.% ratio 87.5:12.5, DAA solvent:TPU polymer display Newtonian behaviours [Figure 7-2 (a)]. The shear viscosity value drops with decreasing polymer Vg, as expected from manufacturers data. There is a small drop in viscosity with shear rate for high Vgs. However, this is likely due to inertia forces within the sample, distorting the more viscous fluids at higher shear rates. It is possible that the gradual downward curve of the 19 and the 25 Vg could be due to polymer alignment in the fluid, the beginning of non-Newtonian behaviour.

In addition, extensional behaviours within inks have been shown to align with Figure 7-2 (a) (118)(124). However, this is unlikely, as this behaviour typically starts at a high shear rate, and therefore would need further testing to verify that there is no machine error in the rheometer and no inertia in the ink.

Regarding the resin, there is little variation in shear viscosity between Vgs for low shear rates [Figure 7-2 (b)], however, the shear viscosity changes with an increase in Vg at higher shear rates.

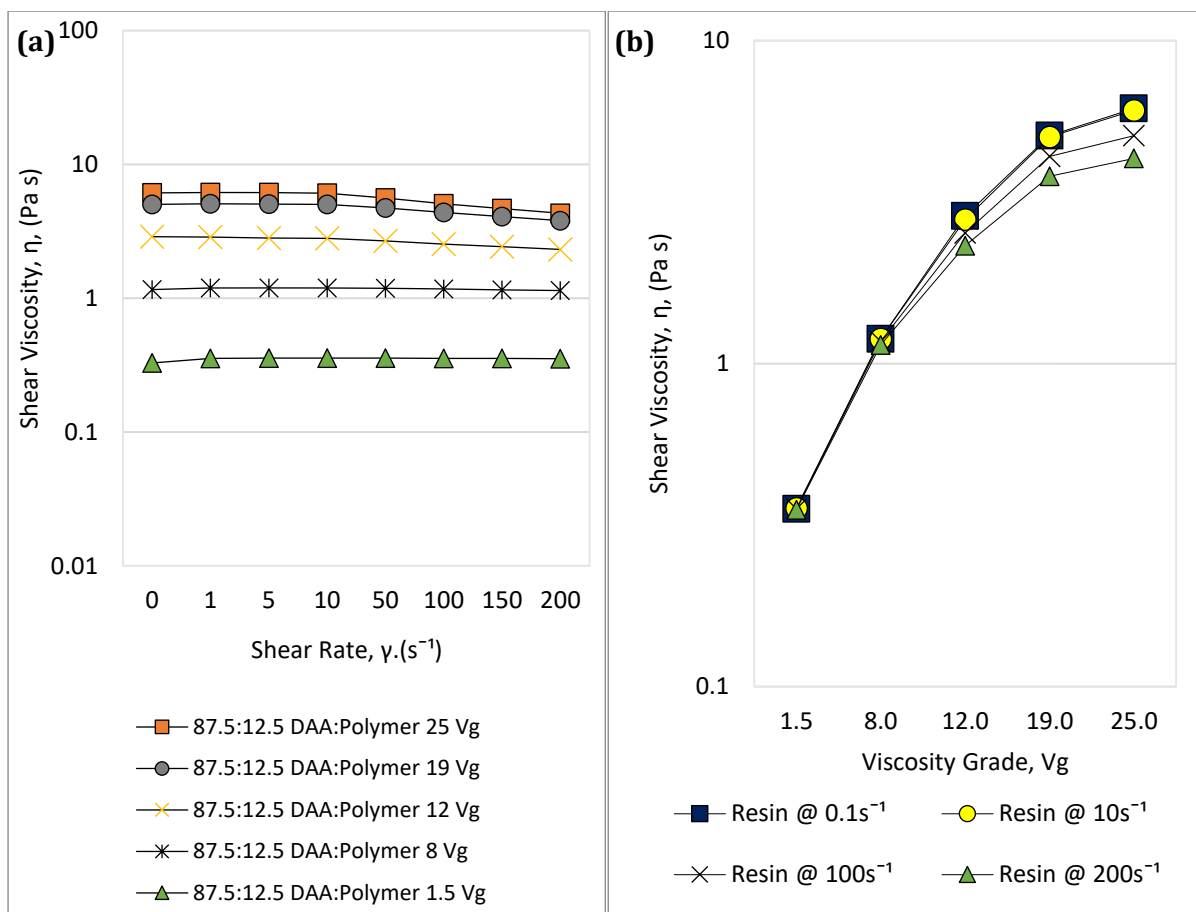


Figure 7-2 – (a) Shear Viscosity against Shear Rate of the five resins composed of DAA and TPU with polymer Vgs (1.5, 8, 12, 19 and 25). Resins of DAA and TPU to ratios of 87.5:12.5 respectively. (b) Viscosity grades in resins at four shear rates.

Silver was added to the carrier formulations shown in Figure 7-2 (a) and shear viscosity-shear rate profiles analysed [Figure 7-3 (a)]. The addition of silver to the resin increases the shear viscosity.

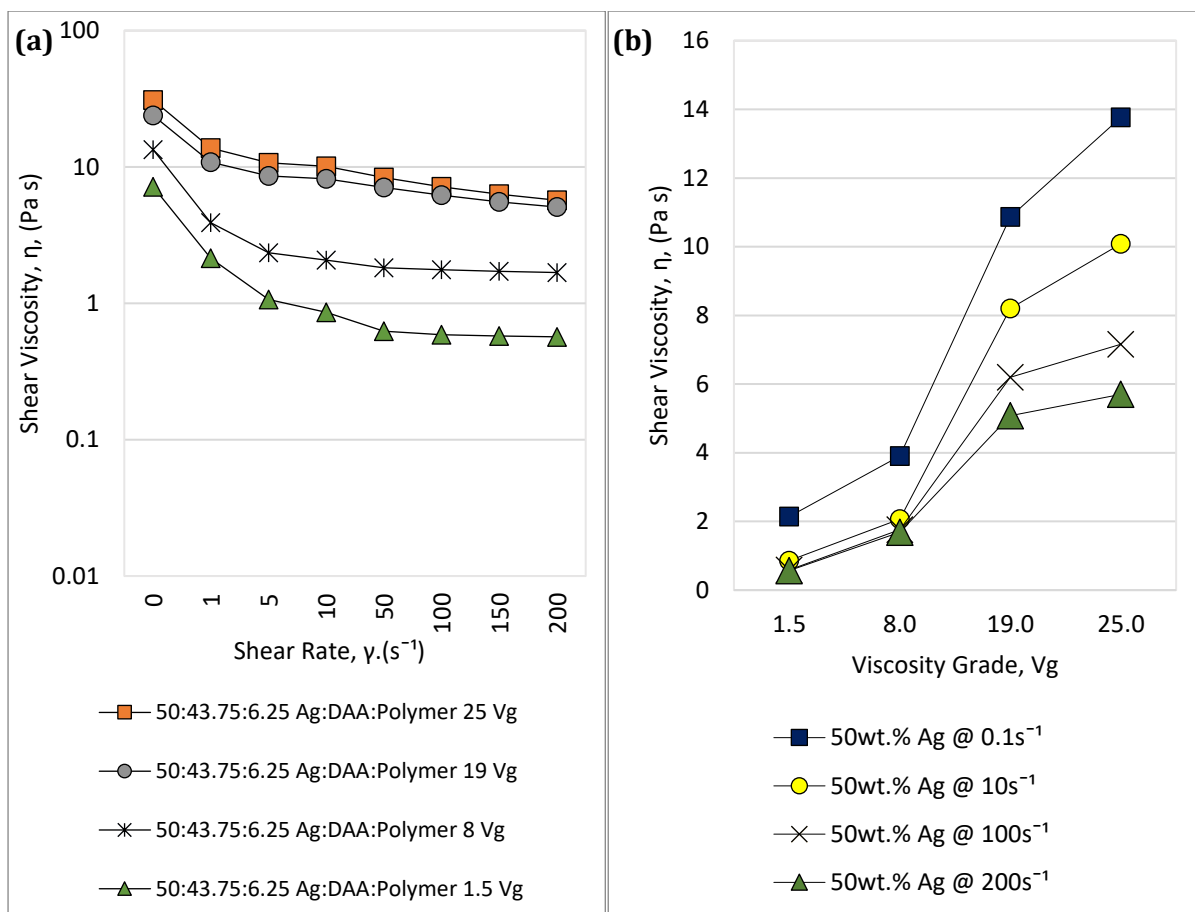


Figure 7-3 – (a) Resins of DAA and TPU for 50wt.% Ag. (b) Viscosity grades in silver-resin formulations at four shear rates.

Ratios of diacetone alcohol to polyurethane resin were adjusted to better align the rheology to commercial ink rheological profiles at the infinite shear viscosity. As previously mentioned, the commercial inks give an operational window in which inks perform on the flexographic printer. To enable study of various elements of the ink, this window has been used to achieve an operational ink.

For the 1.5 and 8 Vg polymer Ag:DAA:TPU solutions, the DAA content was increased to 90.0% and 92.5% from the previous experiment where it was 87.5%. Ag:DAA:TPU (50:46.25:3.75) 8 Vg and 1.5 Vg are the two Ag-Resin inks that show the most promising likelihood of aligning with the continued curve of the commercial ink.

The highest solvent % resins showed the lowest shear infinite viscosity, which is lower than the Gwent ink shear viscosity value of 0.35 Pa.s, measured at a shear rate of $200s^{-1}$. The '50:46.25:3.75 Ag:DAA:Polymer 1.5 Vg' follows the PFI ink profile exactly between shear rates of 10 and $200s^{-1}$. Due to this, a 92.5:7.5 DAA:TPU (50:46.25:3.75 as annotated) polymer resin was selected for further experimentation.

Silver (Ag) flake was added to the resin-solvent formulations at a 50:50 ratio by wt.%. The rheological profiles of the resin-solvent formulations (1.5Vg and 8Vg) and resin-solvent-silver formulations are shown in Figure 7-4 and Figure 7-5 respectively, which can be compared to the commercial silver ink shear profiles in Figure 7-1. Despite the inks not reaching their infinite shear viscosities between the shear rates 0.1 and 200s⁻¹, the graph shows a rise in the infinite shear viscosities compared to the resins without the silver particles.

The component specifications of all three percentage volumes of DAA for the two polymer Vgs are shown in Appendix F: Resin and Silver Ink Formulations (Section 7.3.1.).

All Ag-TPU-DAA inks demonstrate shear thinning behaviour in these shear viscosity – shear rate graphs. Infinite shear viscosity is primarily determined by the polymer rather than the particles. The highest solvent ratios have best alignment with the infinite shear viscosity. The infinite shear viscosity is likely to be the operational range on a flexographic printer. Hence, ink properties were adjusted to align with this parameter. Therefore, these low Vgs (1.5 and 8 polymer Vgs) will be taken forth and silver added to analyse changes in the shear profile.

Figure 7-5 shows, for only the 1.5 and 8 Vg TPU resins with 50wt.% silver content, the three variations of DAA volume % (12, 10 and 7.5). When compared with Figure 7-1, it shows how the formulated inks compare to the commercial range for its shear viscosity against shear rate profile.

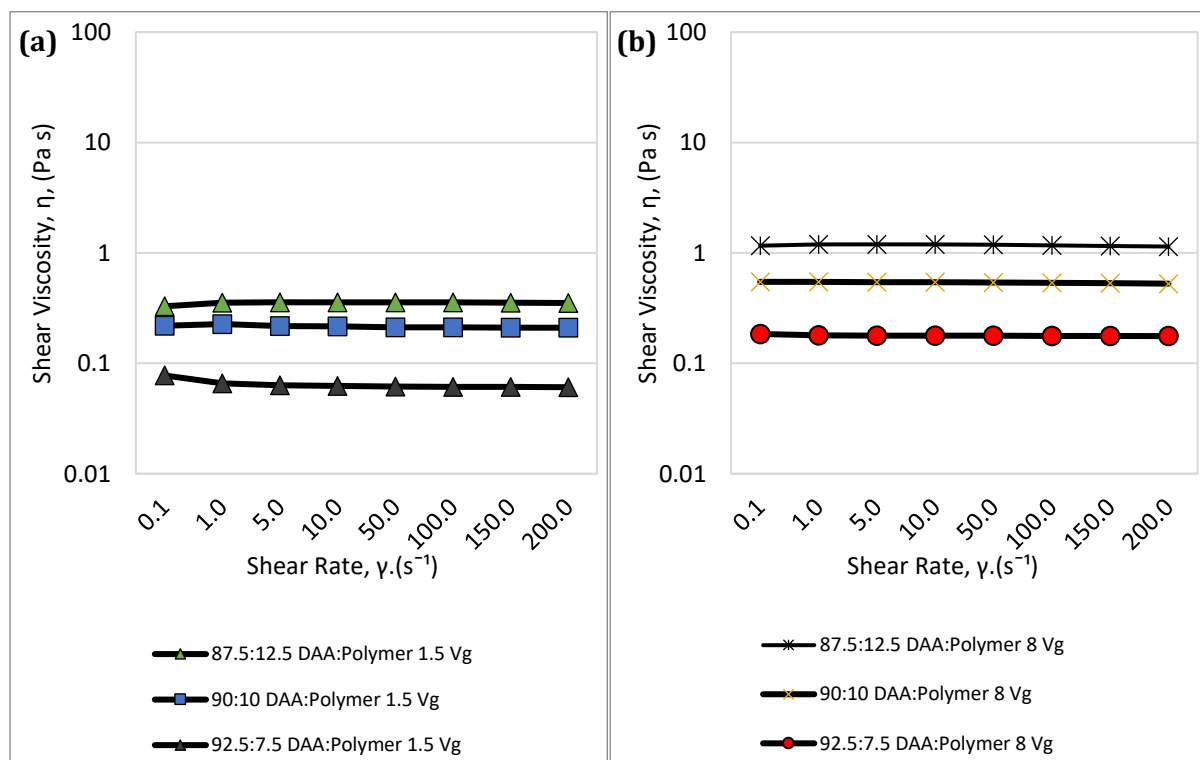


Figure 7-4 – DAA-TPU resins of varying formulation ratios. (a) 1.5 Mw (b) 8 Mw.

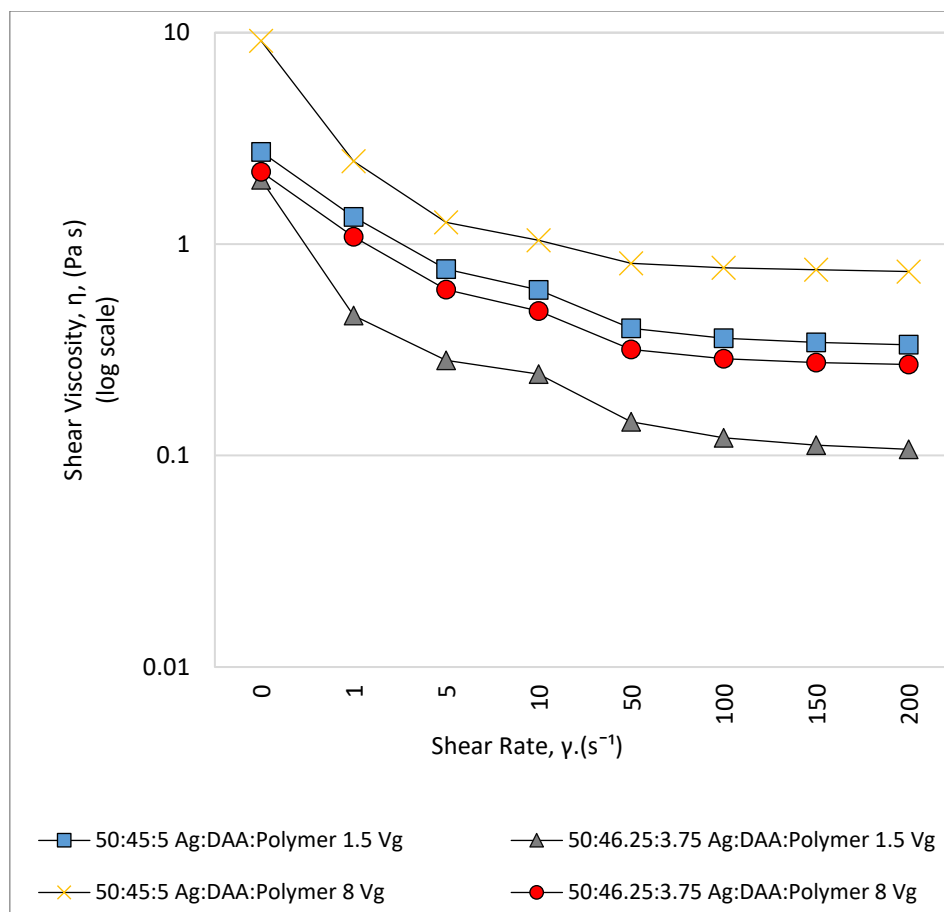


Figure 7-5 – Resins of DAA and TPU. TPU wt.%s 1.5 and 8, in varying ratios of 12.5:87.5, 10:90 and 7.5:92.5 to DAA. All to 50:50 Resin: Ag.

7.3.1 Effect of Silver Loading on Shear Viscosity

An investigation with a 92.5:7.5 DAA:TPU polymer ratio into the effect of silver loading was conducted. This one was selected as it has the lowest shear viscosity at high shears, which best aligns with the viscosity boundaries set by the commercial inks. The ratios of the inks are outlined in Appendix F: Resin and Silver Ink Formulations (Section 7.3.1.). Shear viscosity-shear rate graphs for the silver loading variations for 1.5 Vg and 8 Vg are shown in Figure 7-6 (a) and Figure 7-7 (a) respectively. The 70 wt% was deemed an anomaly and hence removed from the data set. Experiments were repeated but results were similar. These graphs show an increase in the infinite shear viscosity curves as the silver wt.% is increased. Both polymer viscosity and loading as well as silver loading determine the infinite shear viscosity.

All inks align relatively closely to the commercial inks. The 80wt.% silver ink, although follows the Gwent ink profile (Figure 7-1), demonstrates a shallower profile and results in a higher infinite shear viscosity. This is a similar relationship between the 50% silver ink and the PFI-722 ink.

Aside from the highest silver loaded ink, all the inks shown in Figure 7-6 (a) and Figure 7-7 (a), reach relatively Newtonian behaviour/infinite shear viscosities within this typical range. These graphs are important to have for these inks as they describe the behaviour at each part of the printing process. Figure 3-10 highlighted the points on the flexographic printer at which high shear rate will be experienced by the inks. At these points, the inks will move from the left-hand side of the graphs [Figure 7-6 (a)] exhibiting high shear viscosities, rapidly to the right-hand side of lower shear viscosities. Once the ink has been transferred to the next roller, the shear rate returns to zero and begins to viscosity recover. Ink in the anilox cells, on the printing plate and on the substrate will be high, especially for increased silver loading. At the nip junctions between rollers and interaction with the doctor blade, shear rate is high, and viscosity is significantly lower, enabling ink to flow and transfer more readily.

Silver particles have an increasingly higher effect on the viscosity of the inks [Figure 7-6(b)]. Higher wt.%s of silver in a formulation increase shear viscosity. This effect increases further for higher shear rates.

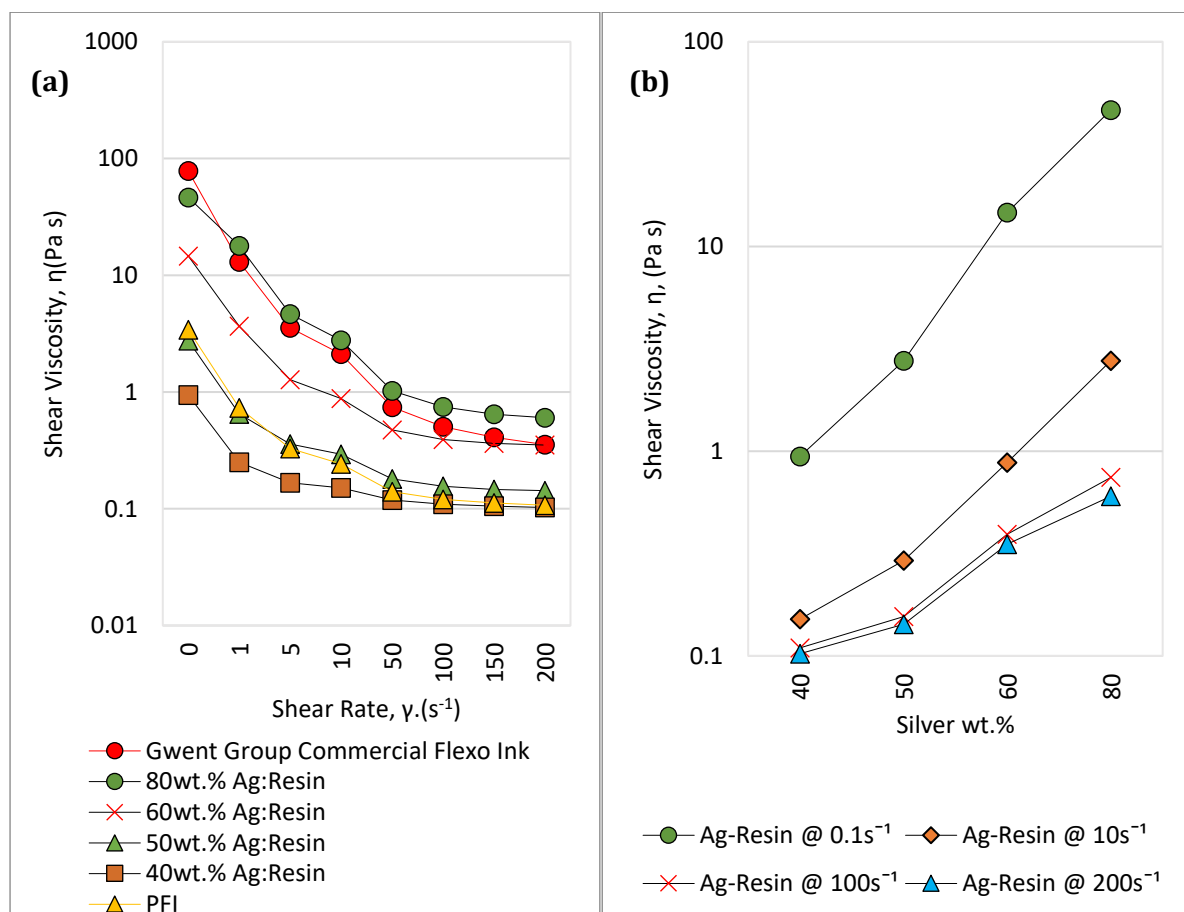


Figure 7-6 – (a) Shear viscosity against shear rate for five inks of 1.5 Vg and 92.5:7.5 DAA:TPU ratio with Ag wt.% of 40, 50, 60, 70 and 80. Commercial inks are also shown. (b) Shear viscosity for silver wt.%s at four shear rates for 1.5Vg resin-silver formulation.

The same DAA:TPU ratio was formulated (as in Figure 7-6) with an 8 Vg polymer [Figure 7-7 (a)]. The shear profiles increased in shear viscosity with an increase in polymer Vg.

As in Figure 7-6 (b), Figure 7-7 (b) shows the effect of silver wt.% for four shear rates on shear viscosity for an 8 Vg resin. The impact of silver particles on shear viscosity is again higher for higher loadings and this effect is also higher at higher shear rates. Up to 10s^{-1} , the shear rate has little impact on the shear viscosity of the ink. Above this shear rate, there is a significant increase in shear viscosities for all silver loadings.

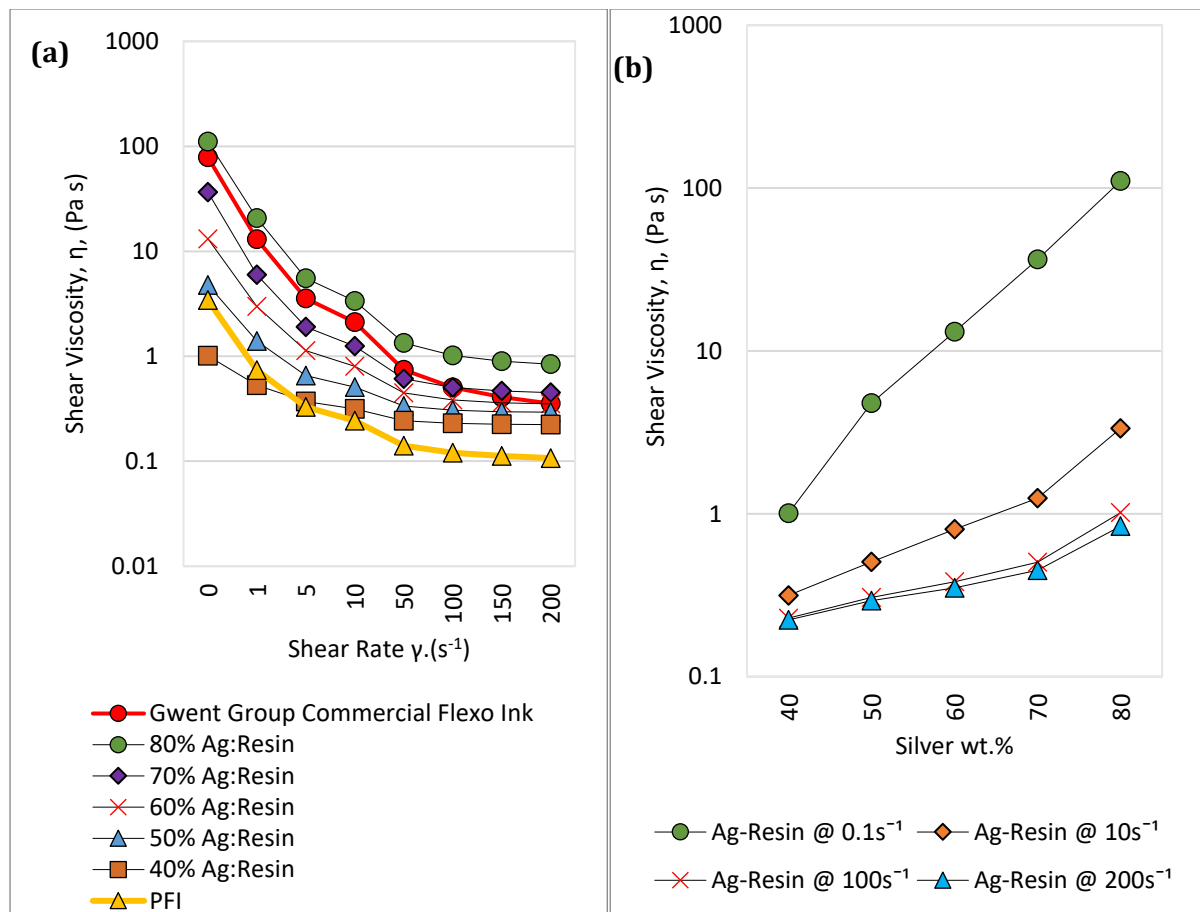


Figure 7-7 – (a) Shear viscosity against shear rate for five inks of 8 Vg and 92.5:7.5 DAA:TPU ratio with Ag wt.% of 40, 50, 60, 70 and 80. Commercial inks are also shown. (b) Shear viscosity for silver wt.%s at four shear rates for 8 Vg resin-silver formulation.

The effect of suspension resins is outlined in terms of their shear profiles in this section. The silver:resin suspensions demonstrate the shear thinning profile required for flexographic printing. In the next section, the application of three suspension models on a full factorial study of inks, with 1.5, 8, 12, 19 and 25 polymer Vgs, and silver wt.%s of 40, 50, 60, 70 and 80, was

studied to investigate their applicability in modelling silver suspensions. An experiment on how this affects printed tracks is presented Chapter 8.

7.4 Effect of Polymer Molecular Structural Changes and Silver Loadings on Rheology

Viscosity grade and silver loading exhibit a significant impact on the shear viscosity-shear rate profile of the ink. To fully understand the range of effects silver loading and viscosity grade can have on printability and electrical performance, a full factorial study of the impact of polymer viscosity grade and silver loading, on rheology was undertaken.

Therefore, a broader range of inks in terms of Vg and silver loading have been tested. Five Huntsman Irostick polymer weights of 1.5, 8, 12, 19 and 25, and five silver loading wt.% of 40, 50, 60, 70 and 80, were tested.

Table 7-2 shows the ink array. The DAA:TPU ratio used (92.5:7.5), was selected from previous work.

Table 7-2 – Polymer viscosity grades and silver loading (wt.%) contents for an ink array study with ink codes.

		Polymer Viscosity Grade (Vg)				
		1.5	8	12	19	25
Silver Loading (wt. %)	40	40 wt.% Ag, 1.5 Vg	40 wt.% Ag, 8 Vg	40 wt.% Ag, 12Vg	40 wt.% Ag, 19 Vg	40 wt.% Ag, 25 Vg
	50	50 wt.% Ag, 1.5 Vg	50 wt.% Ag, 8 Vg	50 wt.% Ag, 12 Vg	50 wt.% Ag, 19 Vg	50 wt.% Ag, 25 Vg
	60	60 wt.% Ag, 1.5 Vg	60 wt.% Ag, 8 Vg	60 wt.% Ag, 12 Vg	60 wt.% Ag, 19 Vg	60 wt.% Ag, 25 Vg
	70	70 wt.% Ag, 1.5 Vg	70 wt.% Ag, 8 Vg	70 wt.% Ag, 12 Vg	70 wt.% Ag, 19 Vg	70 wt.% Ag, 25 Vg
	80	80 wt.% Ag, 1.5 Vg	80 wt.% Ag, 8 Vg	80 wt.% Ag, 12 Vg	80 wt.% Ag, 19 Vg	80 wt.% Ag, 25 Vg

7.4.1 Effect of varying Polymer Viscosity Grade at Various Silver Loading

Figure 7-8 shows an example shear viscosity profile for 60 wt.% silver of five polymer wt.%. Appendix C: Polymer Viscosity Grade at Various Silver Loadings (Section 7.4.1.) shows the graphs for 40, 50, 70 and 80 wt.% loadings and shows the change in shear viscosity for an increasing

shear rate for each silver loaded ink with an increasing polymer viscosity grade. The data presented in this graph is evidently shear thinning and this effect becomes stronger for higher silver loading contents. For lower silver loads within the ink, there is a lower shear thinning effect, tending toward Newtonian behaviour.

For the ink that contained lower polymer viscosity grades, there is a lower shear profile and this increases with increased polymer viscosity grade. The drop in shear viscosity due to is the length of polymer chains aligning within the fluid, and more so as the shear rate is increased. Higher viscosity grades have longer molecule chain lengths and hence develop stronger structures and alignment within the flow of the ink as the shear is applied.

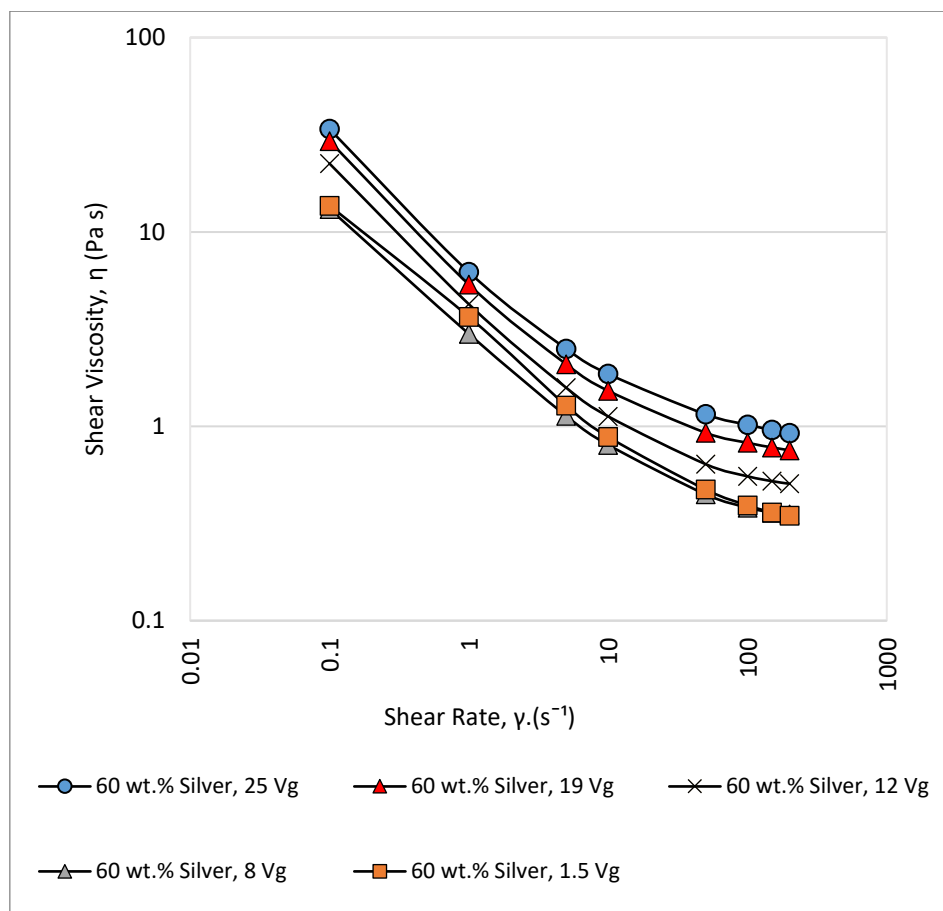


Figure 7-8 – Effect of polymer viscosity grades 1.5, 8, 12, 19 and 25 for: (a) 40 wt.%, (b) 50 wt.%, (c) 60 wt.%, (d) 70 wt.% and (e) 80 wt.% silver loading on shear viscosity. Shown on a shear viscosity against shear rate log-log graph.

7.4.2 Varying Silver Loading

Figure 7-9 shows the changes in shear viscosity for an increasing shear rate for each silver loading with a polymer viscosity grade of 8. Appendix D: Silver Loadings at Various Viscosity Grades (Section 7.4.2.) shows the graphs for 1.5, 12, 19 and 25Vg. All graphs also show an increase in shear thinning as silver loading is increased. The shear thinning behaviour exhibited is due to alignment of particles within the fluid. For Vg 1.5, the change in viscosity from yield point at 0.1s^{-1} to 200s^{-1} is $42.8\text{Pa}\cdot\text{s}$ for 80 wt.% silver and $0.84\text{Pa}\cdot\text{s}$ for 40 wt.% silver. For Vg 25, the change in viscosity from yield point at 0.1s^{-1} to 200s^{-1} is $184.4\text{Pa}\cdot\text{s}$ for 80 wt.% silver and $3.2\text{Pa}\cdot\text{s}$ for 40 wt.% silver. There are significant changes within the structures of the inks. Larger shear thinning effects are seen in high silver loaded unsheared fluids due to the higher forces required to initiate flow indicating that higher interparticle forces are present (Figure 7-8).

When comparing Figure 7-8 to Figure 7-9 and Appendix D: Silver Loadings at Various Viscosity Grades (Section 7.4.2.), the shear thinning is dominated by particle loading effects. Silver loading has a stronger impact on the shear thinning effect exhibited by the ink than that of increased polymer weight.

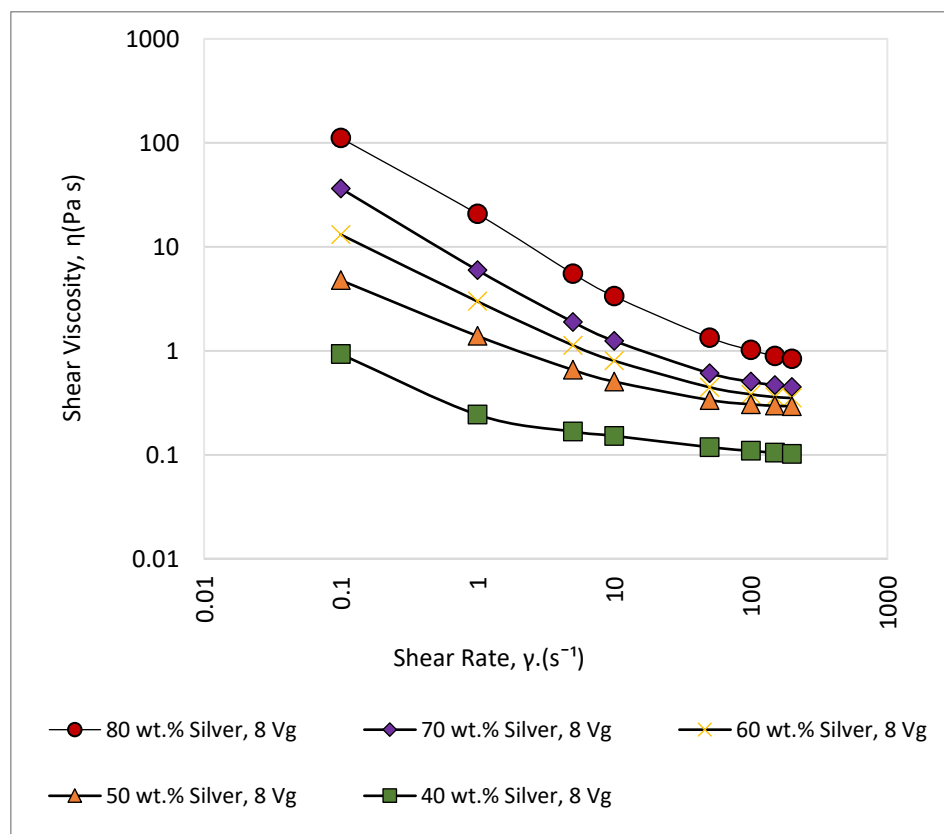


Figure 7-9 – Silver loadings: 40, 50, 60, 70 and 80 wt.% for 8 Vg polymer on a shear viscosity against shear rate.

Table 7-3 and Table 7-4 show a summary of the shear viscosities at $0.01s^{-1}$ and $200s^{-1}$ respectively for the 25 inks with colour coding to demonstrate relative to one another high (dark blue) and low (light blue) shear viscosities. Viscosity at both shear rates increase with both polymer Vg and silver loading. As previously discussed, this effect is especially prevalent for the shear viscosity at a shear rate of $0.01s^{-1}$ for these inks. Viscosities are much closer at high shear rates than at low shear rates; For example, comparing the shear viscosity of 40wt.% and 80 wt.% loading of the 1.5Vg ink has a difference of 42.44 Pa.s at $0.01s^{-1}$ and 0.5 Pa.s at $200s^{-1}$.

70wt.% at 1.5Vg is an error as distinct patterns of increasing viscosity for increases in viscosity grade and silver loading are demonstrated in the data, hence it is not included.

Table 7-3 – Shear viscosity values at $0.01s^{-1}$ for polymer weights and silver loading contents for an ink array study.

	Polymer Viscosity Grade (Vg)					
		1.5	8	12	19	25
Silver Loading (wt. %)	40	0.94	0.93	2.43	2.12	3.68
	50	2.76	4.78	3.95	5.64	6.24
	60	13.65	13.14	22.47	29.34	33.83
	70		36.46	52.25	52.25	61.47
	80	43.38	111.13	153.48	173.84	185.68

Table 7-4 – Shear viscosity values at $200s^{-1}$ for polymer weights and silver loading contents for an ink array study.

	Polymer Viscosity Grade (Vg)					
		1.5	8	12	19	25
Silver Loading (wt. %)	40	0.10	0.10	0.31	0.37	0.52
	50	0.14	0.29	0.32	0.50	0.59
	60	0.35	0.35	0.51	0.75	0.92
	70		0.45	0.61	0.84	0.94
	80	0.60	0.84	1.24	1.52	1.62

7.4.3 Equilibrium Shear Rate-Viscosity Curve

Consistency and reliability of the printing process is essential in large scale printing.

Viscosity over time was measured to establish if there are thixotropic effects for the ink of lowest Vg (1.5) with the lowest silver wt. % and for the ink of highest Vg (25) with the highest silver wt. %. The viscosities were constant, indicating that no thixotropic effects were present.

7.5 Modelling of Polymer Viscosity Grade and Silver Loading Suspension Behaviours for Viscosity and Phase Volume

Viscosity and phase volume play an important role in the behaviour of an ink. The Krieger-Dougherty, Maron-Pierce and Einstein-Batchelor equations were used to estimate viscosity values, which were all plotted against the calculated relative viscosities (Ink Viscosity / Resin Viscosity) at shear rate $1s^{-1}$ and phase volumes of the different Vgs and silver loadings. Table 7-5 shows each of these silver wt.%s with their corresponding phase volumes. Figure 7-10 is an exemplar graph from Appendix E: Modelling of Polymer Viscosity Grade and Silver Loading Suspension Behaviours for Viscosity and Phase Volume (Section 7.5.), which shows the results for the range of silver wt.%s at each of the polymer Vgs. As silver wt.% increases, phase volume increases, as does relative viscosity. A logarithmic scale has been used on the y-axis for relative viscosity to better analyse the data and distinguish between graphs.

Table 7-5 – Phase volumes at $1s^{-1}$ for each Ag wt.%

Ag wt. %	Phase Volume at s^{-1}
40	0.056763
50	0.082795
60	0.119256
70	0.173982
80	0.265287

There is best alignment with the Krieger-Dougherty model and least with the Einstein-Batchelor model. The error sum squared numerically demonstrates the accuracy of the predictive equations. It was expected that the data would least align with the E-B model due to its applicability for lower volumes of suspension material. Maximum packing factor in a fluid is 0.74 and infinite viscosity is assumed to be 1 for the E-B equation, which is not physically possible, hence the lack of correlation. In terms of the K-D and the M-P models, M-P is fundamentally the same model as the K-D with an additional assumption that $[\eta]\phi_m = 2$, which has been determined from much experimental testing and found to be typically 2. For these data sets, the value of $[\eta]\phi_m$ has ranged between 4 and 9, which is much higher than the value assumed for the M-P model,

hence the M-P model does not align well with the results. It is due to this assumption that K-D model is most aligned to the measured data.

As the relative viscosity increases, the divergence from the models increases, with two exceptions. In the figures, the data collected for 70 wt.% sample is one where the data point aligns more closely with the M-P model than the K-D model. 80 wt.% silver for all polymer wt.%s is the second. The latter point is demonstrated in all of the figures, and the data aligns well with both the K-D and the M-P models as this is the point at which they converge.

The relative viscosity for the samples increases with increased silver wt.% at a faster rate than the models predict. It is proposed that due to the high density of silver particles, sedimentation plays a role in the divergence from the models. Sedimentation is not considered numerically by the models but was observed in this rheometric testing. In testing, inks are quickly used after three roll milling to retain the high dispersion.

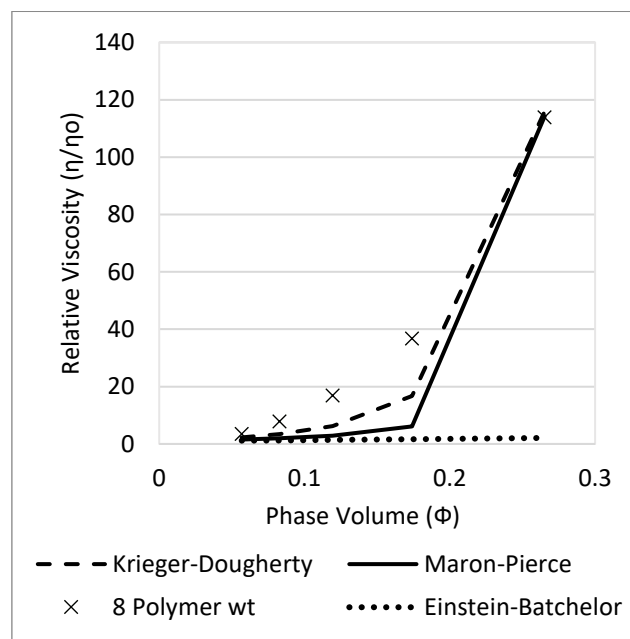


Figure 7-10 – Relative viscosity against phase volume for an Ag-DAA-TPU (1.5 Vg.) flexographic printing ink for inks of 40wt.%, 50wt.%, 60wt.%, 70wt.% and 80wt.% Ag for 8 Vg polymer.

A method of least sum squared was used in conjunction with the Microsoft Excel solver to obtain a converging result for the model. The sum of error squared represents the error between the predictive models with the measured results. Higher sum of error demonstrates a lack of correlation, and close to zero means the models are align well with the data.

Of the three models tested and compared with experimental data, the E-B model, showed little conformity except at lower silver contents, which was as expected. The K-D model showed the highest conformity with the Ag-TPU-DAA ink as it considers intrinsic viscosity. However,

critically, even this model demonstrated a high error sum squared and so not a reliable method of prediction for this ink. One theory for this is the effect of particle shape. Particle shape affects packing factors, and irregular particle shapes have a particular impact on particle interactions. Lower packing densities occur for increasingly irregular shapes.

At the highest silver wt.% for all polymer Vgs, both the K-D model and M-P model accurately predict the relative viscosity and phase volume of the ink. This is also represented by errors lower than $\times 10^{-2}$ for this point. Regardless of the shape or size of the particles, at 80wt.% silver, the ink is nearing its infinite viscosity and maximum packing factor. At this point, silver inter-particle interactions are very significant and particles need to move around one another to align with flow, causing increased viscosity (191).

To account for the higher relative viscosities on the graphs than the model predictions, there is likely to have been an element of phase separation, and hence sedimentation, occurring in the rheometric testing. When removing the silver from the rheometer, there was a visible separation of silver from the resin on the plate. This would create an increased measured viscosity and hence contribute to a higher relative viscosity. Depletion flocculation, whereby the polymer chains are too large to fit between closely aligned particles, causing the osmotic pressure difference and hence causes flocs in the fluid (192)(130). This could also account for the discrepancy between the data collected and the models. Aside from this error, the error decreases for all models as the polymer Vg increases. The longer chains cause more entanglement within the fluid, resisting flow and in turn raising the viscosity. The viscosity value for the resin increases at a faster rate than the viscosities with silver particles, hence creating a lower relative viscosity with increased polymer Vg.

7.6 Inclusion of Density in Viscosity Modelling

In the previous section, the link between packing factor, density and viscosity was highlighted.

The K-D model showed best alignment with the high-density silver particle inks, however, there was room for closer alignment.

Silver is a high-density particle and particle density was not considered in the equations used. A simple ratio between silver particle density and the sum of the suspension fluid densities i.e. the solvent and the resin, has been included into the K-D equation and has demonstrated a significant reduction in the error between recorded results and model predictions using an Excel solver.

$$\frac{\eta}{\eta_0} = \frac{\rho_{Ag}}{\rho_{TPU} + \rho_{DAA}} \left(1 - \frac{\phi}{\phi_m}\right)^{-[\eta]\phi_m}$$

Equation 7-1 – Adaption of K-D model with a density ratio between particle suspension density and density of suspending fluid, for high polymer Vg, high-density-particle loading.

Where:

η = Measured viscosity

η_0 = Newtonian continuous phase viscosity

$[\eta]$ = Intrinsic viscosity

ϕ = Phase volume

ϕ_m = Maximum packing fraction

ρ_{TPU} = Density of TPU

ρ_{DAA} = Density of Diacetone Alcohol

ρ_{Ag} = Density of Silver

Table 7-6 shows the error values for the K-D model. Table 7-7 shows the error values for the newly proposed equation, incorporating a density ratio for all three components. The new model achieves closer alignment with measured results and consequential error reductions of 21%, 217%, 148%, 108% and 105% for 1.5 Vg, 8 Vg, 12 Vg, 19 Vg and 25 Vg respectively. The error for 1.5 Vg ink remains high due to a previously discussed error in the results.

The model appears to show higher applicability to higher viscosity grade polymer inks.

Table 7-6 – Error values between K-D model and measured results.

	1.5 Vg	8 Vg	12 Vg	19 Vg	25 Vg
40 wt.% Ag	1.50	1.23	2.87	0.25	0.74
50 wt.% Ag	9.578	4.50	3.33	1.69	1.43
60 wt.% Ag	48.93	10.75	16.09	10.35	9.52
70 wt.% Ag	-12.86	20.09	26.36	15.44	11.65
80 wt.% Ag	14.19	-1.98	-2.46	-1.96	-1.62
Sum Error Squared	<i>2855.18</i>	<i>544.83</i>	<i>979.00</i>	<i>352.16</i>	<i>231.58</i>

Table 7-7 – Error values between newly proposed model and measured results.

	1.5 Vg	8 Vg	12 Vg	19 Vg	25 Vg
40 wt.% Ag	-1.17	-1.01	-0.71	-1.10	-0.97
50 wt.% Ag	-0.06	-0.65	-0.95	-1.02	-1.02
60 wt.% Ag	6.77	0.09	1.05	0.40	0.33
70 wt.% Ag	-9.28	1.02	2.00	0.92	0.34
80 wt.% Ag	0.35	-0.14	-0.33	-0.16	-0.04
Sum Error Squared	<i>133.35</i>	<i>2.51</i>	<i>6.61</i>	<i>3.27</i>	<i>2.203</i>

The sum error squared values show a significant decrease with the inclusion of the density ratio and the percentage of model results to experimental results show that this model aligns better for higher particle loading (Table 7-8 and Table 7-9). Viscosity for inks above 1.5 Vg and 50 wt.% silver can be predicted within 22.72% accuracy using the newly proposed equation, which is a significant improvement on the 90% accuracy of the K-D model. The model is significantly more applicable to the prediction of this silver wt.% range. Below this Vg and wt.%, there are extremely large errors. Density has a higher impact on the particle suspensions for higher silver loading. Green and red shading of tables signify which model best aligns for that ink formulation of the two equations. Table 7-8 shows the results for $(1 - (\text{K-D Model Results} / \text{Experimental Results}))$ and Table 7-9 shows results for $(1 - (\text{New Model Results} / \text{Experimental Results}))$. An anomaly is in grey.

Table 7-8 – Highlights show improved alignment (green) or diverged alignment (red) compared to results in Table 7-9 for K-D Model. (Grey for anomaly result).

		Polymer Vg				
		1.5	8	12	19	25
wt.% Ag	40	42.72%	35.03%	55.11%	10.63%	26.79%
	50	76.59%	56.81%	48.43%	36.11%	33.12%
	60	90.32%	63.27%	70.92%	67.05%	66.32%
	70	-500.46%	54.57%	59.14%	55.83%	50.81%
	80	4.71%	-1.74%	-1.87%	-2.95%	-2.80%

Table 7-9 – Highlights show improved alignment (green) or diverged alignment (red) compared to results in Table 7-8 for New Model. (Grey for anomaly result).

		Polymer Vg				
		1.5	8	12	19	25
wt.% Ag	40	-163.15%	-142.07%	-67.40%	-232.66%	-172.02%
	50	-2.41%	-40.33%	-67.80%	-107.25%	-116.41%
	60	61.50%	2.56%	22.72%	12.80%	11.21%
	70	-1776.88%	13.61%	22.07%	16.32%	7.28%
	80	0.58%	-0.62%	-1.25%	-1.18%	-0.31%

7.7 Chapter Conclusion

The aim was to select a DAA:TPU resin ratio and a silver:resin ratio that produced a shear viscosity-shear rate profile similar to that of the two commercial inks. A series of silver inks were formulated, and their rheology compared. The commercial silver ink displayed shear thinning behaviour, with particles aligning with flow until, at high shear rates, a plateau was observed in shear viscosity. The formulated polymer resins showed essentially Newtonian shear profiles, with viscosity dependent on viscosity grade and concentration.

Once silver was added, the shear viscosity-shear rate profiles were too high to be within the range defined by the commercial inks. Two trends that were present in the data were: as the silver wt.% was increased, the shear viscosity increased due to more particle-particle interactions within the ink. The second is that as the wt.% of polymer was increased and DAA decreased, the shear viscosity increased due to high entanglement of the polymer particles. Higher volumes of solvent encourage polymer chains to relax and expand from a spherical like shape, leading to high entanglement and hence, higher viscosity.

These viscosities were adjusted to align with the high shear plateaus in the commercial inks to select an appropriate resin concentration and viscosity grade for use in ink manufacture. A 92.5:7.5 solvent to polymer ratio was selected and the lower end polymer viscosity grades (1.5 and 8) showed closest alignment to the shear profiles of the commercial flexographic inks, with 8Vg fitting between the high shear viscosities of the two commercial inks.

Two ratios of higher DAA content (90:10 and 92.5:7.5) were trialled for the lower two polymer Vgs (1.5 and 8) as the higher polymer Vgs had much higher shear viscosities and showed signs of non-Newtonian behaviours or alternatively inertia within the machine was present in the results. The resins generally displayed a Newtonian profile and when silver was added, the ink

demonstrated a shear thinning profile, that tended towards an infinite shear viscosity beyond a shear rate of 200s^{-1} . It is unlikely that polymer alignment is a contributing factor to shear thinning behaviour of these lower Vg polymer inks and is purely due to particle interaction from the addition of silver particles. There are no thixotropic effects in these inks. The highest wt.% of DAA showed best alignment with the commercial inks and hence was used for an experiment investigating the impact of varying silver wt.% on the shear viscosity—shear rate profile.

The main aim of this work was to understand the relationship between ink formulation, rheology, and printability. It was interesting to reduce the silver filler loading to a minimum point at which resistance of a printed track is not compromised. The 8 Vg is chosen for print trials as the 40 wt.% fit comfortably in the range defined by the commercial inks. There is also space at the lower end of the commercial ink range to reduce the silver content further if the 40wt.% is deemed to be a success in printing trials.

A similar pattern of rheological behaviour was observed for the model inks to that of the commercial inks, with shear thinning and plateauing in the 200s^{-1} shear rate range. Increases in silver content and polymer viscosity grade increased the viscosity of the inks. Increased silver loading creates stronger interparticle forces and high yield points, requiring higher initial shear to initiate flow. The increase in silver loading primarily affected the yield point, and high shear viscosities only marginally increased with silver loading and polymer Vg. 60wt.% ink loading was selected as the fixed parameter as it best aligned with the shear viscosity-shear rate profile of the commercial ink.

In terms of the applicability of the K-D, M-P and E-B models in describing the relationship between relative viscosity and phase volume; All equations showed relatively large errors and demonstrated only weak correlations with the data. The K-D model demonstrated the best alignment and could predict experimental results to at least a 55% accuracy for a 40 wt.% silver loading, however, above this silver loading, deviations ranged up to 90%. This does not provide an accurate method of ink behaviour prediction.

The newly proposed equation (Equation 7-1) builds upon the Krieger-Dougherty model. A ratio of silver density to the sum of densities of the remaining components of the ink is used as a multiplier. This begins to consider the effect of density for high-density silver particles, which were previously unaccounted for in the K-D, M-P and E-B equations. This equation shows most applicability for polymer Vgs of 12 and above, and for silver loading of 60wt.% and above. These limits are likely due to strong interparticle forces within the ink.

The next chapter will explore the use of these inks for flexographic printing, with printed samples analysed in terms of topography and electrical characteristics.

Chapter 8: Effect of Polymer Viscosity and Silver Loading on Printability

8.1 Introduction

The previous chapter showed that lower viscosity grades of 1.5 Vg and 8 Vg with a ratio of solvent to polymer 92.5:7.5 produced rheologically similar inks to commercial silver inks. Commercial inks are not necessarily the perfect ink but work well on flexographic printers and hence was used as a starting point for the research. Further investigation is required to understand the printability of these inks. Furthermore, printed tracks demonstrate edge effects, which may leave the central track with lower quantities of ink. Engagement between rollers could relieve edge effects in the print.

This chapter will explore in detail the key operational setting of engagement as engagement plays an important role in sufficient transfer of ink, without compressing the printing plate and causing squeezing effects, as outlined in Engagement Distance Between Rollers. A study to analyse the effects of the varying engagements available on the RK Flexiproof 100 was conducted. Spreading effects seen throughout testing thus far are associated with engagement settings, so a study has been conducted to investigate the effects of both the anilox roller to plate cylinder (A-P) engagement, and plate cylinder engagement to impression cylinder (P-I) engagement. Conclusions from the anilox volume and print speed study showed high spreading effects, and large quantities of the ink were in fact outside of the specified track width. By changing the engagements, the pressures applied between the rollers will differ.

A range of inks, selected for their alignment with the rheological commercial ink range, from the previous work were then printed at the optimised settings.

The impact of rheology on printability was then evaluated for an exemplar selection of the inks to represent the range of Vg and silver loading.

8.2 Effect of Press Engagement

The printing plate previously used in section Revised Monopole Antenna Design for Testing Print Variation was used. The 1mm width line was measured as the thinner lines did not produce a consistently readable resistance. The printed samples are presented in Figure 8-1 and Table 8-1.

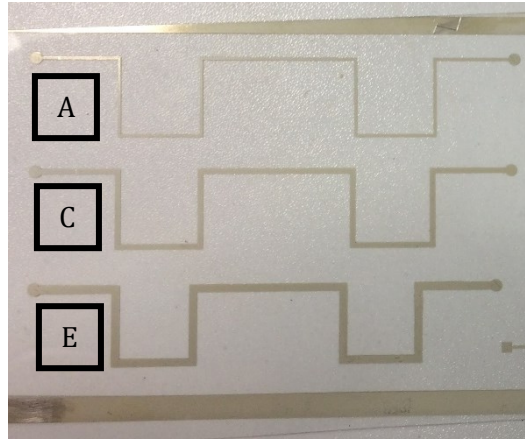


Figure 8-1 – Printed antenna designs A, C and E.

Table 8-1 – Design parameters of a plate with lines of various widths and lengths.

Line Reference	Line Width (mm)	Line Length (mm)
A	0.5	147
C	1	164
E	1.5	181

The silver ink ‘8 Vg polymer:DAA:60 wt.% Ag’, was trialled on the printer using the parameters (50m/s print speed, 24cm³/m² anilox volume) that achieved the lowest resistance for the commercial ink. This ink contains no additives or surfactants so the ink behaviour on the printing press can be correlated to the interactions of the particles, polymer, or solvent in the ink. Print settings for an engagement study are outlined in Table 8-2.

Table 8-2 – Print settings for print engagement trial.

Printer	RK Flexiproof 100		
Ink	8 Vg polymer:DAA:60 wt.% Ag		
Substrate	HiFi Industrial Film SU 320 175µm PET		
Anilox Volume	24 cm ³ /m ²		
Backing Tape	3M E1120 (medium hardness)		
Print Speed	50 m/s		
Drying Method	Vötsch VTL 60/90 Oven 15 mins, 150°C (Recommended from preliminary testing)		
Print Engagements (Further discussed in Methodology)	Only A-P Changes	Anilox Roller-Printing Plate Roller (µm) (A-P)	Printing Plate Roller-Impression Cylinder (µm) (P-I)
		140	280
		200	280
		260*	280*
		320	280
	Both A-P and P-I Change	420	280
		140	160
		200	220
		260*	280*
		320	340
	Only P-I Changes	420	400
		260	160
		260	220
		260*	280*
		260	340
	260	400	

* Using same print for 260, 280 µm settings in table.

8.2.1 Effect of Engagement on Film Thickness

Printed designs and the key to the profiles are shown in Table 8-1 and Figure 8-1. As previously seen in assessing resistance with respect to engagements, as P-I engagement increases, there is less of a squeeze effect up to a distance of 280µm (visually seen in Table 8-3). At this point, the track has a more even ink distribution. As the engagement becomes larger, the ink separates into

three tracks (Figure 8-3). With ink separated into individual tracks, this reduced the quantity of ink in an individual track, hence lowering the resistance (Figure 8-5). In the second column of this figure where both engagements are increased, there is a similar pattern. For the third column, where the A-P engagement is increased, the ink distribution is good for the lowest engagement and slowly separates into three distinct peaks. The higher two engagements show a suppressed middle peak and two larger outside peaks, which is indicative of the squeeze effect, however, the rollers have moved to their furthest distances in this experiment, so it is unlikely to be the squeeze effect. This was an unexpected result and requires further investigation outside of this study. This division of ink reduces the volume of ink that a current can flow through at one time. A smaller cross-section of ink indicates a higher resistance and hence, lower performance.

In contrast to the other two columns, where the printed tracks grow thinner with increased engagement, the track becomes wider for an increased A-P engagement.

With high engagement pressures, ink is squeezed out from its intended deposition pattern, causing a high film thickness, yet little uniformity in the deposition of the ink.

Table 8-3 – Key to image array Figure 8-2Figure 8-1.

	Increasing engagement between Plate Cylinder and Impression Cylinder	Increasing engagement between Anilox to Plate Cylinder	Increasing engagement between Anilox and Plate Cylinder; and Plate Cylinder and Impression Cylinder
	Column 1	Column 2	Column 3
Row 1	260, 160	140, 280	140, 160
Row 2	260, 220	200, 280	200, 220
Row 3	260, 280	260, 280	260, 280
Row 4	260, 340	320, 280	320, 340
Row 5	260, 400	420, 280	420, 400

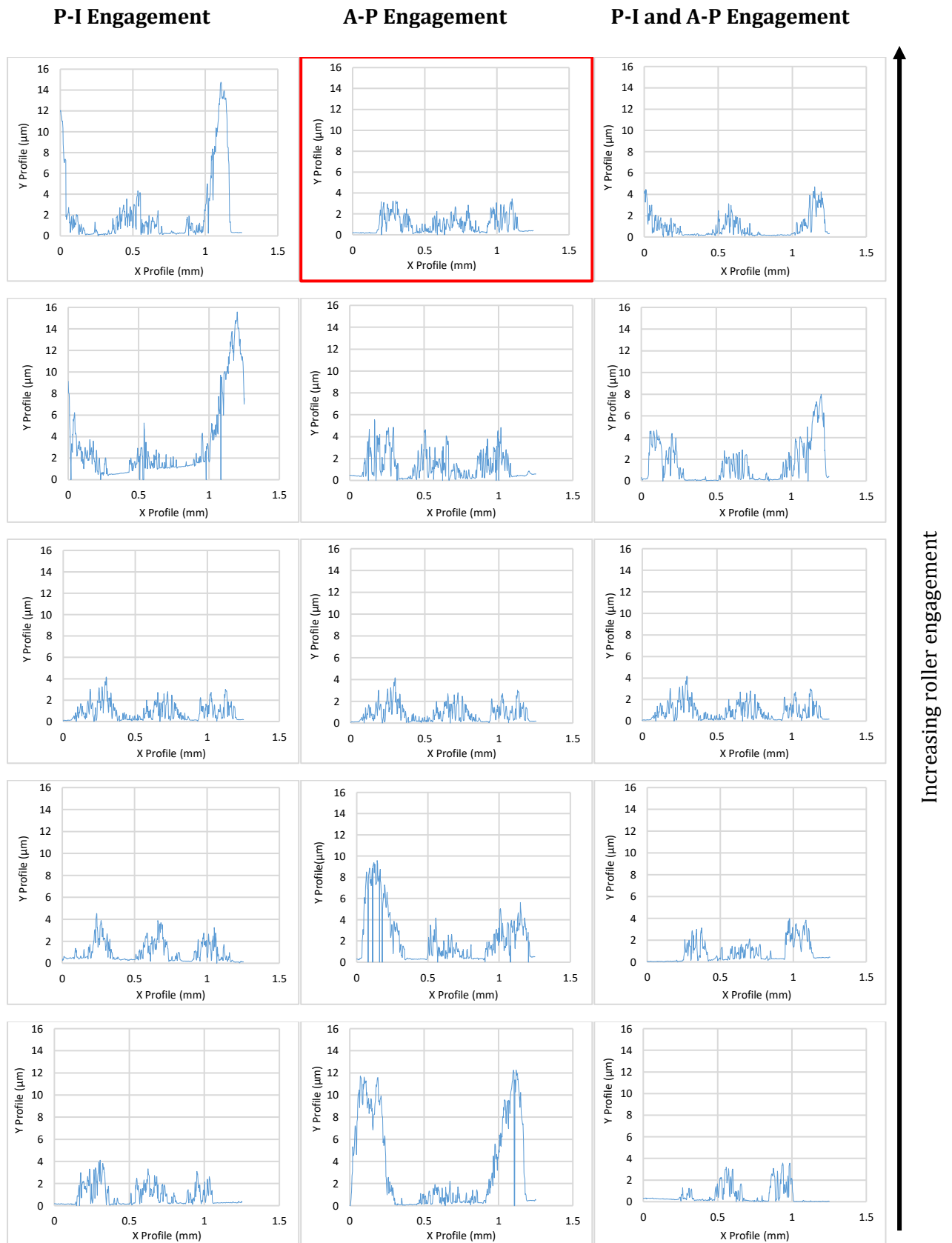


Figure 8-2 – Engagement settings (Anilox Cylinder to Plate Cylinder Plate Cylinder to Impression Cylinder). Optimal profile for low resistance is highlighted in red.

Figure 8-3 shows white light interferometry images of design C (1mm line width) for engagement setting 200, 280 μm (A-P,P-I) which produces a consistent ink deposition profile and in turn a low resistance [Figure 8-5 (a)]. Two other engagement settings 420, 280 μm (A-P,P-I) [Figure 8-5 (b)] and 420, 400 μm (A-P,P-I) [Figure 8-5 (c)] demonstrate surface profiles of poorly conductive tracks. There are areas of high deposition, indicated in red (b), with little ink deposited in the central area. Additionally, the edges of the tracks are inconsistent. Figure 8-3(c) shows fluctuations in deposition both in the horizontal and vertical. Both result in low conductivity. However, Figure 8-3 (a) demonstrates a more consistent print along the length of the track (less areas of excessively low ink deposition) and consequently has low measured resistance.

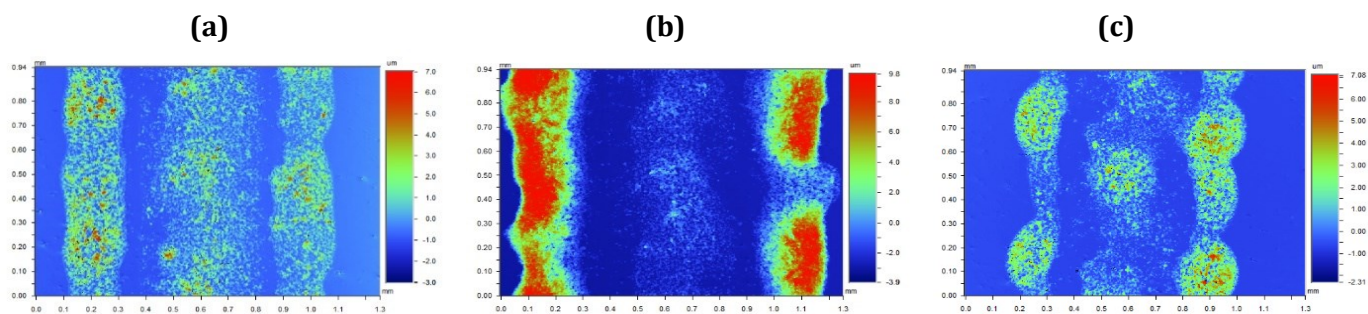


Figure 8-3 – White light interferometry images of 1mm lines for engagements: **(a)** 200,280 μm (A-P,P-I), **(b)** 420,280 μm (A-P,P-I) and **(c)** 420,400 μm (A-P,P-I).

At close A-P engagement, the plate presses into the anilox holes. This applies an extensional force on the ink (118). The viscosity decreases significantly for these shear thinning inks when a shear is applied, as seen from shear viscosity-shear rate graphs in rheological experimentation. Lower viscosity increases the flow of the ink and aids in the extraction of ink from the cells, increasing the volume of ink and decreasing the resistance. However, as the engagement is increased, two distinct peaks at the edges of the printed track are shown in the line profiles (Figure 8-2), leaving little to no ink in the main channel of the printed line. Notably, these peaks that form an ‘M’ shape [also seen in literature (193)] are distinctly higher than other film thicknesses produced. The majority of ink ends up at the edges in this scenario, with little ink in the centre. It could be that the lack of roller-to-roller contact means there is not enough shear applied between rollers and hence, ink is too viscous to transfer sufficiently.

At close P-I engagement, the ‘M’ shape appears, displaying two distinct peaks at the edges of the printed track. As the engagement distance is increased, the peaks widen and then become three distinct peaks, with relatively good film thickness distribution between the three peaks. It is as these peaks increase in width and the third peak begins to form, more ink deposition is noticeable

in the cross-sections and the resistance reaches a minimum. As the engagement reaches the maximum distance tested, less ink is transferred, and the peaks decrease in width.

Average film thickness has not been discussed here due to the geometry of the printed lines with many producing shapes known as 'bunny ears'. An accurate average film thickness is not possible to obtain for this printed line using previous methods.

8.2.2 Effect of Engagement on Printed Line Width

Printed line widths for a meandering line of nominal width 1mm are shown in Figure 8-4 (a), (b) and (c) for engagement settings: A-P changes, P-I changes, and A-P with P-I changes respectively. Figure 8-4 (a) shows spreading between 33% and 50% of designed line width, whereas varying the plate to impression cylinder engagement, [Figure 8-4 (b)], has a much higher range from 26% to 82% with a line gain for all lines which increased with close engagement. Higher engagements for both sets of cylinders achieve line widths more closely comparable to the designed widths on the printing plate [Figure 8-4 (c)], with just 23% line spreading.

Greater A-P engagement distance causes a rise in line width. Figure 8-2 shows that the three ridges that have formed in the printed line cross-section move further away from the centre and form two distinct peaks at the edges of the line and the central ridge depletes. These two peaks almost double in film thickness compared to the film thickness of the closer A-P engagement distances. Initially, it was thought that a similar amount of ink was transferred but it was now at the edges of the print rather than evenly distributed. Comparing with Figure 8-5, resistance increases with larger A-P engagement distance, indicating that less ink is transferred. However, because this 'M' shape in the cross-section has occurred, there is little ink in the centre of the printed line and in effect has created two parallel lines from the relatively similar quantity of ink. With a separation in the printed line, this will reduce pathways for electrons to move through the printed ink and hence create a higher resistance.

Increasing the P-I engagement distance decreases the line width, bringing it closer to the designed line width [Figure 8-4 (b)]. This, however, does not mean lower resistance. Comparisons with Figure 8-2 show the spread of the previously discussed peaks and 'M' shape. The pushing of the ink into the peaks at the edges increases the print width. For larger P-I engagement distances, these peaks move closer to the centre and decrease in width.

A-P engagement aligns well with resistance and P-I has little if any impact. The decrease in line width for increasing P-I engagement distance is more significant than the increase in line width

for an increase in A-P engagement distance, hence it was expected that as both were increased together, the line width would decrease. It is also interesting to note that Figure 8-4 (c) reflects Figure 8-4 (b) well, indicating that the addition of varying the A-P engagement has little to no impact on the line width outcome.

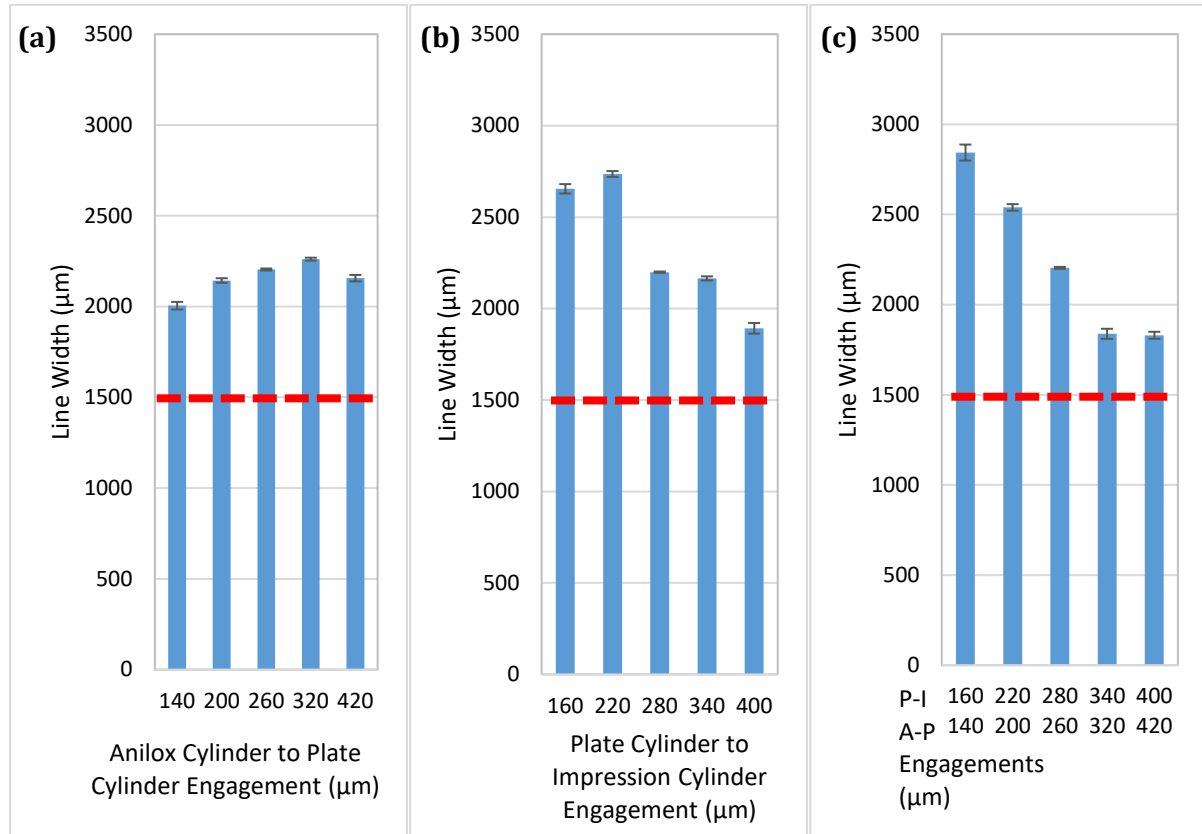


Figure 8-4 – Effect of engagement on line width of a printed 1mm width track where (a) A-P engagement varies, and P-I engagement is set to 240 µm; (b) Varying P-I engagement A-P engagement is set to 260 µm.; (c) A-P engagement and P-I engagement vary simultaneously. Error bars show one standard deviation

8.2.3 Effect of Engagement on Resistance

Figure 8-5 (a) shows the resistance measurements for a 1mm wide line where the engagement distance between the plate cylinder and the impression cylinder is held at 280µm, and the engagement between the anilox cylinder and the plate cylinder is changed between engagements of 140µm, 200µm, 260µm, 320µm and 420µm. The two smaller engagements produce the lowest resistances, with the second highest having a smaller standard deviation. Thereafter, the resistances increase with increasing engagement distance. Additionally, as shown with previous tests, the higher resistances have higher standard deviations.

Figure 8-5 (b) shows the resistance measurements for a 1mm wide line where the engagement distance between the anilox cylinder and the plate cylinder is held at 260µm, and the engagement

between the plate cylinder and the impression cylinder is changed between engagements of 160 μm , 220 μm , 280 μm , 340 μm and 400 μm . The lowest engagement distance produced the highest resistance and also the highest standard deviation. After this setting, the measured resistances gradually increase as the engagement settings increase from 220 μm and 400 μm respectively. Statistical difference is not seen in the larger measured resistances due to large overlap of the standard deviations.

Comparing (a) and (b), it can be seen that increased A-P engagement distance has, by comparison, a small impact on resistance, increasing by $\sim 3\text{k}\Omega$. On the other hand, changes in P-I engagement distance can change resistance from 25k Ω to 0.5k Ω [Figure 8-5 (b)]. Hence, it was assumed that the graph of combined increasing engagements [Figure 8-5 (c)], would look similar to Figure 8-4 (b), and that (A-P, P-I) 200, 240 engagement would produce the lowest resistance. The lowest resistance produced is 200 μm A-P and 280 μm P-I [Figure 8-5 (c)], which are similar gap sizes to those expected. Even comparison of Figure 8-5 (c) to the cross-sections in Figure 8-2 shows a good correlation between profiles for an increase in P-I engagement and increase in A-P,P-I engagement.

It could be that the extremes of the setting tested provide too much squeezing between plates at one end and at the other; there is not enough contact for ink transfer. The two extreme values used produced high resistances with very large standard deviations, meaning that there is insufficient repeatable data to determine any statistical difference.

There is a slight correlation between resistance and low film thickness, high print width and low surface roughness, however, some engagement settings exist that do not fit this correlation. Analysis of the cross-sectional profiles suggests that the surface profile plays a strong role in the impact on the resistance. The profile is accounted for in all print measurables i.e. spreading effects in terms of width, and fluctuations in print consistency in surface roughness and print height.

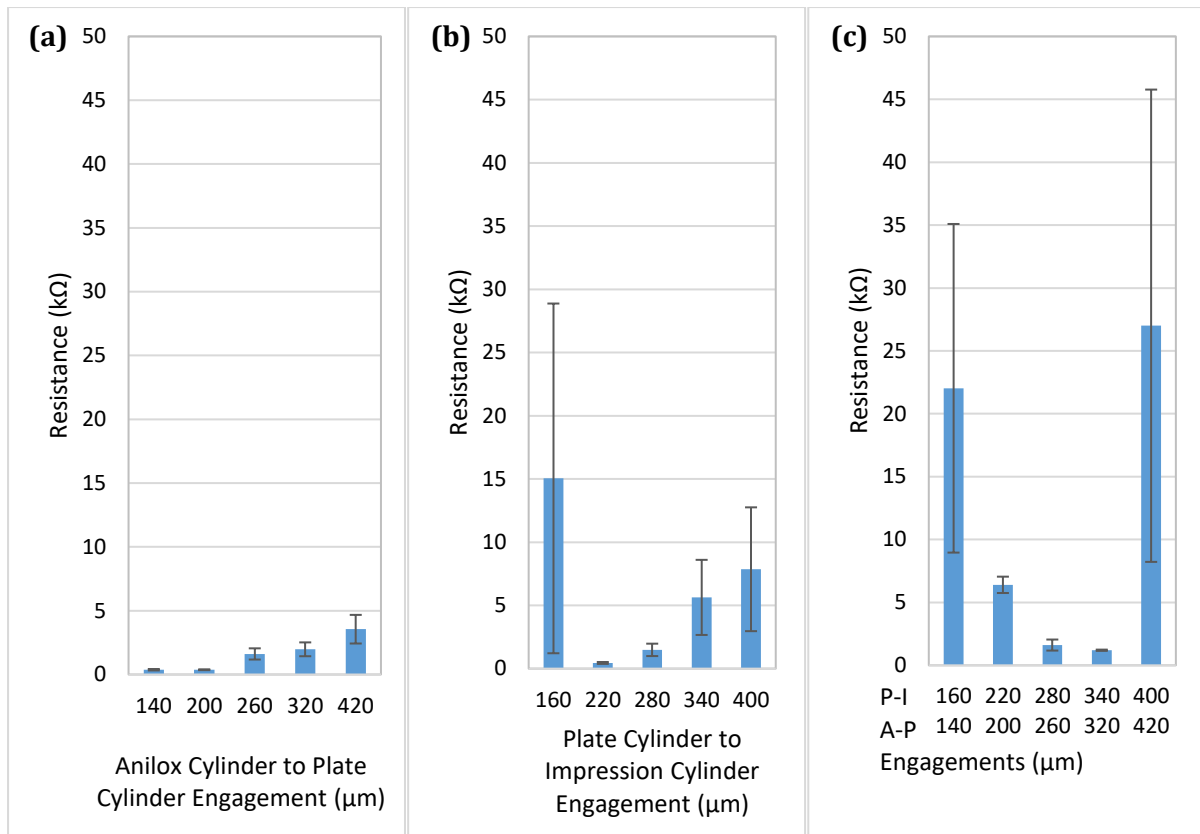


Figure 8-5 – Resistance measurements of a 1mm line width for: **(a)** increasing A-P engagement. P-I engagement is 280μm; **(b)** increasing P-I engagement. A-P engagement is 260μm; **(c)** increasing A-P and P-I engagement. Average resistance measurements are shown with one standard deviation.

8.3 Printing Trials Using Inks of Varying Viscosity Grade and Silver Content

8.3.1 Introduction

Rheological testing has determined the optimal resin to solvent ratio to align the ink formulation to commercial ink shear viscosities. With an understanding that increased polymer Vg and silver loading increases the viscosity, a print study to investigate the impact of these rheological changes on printed samples was conducted (Table 8-4). An ink of 8 Vg polymer for five silver loadings (40, 50, 60, 70 and 80 wt.%), and a silver loading of 60 wt.% for five polymer Vgs (1.5, 8, 12, 19 and 25Vg) were printed. 8 Vg and 60wt.% were chosen for their rheological alignment with commercial inks. Testing the range of Vgs and silver loadings is to provide an understanding of the effect of varying Vgs and silver loading in the flexographic print process.

Table 8-4 – Printed inks (red) from full factorial array.

	Viscosity Grade					
		1.5	8	12	19	25
Silver Loading (wt.%)	40					
	50					
	60					
	70					
	80					

Three designs printed: A, C and E, are shown Figure 5-6 and dimensions are in Table 5-3.

As outlined in the methodology section, all printed inks were three-roll milled prior to use on the printer. Of the inks printed, the resistances, film thicknesses, surface roughness' and print widths were measured, and the resistivities calculated. Printer settings were based on Assessment of Flexographic Process Parameters and Effect of Press Engagement, which optimised anilox volume, print speed, drying conditions and roller engagement settings for the lowest possible resistance.

8.3.2 Effect of Polymer Viscosity Grade and Silver Loading on Line Widths

Figure 8-6 shows the % increase of widths from designed width to printed width for the three printed lines. The lines show the same pattern of behaviour across the changing polymer Vg. The effect of spreading is higher for smaller track widths. There is no significant impact of increased polymer Vg on the line width of the printed track [Figure 8-6 (a)], although 1.5 Vg inks have the highest line widths of all polymer Vg inks used. All designs for both variations in Vg and silver loading show a variation of less than 150µm in line width. Figure 8-6 (b) shows that there is no correlation between silver loading and line widths.

Whilst there is no increase in average line widths for increases in polymer Vg and silver loading, Figure 8-7 and Figure 8-9 show an increase in the waviness of line edges.

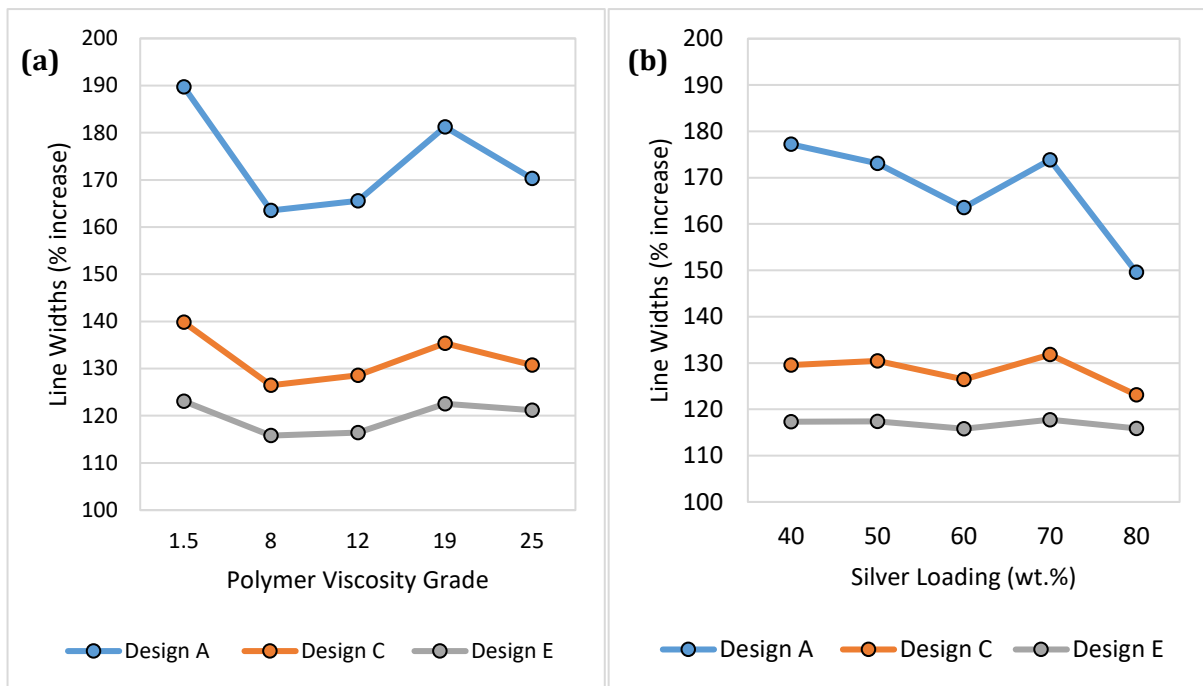


Figure 8-6 – % increase in three line widths (design A:0.5mm, design C:1mm and design E:1.5mm) for changes in the silver ink of 60 wt.% loading with polymer (a) Vg1.5 (b) Vg8. Each point is an average increase for five measurements taken.

Figure 8-7 and Figure 8-9 show images taken on the Alicona microscope of design A printed tracks.

As the Vg increases, the visual waviness of the edges of the tracks increases. The line width reduces from 1.5 Vg to 8 Vg, and then increases in width up to 19 Vg, followed by a slight drop to 25 Vg. The waviness of the track edges shows a similar pattern. The excess ink along the edges of the track, most prominently seen for 25 Vg, are indicative of large anilox volumes. To visually demonstrate this relationship, an overlay of the anilox cell structure and printing plate track demonstrates this (Figure 8-10) on examples of the printed track shown in Figure 8-7 and Figure 8-9. This effect is non-existent for the lowest polymer Vg 1.5.

The lowest Vg visually exhibits the smoothest line edges. As the Vg increases, not only greater effects of waviness are seen but ink coverage at the edges of the track becomes less continuous. Throughout all images of changing Vgs (in Figure 8-7), there is a line where the main body differentiates from the 'edges' of the track, although this is very faint on some tracks. This separates the print into two sections, the main body and the edges. In the main body of the track, the volumes of ink deposited spread to connect and form one large body. The printing plate image impress the image onto the substrate and forces these volumes to amalgamate into one. On the edges of the print, without the impression of the printing plate image pressing the ink into the substrate, the structures of the ink volumes drawn from the anilox cells remain. The correlation

to the anilox geometry is distinct in the printed pattern. After ink is forced into the anilox cells from the ink tray, it forms a strong enough structure at the edges of the printed track to maintain its shape until reaching the substrate. At lower Vg there is higher relaxation of the ink due to a lower viscosity. However, as the Vg increases, this effect become increasingly pronounced. The level of viscosity has overcome not only being withdrawn from anilox cells onto a printing plate but has also maintained its shape throughout a second transfer onto the substrate.

High polymer Vg increases entanglement of particles, meaning that it takes longer for the polymer particles to align with flow. It could be that the ink has not been sheared long enough to reach sufficient flow of the ink as seen with initial shear ramps in rheological testing.

Despite the higher Vg inks showing increased edge waviness and substantial breaks in the film in line with the print direction, the 19 Vg print holds the lowest resistance value for design A.

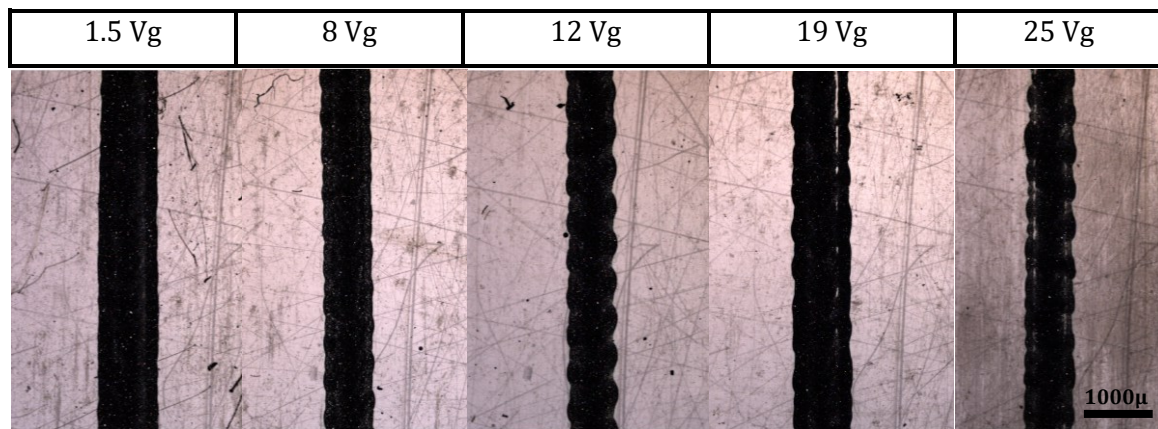


Figure 8-7 – Design A: Silver loading 60wt.%, polymer Vg 1.5, 8, 12, 19, 25.

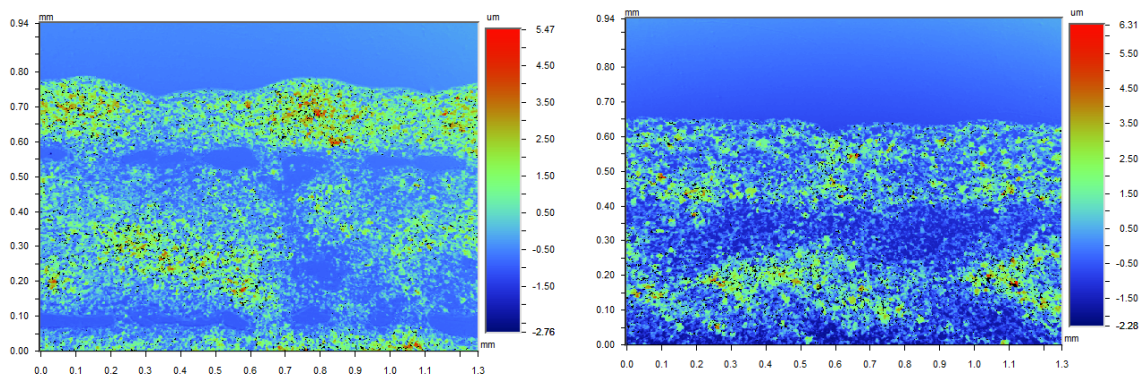


Figure 8-8 – White light interferometry scans of 1.5 Vg (left) and 25 Vg (right) for a silver loading of 60wt.%.

The line in Figure 8-9 becomes inconsistent at high silver loading. While the average line width stays the same, the edge profile becomes uneven and has a marking effect due to the increased ink viscosity in the anilox cells. The high viscosity ink retains the ‘shape’ of the cell rather than

conforming with the line. Figure 8-10 shows an overlay of correctly scaled anilox cell structure and printing plate track over printed lines and demonstrates the relationship. The coarse anilox ruling is as such due to the highest anilox volume being used. Where the track enters another cell, more ink is removed for higher viscous inks and edge waviness of the line increases.

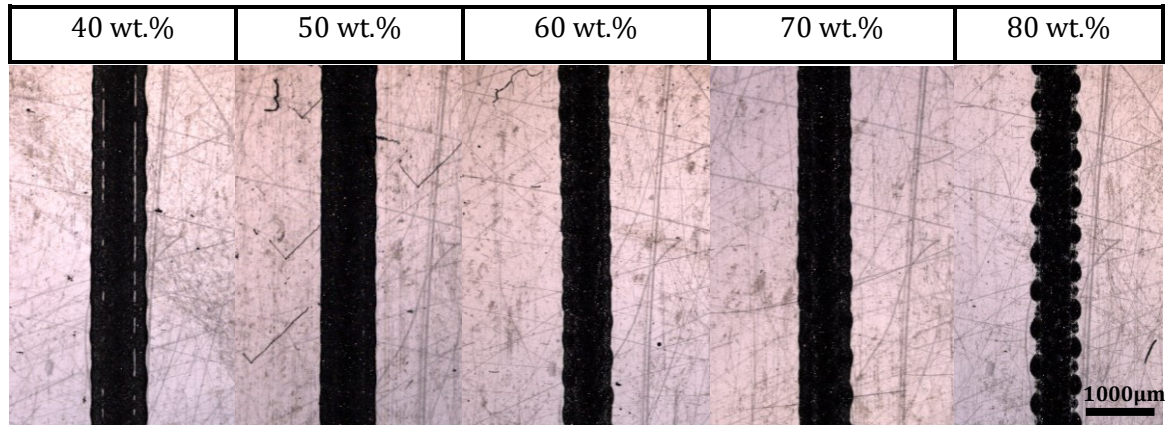


Figure 8-9 – Design A: 8 Vg; Silver loading 40, 50, 60, 70 and 80wt. %.

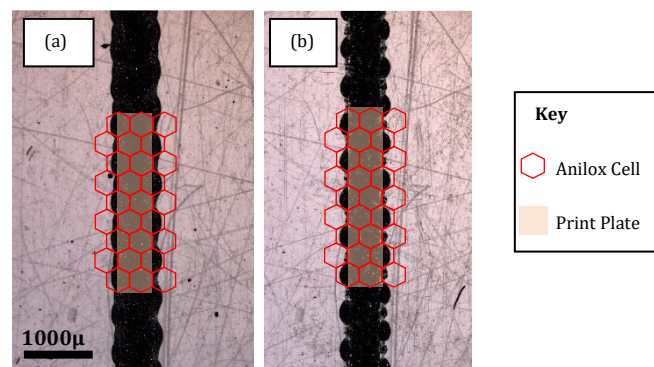


Figure 8-10 – Overlays of anilox cells and printing plate track on (a) 12 Vg ink track (b) 80wt. % silver loading ink track. Anilox cell measurement outlined in Methodology.

Increasing silver loading increases the interparticle forces and hence the measured viscosity. As the silver content is increased, the effect of particle-particle interaction is more prevalent. At 40 wt.%, there are not enough silver particles to have significant particle-particle interaction. The structure between particles is weak enough that the structure does not recover from plate pressure. If the line breaks between the edges and the central track (shown in 40wt.% silver Figure 8-9), it may be due to too a high roller engagement and hence squeezing effects of the printing plate. A potential mechanism for describing the squeeze effects is outlined in Figure 8-11. As the plate, hosting the ink, connects with the substrate, it flattens ink under its surface. Excess ink is then squeezed out from underneath (Figure 8-11). The quantity of ink on the edges of the printing plate has been less affected by shearing forces, in turn, this becomes an excess around

the perimeter of the features. When the ink begins to relax on the substrate, after the plate has left, this excess ink has relatively strong forces present when compared to the sheared main body ink, and can pull ink in, parting it from the main body and causing the lines in the print. High speed cameras can be used to verify this in further testing.

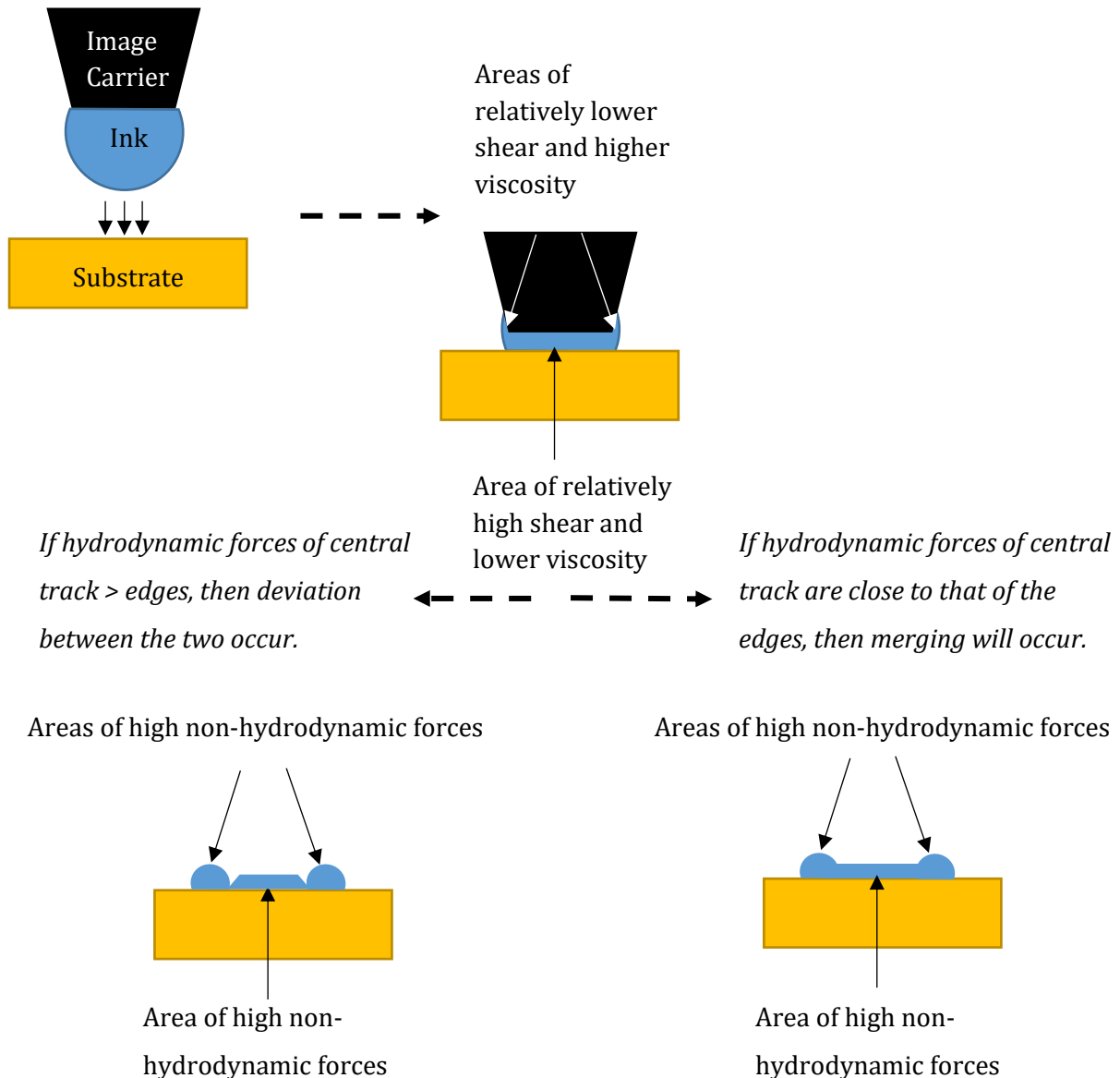


Figure 8-11 – Cross-section of printed track on a flexographic printer. Demonstration of theorised movement of ink under the plate pressure.

50 wt.% loading visually produces the most coverage and lowest waviness of the edges of the track. 40 wt.% shows some edge waviness, which could be due to the lack of silver particles and lessened structure formed through interactions between particles and resin, allowing ink to relax for longer on the substrate after printing. There is good relaxation in the ink, allowing the ink to form smooth edges and a consistent print across the surface. Above this loading, particle-particle

interaction becomes more prominent and distinctly alters the structure of the deposited fluid, particularly seen at the edges of the print. At the highest wt.% of 80, structures have formed in the anilox and been transferred to the substrate. For the main body of the track, ink deposition is relatively smooth. It is in this area that sheared ink is present, as opposed to the ink sitting at the side of the raised image on the printing plate.

If the shear rate was not sufficient to overcome the strong particle-particle interactions and cause shear thinning, then the viscosity of inks would remain high and create volumes of ink on the edges.

8.3.3 Effect of Polymer Viscosity Grade and Silver Loading on Film Thickness

For an increase in V_g , there was seen to be a general increase in film thickness [Figure 8-12 (a)]. However, this trend is not linear and only applies for design C and E. Design A, the smallest line width, shows the most fluctuation, due to relative edge effects.

There is a strong correlation between film thickness and silver loading [Figure 8-12 (b)]. An increase in silver loading increases film thickness due to high solid content and low solvent quantities. Another factor that may be contributing to the high film thickness is the high shear viscosity at all tested shear rates ($0.1-200 \text{ s}^{-1}$) (Figure 7-9), which will reduce spread on the substrate.

Similarities can be drawn between designs A and E for print thickness and print width (Figure 8-12 and Figure 8-6). For increases in the width there are increases in the print thickness, implying that a higher volume is being deposited. Print width is independent of effects by polymer V_g so polymer V_g alterations cannot be used to control the width of the printed track. However, there is a weak control over the thickness and by increasing the polymer viscosity grade, the film thickness can be slightly increased.

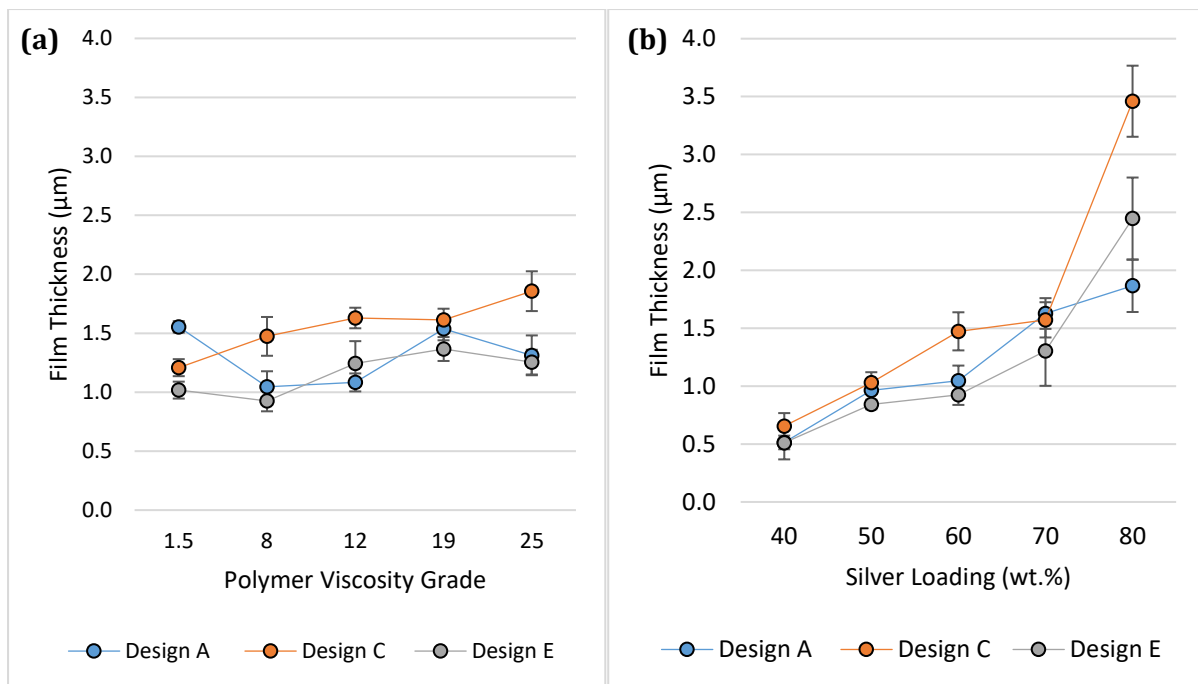


Figure 8-12 – **(a)** Film thickness of three line widths (design A:0.5mm, design C:1mm and design E:1.5mm) for polymer Vg changes in the silver ink of 60 wt.% loading. **(b)** Film thickness of three line widths (design A:0.5mm, design C:1mm and design E:1.5mm) for silver loading changes in the silver ink of polymer 8 Vg. Error bars show standard deviation of 5 samples.

8.3.4 Effect of Polymer Viscosity Grade and Silver Loading on Surface Roughness

There is a lack of relationship between surface roughness and Vg (Figure 8-13). There is a variation of 144nm for designs A and E, however, design C shows a range of 292 nm. There is a strong correlation between surface roughness and silver loading.

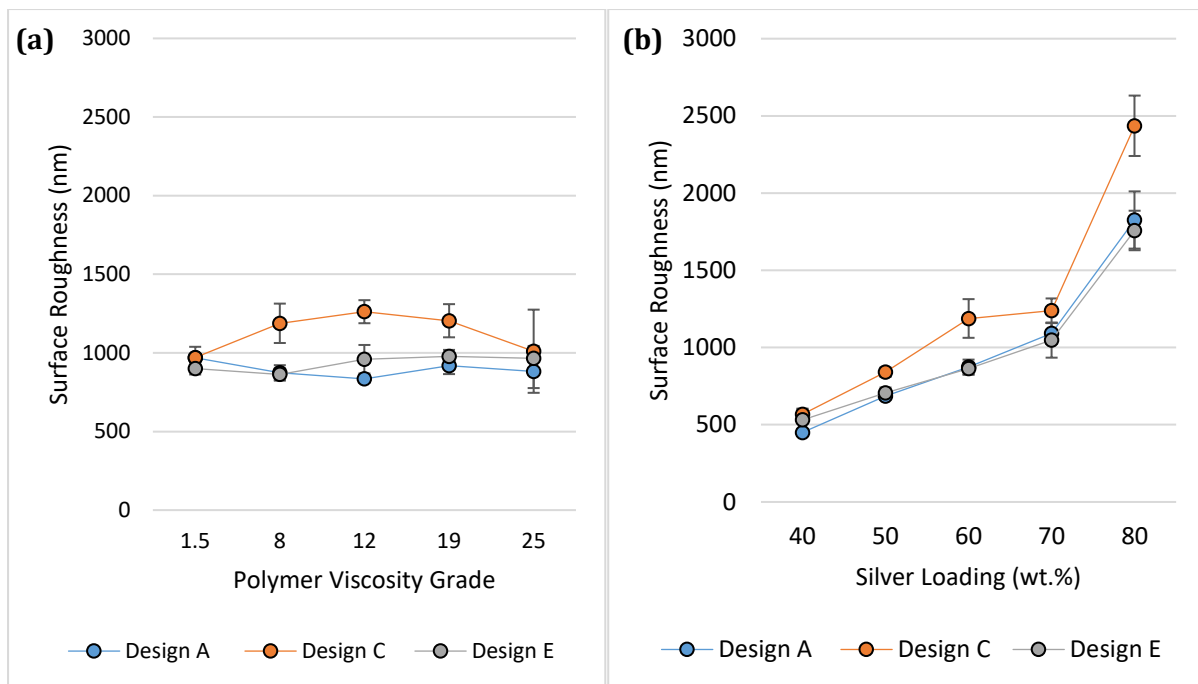
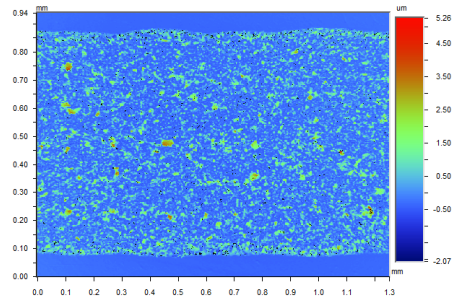


Figure 8-13 – **(a)** Surface roughness of three line widths (design A:0.5mm, design C:1mm and design E:1.5mm) for polymer Vg changes in the silver ink of 60 wt.% loading. **(b)** Surface roughness of three line widths (design A:0.5mm, design C:1mm and design E:1.5mm) for silver loading changes in the silver ink of 8 Vg polymer. Error bars show standard deviation of 5 samples.

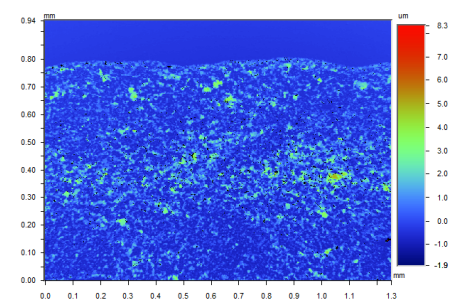
An increase in silver loading shows a higher likelihood of demonstrating a viscous fingering pattern (Figure 8-14 and Figure 8-15). This forms at around 60wt.% and increases with an increase in silver loading and consequently increased viscosity. When comparing Figure 8-14 and Figure 8-15 with Figure 8-13 (b), which presents data extracted from the white light interferometry images presented in (Figure 8-14 and Figure 8-15), the increased surface roughness can be clearly demonstrated by viscous fingering up to 70wt.%. At 80wt.%, there is a large increase in surface roughness, which correlates with the relatively high peaks shown [Figure 8-13 (b)], caused by high viscosity ink being drawn from the anilox. Due to the high viscosity, the ink does not relax and holds its ‘cell’ structure.

Increases in viscosity grade do not demonstrate any effect on viscous fingering surface patterns, which correlate with Figure 8-13 (a).

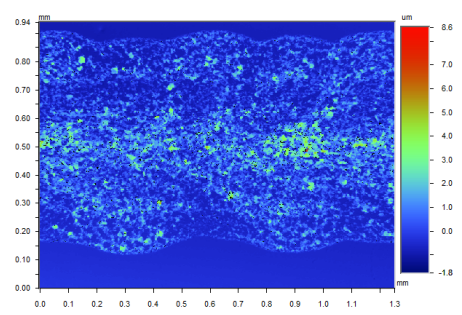
40wt.%



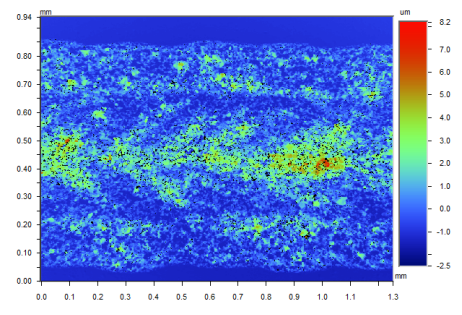
50wt.%



60wt.%



70wt.%



80wt.%

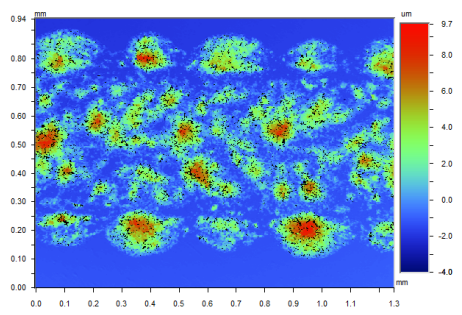


Figure 8-14 – White Light Interferometry images of printed tracks for five silver loadings.1.5 Vg.

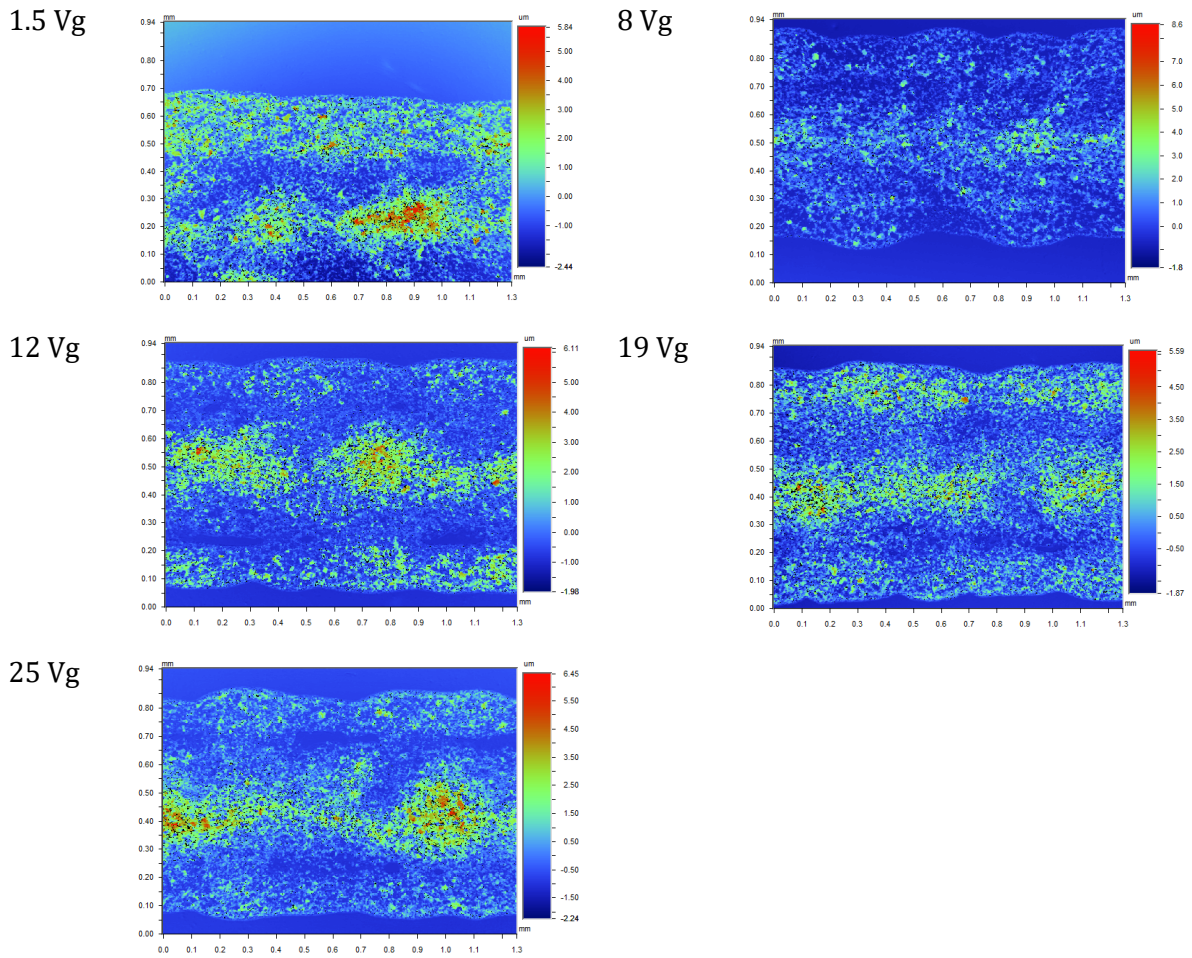


Figure 8-15 – White Light Interferometry images of printed tracks for five viscosity grades.

8.3.5 Effect of Polymer Viscosity Grade and Silver Loading on Resistance

Printed line resistance is shown for the various combinations of silver loading and polymer viscosity in Figure 8-16 (a) and (b). Resistance decreases in value as polymer Vg increases from 1.5 to 12 for all line widths [Figure 8-16 (a)]. This trend follows as such for the 0.5mm and 1.5mm line widths of designs A and C, however, significantly higher resistances were measured for design C, averaging at 51,635Ω, and hence not shown in the figure. After 19 Vg, the resistance increases for all inks.

The lowest resistance achieved was 58Ω for a line width of 1.5mm with a silver loading of 60wt.%, and for a line width of 0.5mm, 181Ω [Figure 8-16 (b)]. For silver concentrations below 60wt.%, resistance is generally high. However, there is no benefit of increasing the silver loading beyond 60 wt.% as there is no clear trend of improved line resistance. Resistance continues to decrease marginally even though Figure 8-13 shows an increase in irregular surface topography. As print

thickness increases with increased silver loading, silver consumption is also increased. When looking at Figure 8-9, distinct parts of the line can be seen. This reduction in consistency and lack of silver content across the line is demonstrated in the resistance as no resistance could be detected for this print. Higher silver content means that a measurement can be taken, and the resistance is lower for higher content as expected. Interestingly for the 80wt.%, the line is very wavy at the edges, but this provides the lowest resistance. The high viscosity of the ink must overcome the large surface roughness for this print.

The wider line widths, designs C and E maintain lower resistances than design A for lower silver loading. For lower silver loading content, no resistance measurements can be detected however, the widest line, E, shows a high resistance of 2,736 Ω for a 50wt.% loading. The lowest resistance achieved of all lines was 52 Ω for design E at 70wt.% loading, however decreasing loading by 10% increases resistance by 15 Ω ; and increasing loading by 10% increases the resistance by 2 Ω .

Surface roughness does not show a correlation with the decreasing resistance for increasing polymer Vg or silver loading.

For loading levels outside of 60 wt.% to 70 wt.%, a resistance could not be detected for the thinnest line, which could be because at lower wt.%s there is not enough silver in the ink to give good conductivity at that line width. Further investigation is required to understand this limitation. This means that silver loadings 40, 50, and 80wt.% were outside of the process window. For the larger line widths, the operating window increased to 60-80 wt.% with relatively low resistances.

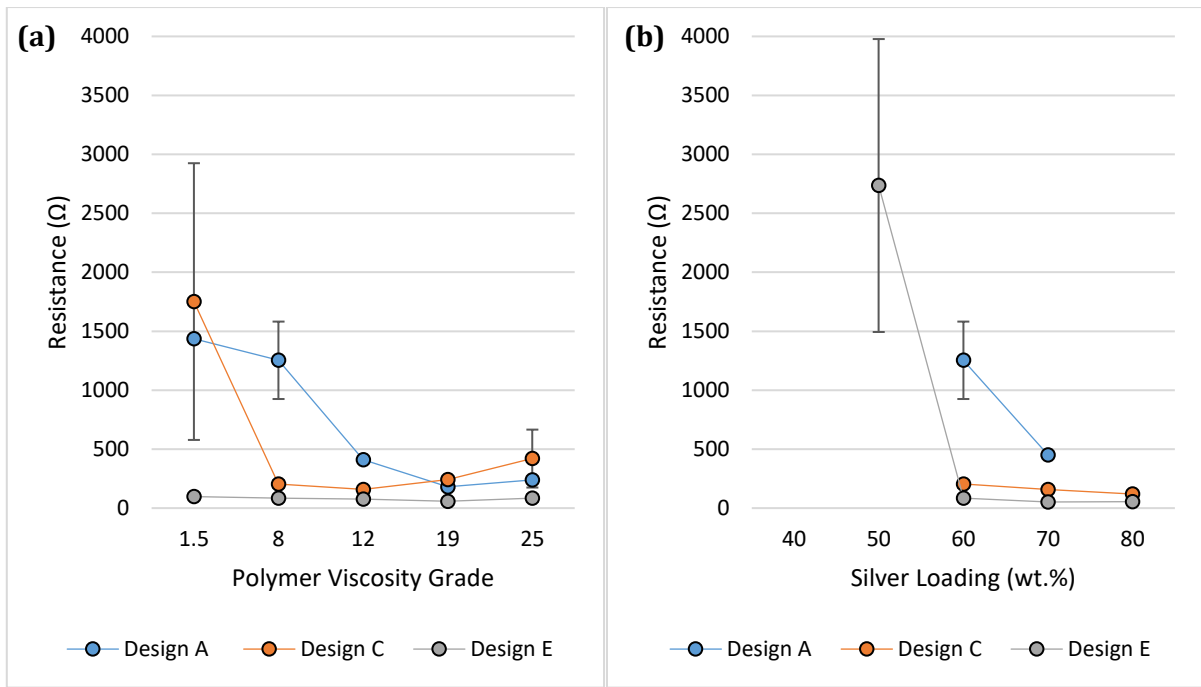


Figure 8-16 – (a) Resistance of three line widths (design A:0.5mm, design C:1mm and design E:1.5mm) for polymer Vg changes in the silver ink of 60 wt.% loading. (b) Resistance of three line widths (design A:0.5mm, design C:1mm and design E:1.5mm) for silver loading changes in the silver ink of 8 Vg. Error bars show standard deviation of 5 samples.

8.3.6 Effect of Polymer Viscosity Grade and Silver Loading on Resistivity

The calculated resistivity of the three line widths printed is shown in Figure 8-17. The two thinner line widths, designs A and C, show the same pattern of behaviour across the changing polymer Vg and decrease in resistivity for an increase in polymer Vg up to 12 Vg. Both designs were measured to have slightly increased in resistivity for the highest Vg tested, 25. For design E, resistivity stays relatively consistent for changes in Vg, highlighting that at the 1.5mm line width, changes in resistivity are very small in comparison to smaller line widths. As the resistance decreases, film thickness plays a stronger role in increasing the resistivity at higher Vg.

For the smaller line widths, Vg has a higher impact on the resistivity, although at higher Vg this is shown to be less prominent for a line width of 0.5mm. This conflicts with results gathered from the 1mm line, design C. Above 12 Vg, the resistance and resistivity of design C increases much higher than the other two designs.

The resistivity for design A at 50 wt.% silver loading is significantly higher at 287,029Ωμm and not included on the graph for better demonstration of the other results. Designs A and E produced very high resistances at 50 wt.%. Low volumes of ink at this wt. %'s mean that there are not

enough bonded silver particles when the ink has dried to allow for sufficient transfer of electrical energy through the printed track.

Only for the widest line of 1.5mm could a resistance be detected at a 50wt.% loading. Resistivities are relatively low in value for 60wt.% and 70wt.% loading. However, 80wt.% loading sees an increase in resistivity. Wider line widths allow for a wider range of polymer Vg to be used in the inks however, an optimal low resistance and resistivity is found for a silver loading of 70wt.% and 19Vg.

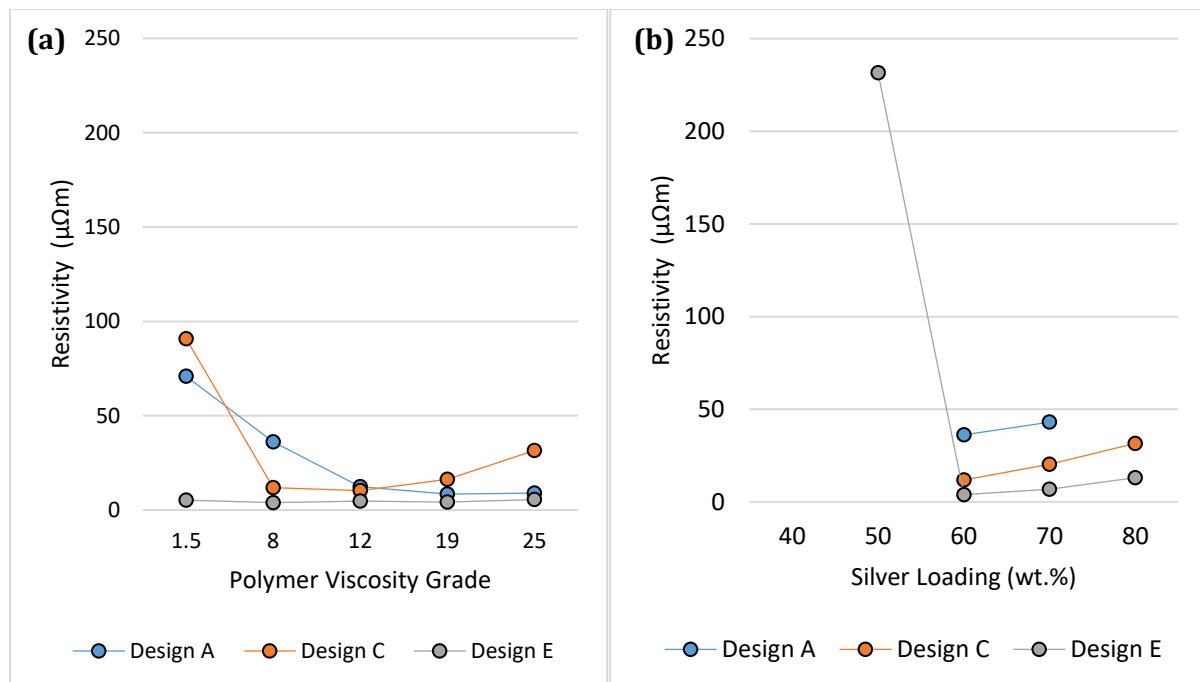


Figure 8-17 – (a) Calculated resistivity of three line widths (design A:0.5mm, design C:1mm and design E:1.5mm) for polymer Vg changes in the silver ink of 60 wt.% loading. (b) Calculated resistivity of three line widths (design A:0.5mm, design C:1mm and design E:1.5mm) for silver loading changes in the silver ink of 8 Vg.

8.4 Antenna Performance Testing for Optimised Silver Ink

Through study of the design at a lower frequency band than that tested in and simulated in Chapter 4, the S22 values tend towards a lower value as the frequency increases. Figure 8-18 shows the frequency and S22 responses of the three designs. Simulation results indicated that the best operating frequency band is at a higher frequency. Initial testing obtained a frequency profile between 100MHz – 1GHz. Tests in this chapter applied a frequency sweep of 1GHz-5GHz. If a reliable frequency profile can be obtained, this can be altered in an application to transmit data through shifts in frequency. For the designs used, PCBs are resilient to design changes in terms of low conductivity. The three designs (A, C and E) as shown in Figure 5-6 and Table 5-3 have been tested using the VNA machine. The ink used is an 8 Vg polymer and silver:resin ratio of 60:40 as this produced the lowest resistivity and resistance 1mm and 1.5mm line widths. To achieve comparable S22 responses to PCBs, printed tracks will need to be at a minimum of 1.5mm in width. Finer lines are unlikely to give comparable conductivities and in turn, antenna performance.

The general slope of the frequency profile tends towards a more prominent S22 value at a higher frequency, implying that a lower resonant peak can be achieved. Hence, in the following experiment the samples have been tested at a higher frequency range of 1GHz to 5GHz. There is a large amount of noise in the samples creating a lot of fluctuation however, the points of clearest distinction are around 1.84GHz and 3.98GHz. It is here that the responses appear to be forming resonant frequencies. At these points, the larger designs dip into a lower S22 value than the smaller design A. This is consistent with the earlier findings with the commercial ink in Chapter 6; where the wider line had a lower overall resistance and a smoother surface. The extra material in the wider lines, may also ensure there was enough room for the signals to flow in the core without being affected by the surface.

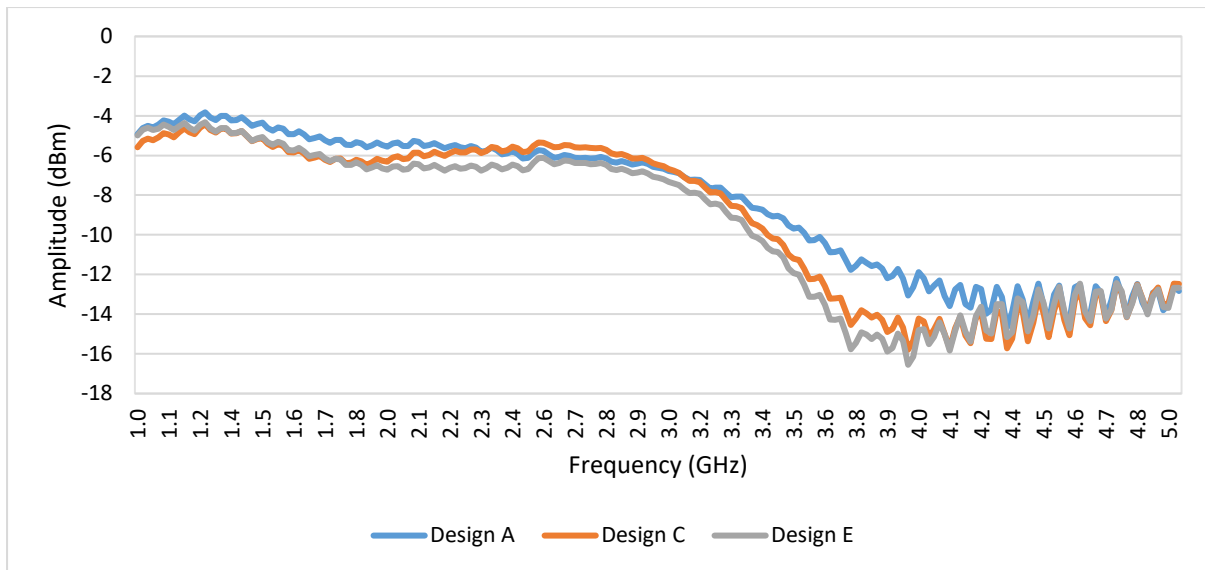


Figure 8-18 – Designs A, C and E tested on a VNA machine at a frequency range of 1GHz to 5GHz.

PCBs are the industry standard for electronic devices. Copper is the primary metal used in PCBs due to its high electrical conductivity. As the printed electronics industry developed, copper was tried in printing inks however, due to its highly oxidising nature, it was not an appropriate solution for printing inks. Printed electronics strive to achieve the same results as PCBs. Therefore, Designs A, C and E are also replicated on PCB's, made via etching, so comparisons can be made between PCB versions and the printed electronic tracks. Figure 8-19 shows the frequency and S22 response for designs A, C and E on a PCB. This was used as a comparison for the printed electronics due to the high conductivity of copper.

There is an increase in the resonant trough around 4GHz (Figure 8-19). There does not seem to be a correlation linking these changes in S22 with design. However, the largest design has by far the most prominent trough. It could be that the two smaller designs were subject to some form of interference, i.e. by metal within the table on which it was tested, but this would require further testing. Additionally, it appears that design A has formed two slight troughs within the area, implying that there is another phenomenon occurring. The sample size of each of these designs was one. Therefore, to achieve more reliable results, more PCB samples would need to be manufactured and tested to conclusively decide on the impact of the designs in this scenario.

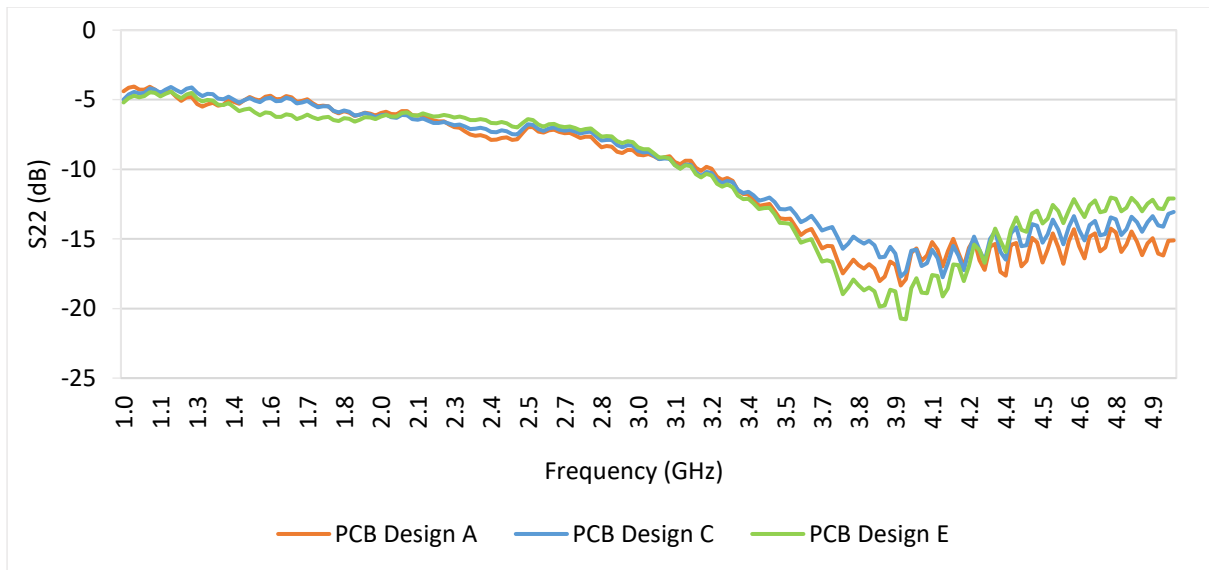


Figure 8-19 – PCB designs A, C and E tested on a VNA machine at a frequency range of 1GHz to 5GHz.

Figure 8-20 compares design A on PET substrate with the design A on a PCB. The PCB design achieves a lower S22 profile. It also demonstrates more than one resonant trough, although less distinct than that at approximately 4GHz. If these smaller troughs were visible in the printed samples, they could be characterised for information transfer. The lowest S22 value achieved of the design on substrate was -15.73 and the lowest for the PCB design was -18.30dB, hence there is a difference of 2.57 in resonant values.

It is perhaps not surprising with the comparatively smooth surface PCB produces a larger response. The printed antenna is showing similar trends although these are partially hidden by the inherently noisy signal. In order to flexo print an antenna, then the quality of the print including the ink would have to be further optimised.

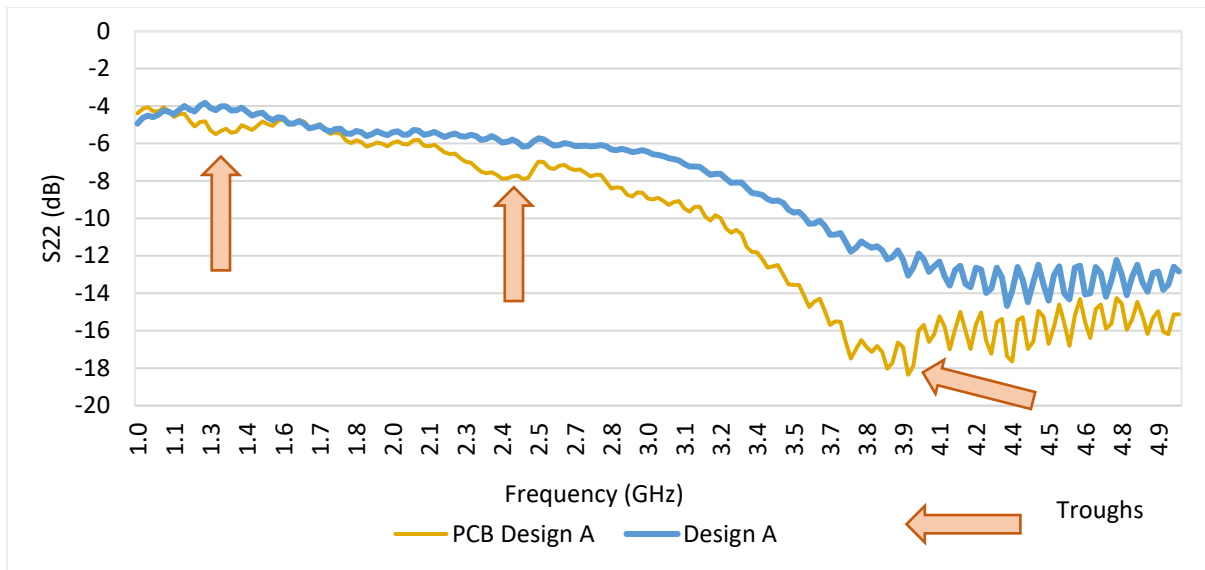


Figure 8-20 – PCB design A, and PET substrate design A tested on a VNA machine at a frequency range of 1GHz to 5GHz.

When comparing the physical test results shown in Figure 8-18 to Figure 8-20 with the CST Studio Suite simulation results in Figure 4-8 and Figure 4-9, there are some similarities and many differences. Firstly, both sets of results show many resonant points. The troughs tend towards a higher magnitude at a higher frequency. The most prominent troughs in the simulation are not present in physical testing. In physical testing, there is a large amount of noise present. Physical tests show small trough magnitudes between 1GHz and 2GHz, and also tend towards a trough below 1GHz. There is a trough between 3GHz and 4GHz on both sets of data. This correlates with the troughs shown on the simulation results. These troughs are weak in the physical test results and loosely follow the simulation frequency profiles. Error is high between the two. Small bandwidths of resonant troughs indicate a high Q-factor value, which are not present in physical testing. High Q-factor is critical for repeatability and performance. The reduction of resistance in the printed tracks can improve the Q-factor as demonstrated in Figure 8-20 where the PCB design is compared to the printed sample. Troughs are more prominent for the low resistance PCB. Despite the low resistances of the PCB, these frequency profiles still do not match the simulation results. Further testing is required to fully understand the extent to which design can enhance the quality of the resonant troughs.

Simulation models cannot be used to describe the physical testing. As outlined, there are some resemblances that demonstrate simulations can give an insight into how they may be able to aid physical testing. More work is required to achieve good alignment between the two.

8.5 Discussion

This study analysed the effect of engagement on an '8 viscosity grade TPU polymer : diacetone alcohol: silver particle' ink developed so that increased control could be had on the investigation of the printing process and ink development.

Three studies were conducted; one varying the A-P engagement from 140 μm to 420 μm , with a fixed P-I of 280 μm ; another fixing the A-P engagement to 260 μm and varying the P-I engagement from 160 μm to 400 μm ; for the third study, both engagements were changed simultaneously.

There are three main phases that the line profile transitions through as the engagements are changed. The first phase is: line profiles form three distinct peaks across the line width, creating three channels in the printed line. In the second phase, these peaks expand in width, forming a more conformed print. These peaks begin to connect. The third phase is where the outer two peaks at the edges of the print, become much larger than the average film thickness and grow in width at the edges of the print, whilst the central peak diminishes in height.

For an increased A-P engagement (rollers moving closer together), the ink profiles move from the third phase to the first and then toward the second as engagement reaches the maximum tested. Initially the ink is drawn predominantly from the surface of the anilox and hence along the edge of the plate, leaving little ink in the centre. As the engagement is increased, the plate has more contact time with the anilox cells and can thus draw ink out from the cells across the whole surface of the line. However, there is a limit to how much ink can be held on the centre of the plate and further increasing the engagement forces ink to the side.

For an increased P-I engagement, the line profiles move through phases one, two and three consecutively. Initially at below "kiss" pressure, as the plate disengages there is insufficient elastic movement to maintain a pressure on the ink in the centre of the line and the ink is drawn elastically to the edge of the plate. In phase 2, there is sufficient ink to compress the plate, which expands elastically to keep the ink evenly spread across the surface. A further increase in engagement forces the ink towards the edges of the line during the contact time, leaving the distinct bunny ears. When both engagements are increased in parallel, the same pattern is followed as that of the P-I engagement increase.

One potential mechanism may be that at closer A-P engagements, a higher shear is being applied to the ink between the rollers, decreasing the viscosity of the ink and making it more 'fluid'. This could cause higher ink flow from the anilox cells and produce lower resistances. When a close P-I engagement is applied, this squeezes the ink between the two rollers and out of the sides of the raised printing plate image, creating an 'M' shape in the printed line profile. Further research is

required to understand the 'M' shape when there is large A-P engagement distance and if this mechanism is correct for this outcome.

Resistance, film thickness and line width results are used to understand the changes in resistivity for changes in the engagement. Compared to the commercial inks, the resistance is much higher; between 1-3 magnitudes higher in some cases. The drop in resistance from 15 k Ω to 0.45 k Ω for P-I engagements 160, 260 μm to 220,260 μm could be attributed to a deformation in the printing plate, as it is squeezing the features into anilox cells. This is shown in the print line cross-sections. When the three peaks are closely aligned and are wide in nature, the resistance is likely to be lower. Changing the P-I engagement has a much more significant impact on the resistance than the A-P engagement. Film thickness, surface roughness and, in turn, resistivity were not presented due to the nature of the line geometries. Averages for lines with two or three distinct parts to the line were not giving accurate information.

Greater A-P engagement distance (rollers further away from one another) causes a rise in line width, although this is not as significant as the impact of varying the P-I roller engagement. The ridges that form at the edges of the print track in the 'M' shape spread wider, creating an overall wider track width. Hence, this does not mean that more ink has been deposited and resistance is not low. P-I engagement has a much more significant impact on line width than A-P engagement for similar reasons to the impact on film thickness. Squeezing between P-I rollers reduced the amount of ink deposited at the centre of the printed line. Ink results in collecting at the edges of the printed track and expands the track width.

As the lowest resistivities and resistances were produced using anilox cylinder to plate cylinder engagements of between 140 μm and 200 μm with plate cylinder to impression cylinder engagement of 280 μm , it is these settings that will be used to achieve the best conductivity for prints. These settings also provide the best ink coverage of the printed track and demonstrate low edge effects.

An investigation was conducted on the effect of five Vgs (1.5, 8, 12, 19 and 25) and five silver loading percentages (40, 50, 60, 70 and 80) on printed lines. From previous research, the 8 Vg polymer was selected to test the effect of silver loading; and the 60wt.% ink loading to test the effect of Vg on the ink.

The lowest resistivity achieved was $7\mu\Omega\text{m}$ for a silver loading of 70wt.%, and 8 Vg, which is two orders of magnitude lower than the formulated ink prior to optimisation 'The Effect of Polymer Viscosity and Silver Loading on Ink Rheology and Printability'. This is one order of magnitude higher than the resistivity achieved for the Novacentrix PFI-722 ink. Despite this ink not achieving a lower resistivity than the commercial ink, this work demonstrates that through optimisation of the print parameters, the resistivity could be reduced. Through the optimisation of silver loading and polymer viscosity grade in the ink, this can be reduced even further. The resistance and resistivity are intrinsically linked and hence follow similar patterns. Generally, from the data collected, lower polymer Vg and lower silver loadings have higher resistances and in turn resistivities. Resistance values reach minimums at silver loading of 70wt.% and 19Vg. However, there was no benefit to conductivity after 60wt.% for line widths 1mm and 1.5mm. This is also similar for resistivity. It is this formulation that demonstrates the optimal ink due to its high conductivity. Measurable lines were limited between 50 wt.% to 80 wt.% for 1.5mm, 60 wt.% to 80 wt.% silver loading for line widths 1mm, and 60 wt.% to 70 wt.% for 0.5mm width. As expected, the wider line widths deposit a higher volume of ink onto the substrate and hence decrease resistance as the line widths increase. Resistivity also decreases for increased volume, however, this could be due to improved consistency in the print. Some average resistances were up to two orders of magnitude larger than the lowest resistances achieved, hence some large variation.

For the lowest line width (0.5mm), the impact of increased Vg continued to reduce the resistance of the print at 12 Vg. As film thickness increases as resistances decrease, there is an optimal point at which the polymer provides good suspension of silver particles and there is good contact between silver particles. 8 Vg gave sufficient improvement in resistance and 12 Vg was shown to be a slight improvement.

Larger line widths are largely unaffected by viscosity grade and silver loading. Hence, to optimise thinner lines, silver loading and viscosity grade are of high importance.

For thinner line production, a 70wt.% 8 Vg ink produces the optimal resistivity. For wider line widths, the resistivity and resistance decrease between the 60wt.% and the 70wt.% ink do not give a large enough advantage to justify the cost of an extra 10wt.% of silver in the ink in this application, hence a 60wt.% ink is optimal for 1mm and 1.5mm line widths. Film thickness and surface roughness increased with increased silver loading, however, this did not always indicate reduced resistance. Vg was not found to affect surface roughness. Print thickness increased with an increase in Vg, for which measured shear viscosity increases as shown in rheological testing. Higher polymer Vg exhibits higher entanglement between particles, causing the higher

viscosities. With greater entanglement between particles, there are strong forces within the ink. Print width was found to be independent of polymer Vg, whereas film thickness increases with increased polymer Vg, implying that ink deposition increases. The increased viscosity is likely to be drawing more ink from the anilox cells due to greater entanglement and interparticle forces. As line widths remain relatively unaffected by increases in polymer Vg and silver loading, the higher viscosity enables the printed ink to not spread. An increase in silver loading was seen to increase the film thickness for all line widths. This increased print thickness for increased silver loading is probably due to the reduction in solvent loss. As silver loading increases, the solvent content in the ink decreases, meaning that more solid content remains on the substrate when solvent is removed, hence an increase in film thickness. Neither an increase in Vg nor silver loading impacted the spreading effects of the printed tracks. Novacentrix PFI-722 ink has a 60wt.% silver loading and is water based, therefore Vg variations are not directly comparable, yet the silver loading variations are. For the 60wt.% silver loaded inks, the film thicknesses were also lower. Surface roughness' for variations in polymer Vg are lower than the commercial ink tests. For a 40wt.% silver loading, the surface roughness is lower than the commercial ink, however, the surface roughness of the commercial ink is exceeded by a 60wt.% loading.

As both polymer Vg and silver wt.% were increased, anilox cell volumes of ink held high levels of structure throughout the transfer of ink from anilox roller to plate to substrate. High levels of structure form within the anilox cells. The structure formed within the anilox cells is visible at the edges of the track on the substrate.

There are two distinct areas seen on the printed track: the central strip, and the ink at the edges of the print. Higher shears reduce viscosity, making the ink more free flowing. This explains the lack of bridging between the main strip and edges when ink is transferred from the anilox to the plate and to the substrate. For higher polymer Vg, there is increased ink viscosity, and this has visual impacts in that at the edges of the print, distinct anilox cell shapes increase the line waviness. This provides strong evidence that viscosity and non-hydrodynamic forces play a strong role in the waviness of the printed track.

Comparing the commercial ink printed design C (Chapter 5) with the printed in-house inks using optimised print settings demonstrates:

- Line widths of the in-house inks are 100-200µm wider for all viscosity grades. This was also the same for all silver loadings tested.
- Film thickness of printed tracks using the in-house inks is between one and seven times thicker than the Novacentrix ink.

- Surface roughness is two orders of magnitude lower than the commercial ink.
- Lowest measured resistances for the in-house inks were double the resistance of commercial inks, and resistivities were one order of magnitude higher.

Hence, despite higher deposition of ink in terms of measured line width and thickness, resistance and resistivity were not lower than the commercial ink printed tracks. Commercial inks include additives and hence demonstrate a different rheology. This could account for differences and enable better contact between particles to provide lower resistances with less ink. However, this method of ink formulation was used to study the components of the ink independently.

A VNA was used to measure the samples at a higher frequency range than the previous test; moving from a test range of 100MHz-1GHz to 1GHz-5GHz. The three designs all exhibited one strong resonant trough and one shallow trough with a wide bandwidth. These responses were compared with a PCB with the designs etched in.

When comparing frequency profiles of the three printed antenna designs with the simulation results, it is evident that resonant troughs occur on both. However, the physical testing demonstrates a high level of noise in the data and resonant troughs are suppressed. There are resonant troughs occurring in ranges 1GHz -2GHz and 3GHz-4 GHz in both simulation data and in physical test results, albeit weak magnitudes for the latter. As discussed in the literature review, research suggests that decreased resistance leads to a higher Q-factor for the resonant trough however, when the samples are compared with the PCB design, there is only a small increase in magnitudes and the bandwidth remains large for the PCB designs. This implies that there is another factor in practise that contributes to energy losses. Further research is required to determine this. The designs on PCB's achieved lower magnitudes, which is as expected as there is less resistance in the copper layer in the PCB than there is in the conductive printed ink.

Wider lines produce magnitudes that correlate better with the PCB response due to lower resistance of the tracks. To achieve antennas with consistent performance and comparable performance to PCBs, wider printed lines are required.

Comparisons with the commercial inks are not possible, as previously mentioned, the testing frequencies are of different bandwidths that do not overlap.

As previously discussed in initial antenna testing, ambiguity remains when correlating troughs in the simulation model to the physical results. For the results presented in this chapter, it could be that phase shift is occurring and the troughs on Figure 8-18 and Figure 8-19 are represented by

another set of troughs on the simulation model. With regards to both theories, the simulation model shows distinct variations between each design in terms of its frequency response, however, the physical testing does not distinctly show these in terms of phase changes.

The physical testing is very variable and influenced by many external factors e.g. metal within the table. Although there are some similarities, the simulation work does not accurately correspond with physical testing. A more extensive complex physical set up, model and analysis would need to be developed. Further experiments would be required inside an anechoic chamber to remove electromagnetic noise, and the use of antenna horns to transmit and receive the signal for through air transmission could help to align the measured signal more closely with the simulated signal. This could contribute to more prominent resonant frequency troughs.

The simulation models cannot be used to describe the physical testing however, it shows some resemblance of physical testing and gives an insight to the potential of this work if closely aligned models were achieved. While the model gives an insight to the potential of the antenna designs, more development is required for it to closely align with actual devices. There is a need to establish the effect of printed features on electrical and antenna performance.

There was no change of note in terms of frequency response made regarding changes in surface roughness due to the print process.

8.6 Closure

Three main phases in which the lines transition through are seen as engagements on the printer are altered. Squeezing effects are also visible in the prints when a close P-I engagement is applied. Closer A-P engagement result in lower resistances in the printed track. Although the resistances were much higher than that of the commercial inks test, good understanding of the relationship between engagement and resistance, film thickness and line width has been established and that through optimisation of the print parameters, the resistivity could be reduced. The P-I engagement has a higher impact on these factors than the A-P engagement. From this study, optimal engagements were selected to achieve the lowest resistivities for the next experiments.

Lower polymer Vg and lower silver loading produced higher resistances and resistivities. Resistance and resistivity values reached minimums at silver loading of 70wt.% and 19Vg. However, there was no benefit to conductivity after 60wt.% for line widths 1mm and 1.5mm.

Larger line widths (1.5mm) are largely unaffected by viscosity grade and silver loading. To optimise thinner lines, silver loading and viscosity grade are of high importance.

VNA testing of the samples demonstrated that they response to a signal and demonstrate some similarities to simulations however, this work requires more development to achieve good alignment. Wider lines produce magnitudes that correlate better with the PCB response due to lower resistance of the tracks.

The next chapter will discuss the results from this thesis.

Chapter 9: Discussion

Chapter 8 builds upon the rheological ink analysis carried out in Chapter 7 by measuring the samples in terms of their antenna performance and print outcomes. The lowest resistivity achieved was $7\Omega\mu\text{m}$ for a silver loading of 70wt.% and 8 Vg. This is two orders of magnitude higher than the resistivity achievable as stated for the PFI-722 ink by Novacentrix and half an order of magnitude higher than the results achieved in laboratory. Generally, from the data collected, lower polymer Vg and lower silver loadings have higher resistances and in turn resistivities. Resistance values reach minimums at silver loading of 70wt.% and 19Vg. Correlations between silver loading and viscosity grade have been found with the print outcomes and the structure of the printed track. In terms of antenna performance, a higher frequency test range of 1 to 4GHz was found to have stronger resonant troughs than initial tests in Chapter 4, indicating better antenna performance.

Through the use of an RK Flexiproof 100 desktop printer and a convection oven, conductive silver tracks were printed and dried for use as an RFID antenna. Three methods of assessing the performance of the printed track for RFID have been assessed including a hand-held scanner for chip reading, an LCR bridge and a VNA. These have allowed comparisons to be made between samples and determine if improvements have been achieved. The resistance is a significant indicator of the operating frequency and a VNA was used to obtain an EM signature. Resistance was found to be an indicator of operating frequency.

A trial investigated the effect of print speed, anilox volume, temperature and length of exposure to heat on: print width, film thickness, surface roughness, resistance, and resistivity. This series of print trials identified 'optimal' settings at which the resistivity was at its lowest value. The lowest resistivities are achieved using lower print speeds of 20 and 50m/min and using the smallest anilox volume $8\text{cm}^3/\text{m}^2$. For larger cell volumes with wider openings, the cell opening can extend beyond the raised printing plate. Excess ink is drawn from the anilox and contributes to higher line widths and film thicknesses.

The prints from these trials were then tested on a VNA to analyse natural resonant troughs and frequencies in the samples. As resistivity is an indicator of the conductivity of the sample and RFID technology is reliant on good conductivity of prints and sufficient film thickness for the signal to pass through, it was thought that higher film thickness would produce higher resonant trough magnitudes and changing resistivities would alter resonant points and frequencies (28). No such trends have been identified in these experiments. It could be that the film thicknesses and resistances do not vary enough to impact the S22 and frequency outcomes, or that the

antenna was not being tested in its correct operating range and does not vary enough for a trend to develop.

At optimised print speed, anilox volume and engagement settings the formulated ink achieves a resistivity of $1.2\text{n}\Omega\text{m}$, which is significantly lower than the $661\text{n}\Omega\text{m}$ achieved by the unoptimised commercial ink in Chapter 5.

Increased anilox volumes increased print width, film thickness and surface roughness of the samples. The relationship between increased anilox volume and film thickness correlates with literature presented in the review (33). More ink in the cells means more ink ultimately transferred to the substrate, which can lead to slumping effects. The highest achieved film thicknesses were $0.7\text{-}0.72\mu\text{m}$ for the lowest resistivities achieved. Smaller anilox volumes increased resistance. Print speed did not influence the resistance. The largest anilox volume, $24\text{cm}^3/\text{m}^2$, produced the lowest resistances and resistivities at print speeds of $50\text{m}/\text{min}$ and $80\text{m}/\text{min}$. Due to a reduction in defects, such as viscous fingering, thicker lines are less likely to be affected by small defects. Also due to the large anilox volume and over extraction of ink, there is significant line spreading when using these settings, losing cell resolution.

Regarding printing defects, the frequency of the viscous fingering effect, described by its peak-to-peak distance (lower peak-to-peak distances meaning higher density of effect), was seen to decrease with increased film thickness for the particular printer set-up outlined in Chapter 5 ($24\text{cm}^3/\text{m}^2$, $90\text{m}/\text{min}$). The effect increased in frequency for increasing print speed which aligns with literature for gravure printing (91). Between parameter changes, this effect did not occur and appears to apply only for particular printer set-ups. No effect between resistance or resistivity and viscous fingering was found and hence it can be said that viscous fingering is not a significant defect in the performance of a silver nano flexographically printed ink on a smooth substrate, which aligns with literature (83).

In terms of ink formulation on surface patterning, formulation has affected ink viscosity at all shear rates. Increased silver loading was found to increase surface roughness; retaining viscous finger patterning on the surface; and increase edge waviness of the tracks.

Printer trials highlighted the limitations of the process on the optimal performance of a printed track. Literature (24)(93)(100) suggested that alterations to ink formulation could enable improved performance further.

Antenna performance was divided into two factors, resonant troughs in the S22 values and the frequency at which this happens. There was no correlation between troughs and print outcomes (print width, film thickness, surface roughness, resistance, and resistivity). Resonant frequencies show no correlation with print thickness. Aside from one anomaly, resonant frequencies increase as surface roughness increases until the relationship plateaus at 430nm. This could be due to skin effects as presented in literature (186). After which point, the surface roughness no longer has an impact on the frequency. Frequency also shows a relationship with resistance, and it is this measurable that can be altered in an application to enable the device to store information. Resonant frequency increases with increases in resistance. Shifts in resistance can affect the signal output by shifting the frequency higher or lower and indicate changes from a sensor integrated into the antenna.

There was no correlation found between print parameters (print speed and anilox volume) and the magnitude of the troughs. Only an increase to the fastest print speed, 80 m/min, decreased frequency. This decrease came with an increase in error. More work is needed to verify results via higher sample numbers. Literature (63)(68)(194) suggests that varying print parameters alters volume of ink deposited onto substrate and increased volume of ink affects frequency due to resistance reduction and film thickness changes, which is important in the way waves travel through the printed track. More samples and experimentation could verify this effect on a flexographic printer.

Increased heat and length of heat treatment significantly reduced resistivity of the printed tracks. As these are increased, the silver particles are reaching sintering temperatures, softening particles to create bonds with adjacent particles. Solid bonds between silver particles in the track increase electron pathways for good conductivity. Generally, higher temperatures of 150°C and 180°C achieve the lowest resistance and resistivities. 15 minutes is found to be the optimal temperature for achieving the lowest values. These increased temperatures cause an increase in print widths due to spreading of the ink as it is heated.

A conveyor dryer could be used to resolve drying patterns in the samples, however, the size of the conveyor dictates the drying time and therefore cannot provide 20 minutes of continuous heating. Near infrared and photonic sintering are two technologies that could be an alternative (23).

Flexographic inks are inherently shear thinning. Particle orientation and alignment with flow is occurring when shear rates are increased from $0.1s^{-1}$ to $200s^{-1}$. This reduces resistance to flow

within the ink and hence viscosity reduces. Increased silver content and increased polymer Vg increase the viscosity profiles of the DAA-TPU-Ag inks. Higher print speeds are required to shear inks with higher silver loading. Increased silver loading creates stronger interparticle forces and high yield points are present at high loadings, requiring higher initial shears to initiate flow in the printer. The increase in silver loading primarily affects the yield point η_0 . Infinite shear viscosities only marginally increase with increased silver loading and increased polymer Vg. These inks are suitable for the high shear rates in full scale printers due to no change in viscosity occurring after 200s^{-1} .

Print width is independent of polymer Vg, whereas film thickness increases up to $0.6\mu\text{m}$ with increased polymer Vg (1.5 to 25 Vg), implying that ink deposition increases. The higher viscosity of the higher Vg inks was associated with an increase in ink transfer. This is also a relationship found in literature (24) between the two for screen printing. This was primarily manifested as an increase in ink film thickness, with no significant change in line width (no slumping). On the shear viscosity-shear rate profiles in Chapter 7, lower Vg showed lower viscosities at low shear rates. This, however, did not lead to lower spreading/reduced slumping as was expected. Vg was not found to affect surface roughness, R_a , of the printed layer. This R_a value incorporates both high frequency surface roughness and waviness of the printed surface and therefore is not necessarily a reliable value to correlate to. Print thickness increased with an increase in Vg, for which measured shear viscosity increases as shown in rheological testing. Greater polymer Vg exhibits greater entanglement between particles, causing the greater viscosities. With greater entanglement between particles, there are strong forces within the ink. The increased viscosity is likely to be drawing more ink from the anilox cells due to greater entanglement and interparticle forces. As line widths remain relatively unaffected by increases in polymer Vg and silver loading, the greater viscosities enable the printed ink to not spread. For wider designed lines widths (1.5mm) the Vg does not alter the resistivity or resistance of the printed track, however, for line widths lower than this, low Vg (1.5) causes the resistivity to be approximately an order of magnitude higher than the 1.5mm width line. Wider line widths deposit more ink and can be more forgiving regarding defects within the printed track. Lower Vg inks have a lower viscosity across all shear rates. At the low shears i.e. when the ink has been deposited on the substrate, the ink holds less structure and although it holds the same spreading effects, it has a lower film thickness. Resistance follows a similar pattern to resistivity with $1,436\Omega$ (1.5Vg) and 239Ω (25Vg) for a 0.5mm line width, and 98Ω (1.5Vg) and 85Ω (25Vg) for 1.5mm. Wide lines were reproduced effectively at all Vgs with consistent resistivity but finer lines, produced using low Vg, had

substantially higher resistivity. Increased resistivity was due to a smaller cross-sectional area of the printed track, hence a smaller area for electrical current to flow.

Fine lines (below 1.5mm) did not show good conductivity with low V_g as the film thickness is much lower and any resulting defects in the lines hold higher impact.

Changes to silver loading of the ink changed the conductivity due to changes in the ratio of silver to binder. However, there was distortion of the ink deposition, which created an uneven film thickness. An increase in silver loading was seen to increase the film thickness by 1.36 μm , 2.80 μm , 1.94 μm for line widths 0.5mm, 1mm, 1.5mm respectively. Much of this film thickness increase is attributed to an increase in the dry solid content, however, at low shear rates, the viscosity can be up to two orders of magnitude higher between a loading of 40wt.% to 80wt.%, which will affect the spreading after deposition onto substrate and consequently this increases the film thickness. This increased print thickness with increased silver loading is due to the reduction in solvent loss and any rheology effects as well. As silver loading increases, solvent content in the ink decreases, meaning that more solid content remains on the substrate when solvent is removed, hence an increase in film thickness. Neither an increase in V_g nor silver loading impacted the spreading effects of the printed tracks.

At lower line widths, lines were not sufficiently conductive to enable a resistance measurement for the various silver loadings. 60wt.% and 70wt.%, 8 V_g inks produced readings for all line widths. For lines wider than 0.5mm, an 80wt.% loading gave the best resistance results. These all had good line width and high film thickness. Despite the thinnest width line having no detectable resistance, the film thickness was very high and line width was good. Surface roughness was particularly high for these samples and there is a high rate of defects that have a substantial effect, which reduces the resistance.

Resistivities differ from the pattern of the resistances for silver loadings in that the optimal silver loading for all line widths is 70wt.% at 8 V_g . This is the ink that produced the optimal conductivity per printed area. Higher silver loading than 70wt.% increases resistivity and provides less 'value for money'.

Novacentrix PFI-722 ink has a 60wt.% silver loading and is water based, therefore V_g variations are not directly comparable due to differences in ink formulation. However, when compared, the 60wt.% silver loading inks had lower film thicknesses than the commercial ink. Surface roughness's for variations in polymer V_g are lower than the commercial ink tests. For a 40wt.% silver loading, the surface roughness is lower than the commercial ink, however, resistance readings were not possible at this wt.%. The surface roughness of the commercial ink is exceeded

by a 60wt.% loading. High silver loading creates high viscosity. These viscosities are so high that the ink fails to relax between rollers and the geometry of the anilox cells is exhibited on the substrate. Lower polymer Vg and silver loading produce higher resistivities. An increase in silver loading increased film thickness for all line widths, whereas Vg had no impact. Higher silver loading means that there is more solid content and less DAA. DAA evaporates under temperature and hence, with a lower wt.% there is more remaining functional materials after the drying.

It is proposed in literature (89) that ink experiences high shear at it enters the anilox cells due to flow under the doctor blade. It is believed that once within these cells, the ink relaxes, and structure begins to rebuild within the silver ink,. Attractive forces between the ink and the printing plate can pull the ink from the cell, exerting a pulling force on the ink. There is a short shear force as the cylinder rotates and the anilox edge breaks the ink removal, however, this would be a primarily attractive/pulling force rather than a shear force as the ink is removed. Little particle alignment or orientation under this short shear stress would be present. For higher Vg and silver wt.%, stronger interparticle forces are thought to form within the anilox than lower Vg and silver wt.%. As the structure of the ink remains high upon exiting the anilox cells, the ink holds the anilox cell shape on the raised printing plate, which is transferred to the substrate and distinct shapes at the edges of the printed tracks are seen in analysis. If this proposed model can be verified further, it would help to conclude that Vg and silver wt.% strongly contribute to the waviness of printed tracks.

The K-D, M-P and E-B models, used to describe the relationship between relative viscosity and phase volume for suspension fluids, were fitted to data collected as in (191). All models showed relatively large error and did not accurately describe the Ag:TPU:DAA formulation. These models applied better to lower silver loadings and also modelling for carbon inks also using TPU in (191) worked well and showed good alignment. However, for higher silver loadings, these could not accurately model the ink with 60wt.% loading and above. For 50wt.% loading at low polymer viscosity grades of 1.5 and 8, these equations also do not describe the silver ink well. Silver's high-density has shown a lack of coherence with the models.. The effect of density plays a more prominent role, as in printed tracks in Chapter 8. A ratio of densities for all components in the ink has been applied to the K-D model (Equation 9-1), which was the closest fitting model. This proposed equation better describes silver loaded inks above 60wt.%.

$$\frac{\eta}{\eta_0} = \frac{\rho_{Ag}}{\rho_{TPU} + \rho_{DAA}} \left(1 - \frac{\phi}{\phi_m}\right)^{-[\eta]\phi_m} \quad \text{Equation 9-1}$$

Adjusting the roller engagements caused the ink to go through various 'phases' whereby distinct peaks in the profile of the line width were seen to sharpen, broaden and move away from one another. Close alignment of these peaks was seen with low resistance. Close anilox-printing plate engagements demonstrate the most even distribution across the printed track and exhibit the lowest resistance and resistivity at an engagement of 140. At close printing plate-impression cylinder engagements, an 'M' shape was seen in the ink due to squeezing effects. This 'M' effect is also seen in literature (193) but not yet correlated to roller engagement. Changing the P-I engagement has a much more significant impact on the resistance than the A-P engagement.

Adjustments of roller engagement distance caused a change in print cross sections, which impacted the resistivity of the printed tracks. The cross sections generally transitioned through three phases whereby distinct peaks are formed, print widths increase due to the expansion of peaks and decrease due to consolidation of these peaks. More detail on these transitions is outlined in the results. Resistivity is low for line widths that have less spreading. A-P engagement has a small impact on resistivity and P-I variations cause a wider change in resistance. Closer A-P engagements causes a high shear to be applied on the ink between rollers. This decreases the viscosity of the ink, making it more fluid. This causes higher ink flow, and a better coverage of ink is deposited onto the substrate. This reduces the resistance. For close P-I engagements, ink is squeezed between the rollers and printing plate, and for very close engagements, the ink squeezes out the sides of the raised printing plate image, creating an 'M' shape in the printed line profile. Further research is required to understand the 'M' shape created by large A-P distances.

For the optimised print parameters (anilox volume, print speed and curing temperatures), the lowest resistivity achieved was $15.6\mu\Omega\text{m}$ for a 0.5mm width line printed with the Novacentrix PFI-722 ink. These samples had low surface roughness and print height. The optimised settings from all these studies were used to print nine inks of varying polymer viscosity grade and silver loading. This indicates that the additives or the blend of nanoparticles within the commercial ink play a big role in the reduction of resistivity of a conductive print. Alternatively, this discrepancy could be due to the commercial ink being water based and the formulated ink a solvent-based ink. Resistance for this achieved resistivity was very low relative to other prints, film thickness was average, line width demonstrated low spreading and surface roughness was low. A combination of the low surface roughness across the print and good film thickness has contributed to a low resistance in the print and hence, low resistivity. For the samples that produced high resistivity values, there was no notable indicator i.e. low film thickness, narrow line width or high surface roughness, hence it has been deduced that there is likely to be a high number of defects in the

line. Surface profiling has been looked at and 'M' patterns are demonstrated, which has been shown to limit the conductivity of the track. However, further investigation would need to be done to view the cross section of the track to determine internal geometry of the silver. This series of experiments demonstrates that through the optimisation of the print process parameters, and correct selection of polymer viscosity grade and silver loading, the ink resistivity can be reduced.

Chapter 10: Conclusions and Future Work

10.1 Conclusions

In order to optimise the flexographic printing process to improve the conductivity of a silver particle ink for RFID applications, it is necessary to understand how the components of the ink influence the antenna performance. Areas of research outlined at the end of Chapter 2 have been investigated. Research questions with regards to the performance, printability and rheology of commercially available inks were evaluated for the effects of print speed, anilox cell volume and heat treatment to provide a benchmark. Model inks have been developed using resins containing a range of viscosity grades, which is equivalent to changing the molecular weight without changing the chemistry. The impact of silver flake loading has been evaluated. More specifically, the following have been concluded.

- Rheology has been shown to be an important factor in flexographic printing because it affects the ink transfer between rollers. Printed line conductivity was a function of both silver content and printed line topography, which is also affected by rheology. High elasticity is associated with high ink release from anilox cells. Thicker prints can be achieved by increasing the polymer viscosity grade.
- Silver loading affects the rheology of the ink and conductivity of line. Reduced resistance from high silver content overcame any increases in resistance resulting from high surface roughness. Larger anilox volumes and higher silver loading both have a significant impact on the reduction of resistance of a silver printed track.
- Silver loading of ink has an upper practical limit of 70 wt.%, above which there is no benefit to conductivity of the printed track. There is a trade-off between silver loading to improve conductivity and resulting topographical characteristics of the print. High silver loading resulted in significant distortion of the surface and edge topography of the printed track. This was mitigated by local conductivity improvements due to the presence of additional silver.
- Flexography has proven to be capable of volume manufacturing for printing RFID antenna. Good film thickness, width and low resistance has been achieved with optimised print settings and ink formulation. Opportunities still exist in reducing resistance and improving reliability in the print process.
- Contrary to expectation, viscous fingering was not found to be correlated with resistance of silver flexographically printed ink films. Increased film thickness and lower print speeds were shown to reduce the occurrence of the ridges. Lower silver loadings also reduce the occurrence of the ridges that occur.

- Lines below 1.5mm are more susceptible to variation in flexographic print parameters. Above this line width, lines are more robust, having a low enough resistance to mitigate against defects in the printed tracks.
- Increasing the ink viscosity by increasing silver particle content has shown to significantly alter the print geometry. Geometry formed within the anilox was seen to transfer between multiple rollers onto the substrate and still hold its form. The geometries formed in the anilox did not relax through the printing process, which means both print parameters and ink viscosity should be considered when printing in applications when geometry is critical.
- The tarnishing of silver print over time (silver sulphide) at the surface causes electrical changes in the track and is the likely cause of changes in Q-factor over time, meaning that silver tracks should be coated to prevent shifts in performance.
- A new equation for estimating the effect of particle loading on ink rheology, building upon the Krieger-Dougherty model, is proposed for high density silver inks. A ratio of silver density to the sum of densities of the remaining components of the ink is used as a scaling factor. This equation shows most applicability for polymers of mid to high viscosity range (12 viscosity grade, a proxy for molecular weight, and above), and for silver loading of 60wt.% and above.

10.2 Future Work Recommendations

10.2.1 Ink Formulation Method for Future Work

An optimal solvent to polymer ratio was found to be 92.5:7.5. The polymer was dispersed in the solvent using an overhead mixer at a raised temperature. This was repeated for each polymer viscosity grade tested. Silver was added to these mixtures, stirred and prior to printing, a triple roll mill was used to ensure good dispersion of the silver particles throughout the polymer-solvent dispersion.

10.2.2 Future Work

It has been shown possible to increase conductivity of a print further through the determination of optimal print settings and ink formulation. One main area of future work is to apply the understanding of the interaction of the flexographic printing process and ink formulation as a building block for improving the quality and printability of RFID antennas.

Other areas of investigation that would be valuable but were not possible in the time scale of this thesis include:

- Investigation of surface tension on the print outcome and its interaction with the ink viscosity.
- SEM cross-sectional analysis of the prints to determine internal geometry of the printed silver and analyse for any defects present within the film.
- Separate out surface roughness high frequency from waviness and determine impact.
- Analysis of another high-density ink to prove/disprove proposed equation.
- Investigation into the impact of a porous substrate on the extent of effects from atmospheric air from both sides of a printed silver track.
- Further investigation into the impact of variable surface topography of printed tracks with high silver loading on RFID antenna is required.
- To develop a predictive model for printability based on the rheology, weight percent and geometry of silver particles in the ink.
- Test monopole antenna with spiral resonators as these give the antenna extra frequencies at which the antenna resonates. This would give the antenna the potential to transfer more information in the form of four bits. An alternative detection regime is required to pick up any effects of the spiral resonator.

References

1. Kattumenu RC. Flexography printing of silver based conductive inks on packaging substrates. West Michigan Univ Dep Pap Eng Chem Eng. 2008;(PhD).
2. Ph.D. GV. Everything you need to know about RFID technology. LabTag. 2018.
3. Stockman H. Communication by Means of Reflected Power. Proc IRE [Internet]. 1948;36(10):1196–204. Available from: <http://ieeexplore.ieee.org/document/1697527/>
4. Preradovic S, Karmakar N. Fully Printable Chipless RFID Tag. Adv Radio Freq Identif Des Appl [Internet]. 2011;132–54. Available from: <http://www.intechopen.com/books/advanced-radio-frequency-identification-design-and-applications/fully-printable-chipless-rfid-tag>
5. Duroc Y, Tedjini S. RFID: A key technology for Humanity. Comptes Rendus Phys [Internet]. 2018;19(1–2):64–71. Available from: <https://doi.org/10.1016/j.crhy.2018.01.003>
6. Chanchaichujit J, Balasubramanian S, Charmaine NSM. A systematic literature review on the benefit-drivers of RFID implementation in supply chains and its impact on organizational competitive advantage. Cogent Bus Manag [Internet]. 2020;7(1). Available from: <https://doi.org/10.1080/23311975.2020.1818408>
7. Hämäläinen H, Salmela E, Happonen A. RFID on Item Level Tagging in Supply Chain with High-Valued Products. 2007;(August 2019). Available from: <https://zenodo.org/record/3376601>
8. Markets and Markets. RFID Market with COVID-19 Impact Analysis by Product Type (Tags, Readers, and Software and Services), Wafer Size, Tag Type (Passive Tags and Active Tags), Frequency, Applications, Form Factor, Material, and Region - Global Forecast to 2026 [Internet]. 2021. Available from: <https://www.marketsandmarkets.com/PressReleases/radio-frequency-identification.asp>
9. Virtanen J, Ukkonen L, Björninen T, Sydañheimo L, Elsherbeni AZ. Temperature sensor tag for passive UHF RFID systems. SAS 2011 - IEEE Sensors Appl Symp Proc. 2011;60(8):312–7.
10. Smits E, Schram J, Nagelkerke M, Kusters R, van Heck G, van Acht V, et al. Development of printed RFID sensor tags for smart food packaging. 14th Int Meet Chem Sensors. 2012;(August 2015):403–6.
11. Gao J, Sidén J, Nilsson H, Gulliksson M. Printed Humidity Sensor With Memory Functionality for Passive RFID Tags. IEEE Sens J. 2013;13(5):1824–34.
12. Vásquez Quintero A, Molina-Lopez F, Smits ECP, Danesh E, Van Den Brand J, Persaud K, et al. Smart RFID label with a printed multisensor platform for environmental monitoring. Flex Print Electron. 2016;1(2):1–13.
13. Vena A, Perret E, Tedjini S, Tourtollet GEP, Delattre A, Garet F, et al. Design of chipless RFID tags printed on paper by flexography. IEEE Trans Antennas Propag. 2013;61(12):5868–77.
14. Zhong T, Jin N, Yuan W, Zhou C, Gu W. Printable Stretchable Silver Ink and Application to Printed RFID Tags for Wearable Electronics. Materials (Basel). 2019;1–14.
15. Catarinucci L, Esposito A, Tarricone L, Zappatore M, Colell R. Smart Data Collection and

- Management in Heterogeneous Ubiquitous Healthcare. Biomed Eng Trends Electron Commun Softw. 2011;
16. Hoon WF, Seok YB, Malek MA, Seng LY, Ibrahim S. Radio Frequency Identification (RFID) Tag Antenna Design at Ultra High Frequency (UHF) Band. Indian J Sci Technol [Internet]. 2017;10:1–6. Available from: [https://www.semanticscholar.org/paper/Radio-Frequency-Identification-\(RFID\)-Tag-Antenna-Hoon-Seok/a73bc741c0beca3ce6a537b0ac6080b2d2f21597](https://www.semanticscholar.org/paper/Radio-Frequency-Identification-(RFID)-Tag-Antenna-Hoon-Seok/a73bc741c0beca3ce6a537b0ac6080b2d2f21597)
 17. GAO RFID Inc. How RFID Tags are Designed, Manufactured and Packaged [Internet]. [cited 2021 Apr 20]. Available from: <https://gaorfid.com/how-rfid-tags-are-designed-manufactured-and-packaged/>
 18. RFID4u. Inductive and Backscatter Coupling [Internet]. [cited 2021 Apr 20]. Available from: <https://rfid4u.com/inductive-and-backscatter-coupling/>
 19. Ramade C, Silvestre S, Pascal-Delannoy F, Sorli B. Thin film HF RFID tag deposited on paper by thermal evaporation. Int J Radio Freq Identif Technol Appl. 2012;4(1):49–66.
 20. RFID and Card Technology. Introduction to RFID antenna manufacturing method and introduction of die cutting technology [Internet]. [cited 2021 Apr 20]. Available from: http://www.rfidandcard.com/en/news_show.php?id=119
 21. Besi. Meco FAP [Internet]. [cited 2021 Apr 20]. Available from: <https://www.besi.com/products-technology/product-details/product/meco-fap/>
 22. Rosen YS, Yakushenko A, Offenhäusser A, Magdassi S. Self-Reducing Copper Precursor Inks and Photonic Additive Yield Conductive Patterns under Intense Pulsed Light. ACS Omega. 2017;2(2):573–81.
 23. Hwang HJ, Oh KH, Kim HS. All-photonic drying and sintering process via flash white light combined with deep-UV and near-infrared irradiation for highly conductive copper nano-ink. Sci Rep. 2016;6(May 2015):1–10.
 24. Phillips C, Al-Ahmadi A, Potts SJ, Claypole T, Deganello D. The effect of graphite and carbon black ratios on conductive ink performance. J Mater Sci. 2017;52(16):9520–30.
 25. M.Dobkin D. Reader Antennas. RF RFID (Second Ed UHF RFID Pract. 2013;2:239–97.
 26. Tutorials Point. Antenna Theory - Wire, Transmission Line [Internet]. Tutorials Point. [cited 2021 Jan 1]. Available from: https://www.tutorialspoint.com/antenna_theory/antenna_theory_wire.htm
 27. Electricalsynergy. Dipole Receiving Antenna-Animation [Internet]. 2016 [cited 2020 Aug 25]. Available from: <https://electricalsynergy.edublogs.org/2016/08/19/dipole-receiving-antenna-animation/>
 28. Siden J, Nilsson H-E. Line width limitations of flexographic-screen- and inkjet printed RFID antennas. In: 2007 IEEE Antennas and Propagation International Symposium [Internet]. IEEE; 2007. p. 1745–8. Available from: <http://ieeexplore.ieee.org/document/4395852/>
 29. Pongpaibool P. A study of cost-effective conductive ink for inkjet-printed RFID application. IEEE Antennas Propag Soc AP-S Int Symp. 2012;1248–51.
 30. Shin DY, Lee Y, Kim CH. Performance characterization of screen printed radio frequency identification antennas with silver nanopaste. Thin Solid Films [Internet]. 2009;517(21):6112–8. Available from: <http://dx.doi.org/10.1016/j.tsf.2009.05.019>

31. Salmerón JF, Molina-Lopez F, Briand D, Ruan JJ, Rivadeneyra A, Carvajal MA, et al. Properties and Printability of Inkjet and Screen-Printed Silver Patterns for RFID Antennas. *J Electron Mater* [Internet]. 2013;43:604–617. Available from: <https://link.springer.com/article/10.1007/s11664-013-2893-4>
32. Jian Dong Lu, Pu Jun Deng, Lu Hai Li, Wei Wei Li. The Research on Gravure Printing RFID Antenna. *Adv Mater Res*. 2014;1033-1034:1142-1148.
33. Deganello D, Cherry JA, Gethin DT, Claypole TC. Impact of metered ink volume on reel-to-reel flexographic printed conductive networks for enhanced thin film conductivity. *Thin Solid Films* [Internet]. 2012;520(6):2233–7. Available from: <http://dx.doi.org/10.1016/j.tsf.2011.08.050>
34. United States Department of Labor. Printing Industry [Internet]. Available from: https://www.osha.gov/SLTC/etools/printing/flexography/flexography_index.html
35. Khan S, Lorenzelli L, Dahiya RS. Technologies for printing sensors and electronics over large flexible substrates: A review. *IEEE Sens J*. 2015;15(6):3164–85.
36. Rentzhog M. Characterisation of Water-Based Flexographic Inks and their Interactions with Polymer-Coated Board [Internet]. 2004. 45 p. Available from: <http://www.diva-portal.org/smash/get/diva2:9129/FULLTEXT01.pdf>
37. Kim S, Sojoudi H, Zhao H, Mariappan D, McKinley GH, Gleason KK, et al. Ultrathin high-resolution flexographic printing using nanoporous stamps. *Sci Adv* [Internet]. 2016;2(12). Available from: <http://advances.sciencemag.org/cgi/doi/10.1126/sciadv.1601660>
38. Zavanelli N, Yeo WH. Advances in Screen Printing of Conductive Nanomaterials for Stretchable Electronics. *ACS Omega*. 2021;6(14):9344–51.
39. Lead Beneficiary: SAL – Silicon Austrian labs. DELIVERABLE D3 . 3 REPORT Materials and process parameters for ink-jet printing and curing. 2020.
40. Podhajny DRM. How Do You Measure Ink Film Thickness? Count the Ways [Internet]. 2002 [cited 2020 Aug 23]. Available from: <https://www.pffc-online.com/magazine/308-paper-measure-ink-film>
41. Kattumenu R, Rebros M, Joyce M, Fleming PD, Neelgund G. Effect of substrate properties on conductive traces printed with silver-based flexographic ink. *Nord Pulp Pap Res J*. 2009;24(1):101–6.
42. Pudas MT. Gravure-offset printing in the manufacture of ultra-fine-line thick films for electronics [Internet]. ProQuest Dissertations and Theses. 2004. Available from: http://proxy.mul.missouri.edu/login?url=http://search.proquest.com/docview/305098192?accountid=14576%5Cnhttp://ew3dm6nd8c.search.serialssolutions.com/?ctx_ver=Z39.88-2004&ctx_enc=info:ofi/enc:UTF-8&rfr_id=info:sid/ProQuest+Dissertations+%26+Theses+A%26I&r
43. Marra F, Minutillo S, Tamburrano A, Sarto MS. Production and characterization of Graphene Nanoplatelet-based ink for smart textile strain sensors via screen printing technique. *Mater Des* [Internet]. 2021;198:109306. Available from: <https://doi.org/10.1016/j.matdes.2020.109306>
44. THE OFFSET PRESSMAN. The Five Fastest Offset Printing Presses in the World [Internet]. [cited 2020 Aug 23]. Available from: <http://offsetpressman.blogspot.com/2011/06/five-fastest-offset-printing-presses-in.html>

45. PromArchive. FLEXOGRAPHIC PRINTING MACHINE - MAX. 800 M/MIN | VISTAFLEX C [Internet]. [cited 2020 Aug 23]. Available from: https://promarchive.ru/en/catalog/industrial_machines_and_equipment/printing_marking_and_engraving/flexographic_printing_machines/flexographic_printing_machine_-_max_800_m_min_vistaflex_c/
46. Rotogravure printing machine [Internet]. Direct Industry. [cited 2020 Aug 23]. Available from: <https://www.directindustry.com/prod/comexi-group-industries/product-75442-1412959.html>
47. VISION RS 5003 - Gravure press [Internet]. Bobst. [cited 2020 Aug 23]. Available from: <https://www.bobst.com/chen/products/gravure-printing/gravure-printing-presses/overview/machine/vision-rs-5003/>
48. L.Gonzalez-Macia, A.J.Killard. Screen printing and other scalable point of care (POC) biosensor processing technologies. *Med Biosens Point Care Appl.* 2017;69–98.
49. McKeegan D. The Evolution of High Production Digital Textile Printers and Single Pass Printing [Internet]. Fespa. 2021 [cited 2021 Aug 23]. Available from: <https://www.fespa.com/en/news-media/features/the-evolution-of-high-production-digital-textile-printers-and-single-pass-printing>
50. Wang Z, Wang X, Fang T. The rheology of the offset inks. *JOCCA - Surf Coatings Int.* 1998;81(5):219–22.
51. Zołek-Tryznowska Z. Rheology of Printing Inks. *Printing on Polymers: Fundamentals and Applications.* 2015. p. 87–99.
52. Claypole T, Davies G, Jewell E, Vigne V. The effect of speed and viscosity on line quality in rotogravure printing with reference to printed electronics. In: *Proceedings of IARIGAI XXXII.* Porvoo, Finland IARIGAI: Proceedings of IARIGAI XXXII;
53. Moongilan D. Skin-effect modeling of image plane techniques for radiated emissions from PCB traces. *IEEE Int Symp Electromagn Compat.* 1997;(2):308–13.
54. The Skin Depth of Copper in Electrical Engineering [Internet]. All About Circuits. Available from: <https://www.allaboutcircuits.com/textbook/alternating-current/chpt-3/more-on-the-skin-effect/>
55. Yang L. Printing Dynamics: Nip Pressure and Its Relationship with Materials' Viscoelasticity. *J Packag Technol Res* [Internet]. 2020;4(2):145–56. Available from: <https://doi.org/10.1007/s41783-020-00091-z>
56. Kenny J. Midweb Flexo [Internet]. Label and Narrow Web. 2008. Available from: https://www.labelandnarrowweb.com/issues/2008-04/view_features/midweb-flexo/
57. Lee B. Design Characteristics Unique to the Flexographic Printing Process. 1998; Available from: <http://scholarworks.rit.edu/cgi/viewcontent.cgi?article=1600&context=theses>
58. Đokić M, Radonić V, Pleteršek A, Kavčič U, Crnojević-Bengin V, Muck T. Comparison between the characteristics of screen and flexographic printing for RFID applications. 2015;45(1):3–11.
59. Yang ZGG, Zhang W, Liu Q, Mo L, Li L. Application Research of Nano Silver Conductive Ink in Flexographic Printed RFID Antenna. *Adv Graph Commun Print Packag.* 2019;480–7.
60. Hösel M, Krebs F. Large-scale Roll-to-roll Fabrication of Organic Solar Cells for Energy Production. Technical University of Denmark; 2013.

61. Izdebska-Podsiadły J, Thomas S. Printing on Polymers: Fundamentals and Applications. Matthew Seans; 2016. 186–187 p.
62. Bohan MFJ, Townsend P, Hamblyn SM, Claypole TC, Gethin DT. Evaluation of Pressures in Flexographic Printing. Proc Tech Assoc Graph Arts, TAGA. 2003;(January 2015):41–3.
63. Foulston S. Anilox Cell Geometries For Printable Electronics and Flexible Packaging. Swansea University; 2020.
64. Bould DC, Hamblyn SM, Gethin DT, Claypole TC. Effect of impression pressure and anilox specification on solid and halftone density. Proc Inst Mech Eng Part B J Eng Manuf. 2011;225(5):699–709.
65. Apex International. Conventional Laser Engraved Anilox Rolls [Internet]. [cited 2018 Feb 1]. Available from: <http://www.apex-groupofcompanies.com/conventional-laser-engraved-anilox-rolls/>
66. Harper Image. Plate Dot vs Anilox Cell [Internet]. [cited 2018 Feb 2]. Available from: <http://www.harperimage.com/AniloxRolls/Anilox-Guides/Plate-Dot-vs-Anilox-Cell>
67. Claypole A. Elite Sport as a Unique Test Arena for Printed Wearable Technology. Swansea University; 2020.
68. Virtanen J, Björninen T, Ukkonen L, Kaija K, Joutsenoja T, Sydänheimo L, et al. The effect of conductor thickness in passive inkjet printed RFID tags. 2010 IEEE Int Symp Antennas Propag CNC-USNC/URSI Radio Sci Meet - Lead Wave, AP-S/URSI 2010. 2010;(1):10–3.
69. Merilampi SL, Björninen T, Vuorimäki A, Ukkonen L, Ruuskanen P, Sydänheimo L. The effect of conductive ink layer thickness on the functioning of printed UHF RFID antennas. Proc IEEE. 2010;98(9):1610–9.
70. He H, Sydänheimo L, Virkki J, Ukkonen L. Experimental Study on Inkjet-Printed Passive UHF RFID Tags on Versatile Paper-Based Substrates. 2016;2016:1–9.
71. TEKRA. Typical Polyester Film Service Temperature Ranges.
72. Vergöhl M, Malkomes N, Szyszka B, Neumann F, Matthée T, Bräuer G. Optimization of the reflectivity of magnetron sputter deposited silver films. J Vac Sci Technol A Vacuum, Surfaces, Film. 2000;18(4):1632–7.
73. Faddoul R, Reverdy-bruas N, Blayo A, Haas T, Zeilmann C. Optimisation of silver paste for flexography printing on LTCC substrate. Microelectron Reliab [Internet]. 2012;52(7):1483–91. Available from: <http://dx.doi.org/10.1016/j.microrel.2012.03.004>
74. Hamblyn S. The Role of the Plate in the Ink Transfer Process in Flexographic Printing. Welsh Cent Print Coat. 2004;PhD(December):329.
75. De Grâce JH, Mangin PJ. A Mechanistic Approach to Ink Transfer Part 1: Effect of Substrate Properties and Press Conditions. In: 17th International Conference of Printing Research Institutes. Saltsjöbaden, Sweden: Ed. Pentech Press, London; 1983. p. 312–32.
76. De Grace JH, Mangin PJ. A mechanistic approach to ink transfer part II-The splitting behaviour of inks in printing nips. Adv Print Sci Technol. 1987;19:146–161.
77. Valdec D, Zjakić I, Milković M. The influence of variable parameters of flexographic printing on dot geometry of pre-printed printing substrate. Tech Gaz. 2013;20(4):659–67.
78. Hamblyn A. Effect of Plate Characteristics on Ink Transfer in Flexographic Printing. 2015;(June):2–5.

79. Johnson J. Aspects of Flexographic Print Quality and Relationship to some Printing Parameters [Internet]. Vol. PhD Thesis, Faculty of Technology and Science Chemical Engineering, Karlstad University. 2008. Available from: www.diva-portal.org/diva/getDocument?urn_nbn_se_kau_diva-1793-1_fulltext.pdf -
80. Bould DC, Claypole TC, Bohan MFJ. An Investigation into Plate Deformation in Flexographic Printing. *Proc Inst Mech Eng Part B J Eng Manuf.* 2004;
81. Liu X, Guthrie JT, Bryant C. A study of the processing of flexographic solid-sheet photopolymer printing plates. *Surf Coatings Int Part B Coatings Int.* 2002;85(4):313–9.
82. Jung YC, Bhushan B. Contact angle, adhesion and friction properties of micro-and nanopatterned polymers for superhydrophobicity. *Nanotechnology.* 2006;17(19):4970–80.
83. Shanahan MER. Simple Theory of “Stick-Slip” Wetting Hysteresis. *Langmuir.* 1995;11(3):1041–3.
84. Lindholm G, Ström G. On-line Measurement of Ink Film Thickness in a Flexo Press. Vol. 23, *Advances in Printing Science Technology.* 1995. p. 337–53.
85. Kalite Sistem Group, Lahti J, Laiho L, EhoPlace Oy, Varitiainen J, VTT, et al. ActInPak Summer School. In: *ActInPak.* Tampere, Finland: ActInPak; 2017.
86. Dahiya AS, Shakthivel D, Kumaresan Y, Zumeit A, Christou A, Dahiya R. High-performance printed electronics based on inorganic semiconducting nano to chip scale structures. *Nano Converg [Internet].* 2020;7(1):1–25. Available from: <https://doi.org/10.1186/s40580-020-00243-6>
87. Ferreir Cruz SM, Rocha LA, Viana JC. Printing Technologies on Flexible Substrates for Printed Electronics.
88. Österbacka R, Fortunato E, Steckl AJ. Focus on Paper Electronics. *Flex Print Electron OE-A [Internet].* 2016; Available from: <https://iopscience.iop.org/journal/2058-8585/page/Focus-on-paper-electronics>
89. Kunz W. Ink Transfer in Gravure Process. In: *TAGA Annual Technical Conference [Internet].* Printing United Alliance; 1975. Available from: <https://www.printing.org/taga-abstracts/ink-transfer-in-gravure-process>
90. Claypole TC, Davies GR. The Effect of Speed on Image Transfer on Rotogravure Printing. In: *Research Conference.* Copenhagen, Denmark; 2004.
91. Schäfer J, Dörsam E. Millisecond Fluid Pattern Formation in the Nip of a Gravure Printing Machine. *Colloids Surfaces A Physicochem Eng Asp.* 2019;575:222–9.
92. Lindholm G, Girard LL, Gustafsson M, Vuillermoz S. Ink Transfer in Flexo Evaluated by X-Ray Fluorescence. In 1996. p. 16.
93. Morgan ML, Curtis DJ, Deganello D. Control of morphological and electrical properties of flexographic printed electronics through tailored ink rheology. *Org Electron [Internet].* 2019;73(May):212–8. Available from: <https://doi.org/10.1016/j.orgel.2019.05.027>
94. Olsson R, Yang L, Stam J Van, Lestelius M. Effects of elevated temperature on flexographic printing. 2007;(May 2014).
95. Rentzhog M. Characterisation of Water-Based Flexographic Inks and their Interactions with Polymer-Coated Board. *Ytkemiska Institutet Institute for Surface Chemistry;* 2004.

96. Mendez-Rossal HR, Wallner GM. Printability and properties of conductive inks on primer-coated surfaces. *Int J Polym Sci.* 2019;2019.
97. Das S, Cormier D, Williams S. Potential for Multi-Functional Additive Manufacturing Using Pulse Photonic Sintering. *Procedia Manuf.* 2015;1(43rd):366–77.
98. Reip P. Developments in nanoscale metal inks for Printed Electronics [Internet]. 2012. Available from: <http://www.lboro.ac.uk/microsites/research/iemrc/documents/EventsDocuments/19thMarch2012PrintedandPlastic/DevinNanoscaleMetalinks.pdf>
99. Fernandes IJ, Aroche AF, Schuck A, Lamberty P, Peter CR, Hasenkamp W, et al. Silver nanoparticle conductive inks: synthesis, characterization, and fabrication of inkjet-printed flexible electrodes. *Sci Rep.* 2020;10(1):1–11.
100. Black K, Singh J, Mehta D, Sung S, Sutcliffe CJ, Chalker PR. Silver Ink Formulations for Sinter-free Printing of Conductive Films. *Sci Rep [Internet].* 2016;6(March). Available from: <http://dx.doi.org/10.1038/srep20814>
101. Liu JF, Yu SJ, Yin YG, Chao JB. Methods for separation, identification, characterization and quantification of silver nanoparticles. *TrAC - Trends Anal Chem [Internet].* 2012;33:95–106. Available from: <http://dx.doi.org/10.1016/j.trac.2011.10.010>
102. Venkata Krishna Rao R, Venkata Abhinav K, Karthik PS, Singh SP. Conductive silver inks and their applications in printed and flexible electronics. *RSC Adv [Internet].* 2015;5(95):77760–90. Available from: <http://dx.doi.org/10.1039/C5RA12013F>
103. Giorgi F, Coglitore D, Curran JM, Gilliland D, Macko P, Whelan M, et al. The influence of inter-particle forces on diffusion at the nanoscale. *Sci Rep.* 2019;9(1):1–6.
104. Rajan K, Roppolo I, Chiappone A, Bocchini S, Perrone D, Chiolerio A. Silver nanoparticle ink technology: State of the art. *Nanotechnol Sci Appl.* 2016;9:1–13.
105. Solouki Bonab V, Manas-Zloczower I. Revisiting thermoplastic polyurethane, from composition to morphology and properties. *J Polym Sci Part B Polym Phys.* 2017;55(20):1553–64.
106. Liang J, Shin S, Lee S, Lee D. Self-Healing and Mechanical Properties of Thermoplastic Polyurethane / Eugenol-Based Phenoxo. 2020;
107. Smith CS, Sondhi K, Jimenez BY, Fan Z, Nishida T, Arnold D. Screen-Printed Inductive Silver Ink Strain Sensor on Stretchable TPU Substrate. 2020 IEEE 70th Electron Components Technol Conf. 2020;
108. Brownell L, Harvard University. Low-cost wearables manufactured by hybrid 3-D printing. *Phys Org [Internet].* 2017; Available from: <https://phys.org/news/2017-09-low-cost-wearables-hybrid-d.html>
109. Mohammed A, Pecht M. A stretchable and screen-printable conductive ink for stretchable electronics. *Appl Phys.* 2016;109(18).
110. Tomašegović T, Poljaček SM, Jakovljević MS, Urbas R. Effect of the common solvents on UV-modified photopolymer and EPDM flexographic printing plates and printed ink films. *Coatings.* 2020;10(2).
111. Cao L, Bai X, Lin Z, Zhang P, Deng S, Du X, et al. The preparation of Ag nanoparticle and ink used for inkjet printing of paper based conductive patterns. *Materials (Basel).* 2017;10(9).

112. Mo L, Guo Z, Yang L, Zhang Q, Fang Y, Xin Z. Silver Nanoparticles Based Ink with Moderate Sintering in Flexible and Printed Electronics.
113. Cronin HM, Stoeva Z, Brown M, Shkunov M, Silva SRP. Photonic Curing of Low-Cost Aqueous Silver Flake Inks for Printed Conductors with Increased Yield. *ACS Appl Mater Interfaces*. 2018;10(25):21398–410.
114. Ortego I, Sanchez N, Garcia J, Casado F, Valderas D, Sancho JI. Inkjet Printed Planar Coil Antenna Analysis for NFC Technology Applications. 2012;2012.
115. Hansuebsai A, Noguchi H, Leelapiwat A. 論文 Application of Flexographic Printing for the Fabrication of Conductive Lines Using Nano-silver Ink. 2013;50(3):251–8.
116. Viscosity NVC Norcross Controls. Flexography Troubleshooting Guide [Internet]. Washington; Available from: http://cdn2.hubspot.net/hubfs/219243/Downloads/NVC_Flexographic_eGuide.pdf
117. Luminite. 'Halo': Not So Heavenly Among Flexo Printing Defects [Internet]. 2018 [cited 2020 Feb 13]. Available from: <https://blog.luminite.com/blog/halo-flexo-printing-defects>
118. Morgan ML, Holder A, Curtis DJ, Deganello D. Formulation, characterisation and flexographic printing of novel Boger fluids to assess the effects of ink elasticity on print uniformity. *Rheol Acta*. 2018;57(2):105–12.
119. Inkjet Insight. Dot Gain [Internet]. 2016 [cited 2020 Mar 2]. Available from: <https://inkjetinsight.com/glossary/dot-gain/>
120. Andersson A, Eklund K. A Study of Oriented Mottle in Halftone Print. *Mater Sci* [Internet]. 2007; Available from: <https://www.semanticscholar.org/paper/A-Study-of-Oriented-Mottle-in-Halftone-Print-Andersson-Eklund/7f2561282ffb89bfba1426c681741a001341f5e6>
121. Luminite. Flexo Printing Defects Diagnostic Chart & Troubleshooting Guide [Internet]. 2021 [cited 2021 Jun 12]. Available from: <https://blog.luminite.com/blog/flexo-printing-defects-diagnostic-chart>
122. Luminite. Flexographic Printing Defects Diagnosis & Troubleshooting Checklist [Internet]. Bradford; Available from: <https://cdn2.hubspot.net/hubfs/2696550/Troubleshooting-Grid.pdf?t=1513971489385>
123. Albina A, Taberna PL, Cambronne JP, Simon P, Flahaut E. Impact of the surface roughness on the electrical capacitance.
124. Barnes HA. *A Handbook of Elementary Rheology*. 1st ed. Wirral: The University of Wales Institute of Non-Newtonian Fluid Mechanics, Department of Mathematics, University of Wales Aberystwth; 2000. 120–170 p.
125. Schaeffer WD, Fisch AB, Zettlemoyer AC. Transfer and Penetration Aspects of ink Receptivity. *Tappi*. 1963;46(6):359–75.
126. Paper C, Karlstads S, Karlstads ML. Effects of elevated temperature on flexographic printing. 2015;(October).
127. Claypole TC, Davies GR. Effect of viscosity on ink transfer in gravure printing. *Iarigai*. 2006;1–12.
128. Żółek-Tryznowska Z. Rheology of Printing Inks. *Print Polym Fundam Appl*. 2016;87–99.

129. Lorenz A, Kalio A, Hofmeister GT, Nold S, Friedrich L, Kraft A, et al. FLEXOGRAPHIC PRINTING – HIGH THROUGHPUT TECHNOLOGY FOR FINE LINE SEED LAYER PRINTING ON SILICON SOLAR CELLS. In: 28th European PV Solar Energy Conference and Exhibition. Paris; 2013.
130. Barnes HA. Rheology of Suspensions. *Rheol Ser.* 1989;3:115–39.
131. Barnes HA. A Review of the Rheology of Filled Viscoelastic Systems. *Rheol Rev.* 2003;2003:1–36.
132. Willenbacher N, Georgieva K. Rheology of disperse systems. *Nature.* 1957;180(4593):957–9.
133. Cassagnau P. Linear viscoelasticity and dynamics of suspensions and molten polymers filled with nanoparticles of different aspect ratios. *Polymer (Guildf)* [Internet]. 2013;54(18):4762–75. Available from: <http://dx.doi.org/10.1016/j.polymer.2013.06.012>
134. Hao T. Physics of Electrorheological Fluids. *Stud Interface Sci.* 2005;22:235–340.
135. Gensdarmes F, Dolez PI. Chapter 1.3 - Methods of Detection and Characterization. *Nanoeng Glob Approaches to Heal Saf Issues*, Elsevier. 2015;55–84.
136. Adair JH, Suvaci E, Sindel J. Surface and Colloid Chemistry. *Encycl Mater Sci Technol.* 2001;1–10.
137. Mueller S, Llewellyn E., Mader HM. The rheology of suspensions of solid particles. *Proc R Soc.* 2009;466:1201–28.
138. Hoffman RL. Discontinuous and Dilatant Viscosity Behavior in Concentrated Suspensions. I. Observation of a Flow Instability. *Trans Soc Rheol.* 1972;16:155.
139. Hoffman RL. Discontinuous and dilatant viscosity behavior in concentrated suspensions. II. Theory and experimental tests. *J Colloid Interface Sci.* 1974;46(3):491–506.
140. Jeffrey DJ, Acrivos A. The rheological properties of suspensions of rigid particles. *AIChE J.* 1976;22(3):417–32.
141. Rutgers IR. Relative Viscosity of Suspensions of Rigid Spheres in Newtonian Liquids. *Rheol Acta.* 1962;2(3):118-122202–10.
142. Shchukin ED, Zelenev AS. Physical-Chemical Mechanics of Disperse Systems and Materials. *Progress in Colloid and Interface Science.* 2015.
143. Willenbacher N, Georgieva K. Rheology of disperse systems. *Prod Des Eng.* 2013;1–57.
144. Kleshchanok D. Polymer-induced colloidal interactions: measured by direct and indirect methods. 2007;(November).
145. Jenkins P, Snowden M. Depletion flocculation in colloidal dispersions. *Adv Colloid Interface Sci.* 1996;68(1–3):57–96.
146. Tay BY, Edirisinghe MJ. Dispersion and stability of silver inks. *J Mater Sci.* 2002;37(21):4653–61.
147. Trefalt G, Borkovec M. Overview of DLVO Theory. *Lab Colloid Surf Chem Univ Geneva* [Internet]. 2014;1–10. Available from: www.colloid.ch/dlvo
148. Mueller S, Llewellyn EW, Mader HM. The rheology of suspensions of solid particles. *Proc R Soc A Math Phys Eng Sci.* 2010;466(2116):1201–28.

149. Thomas DG. Transport characteristics of suspension: VIII. A note on the viscosity of Newtonian suspensions of uniform spherical particles. *J Colloid Sci.* 1965;20(3):267–77.
150. Robinson J V. The viscosity of suspensions of spheres. *J Phys Colloid Chem.* 1949;53(7):1042–56.
151. Brenner H. Rheology of Two-Phase Systems. *Annu Rev Fluid Mech.* 1970;2(1):137–76.
152. Pabst W. Fundamental considerations on suspension rheology. *Ceram - Silikaty.* 2004;48(1):6–13.
153. Jewell EH, Hamblyn SM, Claypole TC, Gethin DT. The impact of carbon content and mesh on the characteristics of screen printed conductive structures. *Circuit World.* 2013;39(1):13–21.
154. Rintoul MD, Torquato S. Computer simulations of dense hard-sphere systems. *J Chem Phys.* 1996;105(20):9258–65.
155. Mai R, Pekarovicova A, Fleming PD. Correlation between ink rheology and press performance of water-based flexographic inks. *Proc Tech Assoc Graph Arts, TAGA.* 2007;(October):416–25.
156. Minyoung S, Sergio C, Punit P c, van Rhoonb G. Chapter 6 - Wearable device for thermotherapies. *Wearable Bioelectron Mater Today.* 2020;179–200.
157. Preradovic S, Karmakar NC. Design of fully printable planar chipless RFID transponder with 35-bit data capacity. *Eur Microw Week 2009, EuMW 2009 Sci Prog Qual Radiofreq Conf Proc - 39th Eur Microw Conf EuMC 2009.* 2009;(October):13–6.
158. Preradovic S, Member S, Karmakar NC. Design of Chipless RFID Tag for Operation on Flexible Laminates. 2010;9:207–10.
159. Preradovic S, Balbin I, Karmakar N, Swiegers G. A novel chipless RFID system based on planar multiresonators for barcode replacement. 2008 IEEE Int Conf RFID. 2008;3169:289–96.
160. Chanda D, Bose B. Dependence of Q-Factor of the Series RLC Circuit on Inductance in Real Practice. 2017;2(11).
161. Shahpari M, Thiel D V. Fundamental Limitations for Antenna Radiation Efficiency. *IEEE Trans Antennas Propag.* 2018;66(8):3894–901.
162. Electronics Notes. Quality Factor / Q Factor; formulas and equations [Internet]. Tutorials. [cited 2018 May 30]. Available from: https://www.electronics-notes.com/articles/basic_concepts/q-quality-factor/basics-tutorial-formula.php
163. Electronics Tutorials. Series RLC Circuit Analysis [Internet]. [cited 2018 May 12]. Available from: <https://www.electronics-tutorials.ws/accircuits/series-circuit.html>
164. Keysight Technologies. N9914A FieldFox Handheld RF Analyzer, 6.5 GHz [Internet]. [cited 2021 Jan 8]. Available from: <https://www.keysight.com/en/pdx-x201924-pn-N9914A/fieldfox-handheld-rf-analyzer-65-ghz?nid=-32495.1150495&cc=GB&lc=eng>
165. Simulia. CST Studio Suite [Internet]. [cited 2020 Feb 1]. Available from: <https://www.3ds.com/products-services/simulia/products/cst-studio-suite/>
166. RK PrintCoat Instruments. RK PrintCoat Instruments [Internet]. [cited 2020 Sep 4]. Available from: <https://www.rkprint.com/products/flexiproof-100-uv/>

167. Riley Surface World. The Marketplace for Surface Technology . New and Used Process Equipment & Machinery . Heraeus Votsch Heating and Drying Oven Type VTU 60 / 90. 1995;(1965748):3-5.
168. Bruning JH, Mahajan VN, Cornejo-Rodríguez A, Malacara D, Malacara-Doblado D, Creath K, et al. Optical Shop Testing. Vol. 26, Optica Acta: International Journal of Optics. 1979. 836-836 p.
169. Veeco. Wyko NT9800 Optical Profiling System. 2006;3-4.
170. Bruker Alicona. Dimensional accuracy & surface finish measurement InfiniteFocusG5 plus [Internet]. [cited 2017 Nov 3]. Available from: <https://www.alicon.com/en/products/infinitefocus/>
171. Exakt Technologies Inc. Exakt 50 I [Internet]. [cited 2020 Sep 8]. Available from: <https://exaktusa.com/dispersion-equipment/basic-models/trm-basic-exakt-50i/>
172. Malvern. Bohlin Gemini [Internet]. [cited 2020 Sep 8]. Available from: http://www.cas-instrumental.com.ar/folletos/bohlin_gemini.pdf
173. Netzsch. Kinexus Pro [Internet]. [cited 2021 Oct 1]. Available from: <https://www.netzsch-thermal-analysis.com/en/products-solutions/rheology/kinexus-pro/>
174. Pharmaceutical Online. Malvern Kinexus Redefines The Rheometer [Internet]. Malvern Instruments. 2008 [cited 2017 Mar 6]. Available from: <https://www.pharmaceuticalonline.com/doc/malvern-kinexus-redefines-the-rheometer-0001>
175. Claypole A, Claypole J, Claypole T, Gethin D, Kilduff L. The effect of plasma functionalization on the print performance and time stability of graphite nanoplatelet electrically conducting inks. J Coatings Technol Res [Internet]. 2021;18(1):193-203. Available from: <https://doi.org/10.1007/s11998-020-00414-4>
176. NXP Semiconductors. SL3S1002FTB1 UCODE G2XM and G2XL [Internet]. Available from: <https://www.nxp.com/part/SL3S1002FTB1#/>
177. Adhikari KK, Jung Y, Park H, Cho G, Kim N. Silver-Nanoparticle-Based Screen-Printing and Film Characterization of a Disposable , Dual-Band , Bandstop Filter on a Flexible Polyethylene Terephthalate Substrate. 2015;2015.
178. Björninen T, Merilampi S, Ukkonen L, Ruuskanen P, Sydänheimo L. Performance comparison of silver ink and copper conductors for microwave applications. IET Microwaves, Antennas Propag [Internet]. 2010;4(9):1224. Available from: <http://digital-library.theiet.org/content/journals/10.1049/iet-map.2009.0241>
179. Farnsworth S, Novacentrix. Novacentrix. In Webinar: OE-A; 2020.
180. Novacentrix. Novacentrix - Metalon Conductive Inks [Internet]. [cited 2017 Aug 1]. Available from: <https://store.novacentrix.com/product-p/pfi.htm>
181. InkTec. InkTec Leads New Paradigm in Printed Electronic Materials. Printed Electronics.
182. Engineering M. Crystallization Behavior of PET Materials. 2011;13(1):26-35.
183. Cherry JA. Ink release characteristics of anilox rolls. 2007;
184. Eco-Craft. Eco-Craft Clear Cellulose Film [Internet]. [cited 2020 Sep 7]. Available from: <https://www.eco-craft.co.uk/500mm-x-25m-roll-clear-cellulose-film.html>

185. HiFi Industrial Film. HiFi Industrial Film SU320 [Internet]. [cited 2020 Sep 7]. Available from: <https://www.hififilm.com/product/su320/>
186. Liew E, Okubo T, Sudo T, Hosoi T, Tsuyoshi H, Kuwako F. Signal transmission loss due to copper surface roughness in high-frequency region. *Ipc Apex Expo 2014*. 2014;(4).
187. Perrenot P, Pairis S, Bourgault D, Caillault N. Sulphur corrosion effect on the electrical performance of silver films elaborated by physical vapor deposition. *Vacuum*. 2019;163:26–30.
188. Huntsman. Technical Data Sheet IROSTIC S 7614. 2004;8304.
189. Merck. Diacetone Alcohol [Internet]. [cited 2020 Jan 20]. Available from: <https://www.sigmaaldrich.com/catalog/substance/diacetonealcohol1161612342211?lang=en®ion=GB>
190. Monument Chemical. Monument Chemical Diacetone Alcohol (DAA) [Internet]. 2018 [cited 2020 Jan 21]. Available from: https://monumentchemical.com/uploads/files/TDS/DAA_-_TDS.pdf
191. Claypole A, Claypole J, Holder A, Claypole TC, Kilduff L. Rheology of high-aspect-ratio nanocarbons dispersed in a low-viscosity fluid. *J Coatings Technol Res* [Internet]. 2020;17(4):1003–12. Available from: <https://doi.org/10.1007/s11998-020-00319-2>
192. Strivens TA. An introduction to rheology. *Paint and Surface Coatings*. 1999. 550–574 p.
193. Lepak-Kuc S, Wasilewska K, Janczak D, Nowicka T, Jakubowska M. Conductive Layers on a Shrinkable PET Film by Flexographic Printing. *Materials (Basel)*. 2022;15(10).
194. Vena A, Perret E, Tedjini S, Tourtollet GEP, Delattre A, Garet F, et al. Design of chipless RFID tags printed on paper by flexography. *IEEE Trans Antennas Propag*. 2013;61(12):5868–77.

Appendix

Appendix A: Discrete Component Model (Section 4.2.1.)

A simple LCR circuit was assembled on a Tic-Tac ® Box using discrete components to understand the effects of each component on the output voltage and frequency. Each component was varied in value and the output voltage of the system was recorded for a range of frequencies (0.01-25MHz). If this physical model could be compared to the physical testing results of the printed transmission line, a model could be built on MultiSim of the discrete components and designs could be adjusted for fine tuning.

The frequencies at which the systems resonate were found for a range of set ups where the values of the resistors, inductors and capacitors were altered.

1.3µH, 4.7µH, 9µH and 14.81µH inductors, 987.5pF, 102.1pF, 22.2pF and 10.3pF capacitors, and 0.97Ω, 4.7Ω and 10Ω resistors were used with the aim of creating a range of values similar to that which may occur in the prints.

Figure A-1 shows the input voltage (yellow) and the output from the circuit (green). There is an increase in amplitude between in the input and the output signal. A phase shift of 45° is also present.



Figure A-1 – Rohde and Schwarz RTM 2024 Digital Oscilloscope output interface showing input and output voltages, input and output frequencies, and phase shifts of the signal.

A sweep of frequencies from 0.01 to 25MHz, was applied for each LCR set-up [Figure A-2 (a), (b) and (c)]. The peak occurs at a higher input frequency and lower output voltage as the inductance in the circuit decreases [Figure A-2 (a)]. The peak occurs at a higher input frequency and higher

output voltage as the capacitance in the circuit increases [Figure A-2 (b)]. The three plots follow very similar patterns and peak towards the higher end of the 0-25MHz test range [Figure A-2 (c)].

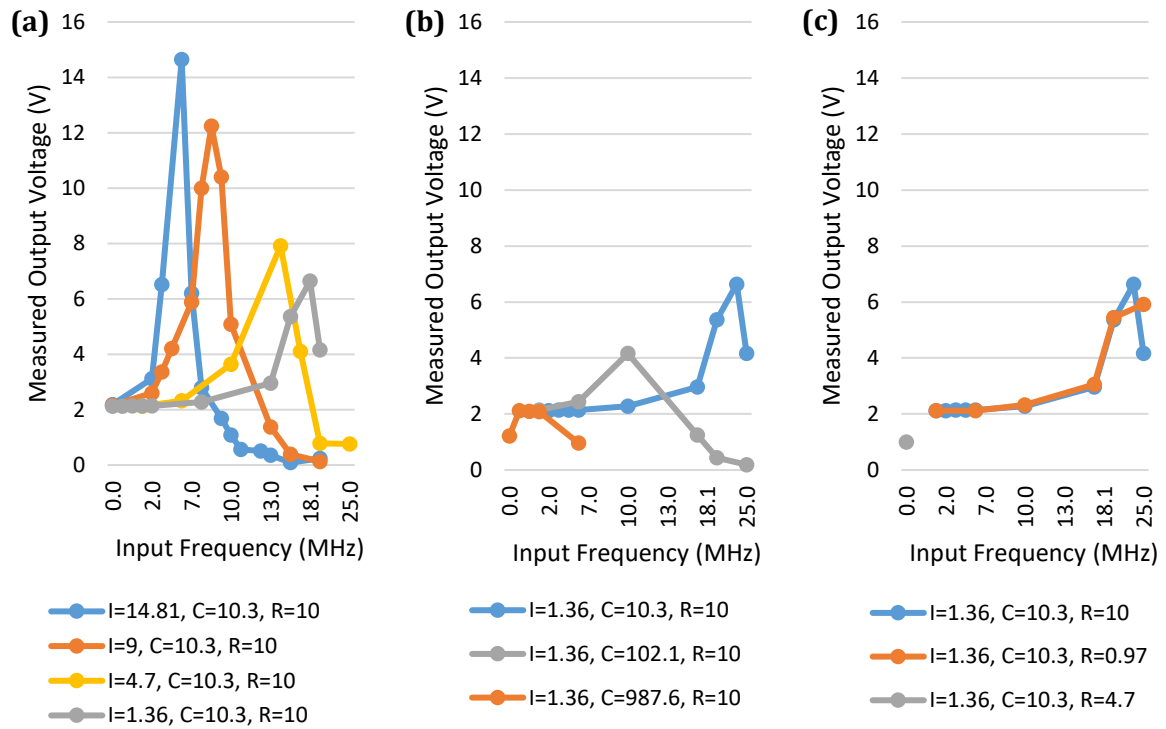


Figure A-2 – Discrete component system showing measured output voltage for: **(a)** varying inductor values across a range of frequencies; **(b)** varying capacitor values across a range of frequencies; **(c)** varying resistor values across a range of frequencies.

Appendix B: Simulation Array for Theoretical Impact of Surface Roughness on Frequency Response (Section 4.3)

Antenna designs were simulated on CST Studio Suite. Parameters used are presented in Table B-1. Average % of spreading was calculated from previous experiments to be 1.18% and is included in the widths presented in Table B-1. Table B-2 shows resonant peak frequencies and trough magnitudes from simulations.

The frequency profiles are presented for each of the nine simulations after the tables.

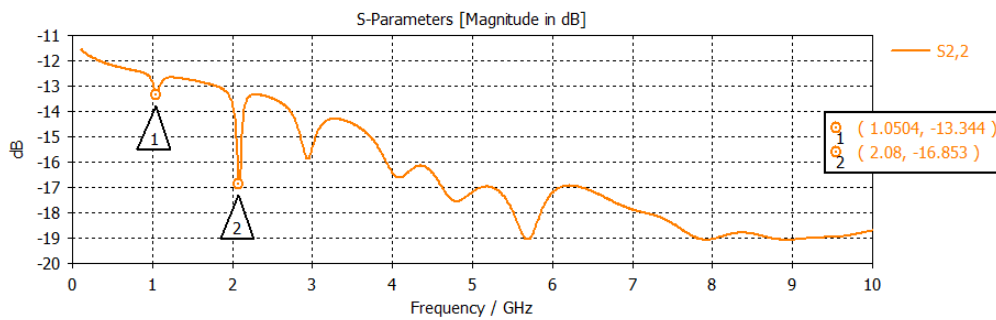
Table B-1 – Track length, widths and surface roughness for antenna design A.

Number denoted on simulations	Width (mm) =0.5*1.18	Line Length (mm)	Silver Surface Roughness RMS aka Ra (nm)	Thickness of Print (µm)	Anilox Vol. (cm³/m²)	Print Speed (m/min)
1	0.59	58.5	367.3433	0.4837	8	20
2	0.59	58.5	294.9833	0.267	8	50
3	0.59	58.5	320.9667	0.262133	8	80
4	0.59	58.5	485.75	0.474933	14	20
5	0.59	58.5	349.6833	0.552367	14	50
6	0.59	58.5	354.3733	0.5235	14	80
7	0.59	58.5	402.37	0.786433	24	20
8	0.59	58.5	428.1567	0.7262	24	50
9	0.59	58.5	630.84	0.710067	24	80

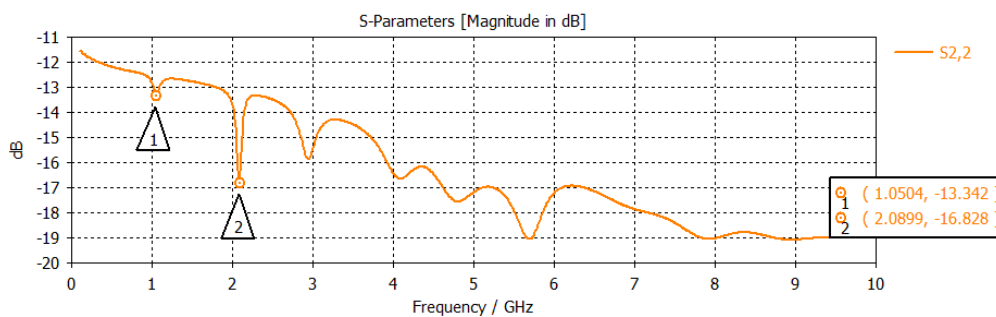
Table B-2 – Summary of resonant peaks from simulation tests of antenna from above table.

	1 st Resonant Peak		2 nd Resonant Peak	
	Frequency (GHz)	S22 (dB)	Frequency (GHz)	S22 (dB)
1	1.0504	-13.344	2.08	-16.853
2	1.0504	-13.342	2.0899	-16.828
3	1.0504	-13.341	2.0899	-16.836
4	1.0504	-13.342	2.0899	-16.796
5	1.0504	-13.344	2.08	-16.85
6	1.0504	-13.344	2.08	-16.851
7	1.0504	-13.347	2.08	-16.869
8	1.0504	-13.342	2.08	-16.855
9	1.0504	-13.343	2.08	-16.883

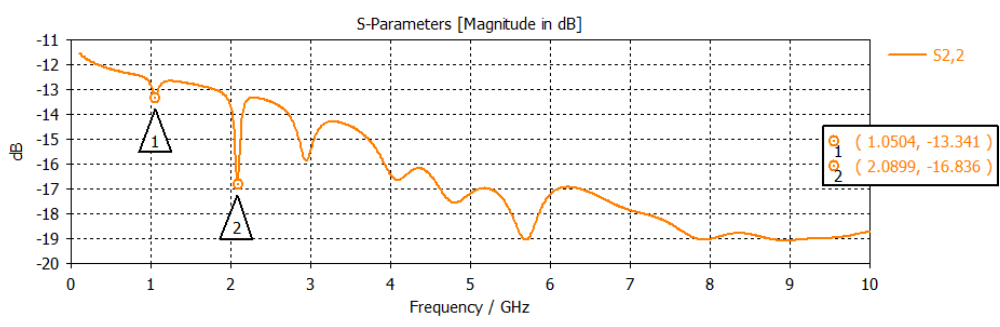
1



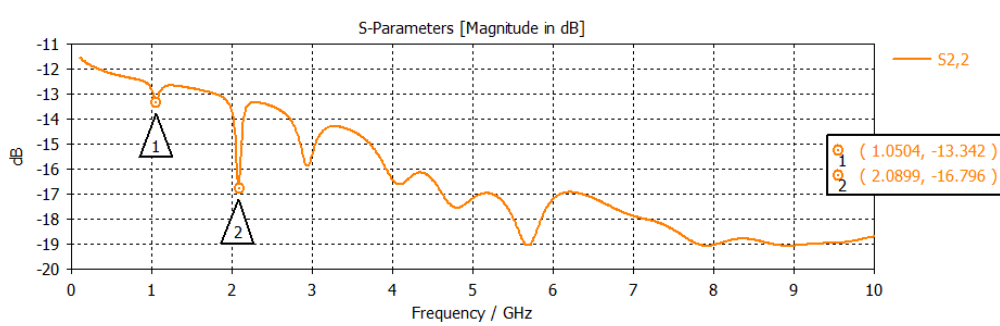
2



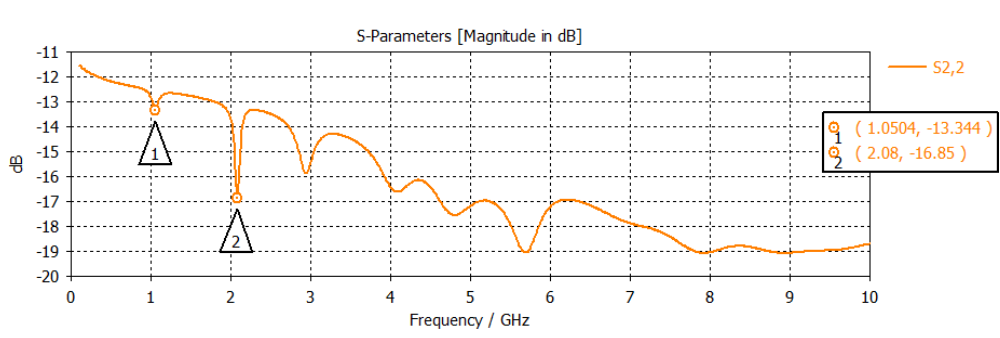
3



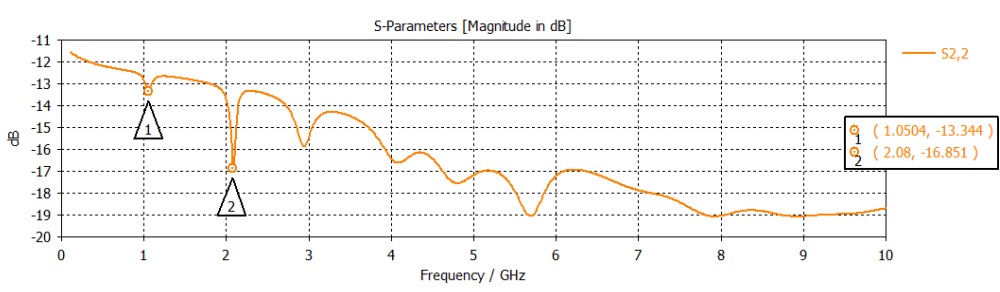
4



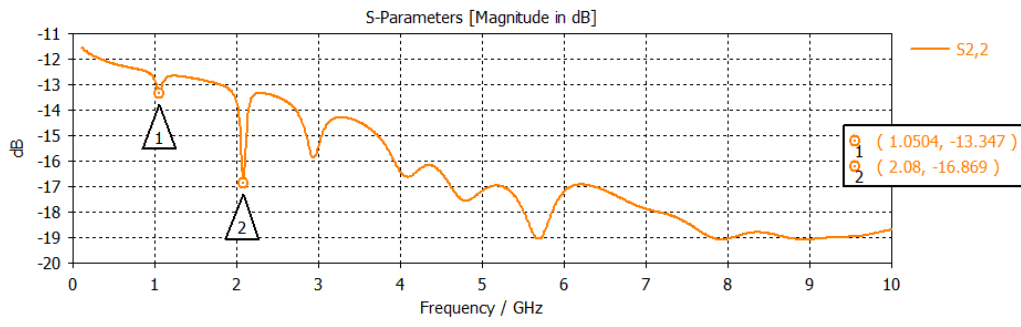
5



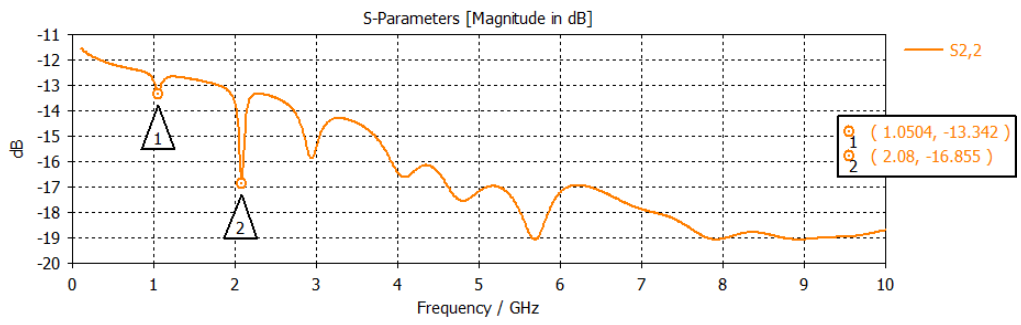
6



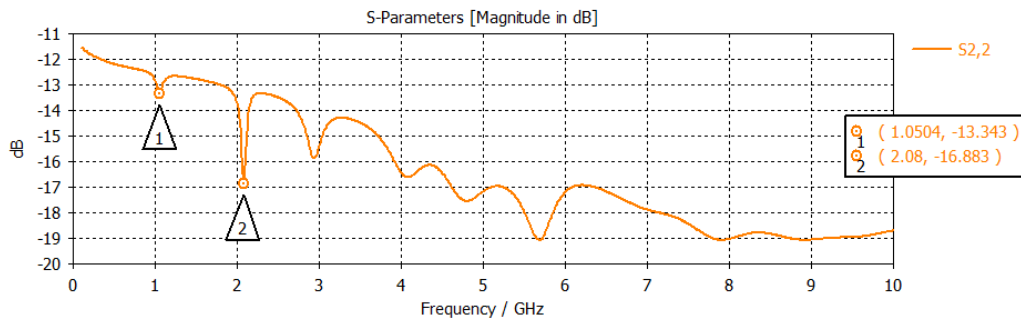
7



8



9

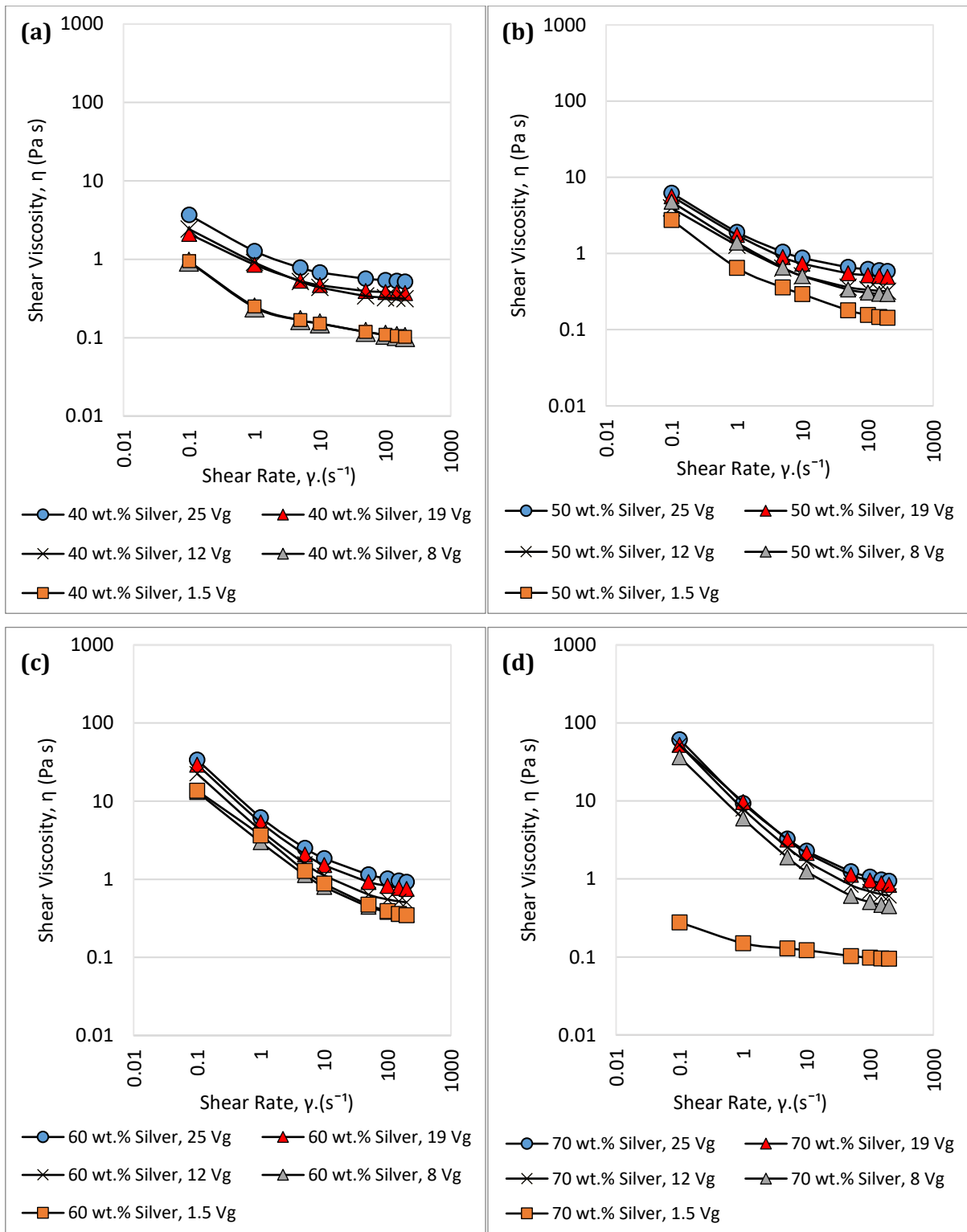


Appendix C: Polymer Viscosity Grade at Various Silver Loadings (Section 7.4.1.)

Figure C-3 (a), (b), (c), (d) and (e) show the changes in shear viscosity for an increasing shear rate for each silver loaded ink with an increasing polymer viscosity grade.

The anomaly (40wt.% silver loading and 8 Vg), in this increasing shear viscosity with increased viscosity grade trend shown in Figure C-3 (a), could be attributed to slip effects, whereby a layer is formed at the surface of the rotating plate due to particles driven away from the wall. Hence, the disk skims across the top of the ink with lower particle interaction. This effect produces lower viscosity values than expected, which is possibly the effect exhibited here. This is also exhibited for 8 Vg, 60wt.% silver loading and 1.5 Vg, 70wt.% loading.

1.5 Vg at $1s^{-1}$ in Figure C-3 (e) is also not in line with the trends seen on the other graphs. It is likely slip occurred when testing at this low rate.



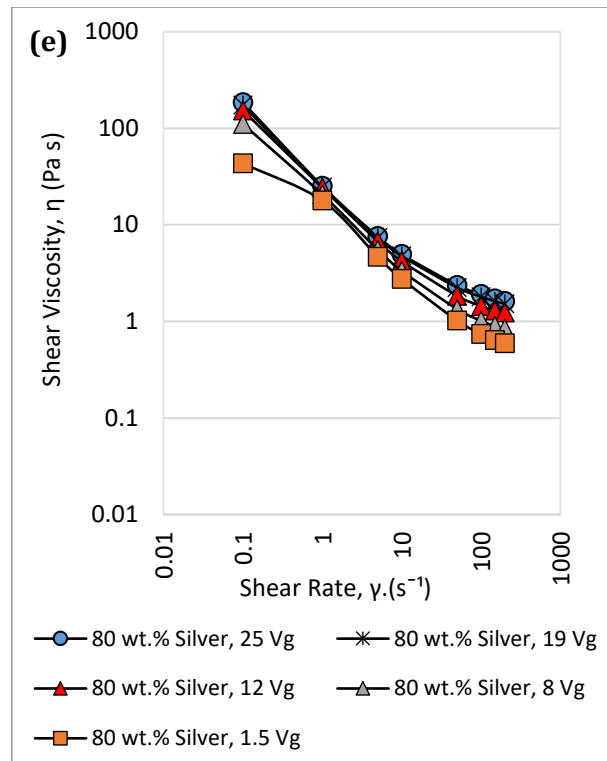
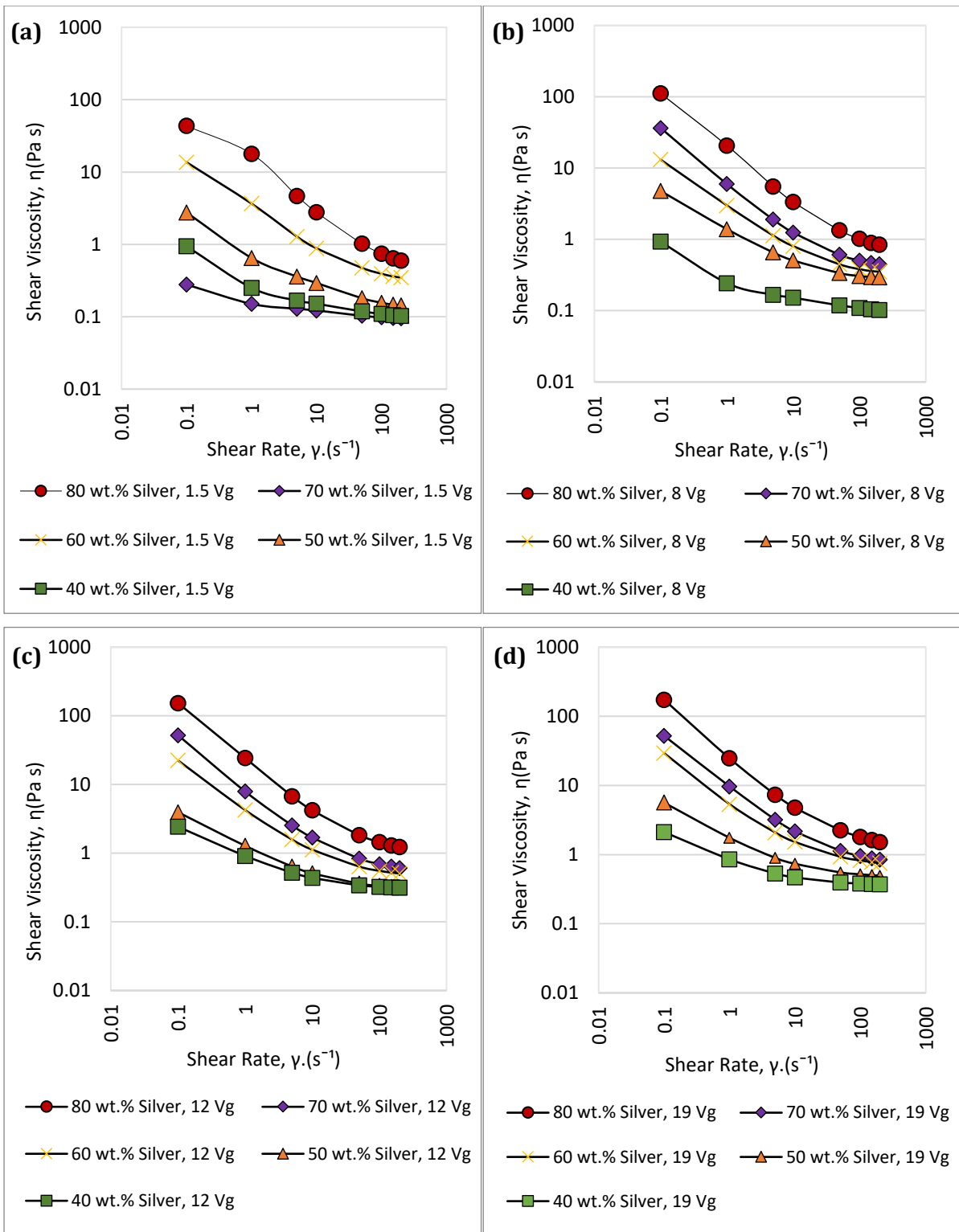


Figure C-3 – Polymer viscosity grades 1.5, 8, 12, 19 and 25 for: **(a)** 40 wt.%, **(b)** 50 wt.%, **(c)** 60 wt.%, **(d)** 70 wt.% and **(e)** 80 wt.% silver loading on a shear viscosity against shear rate log-log graph.

Appendix D: Silver Loadings at Various Viscosity Grades (Section 7.4.2.)

Figure D-4 (a), (b), (c), (d) and (e) show the changes in shear viscosity for an increasing shear rate for each polymer viscosity grade ink with an increasing silver loading. Figure D-4 (a) shows some errors. All other graphs show strong trends but 1.5 Vg at $1s^{-1}$ appears to have experienced some slip in the rheometer. 70wt% for 1.5 Vg also shows an inconsistency with the trend. This experiment was repeated but the result was the same. As the trends are strong when comparing to the other graphs, this result is seen to be anomalous.



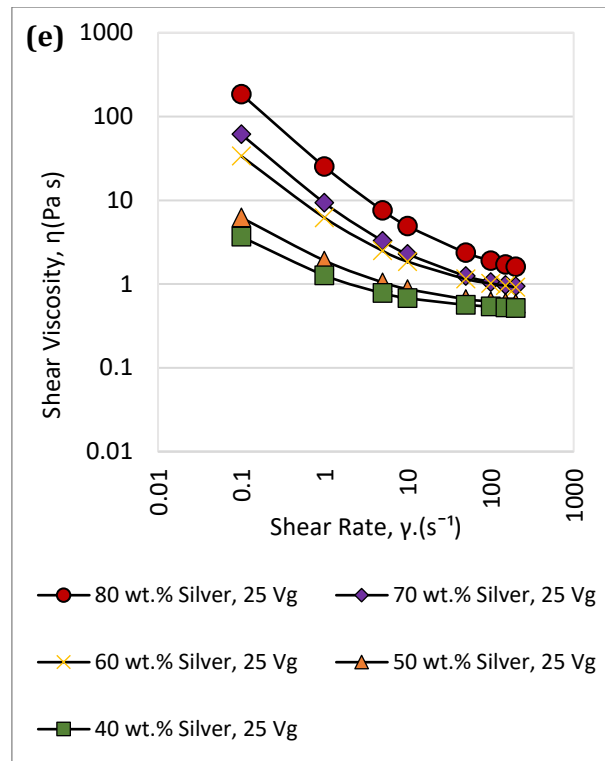


Figure D-4 – 40 wt.%, 50 wt.%, 60 wt.%, 70 wt.% and 80 wt.% silver loadings for polymer: **(a)** 1.5 Vg, **(b)** 8 Vg, **(c)** 12 Vg, **(d)** 19 Vg **(e)** 25 Vg, on a shear viscosity against shear rate log-log graph.

Appendix E: Modelling of Polymer Viscosity Grade and Silver Loading Suspension Behaviours for Viscosity and Phase Volume (Section 7.5.)

Figure E-5 (a), (b), (c), (d) and (e) show the results for the range of silver wt. %s at each of the polymer Vgs (1.5, 8, 12, 19 and 25). It shows that the experimental data for silver inks has poor correlations with each of the models.

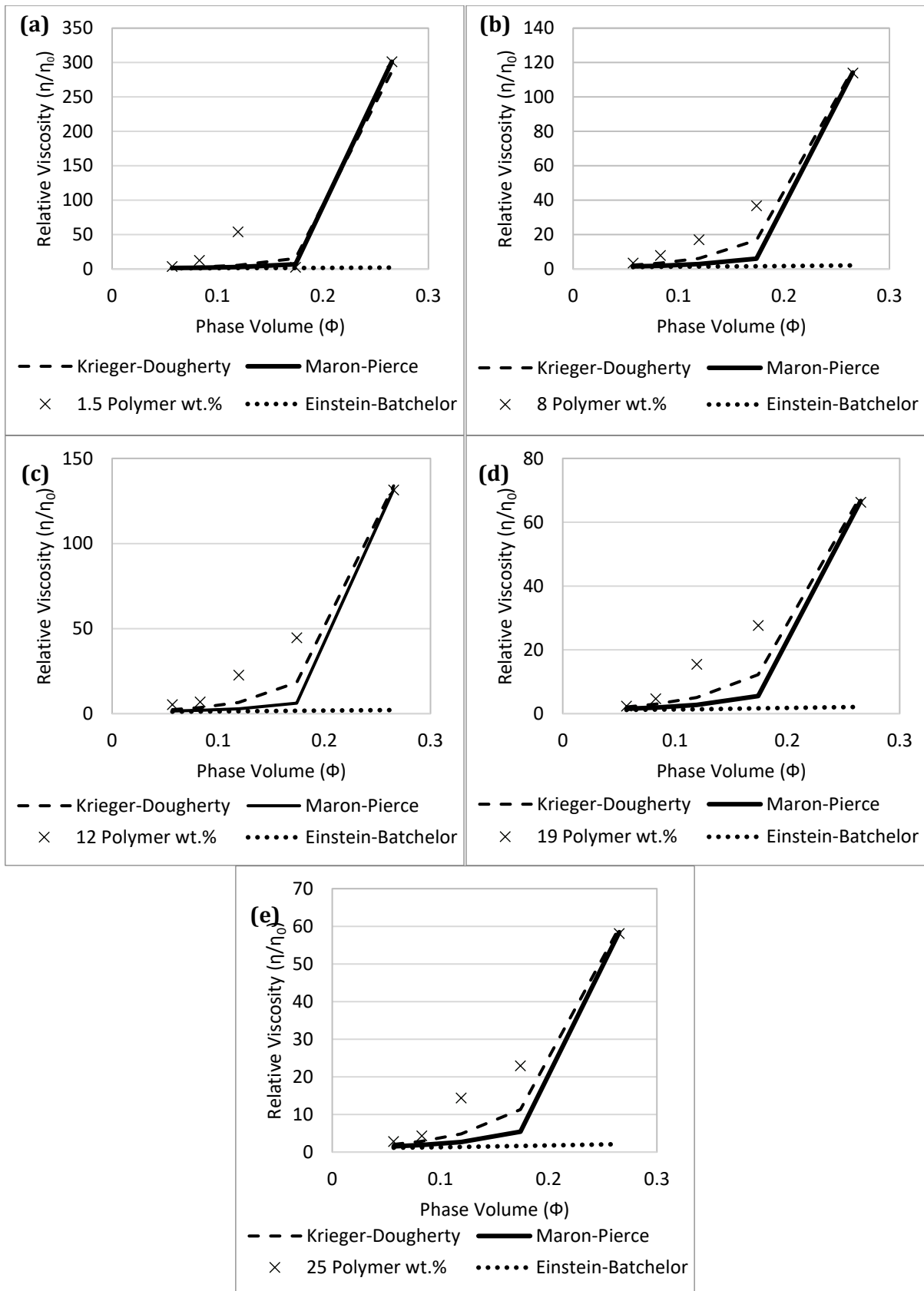


Figure E-5 – Relative viscosity against phase volume for an Ag-DAA-TPU(1.5 Vg.) flexographic printing ink for inks of 40wt.%, 50wt.%, 60wt.%, 70wt.% and 80wt.% Ag. (a) TPU 1.5Vg; (b) 8 Vg; (c) 12 Vg, (d) 19 Vg, (e) 25 Vg.

Appendix F: Resin and Silver Ink Formulations (Section 7.3.1.)

Table F-3 – Ag:DAA:TPU ratios for polymer Vgs 1.5 and 8.

Polymer Vg	Ratios (Ag:DAA:TPU)
1.5	40:55.5:4.5
1.5	50:46.25:3.75
1.5	60:37:3
1.5	70:27.75:2.25
1.5	80:18.5:1.5
8	40:55.5:4.5
8	50:46.25:3.75
8	60:37:3
8	70:27.75:2.25
8	80:18.5:1.5

Table F-4 – Ink formulations of 50:50 wt.% nano-Ag:(DAA-TPU formulation)

	Polymer Vg	DAA to TPU Polymer Ratio	Wt.% Ratio to Ag	Ink Label
Figure 8-3 (a)	1.5	87.5:12.5	-	87.5:12.5 DAA: TPU 1.5 Vg
	1.5	90:10	-	90:10 DAA: TPU 1.5 Vg
	1.5	92.5:7.5	-	92.5:7.5 DAA: TPU 1.5 Vg
	8	87.5:12.5	-	87.5:12.5 DAA: TPU 8 Vg
	8	90:10	-	90:10 DAA: TPU 8 Vg
	8	92.5:7.5	-	92.5:7.5 DAA: TPU 8 Vg
Figure 8-3	1.5	90:10	50:50	50:45:5 Ag:DAA:TPU 1.5 Vg
	1.5	92.5:7.5	50:50	50:46.25:3.75 Ag:DAA: TPU 1.5 Vg
	8	90:10	50:50	50:45:5 Ag:DAA: TPU 8 Vg
	8	92.5:7.5	50:50	50:46.25:3.75 Ag:DAA: TPU 8 Vg